



**VAAL UNIVERSITY
OF TECHNOLOGY**

Inspiring thought. Shaping talent.

***OPTIMIZATION OF A WASTE POLYETHYLENE TEREPHTHALATE/FLY ASH
HYBRID CONCRETE COMPOSITE IN SLABS***

A thesis submitted in fulfilment of the requirements for the degree

Doctorate of Engineering in Mechanical Engineering

In the Faculty of Engineering & Technology

Vaal University of Technology

Name of Student: Nkosilathi Zinti Nkomo

Student Number: 218192223

D.Eng. in Mechanical Engineering

Promoter: Prof L.M.Masu

Co-promoter: Dr P.K Nziu

Date: August 2022

TABLE OF CONTENTS

List of Figures	iv
List of Tables	vii
List of acronyms and abbreviations	viii
List of symbols and nomenclature	x
Declaration of dissertation	xi
Publications and proceedings arising from this thesis.....	xii
Acknowledgement	xiii
Dedication	xiv
Abstract.....	xvi
CHAPTER 1: INTRODUCTION	1
1.1 Background of the study.....	1
1.2 The purpose of the study	3
1.3 Significance of the study	3
1.4 Statement of the problem	4
1.5 Main objective	5
1.6 Specific objectives.....	5
1.7 Scope of the study	5
1.8 Thesis outline	5
CHAPTER 2: LITERATURE REVIEW	7
2.1 Introduction	7
2.2 Portland cement	9
2.3 Fly ash	10
2.3.1 Classification and grading of fly ash.....	13
2.3.2 Physical properties of fly ash	18
2.3.3 Chemical properties of fly ash	20
2.3.4 Effect of fly ash on concrete workability	22
2.3.5 Mechanical properties of concrete slabs containing fly ash.....	30
2.4 Plastics in the environment	32
2.4.1 Microplastics	34
2.5 Fibre spinning.....	35
2.5.1 Melt spinning	35
2.6 Polyethylene Terephthalate.....	36
2.6.1 Recycling Polyethylene Terephthalate.....	38
2.6.2 Physical properties.....	38
2.7 Fibre characterization	39

2.7.1	Fibre strength.....	39
2.7.2	Universal tensile tester	40
2.7.3	Fibre length	40
2.8	Composites materials.....	40
2.8.1	Fibre-reinforced cement composites.....	41
2.8.2	Synthetic polymer fibre reinforced concrete.....	43
2.8.3	Failure mechanisms of fibre reinforced concrete slabs.....	48
2.8.4	Composite fabrication techniques.....	51
2.8.5	Effect of fibre addition on concrete workability.....	53
2.8.6	Water-cement ratio	55
2.8.7	Compressive strength	55
2.8.8	Flexural strength	55
2.8.9	Short duration dynamic loads.....	56
2.9	Materials Testing.....	56
2.9.1	Mechanical testing.....	57
2.9.2	Thermal properties	60
2.9.3	Non-destructive tests.....	62
2.10	Optimization and modelling	65
2.11	Economic implications of fibre reinforced composites	66
2.11.1	Direct material costs	66
2.11.2	Direct labour	66
2.11.3	Manufacturing overhead	66
2.12	Existing knowledge gaps	66
CHAPTER 3: RESEARCH DESIGN AND METHODOLOGY		68
3.1	Introduction	68
3.2	Conceptual framework	68
3.3	Raw materials.....	69
3.3.1	Cement.....	69
3.3.2	Water	70
3.3.3	PET fibres.....	70
3.3.4	Fly ash.....	71
3.3.5	Aggregates	71
3.4	Experimental work.....	72
3.4.1	Characterisation of raw materials.....	72
3.4.2	Fabrication of fibre reinforced cement composite.....	83
3.4.3	Fresh concrete mixture	86

3.4.4	Testing of specimens.....	89
3.4.5	Costing of the fabricated composite.....	95
3.5	Numerical modelling.....	95
3.5.1	Development of model	95
3.5.2	Model validation	99
3.5.3	Response optimizer.....	100
3.6	Applications of fibre reinforced composite in slabs	100
CHAPTER FOUR: RESULTS AND DISCUSSION.....		102
4.1	Introduction	102
4.2	Experimental results	102
4.2.1	Characterisation of raw materials.....	102
4.2.2	Concrete workability	122
4.2.3	Testing of the fabricated specimens.....	126
4.2.4	Analysis of material cost	148
4.3	Numerical modelling.....	151
4.3.1	Optimization of mechanical strength and cost of composite.....	152
4.3.2	Response contour and surface plots.....	157
4.3.3	Model validation	162
4.3.4	Response optimizer for the mix design.....	165
4.4	Applications of fibre reinforced composite in slabs	169
CHAPTER FIVE: CONCLUSIONS AND RECOMMENDATIONS		171
5.1	Introduction	171
5.2	Conclusions	171
5.3	Recommendations for Future Work	174
REFERENCES		175
APPENDIX A: MASTERSIZER REPORT 1.....		A
APPENDIX B: MASTERSIZER REPORT 2.....		B
APPENDIX C: XRD REPORT		C
APPENDIX D: EDS ANALYSIS OF FLY ASH SAMPLE.....		H
APPENDIX E: REBOUND NUMBER.....		I
APPENDIX F: TURNITIN REPORT.....		J

LIST OF FIGURES

Figure 2-1 – Process flow in the production of Portland cement (Barough, et al., 2012).....	8
Figure 2-2 – Flow chart showing the production of fly ash in a thermal power station (Yadav & Fulekar, 2018; Chou, 2012)	11
Figure 2-3 – Formation of calcium hydrates between silanol groups in fly ash and free (Richardson, 2008).....	13
Figure 2-4 – Standard No. 10 laboratory sieve (Wills & Finch, 2015).....	16
Figure 2-5 – Schematic diagram of Laser diffraction principle (Lumay, et al., 2012)	17
Figure 2-6 – Showing the SEM for the cenosphere fly ash particles from different areas (a) Malaysia (b) Hendrina, South Africa (c) Matla, South Africa (Ismail, et al., 2007; Alegbe, et al., 2018) (d) Vereeniging, South Africa fly ash particle (Van der Merwe, et al., 2014)	19
Figure 2-7 – Setting time of concrete mixture containing fly ash (Naik & Ramme, 2002).....	26
Figure 2-8 – Graph showing the stages of the heat of hydration for unreinforced cement (Taylor, et al., 2006; Vazquez & Pique, 2016)	27
Figure 2-9 – Three types of a concrete slump (CEP, 2018).....	29
Figure 2-10 – Effect of fly ash volume fraction on flexural strength of concrete slabs (Vinodsinh & Pitroda, 2013; Solanki & Pitroda, 2013).....	32
Figure 2-11 – (a) Plastic fragments extracted from the digestive tract of a necropsied juvenile green turtle (Nelms, et al., 2015) (b) A turtle wrapped in plastic and washed ashore on the beaches of Brazil (News, 2018).....	33
Figure 2-12 – PET bottles used in construction with cement paste (Turner, 2015).....	34
Figure 2-13 – Melt spinning process (Rawal & Mukhopadhyay, 2014).....	36
Figure 2-14 – Reaction of terephthalic acid and ethylene glycol to produce PET (Sadeghi & Sayaf, 2012).....	36
Figure 2-15 – Potential hydrolysis reaction of PET under alkaline conditions in concrete (Wilinski, et al., 2016)	37
Figure 2-16 – Polyethylene Terephthalate tapes obtained from waste PET bottles (Wilinski, et al., 2016).....	38
Figure 2-17 – Effect of polypropylene fibre loading on compressive strength of concrete (Jassim & Anwar, 2016)	45
Figure 2-18 – Failure mechanisms in FRCC. 1 – Fibre rupture; 2 – Fibre pull out; 3 – Fibre bridging; 4 – Fibre/matrix debonding; 5 – Fibre preventing crack propagating; 6 – Matrix cracking (Zollo, 1997).....	48
Figure 2-19 – Process of fibre debonding failure in concrete (Zollo, 1997).....	49
Figure 2-20 – (a) Hand lay up of sisal fibre/cement composite slab (b) Fabricated slab (Aruna, 2014)	52
Figure 2-21 – Concrete slab moulds (Henderson, 2005)	52
Figure 2-22 -3D printer head for concrete (Bos, et al., 2016).....	53
Figure 2-23 – Three-point bending test for a hybrid concrete slab (Ferreirra, et al., 2016).....	56
Figure 2-24 – (a) Showing Flexural strength test on a concrete sample using four-point loading (b) Test carried out on a fly ash/bamboo fibre reinforced concrete sample (Solanki & Pitroda, 2013).....	58
Figure 2-25 – Concrete cubes for compressive strength tests (Neyestani, 2011)	58
Figure 2-26 – Compressive testing of a concrete cylindrical specimen using a universal compressive tester (Tandon, 2017).....	59
Figure 2-27 – Test setup for measuring resistance to fire of slabs made from glass-reinforced concrete (Sadek, et al., 2006)	62
Figure 2-28 – Schematic diagram of a Schmidt rebound hammer test process (Alyamac, et al., 2017)	64
Figure 2-29 – Maturity test apparatus (Helal, et al., 2015)	64
Figure 3-1 – Flow Diagram of Research Design.....	69

Figure 3-2 – Oven used for drying out fly samples.....	73
Figure 3-3 – Quorum coating machine	74
Figure 3-4 – JEOL SEM Machine	74
Figure 3-5 – Malvern 2000G PSD analyser.....	75
Figure 3-6 – XRD Diffraction analysis of fly ash sample on XRD-7000 Shimadzu.....	76
Figure 3-7 – Specific Gravity Test for Fine Aggregates.....	77
Figure 3-8 – Sieving Apparatus Set Up	78
Figure 3-9 – Sieve shaker.....	79
Figure 3-10 – Coarse Aggregate Flakiness Test	80
Figure 3-11 – Coarse Aggregate Elongation Test.....	81
Figure 3-12 – (a) Aggregate immersed in water for 24 hrs (b) Removal of excess moisture (c) Oven drying for 24 hrs.....	82
Figure 3-13 – Creation of general full factorial experimental design	84
Figure 3-14 – Selection of the level values.....	85
Figure 3-15 – Showing Concrete Hand mixture	87
Figure 3-16 – Curing Tank.....	88
Figure 3-17 – Concrete slump test	89
Figure 3-18 – Flexural Strength set up.....	90
Figure 3-19 – Four Point flexural strength test setup.....	91
Figure 3-20 - ELE 1887B0001 Compressive strength tester machine.....	92
Figure 3-21 – Showing set up used for split tensile strength test.....	93
Figure 3-22 – Rebound Hammer Test.....	94
Figure 3-23 – Defining Response Surface Design.....	96
Figure 3-24 – Responses used to analyse response surface design.....	97
Figure 3-25 – Overlaid Contour plot counters	98
Figure 3-26 – Model Response Predictor.....	99
Figure 4-1 – Dark grey fly ash sample.....	104
Figure 4-2 – Fly ash colour scale (Vishnu, 2016).....	105
Figure 4-3 – Showing the SEM Images of fly ash.....	106
Figure 4-4 – Fly ash particles from ESP hopper (Rohilla, et al., 2018).....	107
Figure 4-5 – Particle size distribution of fly ash	108
Figure 4-6 – Size measurement of fly ash particles	110
Figure 4-7 – EDS Test results showing trace amounts of Titanium element.....	112
Figure 4-8 – XRD Pattern for fly ash particles	113
Figure 4-9 – Fine Aggregate Particle Size Distribution Curve	116
Figure 4-10 – Coarse Aggregate Particle Size Distribution Curve	119
Figure 4-11 – Showing slump values with fly ash replacement of cement.....	123
Figure 4-12 – Showing slump values with PET fibre in FRCC.....	124
Figure 4-13 – Showing Combined Slump Value of Fly Ash and PET Fibre on Concrete	125
Figure 4-14 – Effects of Fibre Addition on Compressive strength.....	126
Figure 4-15 – Effects of Fibre Addition on Compressive Stress of Concrete.....	127
Figure 4-16 – Effects of Fly Ash Addition on Compressive strength.....	128
Figure 4-17 - Effects of Fly Ash Addition on Compressive Stress of Concrete.....	129
Figure 4-18 – Compressive Strength Comparison.....	130
Figure 4-19 – Combined Effect of Fibre and Fly Ash Addition on Compressive strength	131
Figure 4-20 – Combined Effect of Fibre and Fly ash addition on FRCC compressive stress	132
Figure 4-21 – Effect of Fibre Addition on Split Tensile Strength of FRCC.....	133
Figure 4-22 – Effect of fly Ash on the Split Tensile Strength of the FRCC.....	134
Figure 4-23 – Split Tensile Strength Comparison.....	135
Figure 4-24 – Combined Effects of Fibre and Fly Ash on Split Tensile Strength	136
Figure 4-25 – Split Tensile Failure of Concrete Cylinder a) Unreinforced concrete b) FRCC	137

Figure 4-26 – Effect of fly ash on flexural strength.....	138
Figure 4-27 – Flexural Strength Comparison.....	139
Figure 4-28 – Effect of Fibre Addition on Flexural Strength	140
Figure 4-29 – Effects of combined fibre and fly ash addition on FRCC	141
Figure 4-30 – Effect of fly ash addition on rebound number.....	143
Figure 4-31 – Comparison between non-destructive and destructive cube test results.....	144
Figure 4-32 – Average Rebound number for FRCC with PET fibre addition	145
Figure 4-33 - Comparison between non-destructive and destructive cube test results for PET fibre	146
Figure 4-34 – Average Rebound Number of combined fibre and fly ash FRCC.....	147
Figure 4-35 – Bill of Materials in Manufacture of FRCC.....	148
Figure 4-36 – Raw Materials Cost Comparison.....	149
Figure 4-37 - Contour plot and a 3D surface plot showing the effect fibre mass fraction (%) and fly Ash mass fraction (%) on compressive strength.....	158
Figure 4-38 – Contour plot and a 3D surface plot showing the effect of fibre mass fraction (%) and fly ash mass fraction (%) on the slit tensile strength	159
Figure 4-39 - Contour plot and 3D surface plot showing the effect fibre mass fraction (%) and fly ash mass fraction (%) on the flexural strength.....	160
Figure 4-40 – Contour plot and a 3D surface plot showing the effect fibre mass fraction (%) and fly ash mass fraction (%) on the total cost	161
Figure 4-41 - Contour plot and 3D surface plot showing the effect fibre mass fraction (%) and fly ash mass fraction (%) on the slump value.....	161
Figure 4-42 – Predicted vs Actual for	164
Figure 4-43 – Predictive vs Actual for Slump.....	164
Figure 4-44 – Predictive vs Actual for Flexural.....	164
Figure 4-45 – Predictive vs Actual for Split	164
Figure 4-46 – Predictive vs Actual for Total.....	164
Figure 4-47 – Overlaid Contour Plot	167
Figure 4-48 – Numerical Response Optimiser.....	168

LIST OF TABLES

Table 2-1 – Chemical composition of fly and Portland cement (Mohammed & Fang, 2011)	11
Table 2-2 – Showing Differences between Class F and Class C fly ash (Rani & Jain, 2015)	14
Table 2-3 – Various methods that can be used for particle size analysis (Wills & Finch, 2015).....	15
Table 2-4 – Chemical properties of different classes of fly ash and Portland cement (Gamage, et al., 2011; Feng, et al., 2018).	20
Table 2-5 – Chemical composition of fly ash Class F using XRD analysis.....	21
Table 2-6 – Effect of partial replacement of cement with fly ash on the bleeding capacity of concrete (Ravindrarajah, 2003)	25
Table 2-7 – Showing the typical properties of PET (Mark, 1985; Brydson, 1995; Awaja & Pavel, 2005)	39
Table 3-1 – Product specifications for Suretech Cement from PPC (PPC, 2018).....	70
Table 3-2 – Properties of PET fibres (Eco Ace, 2020).....	71
Table 3-3 - Composite experimental design with values X_f of the independent variables.....	84
Table 3-4 – Multilevel full factorial experimental design mix.....	86
Table 3-5 – Showing Optimization targets for model	100
Table 3-6 – Target values used for various applications	100
Table 4-1 – Showing the moisture regain test on the fly ash sample	103
Table 4-2 – PSD fly ash analysis results	109
Table 4-3 – Comparison of PSD distribution of fly ash.....	110
Table 4-4 – Data from energy dispersive X-Ray spectrometer (EDS) elementary analysis of fly ash sample	111
Table 4-5 – XRD based mineralogy of fly ash sample	113
Table 4-6 – Sieve Analysis of fine aggregates	115
Table 4-7 – Showing Classification of Sand based on Fineness Modulus (Amey, et al., 2014; Kagonbe, et al., 2020).....	115
Table 4-8 – Specific gravity of fine aggregates.....	117
Table 4-9 – Sieve analysis results for coarse aggregate	118
Table 4-10 – Flakiness and Elongation of Coarse aggregate	120
Table 4-11 –Water absorption test for coarse aggregate	122
Table 4-12 – Concrete guideline for Rebound Hammer Test (Divvala & Rani, 2020)	142
Table 4-13 – Comparison of Rebound Number	143
Table 4-14 – Cost of Raw Materials	148
Table 4-15 – Materials costing for the FRCC	150
Table 4-16 – Cost Comparison.....	151
Table 4-17 – Response Analysis of FRCC.....	152
Table 4-18 – ANOVA for slump (Minitab 17 output)	153
Table 4-19 – ANOVA for Compressive Strength (Minitab 17 output).....	154
Table 4-20 – ANOVA for Flexural Strength.....	155
Table 4-21 – ANOVA for Split Tensile Strength.....	156
Table 4-22 – ANOVA for Total Cost.....	157
Table 4-23 – Statistical conducted on Predictive Model.....	163
Table 4-24 – Response surface Optimizer	165
Table 4-25 – Multiple Response Prediction	166
Table 4-26 – Validation of the Optimal Results Generated from Minitab	169
Table 4-27 – Optimum composition and strength properties for various applications	170

LIST OF ACRONYMS AND ABBREVIATIONS

The following abbreviations and symbols are addressed in several instances throughout the thesis. Any additional, rarely occurring abbreviations and symbols are noted in the corresponding context.

AEA	Air Entraining Admixtures
AE	Acoustic Emission
AMD	Arithmetic Mean Diameter
ANN	Artificial Neural Network
ANOVA	Analysis of Variance
ASTM	American Society for Testing and Materials
BRT	Bus Rapid Transit
BSE	Back-Scattered Electrons
CCR	Coal Combustion Residue
DOE	Design of Experiments
EDS	Energy Dispersive X-Ray Spectroscopy
FA	Fly Ash
FFD	Full Factorial Design
FRCC	Fibre Reinforced Cement Composite
FM	Fineness Modulus
GHG	Green House Gases (GHGs)
HVFA	High Volume Fly Ash
LOI	Limiting Oxygen Index
MPa	Mega Pascals
NDT	Non-Destructive Testing
OPC	Ordinary Portland Cement
PC	Portland Cement
PET/PETE	Polyethylene Terephthalate
PSD	Particle Size Distribution
ROM	Rule of Mixture
SANS	South African National Standard


SEM	Scanning Electron Microscope
SDG's	Sustainable Development Goals
VUT	Vaal University of Technology
W/C	Water Cement Ratio
XRD	X Ray Diffraction

LIST OF SYMBOLS AND NOMENCLATURE

V_f	Fibre volume fraction
M_f	Fibre mass fraction
ρ_m	Density of resin
ρ_f	Density of fibre
$\mu\text{S/cm}$	Micro-Siemens/cm
W_f	Weight of fibres
W_m	Weight of resin
σ, τ	Shear stress
ε	Strain
T_m	Melting temperature

DECLARATION OF DISSERTATION

I declare that this thesis is my own unaided work. It is being submitted for the degree D.Eng. in Mechanical Engineering at the Vaal University of Technology, Vanderbijlpark, South Africa. It has not been submitted before for any degree for any examination at any other University.

Signature of Candidate ... 

Date: 05 August 2022

Statement 1

This thesis is being submitted in fulfilment of the requirement for the degree of Doctorate Engineering: Mechanical Engineering

Signature of Candidate: 

Date: 05 August 2022

Statement 2


This thesis is the result of my own independent work/investigation, except where otherwise stated. Other sources are acknowledged by giving explicit references. A list of references is appended.

Signature of Candidate: 

Date: 05 August 2022

Statement 3

I hereby give consent for my thesis, if accepted, to be available for online publication, photocopying and for interlibrary loan and for the title and summary to be made available to outside organisations.

Signature of Candidate: 

Date: 05 August 2022

PUBLICATIONS AND PROCEEDINGS ARISING FROM THIS THESIS

No.

Journal Publications

- 1 **N.Z. Nkomo, L.M Masu, P.K Nziu (2019)**, *The effect of fly ash on the workability and mechanical properties of concrete slabs: A Review*, International Journal of Mechanical and Production Engineering Research and Development (IJMPERD), Vol 9, Issue 5
- 2 **N.Z. Nkomo, L.M Masu, P.K Nziu (2019)**, *Synthetic polymer fibre reinforced concrete slabs and their effects on the mechanical properties: A Review*, International Journal of Mechanical and Production Engineering Research and Development (IJMPERD), Vol 9, Issue 6
- 3 **N.Z.Nkomo, L.M Masu, P.K Nziu (2022)**, *Effects of polyethylene terephthalate fibre reinforcement on mechanical properties of concrete*, Advances in Material Science and Engineering, vol. 2022, Article ID 4899298, 9 pages, <https://doi.org/10.1155/2022/4899298>
- 4 **N.Z.Nkomo, L.M Masu, P.K Nziu (2022)**, *Effects of hybrid polyethylene terephthalate fibre and fly ash on mechanical properties of concrete*, Materials Research Express, Vol 9, Issue 5, 1-14, <https://doi.org/10.1088/2053-1591/ac703d>
- 5 **N.Z.Nkomo, L.M Masu, P.K Nziu (2022)**, *Optimization of mechanical properties of polyethylene terephthalate fibre/fly ash hybrid concrete composite*, Case studies in construction materials, vol. 17, <https://doi.org/10.1016/j.cscm.2022.e01395>

Journal Publications under Review

- 6 **N.Z. Nkomo, L.M Masu, P.K Nziu (2021)**, *The effects of cement replacement with fly ash on cost and mechanical properties of concrete*

ACKNOWLEDGEMENT

Firstly, I would like to give thanks to God, the Almighty, for granting me the strength and wisdom to undertake this research and, in the process, meet wonderful people who guided and supported me to complete this work.

I would like to express my deep and sincere gratitude to my main supervisor Prof L.Masu who believed in me and took me to work under him on this research. I am grateful for the guidance throughout the study. I am also thankful to Dr P.Nziu, my co-supervisor, for this work. Thank you for the patience, guidance and relentless effort essential for this thesis to be possible.

I would also like to acknowledge Mr M.Smit, who provided me with a lot of guidance in this work. I would also like to acknowledge Mrs G. Modise for facilitating and allowing me access to the laboratory to carry out experimental work. I would also like to recognise and thank Mr Jabu Mbatha for the excellent assistance rendered during the exploratory phase of this work.

I would like to thank Mr Craig from Eco Ace Pvt Ltd recycling company for supplying the fibres used in the study and Sephaku Ash (Pty) Ltd for the fly ash. I would like to thank Mr. Jaques Steyn from Road lab for allowing me to come and do some tests using their facilities. I would also like to thank my fellow postgraduate students and colleagues in the Department of Industrial & Operational Management and Mechanical Engineering for their support and motivation during this journey. To Bonang, my very good friend, thank you for listening, offering me advice, and motivating me through this entire thesis writing process.

To my parents Mr and Mrs Nkomo, I hope I have made you proud through this humble work. Thank you for the prayers, the caring and the support in my journey to culminate in this achievement.

DEDICATION

To the love of my life, my best friend and my wife, Glenda Julia Nkomo, without whose encouragement and support this thesis would never have seen the light of day.

“Pollution is nothing but the resources we are not harvesting. We allow them to disperse because we’ve been ignorant of their value” – R.Buckminster Fuller (1971)

ABSTRACT

Cracked concrete slabs are a problem due to several factors such as poor maintenance, insufficient reinforcement or steel corrosion leading to crack propagation. There is a need to increase the load-bearing capacity of concrete slabs and increase their life span. The use of waste Polyethylene Terephthalate (PET) fibres and fly ash in a hybrid composite slab dramatically alleviates the problem of crack propagation and failure sustainably. This study aimed to optimize a waste PET fibre/fly ash hybrid cement composite for use in slabs. This study characterized the raw materials used, including fly ash and aggregates. After that, concrete test specimens were fabricated using the PET fibres and fly ash following the full factorial experimental design. The developed specimens were then tested to ascertain their material strength properties. Model development was carried out using Minitab Software Version 14, and subsequent experimental validation was carried out. After that, the PET and fly ash optimisation for maximum favourable response outcome was carried out.

The fly ash was found to belong to the Class F category with particle size ranging from 0.31 μm to 800 μm . The fly ash was mainly spherical and consisted of Ca, Al, P, Si, and trace amounts of Ti and Mg. The spherical shape of the fly ash helped improve the concrete's workability. The river sand had a fineness modulus of 3.69, considered coarse sand. The fine aggregate showed uniform particle size distribution with a uniformity coefficient of 4.007. The coarse aggregate characterisation was carried out and revealed that the aggregate particle size was 13 mm in size. The coarse aggregate had a uniformity coefficient of 4.007, which implied the aggregate was well graded. The coarse aggregate had a high flakiness index of 74.82 % and an acceptable elongation index of 46.72 %.

Full factorial methodology experimental design was employed to fabricate the test specimens by simultaneously varying the independent factors to develop a model for overall response variation. The slump value was observed to increase with the addition of fly ash. However, the addition of PET fibre decreased the slump value with incremental amounts of fibre. The combined effect of fibre addition and fly ash showed a general decreasing slump value for all quantities of fly ash content. The compressive strength of PET fibre only composite had maximum strength at 0.5% fibre addition, and the composite with fly ash alone had the maximum compressive strength at 15%. The combined optimum compressive strength for fibre and fly ash was at 0.5 % and 15 %, respectively, with a 15.54 N/mm^2 . The split tensile strength decreased with an increase in fibre content. However, the fibre provided crack retardation. Fly ash increased the split tensile strength significantly to a peak of 2.35 N/mm^2 for 20 % fly ash addition. The combined addition of fibre and fly ash had an optimum split tensile strength of 2.79 N/mm^2 at 0.5 % fibre and 20 % fly ash. The addition of fibre had an optimum split tensile strength at 0.5% of 1.82 N/mm^2 . The fly ash increased the flexural strength, with optimum strength at 15 %. The combined addition of fibre and fly ash created optimum flexural strength at 0.5% and 30 %, respectively. The

trend observed by the rebound number followed that of the compressive strength. However, the non-destructive rebound hammer method gave significantly lower strength values than the destructive test method. The addition of fly ash had the effect of lowering the cost of producing the slab. However, the addition of fibres marginally increased the cost. The combined effect of fibre and fly ash resulted in a significant cost saving.

Numerical optimisation was carried out concerning the fibre reinforced concrete's fresh and hardened mechanical properties. Predictive modified quadratic equations were developed for slump value, compressive, flexural, split tensile strength and total cost. Analysis of variance test carried out for all the responses indicated that the model could predict the slump value and mechanical properties of the fibre reinforced concrete correctly and effectively with a coefficient of determination in the range of 0.4151 to 0.9467. The developed model can predict the required fibre reinforced fresh and hardened properties in order to assist in decision making in construction in slabs. The optimum constituent combination for maximum mechanical strength at the lowest possible cost was found to be 15.7576 % Fly ash and 0.3232 % PET fibre with optimum responses as shown in Table 4-26. These predictions were validated experimentally, and a good correlation was observed between the actual and predicted values based on the observed standard deviations of 0.1335, 0.031, 0.005, 0.676, 0.02 for compressive strength, flexural strength, tensile strength, slump value and cost, respectively. Concrete slabs were optimised for various possible end uses, and the optimum PET fibre % and fly ash % were ascertained as shown in Table 4-27.

CHAPTER 1: INTRODUCTION

1.1 Background of the study

Recycling plastic materials helps the environment in many ways. It saves landfill space, energy, and natural resources. It also reduces the damage caused by mining, cutting trees and manufacturing (Abdulkarim & Abiodun, 2012). The improper disposal of plastic waste plays on the natural environment is increasingly being criticized. Edugreen (2010) indicates that plastics take about one million years to degrade. Plastics break down into smaller toxic components that eventually pollute the soil and waterways, clog up the drains causing water and sewage to overflow, and become the breeding grounds for germs and bacteria that spread diseases (Akinola, et al., 2014). Plastic bottles make up approximately 11% of the contents of landfills worldwide, causing severe environmental consequences (Hiremath & Shetty, 2014). The importance of managing waste to ensure sustainable development cannot be overemphasised. The environment is threatened because of unhealthy and unsustainable utilization of environmental resources and the ineffective management of solid and liquid wastes; these are also alluded to as targets that must be achieved in the Sustainable Development Goals (SDGs) (Akinola, et al., 2014). The technical and administrative capacity to properly implement sound mechanisms for waste management is weak in most developing countries. This can be traced to lean financial, human, and material resources, which bedevil councils (Makwara & Magudu, 2013).

The idea of using fibres as reinforcement in concrete materials is not new. The Romans included horsehair as reinforcement in the bricks they used in the construction of the Roman coliseum, which was built in 80 AD. Mud bricks, reinforced with straw, were commonly used in ancient Egypt during the first dynasty (old kingdom) c. 3000 years BCE (Flower, 2006). Synthetic fibres are added to concrete before or during the mixing operation. Synthetic fibres benefit the concrete in both the plastic and hardened states. The strength of concrete can be increased significantly by incorporating reinforcing fibres (Nibudey, et al., 2013). The fibres act as micro-crack arresters in cement composites (Nibudey, et al., 2013). The benefits of incorporating fibre in concrete include reduced plastic settlement cracks, reduced plastic shrinkage cracks, increased toughness and impact resistance and provision of energy absorption. Other benefits include improved bending strength, better waterproofing properties, prevention of micro-cracks, improved compressive strength and increased tensile strength (CIP, 2014).

Macro-synthetic fibres, typically at higher volumes, can be used for crack control in hardened concrete or temperature/shrinkage reinforcement in some applications. The ability to resist tensile forces can be enhanced with the addition of synthetic fibres to the concrete. When plain concrete develops tensile stress that exceeds its tensile strength, cracking occurs due to bending or changes in temperature and shrinkage. Synthetic fibres can prevent the effect of excessive tensile stresses by bridging and dispersing cracks and holding the concrete in place. Most synthetic fibres reduce the amount of plastic and post

hardening crack formation. Synthetic fibres assist concrete in developing its optimum long-term integrity by reducing plastic and drying shrinkage crack formation, increasing energy absorption, and improving resistance to impact forces. Synthetic fibres are compatible with chemical admixtures, pozzolans, slag cement, silica fume, metakaolin and cement chemistries (NRMCA, 2014).

Choi (2009) reported that PET waste, which are lightweight aggregates obtained from recycled PET bottles, increased the structural efficiency of the concrete composite's compressive strength and density ratio. Concrete production contributes approximately 5 % of annual anthropogenic global Carbon Dioxide (CO₂) production mainly because of the vast quantities used. The development of new concrete additives could produce a more robust, more workable material whilst reducing the amount of cement required and the resulting CO₂ emissions. The rule of thumb for concrete is for every ton of cement made, one ton of CO₂ is produced (Crow, 2008).

Fly ash is one of the residues generated in the combustion of coal. It is an industrial by-product recovered from the flue gas of coal-burning electric power plants. The coal used in the Republic of South Africa has a high ash content. Therefore the use and disposal of fly ash are of environmental concern. Out of the hundreds of millions of metric tons of fly ash produced annually across the world, approximately 20% - 40% is re-used for productive purposes such as additives or stabilizers in cement. The remaining percentage of fly ash is disposed of in landfills. Fly ash particles are mostly spherical in shape and range from less than 1 µm to 100 µm with a specific surface area, typically between 250 and 600m²/kg. The specific gravity of fly ash varies in the range of 0.6 to 2.8x10³ kg/cm. Coal fly ash has many uses, such as cement additive in masonry blocks, a concrete admixture, lightweight alloys and a concrete aggregate. Fly ash enhances the performance of concrete in several ways. It reduces the requirement for mixing water and improves the paste flow behaviour (Upadhyay & Kamal, 2007). The largest application of fly ash is in the cement and concrete industry, although creative new uses for fly ash, such as fly ash for the fabrication of MMCs, are actively being sought (Seslija, et al., 2016).

Unreinforced concrete slabs now have limited use, and engineers now favour reinforced concrete slabs. This is due to the strength to weight ratio and the favourable economics offered by reinforced concrete slabs. The fabricated Fibre Reinforced Concrete (FRCC) is suitable for domestic and industrial applications as suspended slabs. The advantages of the fabricated FRCC in the present study are like that found in other fibre reinforced polymer materials: lightweight, high strength, non-corrosive and non-magnetic (Ebead & Marzouk, 2004). The developed FRCC can increase the flexural capacity of concrete beams and slabs by bonding the FRCC as sheets or strips to the tension side. The FRCC significantly improve the splitting tensile strength and flexural strength if used in this manner, as several researchers have shown for various polymeric reinforced slabs (Ritchie, et al., 1991; Sulaimani, et al., 1994; Challal, et al., 1998; GangaRao & Vijay, 1998). Furthermore use of fibres in concrete tends to improve its fire and thermal resistance due to abrupt change in temperature. For instance, at higher

temperatures the fibres melt and are absorbed within the concrete. Moreover, the fibres generate a permeable network to allow gas mitigation. This migration of gas eliminates and possibility of concrete explosive spalling (Sovjak, et al., 2016). Though, very little information on the reduction in explosive spalling using different types of synthetic fibres is available. The choice of use of PET fibre in this research was taken in cognisance of the potential benefits it has in thermal resistance for safety in use of the reinforced concrete slabs. Normal concrete has a thermal conductivity of $1.603 \text{ W m}^{-1} \text{ K}^{-1}$ which has been shown to decrease significantly with 30% addition of fly ash to approximately $1.599 \text{ W m}^{-1} \text{ K}^{-1}$ as shown in study by Wang et al (2017). However the thermal conductivity is also depended on the water content in concrete and its stage in the curing process. The use of fly ash is expected to give concrete with lower thermal conductivity.

1.2 The purpose of the study

The primary goal of this study is to develop a concrete composite using waste plastic material and fly ash. The developed composite has a lower carbon footprint due to the lower quantity of concrete required and the use of waste plastic material in a sustainable manner. This is in line with Sustainable Development Goal (SDG) twelve, which stresses the importance of responsible production and consumption.

1.3 Significance of the study

Recycling plastic waste to produce new materials such as aggregate in concrete could be one of the best solutions for its disposal (Saikia & Brito, 2013). The benefits of recycling are numerous. USEPA (2009) allude to reducing material hauling and disposal costs, preservation of landfill capacity, which lead to elongation of landfill design life, and sometimes cheaper materials compared to virgin materials. Recycling helps in greening our infrastructure by conserving natural resources, making our infrastructures more durable due to high-performance mixtures, and decreasing energy use. Other benefits of recycling include reducing greenhouse gas emissions and air pollution, minimizing water consumption and groundwater contamination (Celauro, et al., 2010).

The utilisation of waste PET material and fly ash lowers the carbon footprint in the production of concrete by reducing the amount of concrete material consumed. The developed composite material has superior properties by reinforcing the concrete material at a lower cost and reducing the problem of plastic waste material disposal. The use of reinforcement in concrete speeds up construction time because less concrete is required for the slabs and adds strength, allowing thinner and less supported slabs.

1.4 Statement of the problem

Concrete production contributes approximately 5% of annual anthropogenic global CO₂ production mainly because of the vast quantities used, with cement being the second most consumed material next to water (Kumar, et al., 2015). This contributes significantly to global warming and climate change plaguing the world. The utilisation of waste materials such as fly ash and plastic material can lower the quantity of cement necessary and reduce the carbon footprint in the construction industry. Plastic waste is now a serious environmental threat to modern living. A major drawback to dumping plastics in landfills from a sustainability aspect is that none of the material resources used to produce the plastic is recovered – the material flow is linear rather than cyclic (Hopewell, et al., 2009). There is a need to use this waste plastic material sustainably to create value-added products.

Cracked concrete slabs have become prevalent due to poor maintenance, increase in legal load limit, insufficient reinforcement or steel corrosion which leads to cracks (Ali & Yehia, 2016). There is a pressing need to enhance the cracking load and mode of failure of slabs as flexural elements. Unreinforced concrete slabs are quasi-brittle materials at all loading conditions that undergo very little deformation before failure and have low fracture toughness. The tensile strength of concrete is 1/10th of its compressive strength, which is too weak in many structural applications necessitating the introduction of reinforcement material. Unreinforced concrete is characterized by several defects such as low ductility, low toughness, and heavyweight (Badave & Pise, 2018). Steel reinforced slabs, when cracked, tend to allow channels for water to reach steel reinforcement and initiate corrosion which compromises the strength of the slabs. Premature deterioration of slabs due to reinforcing steel corrosion represents one of the most serious threats to the future of concrete as the foremost construction material for slab manufacture. The cracking of concrete originates from different reasons during the service life of slabs. Micro cracking can initially occur induced by thermal and shrinkage properties of hydrates and aggregates. At advanced stages, load and shrinkage induced stress may result in major cracking compounded by environmental effects. However, there are several other factors that can cause cracking of concrete both in service and prior to service such as plastic shrinkage due to excess water and premature drying. There is a need to optimise the composite material's strength properties to ensure its durability and safety in its use. There has been some research carried out on the optimisation of various synthetic fibre reinforced concrete however, insufficient research has been done on the optimization of waste PET fibres used in conjunction with partial cement replacement with fly ash. This study seeks to address this gap in knowledge by use of full factorial experimental design and subsequently optimisation to develop a model to predict mechanical and cost properties of a PET fibre and fly ash hybrid concrete composite.

1.5 Main objective

The main objective of this study is to develop and characterise a polyethene terephthalate/fly ash hybrid cement composite for optimal strength in slabs.

1.6 Specific objectives

The specific objectives of the study are:

- i. Characterisation of the fly ash, fine and coarse aggregates.
- ii. Fabrication of hybrid waste PET fibres/fly ash concrete composite slabs.
- iii. Analyse the total cost for the fabrication of the composite slabs.
- iv. Perform selected destructive and non-destructive tests on the fabricated composite slabs.
- v. Development of a numerical model to predict the fabricated composite slabs' total cost and strength properties.
- vi. Comparison of the experimental results obtained in parts iii and iv with numerical ones from part v for validation.
- vii. Optimization of the selected strength properties and respective total cost of the fabricated composite slabs for various applications.

1.7 Scope of the study

Only waste PET material extruded into fibres was used as concrete reinforcement in this study. Fly ash collected from the Republic of South Africa Eskom plants fabricates the hybrid composite.

1.8 Thesis outline

This thesis consists of five chapters. Chapter One gives a brief introduction and background to the research topic. This chapter includes the main objective, specific objectives, and thesis outline.

Chapter Two reviews the properties of cement and fly ash. The characterisation methods and types of fly ash available are reviewed. Thereafter, the effect of fly ash on concrete properties is extensively studied. The effect of plastics in the environment, and the possibility of using these plastics in concrete composites, is explored and reviewed. Furthermore, the manufacturing method of fibres from waste plastic material is reviewed and their feasibility in concrete composites. The problems and methods that have been used to improve the integrity of concrete are researched, with emphasis on fibre-reinforced composites. The manufacturing methods of the FRCC is explored, and their effect on the concrete is reviewed. Thereafter, various mechanical testing methods that are available for characterisation of the FRCC are reviewed. Lastly, the economic implication and feasibility of fibre reinforced composites are also reviewed.

Chapter Three describes the experimental methods that were employed in this study as well as the model development. The chapter is divided into four sections. The first section looks at the characterisation of the raw materials, including the fly ash and aggregates to be used in the fabrication of the FRCC. After that, the following section looks at the full factorial experimental design to be followed and the fabrication of the test specimens. Section three of this chapter looks at the testing methods that were used in the characterisation of the FRCC. The final section of this chapter looks at the development and validation of the model to optimise the properties of the FRCC.

Chapter Four explains the results obtained from experimental data as well as the correlation between the theoretical and experimental results. Furthermore, validation of the model developed is carried out.

Chapter Five concludes the research work of this study. This chapter summarises the main findings from this research. Recommendations for further work is also suggested in this chapter.

Reference and Appendix is the final section in this work and gives references and appendices in this research. Appendix F provides the Turnitin report for this thesis.

CHAPTER 2: LITERATURE REVIEW

2.1 Introduction

Concrete is a popular construction material that is composed of a mixture of fine aggregates, cement, and water. Admixtures can be added to concrete to alter certain characteristics of the concrete, such as its hardening time, durability, workability, and strength (Rohman & Aji, 2014). Concrete has gained immense popularity due to its durability, fire resistance, and ability to be moulded into any required shape. Fly ash is an admixture that can be added to concrete to improve its properties. Fly ash is a pozzolanic material that can partially replace cement, reducing the quantity of cement required in the mixture.

Concrete has several inherent flaws, including micro-cracks in the material and at the interfaces. The defects originate from strain and stress from external restraints, bleeding, excess water, plastic settlement, and thermal shrinkage (Banthia, et al., 2014). When the load is applied to unreinforced concrete, the micro-cracks within the concrete coalesce to form macro-cracks. Further loading the macro cracks can lead to a global catastrophic failure. This micro and macro fracture process can be mitigated by using reinforcement material in the form of fibres such as steel, glass, polyester, nylon, cellulose, polypropylene, and carbon. These fibres assist by stopping the propagation and growth of cracks within the concrete (Banthia & Gupta, 2006; Li, 2003).

Cement production has a significant impact on the world environment, economy, and energy consumption (Barough, et al., 2012). Cement production has a substantial impact on the environment as it generates approximately 5 % of the global CO₂ emissions (Banthia, et al., 2014). There is a need to use cement in a manner that prevents resource depletion, pollution to the environment and minimise water consumption. Furthermore, cement production is an energy-intensive process, with the clinker process being the highest consumer of raw materials and a mass emitter of carbon dioxide. During the clinker process, the raw material is heated in a rotary kiln at high temperatures and then cooled by forced air circulation. Figure 2-1 shows the process flow in the production of Portland cement.

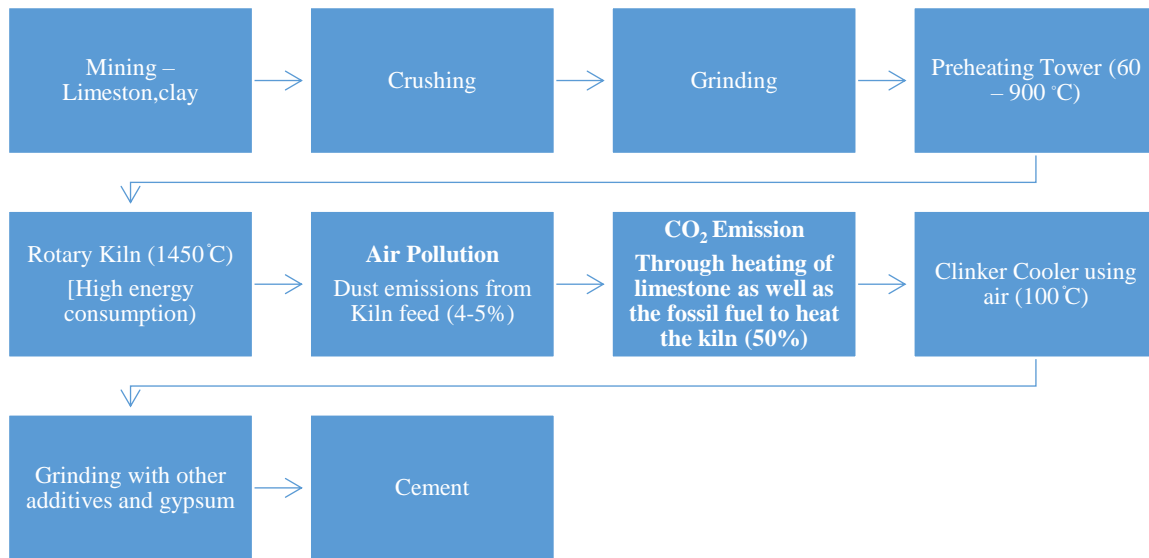


Figure 2-1 – Process flow in the production of Portland cement (Barough, et al., 2012)

Much research has been done on the various methods to reduce the amount of cement required in concrete and substitute it with some other more environmentally friendly materials. Fly ash, rice husk ash, slag and silica fume are some of the materials that have been identified that can partially replace cement in concrete (Saha, 2018).

Fly ash has been widely adopted as a partial cement replacement due to its pozzolanic activity, reduced water demand, reduced bleeding, and less heat evolution. Kumer (2018) carried out research that recommended partial replacement of cement with fly ash at 15-25% for high strength concrete. Fly ash gives dense concrete paste with high particle packing due to the spherical shape of the fly ash particles (Ahmaruzzaman, 2010). In the last decade, approximately 6 million tons of greenhouse gas emissions have been avoided in the South African construction industry by utilizing waste fly ash (Zulu & Allopi, 2015). Furthermore, the use of fly ash in concrete improves the strength (Wongkeo, et al., 2014), wear resistance (Gao, et al., 2017), acid resistance and leaching properties (Saha & Sarker, 2017) of the concrete.

Eco-friendly construction materials are gaining increased popularity worldwide. This is due to environmental regulations, human health, and sustainability in material usage (Kizinievic, et al., 2018). Plastic waste is a significant environmental threat due to its non- biodegradability, and polyethylene contributes the largest quantity of waste plastic in the environment, followed by Polyethylene Terephthalate (PET). Polyethylene terephthalate is a polymeric material with good mechanical properties and dimensional stability.

The addition of polymeric fibres into concrete can significantly improve the properties of concrete as the fibres act as crack retarders, increasing the flexural, tensile, and impact strength of concrete. Furthermore, fibres can also increase the cracking resistance and ductility of concrete (Badave & Pise, 2018). The use of polymeric material in this manner minimises their environmental impact and uses the waste material in a sustainable manner. Polyethylene terephthalate reinforced concrete has been shown by research to have good properties and allows easy jetting of concrete as well as greater control of plastic shrinkage cracking (Dora, 2011).

2.2 Portland cement

Cement is defined as a fine powdery material containing silicates of calcium, formed out of raw materials consisting of calcium oxide, silica, aluminium oxide, and iron oxide (Gaharwar, et al., 2016). Modern life without cement is almost impossible to conceive as cement is the inorganic binder for concrete material for buildings and civil engineering constructions. Furthermore, the cement and concrete industry are important sectors of the world economy and in every country, and it is responsible for job creation and numerous benefits in secondary industries. Concrete is the second most used material in the world next to water. In terms of production, it surpasses its closest rival, steel, by 30 times in volume and ten times in mass (Hanson, 1995). Concrete material is used widely as it does not require sophisticated equipment to use, is easily mouldable and sets rapidly within a few hours (Potgieter, 2012). However, cement production is energy-intensive and environmentally unfriendly. Furthermore, it uses a lot of non-renewable natural resources in the process of generating significant amounts of CO₂. Statistics show that 5-6% of all CO₂ gases generated worldwide is from cement production alone (Rodrigues & Joekes, 2010).

There are over ten different types of cement that are used in the construction industry, and they differ significantly in their composition and are manufactured for different end uses. Some of these types of cement types include Ordinary Portland cement (OPC), Portland Pozzolana Cement (PPC), Rapid Hardening Cement, Quick Setting Cement, Low Heat Cement, Sulphates Resisting Cement, Blast Furnace Slag Cement, High Alumina Cement, White Cement, Coloured cement, Air Entrained Cement, Expansive Cement and Hydrographic Cement (Dunuweera & Rajapakse, 2018). Generally, Ordinary Portland cement is the most suitable for concrete slabs. Henceforth, this study will from this point on focus solely on the use of Ordinary Portland Cement hence after referred to as just Portland cement.

Portland cement got its name from Joseph Aspdin in 1824, who named it after the cliffs on the isle of Portland in England (Bediako & Amankwah, 2015). The manufacturing process of Portland cement involves mining, crushing, grinding of limestone and clay, blending raw materials, and calcining the materials in a kiln and after that, cooling the resulting clinker, mixing the clinker with gypsum, and milling, storing and bagging the finished cement. The chemistry of cement production begins with the decomposition of clay minerals into Silicon dioxide (SiO₂) and Aluminium Oxide (Al₂O₃) on the one

hand and of calcium carbonate (CaCO_3) at about 900°C to give CO_2 on the other hand in a process known as calcination. After that clinkering process is carried out in which the Calcium Oxide (CaO) reacts at approximately 1450°C with silica, alumina, and ferrous oxide to form silicates, aluminates, and ferrites of calcium. The resultant clinker is ground with gypsum and other additives to produce cement.

There is a serious environmental problem in cement production. One possible way to increase sustainability and reduce pollution levels is to use alternative raw materials from those being used currently. One such method involves using fly ash which has been identified as a potential source of silica and alumina in the cement manufacture process (Campolat, et al., 2004; Sahu & Majling, 1994). The other option which is also viable is to use gypsum as starting material to produce sulphuric acid and cement. However, another less researched method that has not been well researched and understood is economically viable, combining fly ash and gypsum as raw materials in the manufacture of cement (Potgieter, 2012). The other available method is the partial substitution of Portland cement with fly ash during the manufacture of concrete slabs, which is the focus of this study.

2.3 Fly ash

Fly ash, also known as coal combustion residue (CCR), is a residue in the combustion of powdered, pulverized coal or lignite coal at high temperatures (Sevim & Demir, 2019). Fly ash is a complex heterogeneous material that consists of amorphous alumina silicate spheres, trace amounts of iron-rich spheres, crystalline phases, and small quantities of unburned carbon (Kiilaots, et al., 2004). Approximately 900 million metric tonnes of fly ash is produced worldwide, and a small percentage of approximately 30-40% is being utilized for various value-added products (Gamage, et al., 2011). In South Africa alone, 29 million tonnes of fly ash is produced per annum, with approximately 5% being used for value-added services (Mahlaba, et al., 2011). The emission of fly ash particulates into the environment is controlled using scrubbers and mechanical and electronic precipitators in power stations. Fly ash makes up approximately 85% of the total coal residue and has a particulate diameter ranging from 0.5 to $100\ \mu\text{m}$ (Rani & Jain, 2015).

Fly ash is generated in the thermal stations after coal is loaded into mills that pulverize the coal then feed it to a boiler. In the boiler, combustion takes place, producing heat and fly ash. The fly ash is carried by the flue gas and passes through the super-heater, then to the re-heater, economizer and preheater, as shown in the flow chart in Figure 2-2.

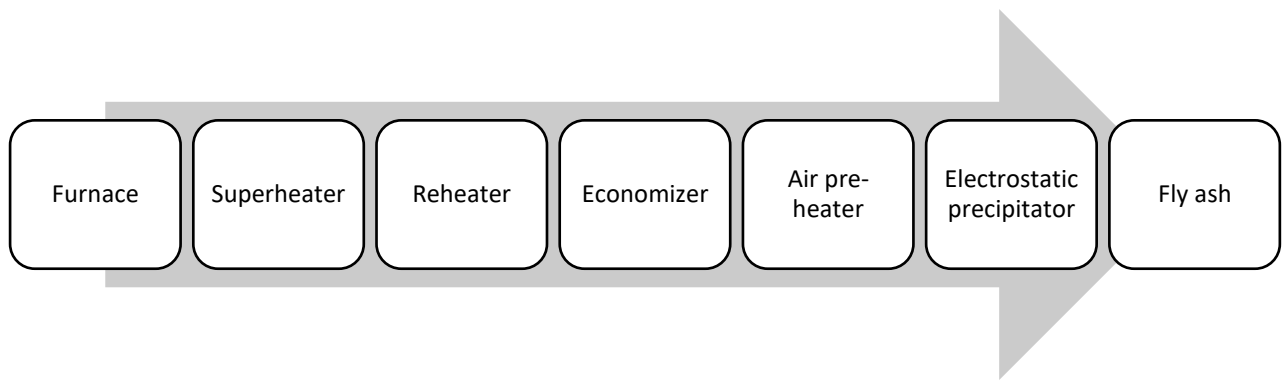


Figure 2-2 – Flow chart showing the production of fly ash in a thermal power station (Yadav & Fulekar, 2018; Chou, 2012)

Thereafter, the fly ash is collected as dry ash and wet ash. The wet ash is collected in the bottom hopper, and the dry ash is collected in the economizer hopper, air preheater and electrostatic precipitator hoppers (Rani & Jain, 2015). Fly ash is a by product of combustion process of coal in various applications hence uses less energy to produce in comparison to cement which is a deliberate and energy intensive exercise.

Table 2-1 shows a comparison of the chemical composition of Portland cement and class f fly ash. It is apparent that the chemistry of fly ash is very similar to that of Portland cement. However, fly ash contains much higher SiO₂ and less CaO which is the main cementitious chemical compound of Portland cement. This phenomenon explains why fly ash cannot be used as a complete replacement of cement as it would not have sufficient cementitious properties to give adequate mechanical strength.

Table 2-1 – Chemical composition of fly and Portland cement (Mohammed & Fang, 2011)

Chemical composition	Portland cement, %	Class F fly ash, %
SiO ₂	21.54	62.5
Fe ₂ O ₃	3.63	3.5
Al ₂ O ₃	5.32	23.4
CaO	63.33	1.8
MgO	1.08	0.34
SO ₃	2.18	1.2
K ₂ O	-	0.95
Na ₂ O	-	0.24
Loss in ignition	2.5	5.61

The cost per unit of concrete can be reduced significantly by incorporating fly ash, thereby reducing the amount of cement required in the mixture (Pravallika & Lakshmi, 2014). Cement is the costliest ingredient in the manufacture of concrete. Significant quantities of cement are necessary to produce

large quantities of slabs. This tends to lead to a high pollution rate due to increased carbon emission during the manufacture of cement (Rahman, et al., 2018). Due to the high cost of cement and its high usage rate, extensive research has been carried out into incorporating waste material into concrete mixtures (Shah, 1993). There have been successful research into incorporating fly ash, silica fume, and other types of inorganic waste materials in concrete (Parasivamurthy, 2007). Fly ash's physical and chemical properties contribute towards improved durability when used with cement as the matrix. The use of fly ash in concrete mixture brings about numerous economic, technical, and environmental benefits through the conservation of natural resources and reducing greenhouse gases emitted during cement production (Erdogdu & Turker, 1998).

Fly ash consists of inorganic, incombustible matter present in the coal that has fused during combustion into a glassy, amorphous structure (Ismail, et al., 2007). Disposal of fly ash in dumps results in environmental pollution, including contamination of groundwater (Belardi, et al., 1998; Hui, et al., 2009). Eskom's coal-fired power stations consume approximately 109 million metric tons of coal per annum, producing 25 million metric tons of ash to supply the bulk of South Africa electricity (Eskom, 2019). Approximately 1.2 million tons of fly ash is sold per year, and the rest is dumped at disposal sites or back stacked at open cast mining sites (Eskom, 2019).

Kumar (2011) showed that fly ash as a partial replacement of cement is gaining importance due to the improved long-term durability of concrete coupled with the ecological benefits of incorporating fly ash (Bendapudi & Saha, 2011). Fly ash is regarded as a toxic material due to the high concentration of leachable heavy metals present within the ash. Leaching tests show that the concentration of heavy metals in fly ash such as Cd, Cr and Zn exceed the regulatory limits implying that fly ash must be treated or disposed of in a controlled manner (Shim, et al., 2005). Landfilling is the normal method of disposal of fly ash. However, it requires large spaces. Thus, alternative reuse applications of fly ash are preferred. Furthermore, the use of supplementary cementing materials in the concrete mixture helps reduce the quantity of cement and improves the strength, workability, and durability of concrete (Bilodeau, et al., 1994; Siddique & Khan, 2011; Bilodeau & Maholtra, 2000). Previous research shows that it is possible to replace up to 50% of Portland cement with fly ash. The replacement of cement with fly ash reduces the cost and permeability of the concrete slab. On the other hand, there is an increase in strength, the durability of the concrete slab.

The use of fly ash as a partial replacement of cement takes advantage of the pozzolanic property of fly ash. There is a relationship between the pozzolanic activity and the size of the fly ash. The coarser the fly ash, the lower the pozzolanic activity (Kumar, et al., 2001). When the fineness of the fly ash increases, the surface silanol groups also increase proportionally. The increase in silanol groups assists in further crystalline hydrate formation when the fly ash reacts with free lime from the hydration of

cement. The reaction in Figure 2-3 shows the construction of calcium silicate hydrate between surface silanol groups in fly ash which aids in forming a strong cement.

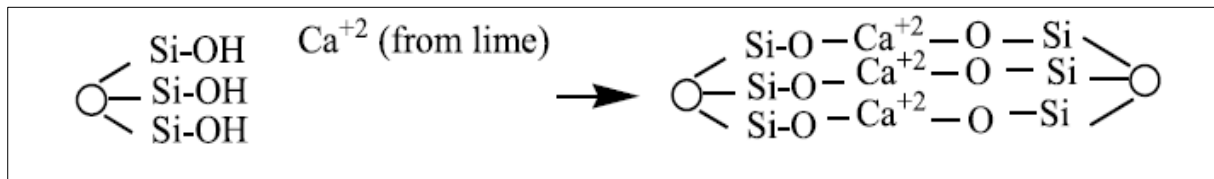


Figure 2-3 – Formation of calcium hydrates between silanol groups in fly ash and free (Richardson, 2008)

The size of fly ash is of great importance hence the need to characterize its grade and size prior to use. Fly ash improves the properties of other polymers/rubber composites when used as a filler material. The shape of the fly ash is also a parameter of considerable importance. Fly ash tends to improve the workability of concrete due to its spherical shape as it gives what is known as a ball bearing effect, increasing the flowability of the concrete mixture (Kumruzzanman, et al., 2003). Irregularly shaped fly ash particles tend to lead to non-uniform compaction. This results in the formation of interparticle voids within the concrete mixture, giving concrete of low mechanical strength (Sarkar, et al., 2012).

Use of finer fly ash particles with a size of $\leq 10 \mu\text{m}$ has the following advantages (Sun, et al., 2003; Kuroda, et al., 1993; Sarkar, et al., 2012):

- Reducing the amount of water required in the concrete mixture;
- Increasing strength of the transition zone;
- Lowering the bleeding during the preparation of concrete mixture;
- Increasing the compressive strength of the concrete.

In Rustenburg, South Africa, engineers used 60% of cement and fly ash mixture in the Bus Rapid Transit (BRT) project. The fly ash used was obtained from Eskom's thermal power stations. This project was considered a great success (Zulu & Allopi, 2015). The concrete at this high level of fly ash addition had compressive strength of 34.5 MPa at 28 day strength which was more than adequate for the application in the project. The compressive strength indicated potential in high volume fly ash however, some of the other properties such as flexural strength and split tensile strength were adversely affected. The use of high volume fly ash is feasible if used with some form of reinforcement material.

2.3.1 Classification and grading of fly ash

Fly ash is a complex material containing amorphous and crystalline phases. Furthermore, the quality of the fly ash varies widely with the type of coal used as well as its combustion properties (Quan & Kasami, 2014). The variability in the fly ash properties makes it necessary to grade and classify fly ash as no

two ashes from different power plants share the same properties (Tanikella & Olek, 2017). It is imperative to note that different standards across the world classify fly ash differently. However, most of the standards use the ASTM C618 standard as the basis. ASTM C618 defines two main classes of fly ash, namely Class F and Class C. These are defined by the origin of the coal and the resultant chemical and mineralogical composition.

Class F fly ash is produced by burning anthracite bituminous coal, also called low calcium fly ash. Whereas Class C fly, ash is produced by burning sub-bituminous lignite (Islam & Islam, 2013). The two classes of fly ash are differentiated primarily based on the total oxides of silicon, aluminium, and iron. If the oxide levels exceed 70%, the fly ash is classified as Class F. On the other hand, if the oxide levels are less than 70%, the ash is classified as Class C. Furthermore, some other parameters govern fly ash classification, as shown in Table 2-2. The replacement level of cement in concrete for Class F fly ash is done between 15-25% by mass whereas, it is between 15-40% by mass for Class C fly ash (Feng & Clark, 2011). Class F fly ash has pozzolanic properties only, and on the other hand, Class C has pozzolanic properties and cementitious properties in addition due to free lime (Ismail, et al., 2007).

Table 2-2 – Showing Differences between Class F and Class C fly ash (Rani & Jain, 2015)

Class F	Class C
Constitutes < 20% of lime	Constitutes > 20% lime
Produced by burning harder anthracite and bituminous coal	Produced by burning of younger lignite or sub-bituminous coal
Lower alkali and sulphate contents compared to Class C	Higher alkali and sulphate contents compared to Class F
Higher quantity of Si, Fe and K oxides than Class C	Lower quantity of Si, Fe and K oxides than Class F
Lower quantity of CaO, MgO, SO ₃ and Na ₂ O than Class C	Higher quantity of CaO, MgO, SO ₃ and Na ₂ O than Class F
Low pozzolanic reaction with water compared to Class C	High pozzolanic reactions compared to Class F.

The pozzolanic reactivity of fly ash is influenced by several factors: its fineness, glass content, and acidic oxide content (Feng & Clark, 2011). Therefore, the variability in the properties of fly ash necessitates its characterization prior to use.

However, besides the two main broad classes of fly ash mentioned above, fly ash can also be classified differently according to its fineness. Fly ash is classified according to two broad grades: normal grade and special grade. Furthermore, normal fly ash grade is further subdivided into fine, medium, and coarse grades. The grading system is based on the fineness, loss of ignition, moisture, and sulphite content

(SO₃). Though this grading system is used sometimes, it is not very informative on the reactivity of the fly ash, and the former grading system is preferred.

2.3.1.1 Fly ash particle size analysis techniques

Fly ash particle size analysis is of paramount importance as it governs the suitability and applications of fly ash. Fly ash rheology influences the water demand in concrete depending on the fly ash particle size distribution. Furthermore, the rheology influences the floc structure of the cement paste. The pore structure of the hardened paste is influenced by the particle size distribution, which also has a direct bearing on the permeability and durability of the hardened concrete. In addition, the fly ash particle size influences the rate of strength gain of concrete, with the finer fly ash reacting more rapidly than, the coarser fly ash (Diamond, 1988).

Particle size can be ascertained by using dry testing conditions such as sieving, optical microscopy, transmission electron microscope and scanning electron microscope (Nziu, et al., 2014). On the other hand, particle size can also be ascertained by wet testing conditions using laser scattering and laser diffraction methods (Takeshi, 2001). But some testing methods allow for both dry and wet testing, such as sieve analysis and laser diffraction. Table 2-3 shows the different particle size analysis methods and the particle size range that each method can measure with accuracy.

Table 2-3 – Various methods that can be used for particle size analysis (Wills & Finch, 2015)

Method	Wet/Dry	Fractionated sample	Approximate range (µm)
Sieve analysis	Both	Yes	5 – 100 000
Laser diffraction	Both	No	0.1 – 2500
Optical microscopy	Dry	No	0.2 – 50
Electron microscopy	Dry	No	0.005 – 100
Elutriation	Wet	Yes	5 – 45
Sedimentation (gravity)	Wet	Yes	1 – 40
Sedimentation (centrifuge)	Wet	Yes	0.05 – 5

As Table 2-3 shows, there are several methods at our disposal to measure fly ash particle sizes, such as sieving, sedimentation, Blaine’s apparatus, and the use of laser diffraction. However, some criticism has been levelled against Blaine’s method to ascertain the particle size of fly ash as the results may be affected by the porous unburned carbon particles (Tanikella & Olek, 2017).

As already alluded to, there are various instruments available to determine to fly ash particle size. These include sieving analysis, optical imaging, laser diffraction, scanning electron

microscope imaging and electrical impedance. Each of these methods will be critically discussed in the following subsections.

2.3.1.1.1 Sieve Analysis

The sieve analysis method involves using mesh screens of varying sizes and mechanical shakers. The sieving process can separate particle diameters of 46 – 710 μm in either wet or dry medium (Poondla, et al., 2009). Furthermore, this method is simple and allows the separation of various sizes of particles. However, the sieving method has significant disadvantages of powder material sticking to the sieve surface clogging up the pores. This is known as blinding and occurs when too much powder is allowed to fall through the mesh at any given point in time. This results in the finer particles not being able to fall through the mesh. The standard used for fly ash particle sieving is ASTM C146 (ASTM C146-21, 2021). In addition, there is also a challenge with the development of static attraction within the powder and the mesh. When there is high moisture content in the atmosphere, it creates particle-mesh adhesion. Furthermore, with continued use and ageing of the sieves, the pores become larger due to abrasion and allow larger particles than desired through the holes. Ageing also brings about the disintegration of the sieve as it can tear over time. The sieving method's effectiveness depends on the number of particles introduced to the sieve at any given point in time and the type of movement of the sieve. Sieves can be found in a wide range of diameters. The common laboratory sieve has apertures of a diameter 2 mm. Figure 2-4 shows a standard laboratory sieve that can be used for particle size grading.



Figure 2-4 – Standard No. 10 laboratory sieve (Wills & Finch, 2015)

Wet sieving can be carried out with the use of water as a medium which might be a necessity with powders that tend to form aggregates when dry sieved.

2.3.1.1.2 Optical Image Analysis

This method has been used widely. However, it has the disadvantage of having a low depth of focus, and the resolution depends on the wavelength of light used (Katja, et al., 2013). With the advancement in computer technology and fuzzy logic, optical imaging is replacing manual methods of particle size analysis. The advantage of optical imaging is that it allows particle sizes to be quantified. The cross-sectional area of the particles can be ascertained with a high degree of accuracy (German, 1997). On

the other hand, a disadvantage of optical image analysis is that if the particle size is small, there is a need to use high magnification, making it difficult to distinguish between different particles due to the limited optical field depth. The optical microscope method applies to particle sizes which range from 0.8 – 150 μm .

2.3.1.1.3 Laser Diffraction Analysis

Laser diffraction is based on the principle of Fraunhofer diffraction and Mie scattering theory which measures the particle size distribution by measuring the diameter of the particles and the diffraction pattern relationship. Fraunhofer approximation for particles makes certain assumptions which are that the particles are spherical, opaque, scatter equivalently at wide and narrow angles and interact with light in a different manner than the medium. The Mie scattering theory was developed to overcome the shortcomings of the Fraunhofer diffraction. Furthermore, Mie scattering theory includes sensitivity to wide-angle scatter, a wide range of opacity, and the operator only needs to provide the refractive index of particle and dispersing medium. Figure 2-5 shows the principle of operation of the laser diffraction instrument. Particles pass through a laser beam, scattering light at angles related to the particle size where smaller particles will scatter the light rays at a wider angle and lower intensity than larger particles (Nziu, et al., 2014). The sizes that are obtained represent the diameter of the particles (Lumay, et al., 2012). A cumulative curve is obtained from the analysis that represents the particles' volumetric diameter. Parameters which include D 0.10, D 0.50 and D 0.90, represent the particle size range diameters. D 0.10 represents the smallest, D 0.50 the average size and D 0.90 the maximum particle diameter (Matsusaka, et al., 2012).

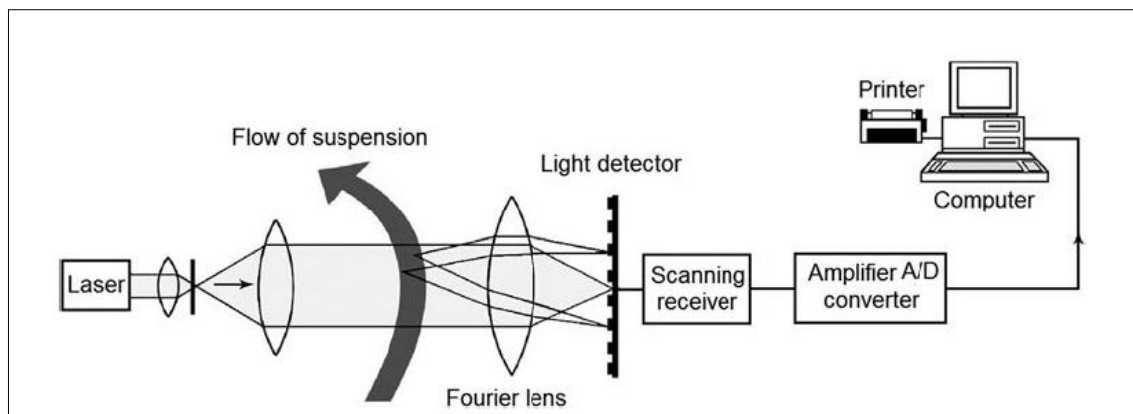


Figure 2-5 – Schematic diagram of Laser diffraction principle (Lumay, et al., 2012)

Due to the nature of the laser diffraction method of particle size analysis, it provides an accurate as well as a rapid method of obtaining particle size distribution information. Therefore, this is the preferred method of fly ash particle size analysis. However, the disadvantage with the use of the laser diffraction method is the high cost of purchasing the instrument.

2.3.1.1.4 Scanning Electron Microscope Analysis

The specimens are prepared before Scanning Electron Microscope (SEM) analysis by depositing a thin layer of metallic or carbon coating to avoid specimen charging. The images formed are analysed by size digital programmed software (Nziu, et al., 2014). An adequate number of images from the SEM have to be processed on the software, and image calibration has to be carried out before analysis. SEM is suited for the characterization of surface material on a micro-scale. The surface characteristics are seen from above, and there is little indication of the height of the particle as the images are seen as 2D objects (Hegel, et al., 2014).

2.3.1.1.5 Electrical Impedance Analysis

Particles are suspended in a conductive fluid and flow through two electrodes. Each particle displaces electrolytes within the two electrodes changing the resistance producing a spike in the voltage, which corresponds to the size of the particle. This voltage spike is then amplified and analysed. The voltage change can then determine particle size. The particle diameter can be calculated for particles ranging in size from 0.4 – 1200 μm .

2.3.2 Physical properties of fly ash

Due to the variability of the fly ash properties, it is necessary to characterize the physical properties of the fly ash. The main physical parameters of great importance in the use of fly ash in concrete include the morphology and particle size of the fly ash particles.

2.3.2.1 Particle Size Analysis

The size of fly ash particles ranges from 10 to 100 microns and is normally finer than that of Portland cement particles (Tutuallo & Mallisa, 2018). There is a relationship between the pozzolanic activity and the size of the fly ash particles. The coarser the fly ash particles, the lower the pozzolanic activity (Kumar, et al., 2001). The lower pozzolanic activity can be attributed to the fact that when the fineness of the fly ash increases, the surface silanol groups also increase proportionally. The increase in silanol groups assists in further crystalline hydrate formation when the fly ash reacts with free lime from the hydration of cement. Fly ash tends to improve the workability of concrete due to its spherical shape as it gives what is commonly referred to as a ball-bearing effect. The ball bearing effect increases the flowability of the concrete mixture (Kumruzzanman, et al., 2003). On the other hand, irregularly shaped fly ash particles tend to lead to irregular compaction. This results in the formation of interparticle voids within the concrete mixture (Sarkar, et al., 2012). Concrete slabs made from finer fly ash particles of size $\leq 10 \mu\text{m}$ give benefits such as reduction in the amount of water required in the concrete mixture and increasing strength of the transition zone. Other benefits are lowering the bleeding during the preparation of the concrete mixture as well as increasing the compressive strength of the concrete slabs (Sarkar, et al., 2012; Sun, et al., 2003; Kuroda, et al., 1993).

2.3.2.2 Scanning Electron Microscope

A Scanning Electron Microscope (SEM) works by directing an electron beam across the surface of the sample, generating X-ray fluorescence from the atoms in its path. The energies of the X-ray photons are characteristic of the element which produced them. Particles normally have a complex morphology that is not uniform, and from the SEM analysis, the particle morphology and size can be ascertained.

Khairul (2007) studied fly ash from Malaysia thermal power stations under an SEM. The SEM images showed that the fly ash was composed of mostly small spherical particles ranging from 2 – 14 μm in diameter. Figure 2-6 shows SEM images for fly ash from Malaysia power plants and fly ash from South Africa thermal power stations. The images show that the fly ash has the same characteristic spherical appearance from both countries.

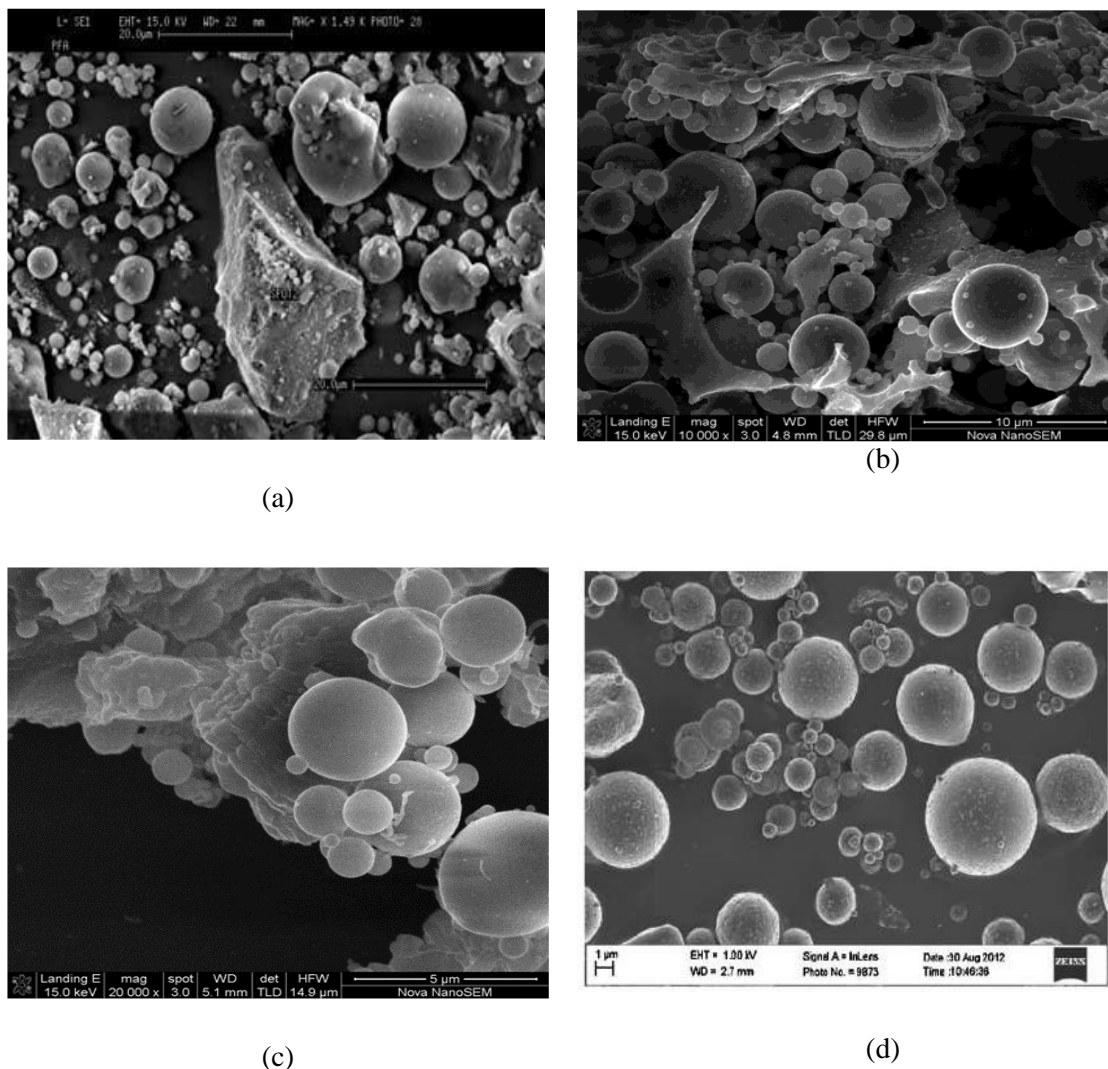


Figure 2-6 – Showing the SEM for the cenosphere fly ash particles from different areas (a) Malaysia (b) Hendrina, South Africa (c) Matla, South Africa (Ismail, et al., 2007; Alegbe, et al., 2018) (d) Vereeniging, South Africa fly ash particle (Van der Merwe, et al., 2014)

Figure 2-6 shows that the fly ash particles are mostly spherical in shape, with only a small percentage of the fly ash particles attached forming agglomerates. The spherical shape was concluded as being the dominant shape after taking length measurement of several particles and averaging these results. This was done using direct measurement on the SEM and range of particle size determined. Fly ash from Matla, South Africa, has more angular shaped fly ash particles due to the incomplete combustion of coal in the furnace. However, in Vereeniging, South Africa, fly ash shows fine particles with minimal agglomerates.

2.3.3 Chemical properties of fly ash

Fly ash is produced at temperatures ranging between 1200 - 1700 °C from coal which contains organic and inorganic materials. The quality of fly ash is dependent on the type of coal, chemical composition, boiler operating conditions and the process before combustion (Alegbe, et al., 2018). Table 2-4 shows the chemical composition of the different grades of fly ash.

Table 2-4 – Chemical properties of different classes of fly ash and Portland cement (Gamage, et al., 2011; Feng, et al., 2018).

Chemical compound	Pozzolan type			Cement
	Class F	Class C	Class N	
SiO ₂	54.90	39.90	58.20	22.60
Al ₂ O ₃	25.80	16.70	18.40	4.30
Fe ₂ O ₃	6.90	5.80	9.30	2.40
CaO	8.70	24.30	3.30	64.40
MgO	1.80	4.60	3.90	2.10
SO ₃	0.60	3.30	1.10	2.30
Na ₂ O & K ₂ O	0.60	1.30	1.10	0.60
Cl ⁻	---	---	---	0.01

Fly ash is a siliceous/aluminous material that, on its own, is not cementitious. However, when reacted with calcium hydroxide and water, it forms a cementitious compound. This is due to the chemical composition of fly ash, which contains elements such as amorphous silica and quartz. Portland cement used in concrete is rich in lime content (60-70%), whereas in contrast, fly ash lime content is low (<7%) (Nawaz, et al., 2016). Fly ash contains mainly reactive silicates (28.87%), as shown in the study by Akbar (2016) while Portland cement, on the other hand, contains smaller amounts. Free lime is generated when Portland cement reacts with water, as shown in equation 2-1. The chemical properties of fly ash allow the pozzolanic activity of the fly ash to combine with the free lime from cement, producing a cementations compound as shown in 2-2.

Portland Cement + Water → Calcium silicate hydrate + Free Lime

2-1

Free Lime + Fly Ash + Water → Calcium silicate hydrate

2-2

The pozzolanic reaction gives additional strength to the concrete. In addition, efflorescence is also prevented due to the mopping up of free lime in the reaction which is responsible for the efflorescence phenomenon (Gamage, et al., 2011).

Therefore, fly ash serves as a pozzolanic material and a partial replacement for cement in concrete manufacture (Han, et al., 2003). Fly ash reacts with the Calcium hydroxide [Ca (OH)₂] released during the hydration of concrete. Fly ash consists of a major amorphous phase and a small crystalline phase (Jimenez & Palomo, 2005; Ward & French, 2006).

2.3.3.1 X-Ray Diffraction analysis

X-ray diffraction (XRD) is used for the identification of crystalline mineral components. It is a suitable means of identifying minerals and other crystalline phases in a wide range of materials (Ward & French, 2005). XRD analysis is a useful tool for analysing fly ash because its crystals are too small to be accurately and reliably determined using other methods. Hence, XRD is the most powerful and probably the only method for directly identifying and defining the fly ash constituent minerals.

In general, the elements present in fly ash include Oxygen (O), Silicon (Si), Aluminium (Al), Iron (Fe), Titanium (Ti), Potassium (K), Calcium (Ca), Phosphorus (P) and Magnesium (Mg). Furthermore, some trace elements can be found in some fly ash samples include Manganese (Mn), Chromium (Cr), Nickel (Ni) and Copper (Cu) (Mishra & Das, 2010). However, more than 55 types of minerals have been identified in fly ash. Research carried out by some authors gave rise to the findings shown in Table 2-5 on the composition of fly ash.

Table 2-5 – Chemical composition of fly ash Class F using XRD analysis

SiO ₂	Al ₂ O ₃	Fe ₂ O ₃	CaO	MgO	SO ₃	LiO	TiO ₂	K ₂ O	Na ₂ O	P ₂ O ₅	Reference
51.49	29.03	7.67	5.51	2.35	-	-	-	2.83	0.66	-	(Puertas, et al., 2000)
71.046	32.077	5.908	0.626	0.819	0.039	-	1.776	0.962	0.136	0.349	(Salumkhe & Mandal, 2014)
62.22	7.63	0.13	5.30	6.09	3.00	9.98	-	1.80	0.24	-	(Belani & Pitroda, 2013)
45.98	23.55	4.91	18.67	1.54	1.47	2.13	-	1.80	0.24	-	(Yazici & Arel, 2012)

2.3.3.2 Energy Dispersive Spectroscopy analysis of fly ash

Energy-dispersive X-ray spectroscopy (EDS), also known as energy dispersive X-ray analysis (EDXA), is a technique for the elemental analysis of a sample. EDS is useful for mapping out the lateral distribution of elements. Furthermore, EDS is useful for compositional information on quasi-bulk specimens or specific particles. EDS systems are typically integrated into either SEM, TEM or Scanning Transmission Electron Microscopy (STEM) (Ebnesajjad, 2014). EDS consists of a detector containing a crystal that absorbs the energy from incoming X-rays by ionization, giving free electrons in the crystal that become conductive and produce an electrical charge bias. After that, the energy from the X rays absorbed is converted to electrical voltages of proportional size. These pulses correspond to the x-ray characteristic of an element.

2.3.4 Effect of fly ash on concrete workability

The use of fly ash in concrete has gained increased popularity over the past years. This is because of the improved durability, workability, and ecological benefits of using concrete containing fly ash in the mixture. Furthermore, advancements in thermal power station processes have also improved the quality of fly ash obtained, making it more suitable for cement composites (Kesharwani, et al., 2017). Fly ash increases the durability of concrete by mitigating the alkali-silica reactions, increasing resistance to sulphate attack and reduced ingress of chloride and water (Hill & Folliard, 2006). Fly ash is normally used in volume fractions of between 0 – 30 % in concrete mixtures, and fly ash used in quantities above 50 % volume fraction is known as High Volume Fly Ash Concrete (HVFA) (Crouch, et al., 2007). Furthermore, fly ash in concrete has been shown to reduce the quantity of water required in the concrete paste. Fly ash addition has an effect of lowering the thermal conductivity of concrete. This phenomenon can be attributed to increase in porosity and pore size in concrete containing fly ash (Kunthe, et al., 2018). Pure concrete has a thermal conductivity of approximately 1.38 W/m-K compared to concrete containing fly ash with thermal conductivity of approximately 1.22 W/m-K for 30% fly ash addition (Kunthe, et al., 2018). The effect of fly ash on concrete and concrete paste is discussed under the following ten sub-sections.

2.3.4.1 Concrete workability

Concrete mixture workability is defined as the effort required to manipulate a freshly mixed quantity of concrete with minimum loss of homogeneity (Yeh, 2007). In a broader context, workability influences the concrete mixture's consistency, flowability, pump-ability, compatibility, and harshness (Oztas, et al., 2006; Yeh, 2006; Li, et al., 2016). The workability of concrete determines the ease with which concrete can be placed, compacted, and moulded. The addition of fly ash into a concrete mixture has a beneficial effect on the rheological properties of concrete and increases its workability. Fly ash increases the paste volume, increasing elasticity and cohesion (Marthong & Agrawal, 2012).

Moreover, due to their spherical nature, fly ash particles tend to act as a lubricant to the aggregates interface, reducing friction and increasing the workability of the concrete mixture. Generally, the higher the volume fraction of fly ash, the better the workability of the concrete mixture (Zulu & Allopi, 2015). Ismail et al. (2007) studied fly ash particles from Malaysia thermal power station under a Scanning Electron Microscope (SEM). Figure 2-6 shows scanning electron images obtained for the fly ash from Malaysia power plants and South Africa thermal power stations. The SEM images show that fly ash has the typical spherical appearance from both countries. Hence, Ismail et al. (2007) study concluded that the fly ash was composed of mostly small spherical particles ranging from 2 μm to 14 μm in diameter.

The spherical shape of the fly ash particles, as shown in Figure 2-6, improves the workability of concrete, making it easier to handle, place and finish. This shape of the particles allows the concrete to flow smoothly and increases its workability significantly. The workability of concrete is also linked to the water content. Moreover, fly ash lowers the required amount of water in the manufacture of concrete. In fact, for each 10% volume fraction of fly ash added to concrete, there is a water reduction of about 3% (Thomas, 2007).

However, Ramaswamy et al. (2011) concluded that the water reduction amount is dependent on the fineness of the fly ash particles. That is, the finer the fly ash particles, the greater the reduction in water demand. The finer fly ash is preferred as it leads to a bigger saving in cost by reducing water demand. There is an increase of 21% in the flow of concrete for a 50% volume fraction of fly ash (Ramaswamy, et al., 2011). This is considered by Ramswamy et al. (2011) the best replacement level of fly ash replacement in concrete to obtain the best workability.

2.3.4.2 Air content

Air entrapment in concrete leads to a loss of its strength. Fly ash plays a significant role in air entrapment in concrete. Fly ash contains residual unburned carbon measured by loss of ignition (LOI). The residual carbon in the fly ash acts as an adsorbent of organic material. However, the literature indicates that the most effective method of measuring fly ash's potential to affect air entrapment is to carry out laboratory mixtures. Replacement of cement with fly ash as cementitious material can increase the required quantity of air-entraining admixtures (AEA).

2.3.4.3 Bleeding of concrete

Bleeding of concrete is the physical migration of water towards the top surface of the concrete. Bleeding of concrete increases finishing times produces laitance at the surface, decreases the mechanical strength, wear-resistance and bond strength of concrete (Ravindrarajah, 2003). However, bleeding is necessary as it helps to replace the water from the surface that has been lost by evaporation and assists to prevent the drying out of concrete, resulting in cracks occurring.

Plastic shrinkage cracking occurs if there is rapid drying on the concrete surface when the evaporation rate exceeds the rate of concrete bleeding. Plastic cracks tend to occur within 3 to 5 hours while the concrete is still in its plastic state if it dries out prematurely (Ravindrarajah, 2003). On the other hand, plastic settlement cracks occur if excessive bleeding and settlement from the concrete. Bleeding capacity is calculated using equation 2-3.

$$\text{Bleeding Capacity (\%)} = \frac{Q * M}{S * V * 10} \times 100 \quad \text{2-3}$$

Where: Q is the total bleed water (ml)

M is the total batch mass of concrete (kg)

S is the mass of concrete in the sample (kg)

V is the free mixing water in the concrete (l)

Ravindrarajah (2003) tested the bleeding of concrete within 10 minutes of mixing by placing the concrete mixture in a steel mould of diameter 254 mm and 280 mm high in two layers and then vibrating it with a vibrating table. A pipette was used to extract the bleed water at intervals of 30 minutes until 3 hours. The extracted water was weighed on an analytical scale, and the bleeding capacity was calculated using equation 2-3. Ravindrarajah (2003) concluded that bleeding rate capacity increase with increased fly ash replacement of cement, as shown in Table 2-6. For the first 90 seconds, there was a significant increase in the quantity of bleed water. However, after 120 minutes, the bleeding rate stabilises and does not increase significantly with time. According to Ravindrarajah (2003), 30% fly ash volume fraction gives the highest water bleed quantity at 90 minutes.

Table 2-6 – Effect of partial replacement of cement with fly ash on the bleeding capacity of concrete (Ravindrarajah, 2003)

% Fly Ash	Time after mixing (min)	Quantity of bleed water (ml)
0	30	10
	60	25
	90	35
10	30	12
	60	30
	90	45
20	30	15
	60	28
	90	40
30	30	13
	60	32
	90	50
40	30	13
	60	33
	90	46

However, some contradicting research has been presented by other authors such as Yao et al. (2015), who concluded that there is a decrease in bleeding with increased fly ash replacement levels (Yao, et al., 2015). The variation in the findings of the two authors could be attributed to the origin of the coal, which impacts its chemical constituents.

2.3.4.4 Setting of concrete

The setting of the concrete mixture is the onset of rigidity in the concrete mix. The Cement matrix is the principal ingredient in the setting of concrete. The setting time of concrete is associated with the workability of concrete. Moreover, setting time influences the time available for transportation, placing and compaction of concrete (Siyal, et al., 2016). The rate of setting of concrete influences how the concrete paste can be used and its shelf life. The addition of fly ash influences the concrete setting rate. Fly ash tends to increase or decrease the setting time of concrete depending on its volume fraction within the mixture and the class of fly ash used (Kesharwani, et al., 2017). With Class F (low lime) fly ash, the setting and hardening of concrete are delayed. HOWEVER, Class C (high lime) fly ashes either rapid or delayed setting time depending on the constituent properties of the fly ash (Naik & Ramme, 2002). Naik & Singh (1997) carried out research into the influence of fly ash volume fraction on the setting and hardening of concrete. The study concluded that the addition of fly ash of volume fraction up to 60% caused a significant delay in the setting of concrete. Generally, at volume fractions above 10%, the effect of fly ash on concrete setting time starts to become more pronounced (Naik & Singh, 1997).

Brooks (2000) study came up with a model able to predict the initial setting time of concrete with fly ash and without fly ash. The study concluded that the initial spacing of un hydrated cement particles divided by a rate coefficient gives the initial setting time. This analogy applies to cement with partial replacement of about 60% fly ash. The final setting time is related to the initial setting time by a factor of 1.35 with an average error of 13% (Brooks, 2000). However, this study failed to consider the variations between fly ash from different geographical locations and the different classes of fly ash.

Research carried out by Naik (1997) concluded that generally, the addition of fly ash up to about 60% caused a significant delay in both the initial and final setting time of concrete. The trend reversed beyond 60% fly ash volume fraction with both the initial and final setting time reducing. Figure 2-7 shows the general trend of setting time with increased fly ash content (Naik & Singh, 1997). At 70% and higher fly ash volume fraction, concrete setting occurs at a faster rate. This phenomenon necessitates the addition of a retarding admixture to allow enough time for good workability of the concrete paste. The increase in setting time is unfavourable as the concrete sets before it is moulded into the desired slab.

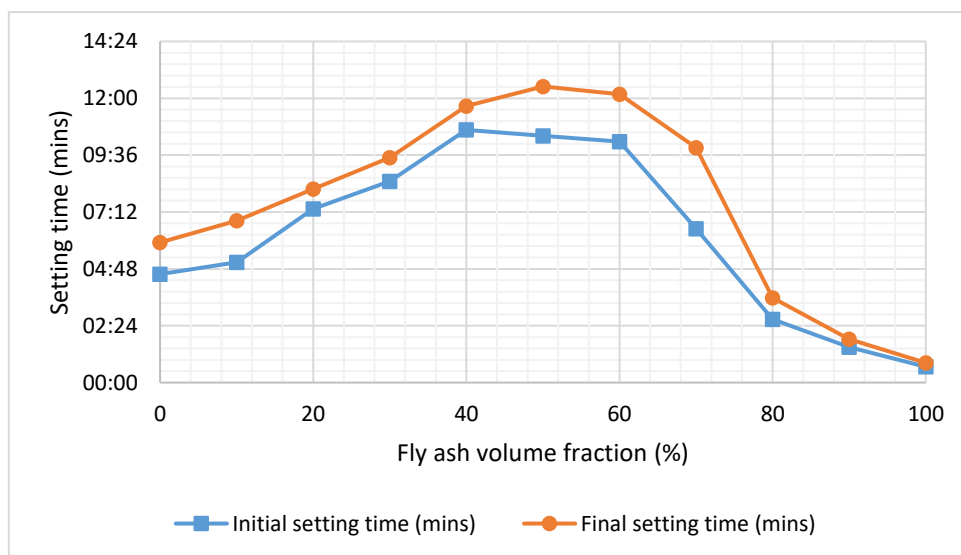


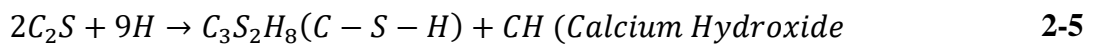
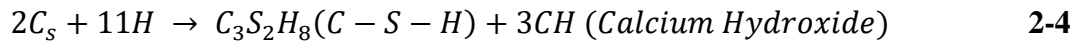
Figure 2-7 – Setting time of concrete mixture containing fly ash (Naik & Ramme, 2002)

The decrease in settling time beyond 60 % fly ash content can be attributed to the lower reactivity of the fly ash. The content of the reactive CaO which is the main cementitious reacting compound is decreased with incremental amounts of fly ash this leads to reduced amount of dissolved Ca^{2+} ions. This phenomenon leads to a deceleration of the activation reaction (Lee & Lee, 2013; Fang, et al., 2018; Nedunuri & Muhammad, 2021).

2.3.4.5 Heat of hydration

The heat of hydration of concrete is defined as the heat generated because of an exothermic reaction between cement and water (Brooks, 2000). The hydration process in concrete containing fly ash is a

complicated reaction due to two interrelated time-dependent processes, cement hydration and the pozzolanic reaction of fly ash (Pane & Hansen, 2005). When Alite (C_3S), Belite (C_2S), aluminate (C_3A) and lumina ferrite (C_4AF) contained in cement are mixed with water, hydration products are produced. The hydration products include calcium silicates composed of (C_3S) and (C_2S). These then produce hydration reactions, as shown in Equations 2-4 and 2-5.



The C-S-H gel is a binder of cement paste and significantly influences the strength of concrete. The heat of hydration of concrete can be broken down into five stages, as shown in Figure 2-8. When cement particles react with water immediately after mixing, and ettringite is formed from tricalcium aluminate (C_3S) reacting with water. Furthermore, this reaction is associated with the release of a burst of energy in the form of heat. This is the first sizeable exothermic peak in the coulometric hydration curve, known as stage (I).

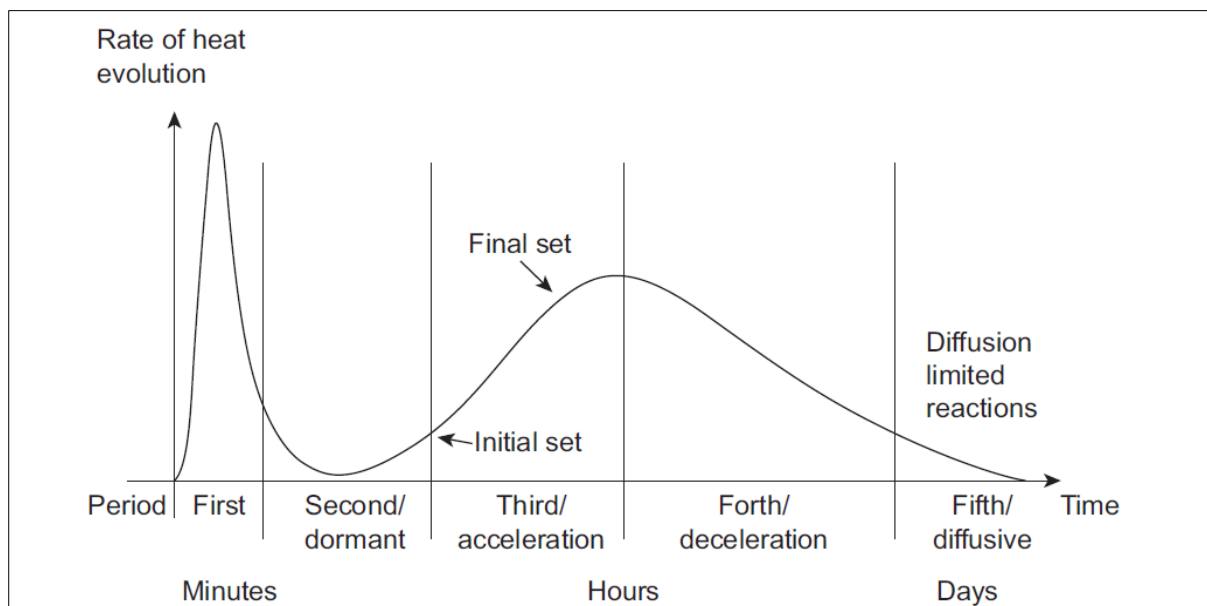


Figure 2-8 – Graph showing the stages of the heat of hydration for unreinforced cement (Taylor, et al., 2006; Vazquez & Pique, 2016)

In the second stage (II), little heat is produced, and this stage is commonly referred to as the dormancy stage and occurs for about 2 to 4 hours after the initial mixing of cement and water. Several theories exist to explain the exact reaction that takes place (Odler, 1998; Taylor, et al., 1984; Jennings, 1986; Brown, et al., 1985). However, the important part of this stage is that the cement paste delimits the period in which it can be manipulated without further altering its chemical structure. The third stage

(III), also known as the acceleration stage, is when calcium silicate hydrate and crystalline calcium hydroxide form in an exothermic reaction. This stage has a second peak of hydration. However, the reaction rate is controlled by the nucleation rate and growth of the hydration products. In the fourth stage (IV), also known as the deceleration stage, the reaction between calcium silicate hydrate and crystalline calcium hydroxide, with water and undissolved cement, slows down the reaction, giving a decline in the speed of hydration. In stage five (V), Belite dissolves, releasing calcium ions slowly. This is a slow reaction and continues if water is available for the hydration products to react.

Moghaddam et al. (2018) carried out a study on fly ash volume fraction on the heat of hydration. Moghaddam et al. (2018) used three types of fly ash (CFA, RFA and GRFA). The graphs of time against the amount of heat evolved show a decreased cumulative heat evolution with the fly ash volume fraction increase. The finer the fly ash grade, the more heat it produced compared to the coarser grade fly ash produced. The increase in peak for the higher fly ash volume fraction could be attributed to the reaction between tri-calcium aluminate and the subsequent conversion of ettringite to mono sulphate. This phenomenon is attributed to the fact that fly ash increases the reaction by providing a high number of nucleation sites for the hydration products of calcium alinate to precipitate (Bullard, et al., 2011; Wang, et al., 2019).

Several studies carried out arrived at the same conclusion that heat of hydration of high-volume concrete is reduced with the addition of fly ash (Zhang, et al., 2002; Amnadhua, et al., 2013; Fanghui, et al., 2014). Feng et al. (2018) measured the heat of hydration of the concrete sample using ToniTechnik7338 Isothermal Differential Calorimeter. The hydration heat was measured within 72 hours at 25°C. Feng et al. (2018) also concluded that ground fly ash lowered the hydration heat when compared to pure cement.

2.3.4.6 Permeability

Concrete permeability of concrete is the ease with which a fluid can pass through the concrete under a pressure difference and is measured in terms of coefficient of permeability (Fanghui, et al., 2014). Water permeability of concrete is of paramount importance as it directly bears the durability of the concrete, more so on concrete subjected to aggressive environments. If concrete is highly permeable, water can enter freely and becomes an agent for the deterioration of concrete or, in a much worse scenario, becomes a transport medium for species such as chloride or sulphate ions. (Li, et al., 2016). The permeability of concrete is directly related to its porosity—the greater the porosity, the larger the permeability coefficient (Yang, et al., 2017).

Supit and Shaikh (2015) research concluded that the inclusion of fly ash in the concrete mixture reduces the volume of permeable voids by as much as 6-11% compared to unreinforced concrete. Supit and Shaikh (2015) showed that 40% replacement of cement with fly ash decreased the permeable voids

significantly. However, 60% replacement exhibited higher permeable voids than the control specimen (Supit & Shaikhh, 2015).

Literature shows a contradiction in terms of the effect of increasing volume fraction of fly ash in concrete samples. Chindaprasirt et al. (2017), in contrast to Supit & Shaikhh (2015), concluded that the addition of fly ash increased the porosity of concrete with an increase in volume fraction of fly ash. This contradiction can be explained by looking at the class of fly ash used and its source. Fly ash's chemical and physical properties tend to vary with its geographical location, and researchers realised contradictions from different geographical locations. This analogy shows the need to thoroughly test fly ash from any new source before its use. A lot of research has focused on ways of improving the permeability and durability of concrete. Literature shows that generally, for most types of fly ash, the addition of admixtures such as pozzolanic materials reduces the porosity of concrete, leading to increased impermeability of concrete (Guneyisi, et al., 2008).

2.3.4.7 Slump of concrete

Slump is a relative measurement in concrete consistency and fluidity. It shows the flow and overall workability of freshly mixed concrete. The primary purpose of the slump test is to assess the consistency of fresh concrete. Indirectly the slump test ensures that the water content of the concrete does not deviate significantly from the required design. The slump of concrete is related to the workability of concrete as it measures the water content in concrete. The concrete slump is in three general forms, as shown in Figure 2-9. In a collapsed slump, the concrete collapses. In a shear slump, the top part of the concrete shears off sideways and in a true slump, the concrete sample keeps its shape. A collapsed slump is an indication of concrete containing too much water.

Ravina (1984) study established that partial replacement of cement with fly ash reduces the slump of concrete. The lower slump loss of concrete mixture containing fly ash can be attributed to the lower amount of water in the concrete containing fly ash.

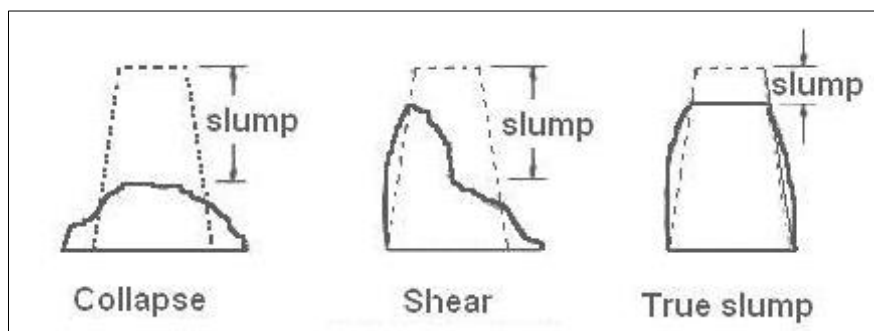


Figure 2-9 – Three types of a concrete slump (CEP, 2018)

However, the lower water quantity required might have an adverse effect on workability yet show a good slump value. The concrete paste might not flow as well due to the lower amount of water, making it harder to mould accurately.

2.3.5 Mechanical properties of concrete slabs containing fly ash

Partial replacement of cement with fly ash in concrete slabs positively affects the compressive and flexural strength of concrete. Concrete is mainly subjected to compressive stress as a load-bearing structure. However, flexural forces are also acting on the concrete slab. Flexural strength measures the ability of the concrete to withstand failure under bending stress. The effect of fly ash on the concrete slab strength properties was reviewed in this study under the following subheadings.

2.3.5.1 Compressive strength

Compressive strength in concrete structures is one of the most important strength parameters. This is mainly because, during the working life of concrete slabs, the main forces exerted are compressional forces. Fly ash, as a partial replacement of cement, on the one hand, tends to have a negative effect on the compressive strength for the first 28 days. On the other hand, fly ash has a positive effect on the long term ultimate compressive strength of the concrete due to the pozzolanic nature of fly ash (Zulu & Allopi, 2015). Research carried out by Barbuta et al. (2017) reported that the highest compressive strength of the fibre and fly ash reinforced concrete slab is obtained at 10% fly ash volume fraction after 28 days.

Rohman et al. (2010) studied the effect of fly ash concentration on the compressive strength of concrete. They concluded that the compressive strength of concrete improved at 16.4% volume fraction of fly ash and then decreased significantly up to 20%. An increase in the quantity of fly ash volume fraction decreases the compressive strength of concrete. This phenomenon implies that the addition of fly ash must be limited to less than 20% to get the best short term compressive strength (Rohman & Aji, 2018; Deepa, et al., 2010).

Class F fly ash has a low lime quantity. This reduces the compression strength of concrete made from this type of fly ash with an increase in its fly ash mass fraction. However, the ultimate compressive strength of the concrete increases in time as the concrete cures due to the pozzolanic activity of the fly ash (Sumer, 2012; Siddique, 2004). The compressive strength increment for concrete slabs containing fly ash continues over a longer period spanning months than concrete unreinforced with fly ash (Saha & Sarker, 2017). The hydration of fly ash within concrete occurs slowly, and significant strength is realised after 28 days. This explains the low compressive strength during the initial stages of curing. After fabrication of concrete slabs containing fly ash, the concrete microstructure has a copious amount of un-hydrated fly ash. However, after approximately a year, the fly ash is more compact and has no sign of un-hydrated fly ash (Li, 2003). Concrete that shows the highest compressive strength was

containing fly ash with the highest degree of fineness of between 1.9 and 17.2 microns (Kiattikomol, et al., 2001). The use of 5%, 10% and 15% of fine fly ash volume fraction gives ultimate compression strength ranging between 3% and 16% higher than concrete without fly ash content (Yazici & Arel, 2012). Ramaswamy et al. (2001) reported that the replacement of 40% volume fraction of fly ash gives the optimum long term compressive strength. Research carried out by Celik et al. (2008) concluded that fly ash particle size had the most dominant effect on the compressive strength over the chemical composition. However, not much conclusive research has been done on the effect of fly ash particle size on the ultimate compressive strength. A study by Reddy (2013) reported that the best compressive strength in the 7- and 28-day range is obtained at about 20% fly ash volume fraction.

2.3.5.2 Flexural strength

Flexural strength is defined as a measure of a concrete slab resistance to failure in bending. The flexing behaviour and cracking of the concrete slab depend on the flexural strength of concrete in addition to some other factors (Mohd, et al., 2016). The flexural strength of concrete can be calculated by using equation 2-6.

$$f_r = bf^n \quad \text{2-6}$$

Where: f_r – Flexural tensile strength

f – Compressive strength of the concrete

b - Constant that ranges from 0.33 - 0.94

n – $\frac{1}{2}$ or $\frac{2}{3}$ coefficient

The constant b and n depend on several factors such as strength levels, aggregate properties and mineralogy, admixture type, moisture content, compaction, and concrete curing conditions. Furthermore, the coefficient is affected by specimen geometry and confinement and the age of the concrete (Mohd, et al., 2016). However, this formula failed to consider the properties of the reinforcement fibres in the concrete.

According to research carried out by Barbuta et al. (2017), the maximum flexural strength for a cement composite containing glass fibre and fly ash was obtained at a fly ash volume fraction of 40%. For fly ash concrete composite with polyester fibres as reinforcement, the maximum flexural strength was observed at 20% volume fraction fly ash (Barbuta, et al., 2017). Feng et al. (2018) researched the addition of fly ash at 25% volume fraction and ground fly ash at the same volume fraction. Tests were carried out on the flexural strength over time. The study concluded that the fly ash particles' fineness influenced the concrete's ultimate flexural strength. This explanation is due to fine fly ash particles that fill the pores between the hydration products. This increases the density of the microstructure and,

hence, improves flexural strength. The maximum obtainable flexural strength has been observed at 50% addition of fly ash content for all ages of the concrete (Upadhyay, et al., 2014). Solanki et al (2013) concluded that the highest flexural strength of concrete with fly ash is obtained at 20%, as shown in Figure 2-10.

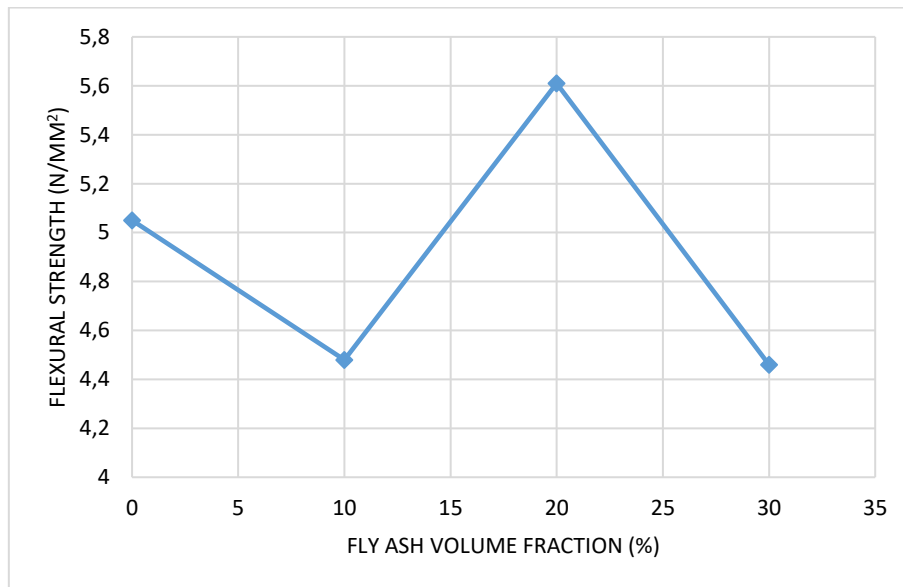


Figure 2-10 – Effect of fly ash volume fraction on flexural strength of concrete slabs (Vinodsinh & Pitroda, 2013; Solanki & Pitroda, 2013).

2.4 Plastics in the environment

Plastic pollution has evolved to be a global threat to the ecology. This threat is largely due to the resilient nature of plastics against degradation. Plastic illegally dumped in the environment pose a threat to wildlife and domestic animals through entanglement and ingestion of the waste plastic (Derraik, 2002). Plastics are popular because they are lightweight, durable, and cheap. They find use in a number of applications such as personal clothing, packaging, and construction materials. Plastics, after use, find their way into the environment as they tend to be single-use items. This lack of recycling necessitates study and research into innovative and imaginative ways of reusing plastics. Furthermore, the scarcity of landfill space and the cost of managing such sites makes it necessary to find alternative methods to deal with plastic waste (Foti, 2013).

The toxicity of plastics in the environment is determined by their particle size and shape, surface area, type of polymer and the additives within the polymer. Plastics contain additives which include organic plastic additives, antimicrobial agents, surfactants, plasticizers, flame retardants, antistatic agents, nanoparticles, dispersants, fillers and pigments (Da costa, et al., 2016; Lambert, et al., 2017; Wright & Kelly, 2017). All these factors affect the level of toxicity of plastics in the environment. When plastics enter rivers and oceans, they undergo degradation in various ways, which include biodegradation,

photodegradation, thermos-oxidative degradation, and hydrolysis (Andrady, 2011; Do Sul & Costa, 2014). Furthermore, turtles and other aquatic creatures can ingest plastic waste in two main methods, namely direct or indirect. Accidental ingestion of plastic may occur when the plastic waste is mixed with normal dietary food. Some aquatic creatures, such as turtles, are visual feeders and may mistake plastic as prey and selectively consume them (Nelms, et al., 2015). Horeau et al. (2014) found plastic bottle tops inside loggerhead turtles and concluded that the turtles mistook the plastic lids for neutronic organisms they normally prey upon. Figure 2-11 shows some effects of plastic on turtles.



Figure 2-11 – (a) Plastic fragments extracted from the digestive tract of a necropsied juvenile green turtle (Nelms, et al., 2015) (b) A turtle wrapped in plastic and washed ashore on the beaches of Brazil (News, 2018)

PET plastics are the second most abundant waste plastic material after polyethylene (Foti, 2013). Research has been done into alternative environmentally friendly ways of disposing of PET bottles. One such research conducted by Himanshu Sharma (2017) used PET bottles in the construction of Eco-bricks. Eco-bricks are PET bottles filled with sand, soil, fly ash, and cement to bind the PET bottles together to make bricks, shown in Figure 2-12.



Figure 2-12 – PET bottles used in construction with cement paste (Turner, 2015)

The Eco-bricks are lightweight and have similar thermal properties as traditional bricks. The Eco-bricks were found to have a high sound reduction index comparable to concrete blocks (Sharma, 2017).

2.4.1 Microplastics

When plastics are exposed to water and sunlight, they tend to degrade to what is known as microplastics. Microplastics (MPs) are plastics under 5 mm in size, and this definition is inclusive of nano-size microplastics (Smith, et al., 2018). The plastic degradation rate to microplastics depends on the polymer type, shape, and density (Lambert, et al., 2017).

Globally an estimated 8.3 billion tonnes of plastic have been manufactured since mass production began in the 1950s. 80% of this mass has accumulated in landfills or the natural environment (Geyer, et al., 2017). Plastics degrade, forming microplastics with the size of approximately 5 mm. Microplastics are becoming recognized as a global concern, and research has been directed towards their effect on human health and the ecosystem. Microplastics have diameters ranging between 330 μm and 5 mm. The discovery of microplastics has raised concerns among environmentalists. MPs make up 94% of an estimated 1.8 trillion pieces of plastic in the garbage patches and have been found in all forms of marine life from zooplankton to whales (Dris, et al., 2016; Besseling, et al., 2015).

Other microplastics enter soils through landfill leachate or improper disposal. Although plastics do not readily biodegrade, they break up into smaller pieces when exposed to ultraviolet light and physical abrasion (Andrady, 2011). When plastics break down into microplastics, they are inadvertently consumed by a wide range of marine organisms (Lusher, 2015; Auta, et al., 2017; Foley, et al., 2018). Consumption of microplastics by organisms at the base of food webs such as mussels (Derraik, 2002)

and plankton (Critchell & Hoogenboom, 2018) has raised concerns about the potential for transfer of plastic associated toxins throughout marine food webs (Farrell & Nelson, 2013).

When plastics break down into smaller particles, now commonly referred to as microplastics, different plasticizers tend to leach out into the surrounding water sources where they can have endocrine-disrupting effects on organisms (Park & Gan, 2014; Rochman, 2014). Water organisms such as molluscs, fish, mammals, and crustaceans tend to confuse microplastics with food. Avio et al. (2015) carried out research into the aquatic life that had traces of ingested microplastics. The author found that *Sardine pilchardus*, *Squalus acanthias*, *Merluccius Merluccius*, *Mullus barbatus*, and *Chelidonichthys lucerna* had ingested microplastics. The most dominant type of plastic found in the fish was polyethene (Avio, et al., 2015).

There is still a need for further research to establish the toxic effects of microplastics on living organisms and limits that the body can take upon inhaling or ingesting the plastics (Wright & Kelly, 2017). This information must be correlated to the type of plastic and exposure amount to fully understand the impact of microplastics on human and animal health.

2.5 Fibre spinning

Fibre spinning is defined as the extrusion process of fluid polymer, which is carried out through bored devices commonly referred to as spinnerets (Andredi, 2004). The two main methods of spinning polymer materials to give fibres are melting or solution. The melting method can be used on thermoplastic polymers, and the solution method involves dissolving the polymer in a solvent to give a viscous liquid which can then be extruded.

2.5.1 Melt spinning

Melt spinning is one of the most popular and most economical methods of making polymer fibres. Melt spinning is simpler compared to other types of spinning methods as it does not involve problems associated with using solvents. Polymers such as polyethylene terephthalate, polyurethanes, polyolefin and polyamides are generally melt spun. Polymer pellets or granules are fed into an extruder which consists of a heated screw for melting the polymer, as shown in Figure 2-13. When polymer granules or pellets are used as the raw material, they are first dried and then melted in the extruder. The polymer is melted and extruded from a spinneret under pressure, forming polymer strands. The polymer is extruded into a monofilament or multifilament yarn, drawn and solidified by cooling. After that, the filament is wound onto spools.

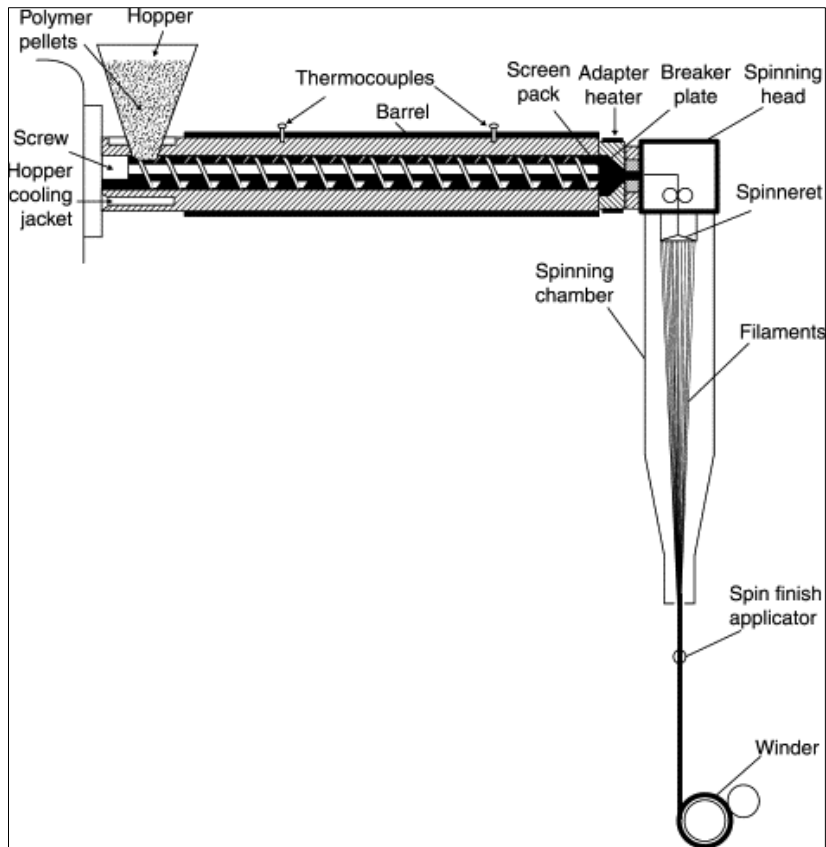


Figure 2-13 – Melt spinning process (Rawal & Mukhopadhyay, 2014)

Melt spinning is generally followed by drawing, which assists in aligning the polymer molecules along the filament axis, and this gives improved physical and mechanical properties to the filament.

2.6 Polyethylene Terephthalate

Polyethylene Terephthalate (PET) is a very popular plastic resin with increased recycling rates every year. However, a large percentage of PET material still finds its way into incinerators or is buried in landfills. PET in cement composites could allow an environmentally friendly disposal method with value addition (Ataei, et al., 2017). PET is produced by combining two monomers, ethylene glycol and purified terephthalate acid. Figure 2-14 shows the reaction to produce polyethylene terephthalate.

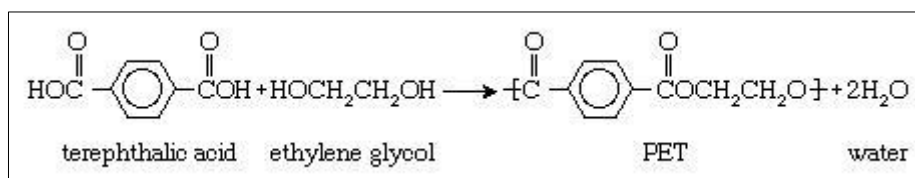


Figure 2-14 – Reaction of terephthalic acid and ethylene glycol to produce PET (Sadeghi & Sayaf, 2012)

The large aromatic ring in PET repeating unit gives the polymer its stiffness and strength. Polyethylene Terephthalate bottle waste can be used as concrete reinforcement. The use of waste PET fibres in this manner can reduce the volume changes in concrete, preventing shrinkage cracks and propagation thereof (Banthia, et al., 2014). Furthermore, there is an urgent need to create sustainable cement slabs which are environmentally friendly and are durable. PET has high mechanical strength, impact resistance, rigidity, and resistance to environmental degradation factors (Lepoittevin & Roger, 2011). This property makes it an ideal material for use in concrete reinforcement.

PET material can be used in two main and completely different ways in construction. The PET material can be used as the matrix an unsaturated resin to manufacture polymer concrete (Rebeiz, 1995; Rebeiz & Craft, 1995; Jo, et al., 2008; Tonet & Proszek, 2013). On the other hand, the PET material can be used as reinforced material in the form of flakes, particles or fibres in the concrete mixture (Choi, et al., 2005; Albano, et al., 2009; Akcaozoglu, et al., 2010; Frigione, 2010).

One of the challenges in using PET fibres as reinforcement material is that it has poor wettability and adhesion to cement (Machovik, et al., 2013). Wilinski (2016) researched treated waste polyethylene terephthalate fibres for use as reinforcement in a concrete composite. Wilincki (2016) reported that treated fibres or yarn should be treated so that the fibres are not smooth but have a rough texture or are crimped. This treatment improved the bonding between the fibres and the cement. Another study by Won et al. (2010) reported that reinforcing concrete with PET material gave a composite with greater frost resistance. The fibres used by Won et al. (2010) were treated with an alkaline solution of pH 12.6. Polymers containing ester groups are susceptible to hydrolysis reaction, which degrades the polymer. However, a major challenge is the degradation of the polymer fibres with time in the concrete leading to decreased mechanical strength. There is a need to find a way to overcome this in the hybrid composite that was fabricated. Figure 2-15 shows how the hydrolysis reaction of PET takes place under alkaline conditions leading to diminished mechanical properties.

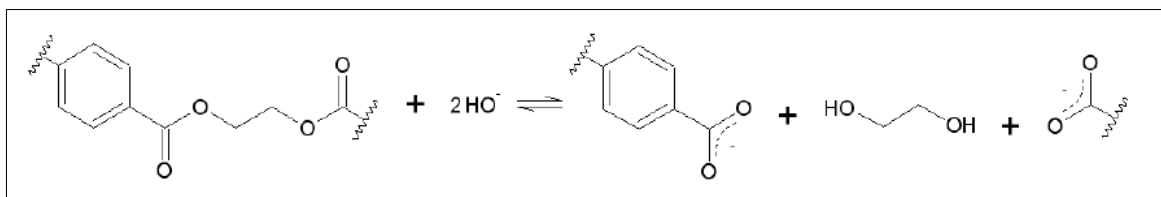


Figure 2-15 – Potential hydrolysis reaction of PET under alkaline conditions in concrete (Wilinski, et al., 2016)

Wilinki et al. (2016) study used recycled PET tapes to create a concrete composite. The tapes had a length of between 50-70 mm and a width of 2-3 mm. The thickness of the tapes was 0.20-0.25 mm, and the density was 1.38 gcm³. Figure 2-16 shows the recycled PET tapes obtained by Wilinki et al. (2016).



Figure 2-16 – Polyethylene Terephthalate tapes obtained from waste PET bottles (Wilinski, et al., 2016)

However, the tapes that were made by Wilinski et al. (2016) lacked adequate strength and were not extruded, compromising the strength of the composite significantly. There is a knowledge gap in the effect on the mechanical properties of extruded PET fibres as reinforcement in concrete that has been impacted additional strength through polymer alignment.

2.6.1 Recycling Polyethylene Terephthalate

Plastics can be broadly divided into two groups which are thermosets and thermoplastics. Thermoplastics can be heated to a viscous fluid and remoulded. However, thermosets cannot be turned from solid to liquid by purely applying a heat source.

PET can be recycled by first obtaining flakes from the PET bottles. PET flakes are obtained from waste PET materials and thereafter after sorting, washing, grinding, and drying the particles. PET flakes can then be made into fibres using either chemical or mechanical methods (Telli & Ozdil, 2015). Using the mechanical method is the most economical method, which includes extruding the PET through spinnerets to obtain fibres. The chemical method involves degrading the PET into its oligomer and monomer former and performing a polymerisation reaction again. Glycolysis, methanolysis, hydrolysis, ammonolysis and aminolysis are some chemical recycling methods that can be used for PET (Telli & Ozdil, 2015). The use of chemical methods has not gained much traction since it does not have much economic value (Aguado & Serrano, 1999; Mancini, et al., 2009; Shen, et al., 2010; Al-Salem, et al., 2009; Goodship, 2007).

Recycling PET material to produce fibres has numerous economic advantages mainly due to lower raw material costs as it is generally considered waste. However, it is worth noting that during mechanical recycling, the molecular weight of the polymer changes which can influence the properties of the PET fibres.

2.6.2 Physical properties

Polyethylene terephthalate is used widely in bottled drinks and water, food items, and other packaging materials. The growing use of PET bottles has led to a boom in their production to cater to growing

demand. Approximately 20 million tonnes of PET bottles are produced each year, and this figure is rising at a rate of 15% annually (Yao, et al., 2014). However, the recycled quantity of PET material is as low as 29.3% (Frigione, 2010). Commercially used PET has a melting temperature (T_m) of between 255 °C and 265 °C, and the more crystalline PET has a melting temperature of 265 °C (Brydson, 1995). Table 2-7 shows some of the significant physical properties of Polyethylene terephthalate, which are important in their use in composite materials.

Table 2-7 – Showing the typical properties of PET (Mark, 1985; Brydson, 1995; Awaja & Pavel, 2005)

Property	Value
Density	1.41 g cm ³
Glass transition temperature	69-115 °C
Melting temperature	265 °C
Heat of fusion	166 J/g
Tensile Breaking strength	50 MPa
Tensile strength (Young's Modulus)	1700 MPa
Yield strain	4 %
Impact strength	90 J m ⁻¹
Water absorption (after 24hrs)	0.5%

The major reason that PET has gained considerable importance is due to its excellent chemical resistance, processability, colour ability and reasonable thermal stability (Awaja & Pavel, 2005).

2.7 Fibre characterization

Fibres are defined as matter characterized by flexibility, fineness, and a high ratio of length to thickness (Morton & Hearle, 2008). The requirements in fibre tests are that they must be reproducibly and that they indicate how the material performs in its intended end-use. There are a number of fibre tests that can be carried out as outlined in this section.

2.7.1 Fibre strength

Single fibre tests are often carried out for research purposes, not as routine industrial control tasks. Tests on single fibres can be carried out on a universal tensile tester with the appropriate load cell and lightweight clamps. If fibres cannot be gripped directly in the testing machine jaws, they are often cemented into individual cardboard frames, which are themselves then gripped by the jaws. Factors affecting the strength of fibres are molecular weight, number and intensity of weak places, coarseness or fineness of fibre, relative humidity, and elasticity.

In bundle fibre strength testing, a universal tensile tester is used to test the strength of the fibre bundle. The breaking load and elongation at break are recorded and used to calculate the tenacity of the fibres, as shown in Equation 2-7.

$$\text{Tenacity of fibre} = \frac{\text{Breaking load (kg)} \times \text{Length of sample (mm)}}{\text{Mass of fibres (mg)}} \quad 2-7$$

To get comparable laboratory results, it is advisable to use the same gauge length for all tests, selecting it to accommodate the shortest fibres available in the test batches.

2.7.2 Universal tensile tester

The Universal tensile tester works on the principle of a constant elongation rate. At a constant elongation rate, the specimen is extended at a constant rate, and the force is a dependent quantity. One end of the sample is clamped into jaws controlled by a crosshead traversed at a constant rate by mechanical drive. The drive originates from a computer-controlled stepper motor. The other end of the sample is clamped in jaws that are mounted on a stiff load cell containing a strain gauge. The load and elongation test results are transferred to computer software, and the data is plotted in graphs for analysis.

2.7.3 Fibre length

When measuring fibre length, there is a need to measure numerous fibres to get accurate results. However, this process can take a lot of time as it would involve individually measuring each of the fibres in the sample batch. There are two main methods of measuring fibre length: the direct and automated methods. The fibre is held in place and measured in its non-crimped state alongside a ruler in the direct method. Fibre length measuring machines automate the manual process to make it faster. The advantage of using automated machines is that they are faster and may give more accurate results as they remove crimp of fibres at constant tension for all the fibres compared to the manual method, which may have variations in tension.

2.8 Composites materials

Composites are materials consisting of two or more chemically distinct constituents, on a macro scale, has a distinct interface. One of the constituents is known as the reinforcement phase, and the other is the resin or matrix. Hybrid composites include additional materials on either of the two basic: reinforcement and matrix. Incorporation of fibres in the cement composite is an efficient practice that gives improved impact, fracture, fatigue resistance and flexural toughness (Ferreira, et al., 2016).

Hybrid composites allow engineers to tailor the properties of the composite to meet specific requirements compared to conventional composites (Selmy, et al., 2019). Meszaros (2014) classifies hybrid composites into three basic categories. The first is when the composite has two matrices. The

second is when the reinforcing materials are of two types: fibre, flakes, nanoparticles, and whiskers. The third classification is when the two reinforcing materials are hybridized (Meszaros & Turcsan, 2014). Hybrid composites have gained increased popularity by allowing the customization of composites to specific end uses by varying the fibre volume fraction, fibre orientation, stacking sequence and hybrid configuration (Pandya, et al., 2011; Tehrani, et al., 2015).

2.8.1 Fibre-reinforced cement composites

Concrete is an inherently brittle material, and to overcome this, research has been carried out into the development of high ductility fibre reinforced cement composites (FRCC). Concrete is a particulate ceramic composite in which the aggregates are embedded in a microcrystalline silicate resin. Concrete consists of cement, the matrix, coarse aggregates as the framework, fine aggregate and fly ash as filler materials, water, and other specific additives. Concrete is widely used due to its high compressive strength and relatively low cost of production. Yet, it has numerous disadvantages, including brittleness, low tensile strength, and low crack propagation resistance. The use of polymeric fibres to create fibre reinforced concrete composites allows the mitigation of the inherent weaknesses of concrete composite (Wilinski, et al., 2016). Fibres effectively increase shock resistance, toughness, and resistance to plastic shrinkage of concrete (Bagherzadeh, et al., 2011).

Cracks and fissures tend to appear on concrete when it is subjected to flexural and tensile loading due to its low toughness (Lura & Terrasi, 2014). Cracks develop in concrete for several reasons, namely (ACI Committee-544, 1996; Brandt , 2009; Pakravan, et al., 2010; Song, et al., 2005):

- Loss of water from evaporation results in plastic shrinkage;
- Reduction in the surface water due to the hydration process;
- Decrease in temperature after the setting of the concrete leads to thermal contraction;
- Loss of water in the hardened state leads to drying shrinkage;
- The reaction of hydrated cement with CO₂ in the presence of moisture leads to carbonation shrinkage.

Research has been carried out into reinforcing concrete using fibres from asbestos, polymers, glass, and steel. Research has been carried out in this area to produce stronger and stiffer structural materials. The challenge with introducing fibres is the cost associated with producing the fibres, leading engineers to refer to using thicker concrete for greater strength (Harris, 1999). However, in some instances, it is not possible to increase the thickness of a slab due to dimensional or material constraints. There are various fibres in commercial use such as steel fibre, synthetic fibres such as polypropylene, glass, carbon, polyvinyl and waste fibre material. The use of any of these synthetic fibres has a considerable effect on the strength properties of FRC.

In addition, there has been some success in the use of metallic, polymeric, carbon, glass, nylon, and waste tyre fibres as reinforcement material that limits crack propagation in concrete and widening of the crack through fibre bridging (Yoo, et al., 2018). Research has been carried out into the use of natural fibres as reinforcement in cement-based composites. These fibres have been considered a potential reinforcement due to their low cost and low energy consumption (Aruna, 2014). But most natural fibres are susceptible to environmental degradation and lack adequate strength, and this limits their applicability as reinforcement in concrete.

Fibre-reinforced composite strength is dependent on the fibre mechanical properties, interface between fibre and matrix, the quantity and orientation of the fibres within the matrix (Alhozaimy, et al., 1996; Kim, et al., 2008). Depending on the geometry and shape of the fibre, reinforcing fibres in concrete can amplify the ductility, impact resistance, fracture energy, fire resistance and durability of concrete (Oh & Park, 2005; Oh & Kim, 2007). Polymeric fibres have generated a lot of research interest in concrete reinforcement due to their toughness, post cracking load carrying capacity and higher deformation at peak load. Furthermore, polymeric fibres have lower cost, weight and resistance against corrosion and acids in comparison to other types of fibres (Alhozaimy & soroushian, 1996; Banthia & Gupta, 2006).

Industrial and agricultural waste products have been added to concrete to increase its strength and lower the environmental impact. Fibres such as carpet waste, sisal and flax have been successfully added to the concrete mixture. Fibre additions to concrete can significantly improve the mechanical and physical properties of the concrete (Heniegal, et al., 2015). Mohd (2015) researched using polypropylene fibres as reinforced in cement composite and concluded that the length of fibre recommended is related to the nominal maximum size of aggregate in the mixture. Mohd (2015) recommended that the length of the fibre be greater than twice the diameter of the aggregate. For use in paving applications, the recommended volume fraction of polypropylene is 0.1%. Fibre volume fraction exceeding 0.5% requires air-entraining and water-reducing admixtures (Mohod, 2015). Polypropylene fibres are also used in the construction of blast resistant concrete and pavements (Labib, 2018).

Failure of cement composites is a multi-stage process that is dependent on the internal structure of the multiphase materials. The main factors that govern the contribution of the fibres to the strength of the composite are:

- The physical properties of the fibre;
- The fibre and interface bond;
- The fibre volume fraction;
- The orientation of the fibres within the composite.

Mazaheripour et al. (2011) studied the use of polypropylene fibres in concrete and noted that a high volume fraction of the fibres increased the tensile and flexural strength of the concrete. Polypropylene fibres have been used as reinforcement materials for cement composites to improve their energy absorption capabilities. Additionally, cement composites with polypropylene fibre reinforcement are used in several applications, such as rigid pavement and self-compacting concrete (Sohaib, et al., 2018). Literature shows some research has been carried out into the use of different fibres in cement composites; however, not much research has been done on optimizing the volume fraction of synthetic fibres in the concrete (Bagherzadeh, et al., 2011). Fibre reinforced concrete is not widely used due to the reduced workability that results from the incorporation of fibres in the concrete mixture. There is need for high technical knowledge in coming up with the optimum mix design that balances cost and strength properties. Hence fibre reinforced concrete is still mainly used in big projects where knowledgeable technicians can utilise fully the effect of fibre reinforcement in concrete.

2.8.2 Synthetic polymer fibre reinforced concrete

Several synthetic fibres, namely, polypropylene, polyethylene terephthalate, olefin and polyamide fibres, have been used successfully in reinforced concrete slabs. The effects of these synthetic fibres on the strength properties of concrete slabs are reviewed under the following four subheadings.

2.8.2.1 Polypropylene fibre reinforced concrete

Polypropylene is a thermoplastic polymer that is commonly used in bundling materials, stationery, amplifiers, research facility gear and several car segments (Sohaib, et al., 2018). These fibres are produced in large quantities and are the fourth most produced synthetic fibres after polyesters, polyamides, and acrylics (Jassim & Anwar, 2016). Polypropylene fibres have been used as reinforcement materials for concrete slabs to improve their energy absorption capabilities. Polypropylene fibres were first used as reinforcement in concrete slabs intended for the construction of blast resistant buildings (Madhavi, et al., 2014). Generally, polypropylene fibre reinforced concrete is used commercially in secondary temperature shrinkage reinforcement, overlays, pavements, and slabs. Other common applications include flooring systems, crash barriers, precast pile shells, shotcrete for tunnel linings, rigid pavement as well as self-compacting concrete (Ramujee, 2013; Sohaib, et al., 2018). Largely, polypropylene fibres are commercially utilized at relatively low volume fractions in order to control the plastic shrinkage cracking of concrete slabs (Alhozaimy, et al., 1996).

Mazaheripour et al. (2011) studied polypropylene fibres in concrete slabs. The author noted that a high volume fraction of polypropylene fibres increased the tensile and flexural strength of the concrete slabs significantly. However, not much research has been done on optimising the volume fraction of the polypropylene fibres in concrete slabs (Bagherzadeh, et al., 2011).

Fibrillated fibres have been extruded into very fine and slender fibrils. The fibrils offer outstanding mechanical bond strength in concrete due to their irregular and square shape. Fibrillated polypropylene fibres have been recommended for paving concrete as they reduce plastic shrinkage and permeability and increase impact and abrasion resistance (Mohod, 2015). Generally, fibre loading for paving concrete is 0.1%. Though, some research has been carried out with up to 7% polypropylene fibre loading. However, fibre loading $> 7\%$ reduces the concrete paste workability significantly (Mohod, 2015). Unfortunately, there has not been much research on hybrid polypropylene fibre reinforcement in concrete slabs. The use of fibrillated polypropylene fibres and unfibrillated fibres and their effects on the strength properties of concrete slabs have to be investigated thoroughly.

Saduun et al. (2016) study reported that low volume fractions of polypropylene fibres of between 0.05 and 0.5% have a negligible effect on the compressive strength of fibre reinforced concrete. However, other studies by Zollo (1982) and Mindess & Vondran (1988) gave contradictory conclusions on the effects of polypropylene fibres on concrete's compressive and flexural strength. Moreover, the differences in the conclusions from the two authors on the effects of fibres on strength may be attributed to variations in matrix composition, type of polypropylene fibre and conditions of polypropylene fibres manufacture. An additional study by Saadun (2016) on flexural strength of concrete reinforced with polypropylene concluded that the flexural strength increased as the fibre volume fraction of polypropylene increased. At 1 kg/m^3 the flexural strength is 3.50 MPa. Whereas, at 2 kg/m^3 the flexural strength is 3.92 MPa (Saadun, et al., 2016). Another study by Dharan & Aswathy (2016) reported that the best flexural strength of polypropylene fibre reinforced concrete slabs occurs at a 1.5% volume fraction. After 28 days of concrete curing time, the resulting flexural strength from the ratio is 5.71 MPa, which is an increase of 31.57% over unreinforced concrete.

Mohod (2015) carried out further research to establish the composition of fibre volume fraction of polypropylene fibres in concrete slabs that gives the optimal flexural strength. The author recommended the use of 0.1% volume fraction of polypropylene fibre in paving slabs. Besides, fibre volume fraction exceeding 0.5% requires the use of admixtures.

Saadun et al. (2016) reported that the compressive strength of polypropylene fibre reinforced concrete decreased with an increase in fibre volume fraction. At 1 kg/m^3 , the compressive strength is 34.87 MPa while at 2 kg/m^3 the compressive strength is 28.08 MPa (Saadun, et al., 2016). However, another research carried out by Mindess (2003) concluded that long term compressive strength increased by 25% at 0.5% polypropylene fibre volume fraction. Furthermore, the same study by Mindess et al. (2003) reported an increase in the short-term compressive strength at low polypropylene fibre loading.

Dharan & Aswathy (2016) studied the effects of polypropylene fibres on the compressive strength of concrete. The study reported that fibres increased the short-term compressive strength marginally. However, polypropylene fibres have a more significant effect on the long-term compressive strength of

the concrete. Dharan & Aswathy (2016) concluded that the best fibre volume fraction is 1.5%, giving a 28-day compressive strength of 46 MPa. This volume fraction gives a 17% increase in compressive strength over unreinforced concrete. This optimum fibre volume fraction of 1.5% was confirmed by another study by Ramujee (2013). Hughes (1976) study established that the compressive strength of concrete containing polypropylene fibres decreases with fibre volume fraction.

On the other hand, the study reported improved flexural properties with increased polypropylene fibre volume fraction. Further study by Parveen & Sharma (2013) noted an increase in compressive strength at low fibre loading of up to 0.2%. Thereafter, there is a reduction in compressive strength with an increase in fibre loading beyond 0.2%

Jassim & Anwar (2016) study showed the effects of polypropylene fibres on concrete strength as shown in Figure 2-17. The study concluded that polypropylene fibres increase the short term (< 28 days) compressive strength. On the other hand, the long-term compressive strength (> 28 days) reduces with increase in fibre loading. However, the effects of fibre length in conjunction with fibre loading on compressive strength in concrete slabs has not been fully researched.

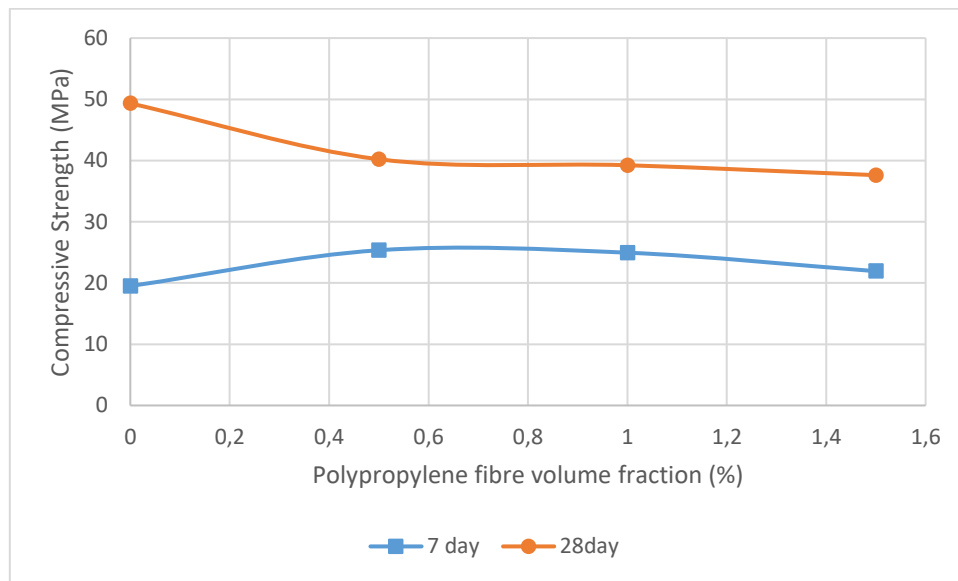


Figure 2-17 – Effect of polypropylene fibre loading on compressive strength of concrete (Jassim & Anwar, 2016)

Another study by Mukhopadhyay & Khatana (2015) reported a dense microstructure around polypropylene fibre in FRC, which gives a strong interfacial adhesion and anchoring of the fibres within the fibres cement matrix. However, there has not been much research into the interfacial adhesion strength of different synthetic fibres.

2.8.2.2 Polyethylene Terephthalate Fibre Reinforced Concrete

Polyethylene Terephthalate (PET) is a thermoplastic used mainly in textiles, fibres, beverages, and other liquid containers (Patil & Shukla, 2017). PET fibres have generated a lot of attention in the FRC industry, and this is because the fibres can be easily mixed into the concrete paste. Ataei et al. (2017) studied the compressive strength effect of recycled PET particles in concrete. The research reported a decrease in compressive strength after adding PET particles. This occurrence was attributed to the weak cohesion between the particles and the cement resin. Rahmani et al. (2013) gave a similar conclusion of a general decrease in compressive strength with PET particles to concrete. Rahmani et al. (2013) reported that the compressive strength of PET particle reinforced concrete had an increase in compressive strength of 8.86% at a 5% particle mass fraction. However, at 10% PET particle mass fraction, the compressive strength was found to remain the same as that of unreinforced concrete (Rahmani, et al., 2013). The compressive strength decreases to 5.14% at a PET particle mass fraction of 15%.

Choi et al. (2005) also studied the effects of increasing the mass fraction of PET particles on compressive strength. The author showed a decline in compressive strength with an increase in the mass fraction of PET particles. At 50% PET particle mass fraction, the loss in compressive strength was found to be 14.52%. Whilst, at 75% PET particle mass fraction, the compressive strength loss was 33.06% in reference to unreinforced concrete slabs (Choi, et al., 2005). The conclusion reached by Choi et al. (2005) work was consistent with that of previous studies by Ataei et al. (2017) and Rahmani et al. (2013).

Mukhopadhyay & Khatana (2015) studied the use of hybrid PET and steel fibres to give superior toughness to concrete slabs. The study reported an increase in ultimate tensile strain capacity at peak with an increase in PET fibre loading. However, beyond a certain fibre loading, the ultimate tensile strain starts to decrease. Further, the author noted that an increase in PET fibre length improves strain hardening and multiple cracking behaviours. This improvement increases the ultimate strain capacity of the concrete slab. However, the study failed to account for the critical length phenomenon, whereby the strength of the concrete starts to reduce at certain fibre lengths. Besides, not much research has been done into the use of hybrid fibres consisting of PET and other synthetic polymer fibres such as polypropylene in concrete slabs.

Ismail et al. (2008) studied the flexural strength properties of waste PET particle reinforced concrete. This study concluded that at 20% PET particles mass fraction, there was a decrease of 30.5% in flexural strength. This decrease in flexural strength was attributed to a reduction in adhesive strength due to the hydrophobic nature of PET. Furthermore, the reduction in flexural strength can also be attributed to the plastic aggregate's elastic nature and non-brittle loading characteristics. Nonetheless, the flexural

strength can be increased using PET fibres, which have a high aspect ratio. However, more research needs to be conducted to establish PET aspect ratios that give optimal flexural strength properties.

2.8.2.3 Olefin Fibre Reinforced Concrete

Olefin fibres have good tensile properties, good abrasion resistance and excellent resistance to chemicals. The tensile strength of polyolefin fibres is > 400 MPa. Furthermore, these fibres tend to form a good bond within the concrete when used as reinforcement material due to their rough surface.

Olefin's macro fibre volume fractions is commonly used in the concrete range from 0.3 to 1.5% (Mindess, et al., 2003). Reviewed literature by Neeley & O'Neil (1996), Ramakrishnan (1996), and Hamou et al. (2005) showed that the proper use of olefin fibre in concrete slabs gives similar strength to that of steel fibre reinforced concrete at a much lower weight. In addition, the use of olefin fibre has been proved to give a 13% increase in strength than unreinforced concrete slabs (Hamou, et al., 2005). Moreover, olefin fibre reinforced concrete reduces the propagation of cracks by up to 70% in comparison to unreinforced concrete (Lin, et al., 2011). Further, research carried out by Lin et al (2011) concluded that olefin fibre reinforced concrete of similar volume fraction has impact strength two times stronger than steel fibre reinforced concrete slabs. This superior strength of olefin fibre makes the olefin reinforced concrete slabs fourteen times greater in impact strength than unreinforced concrete (Lin, et al., 2011). The high strength of the concrete slabs can be attributed to the remarkable good bond generated between the fibres and the concrete due to their rough surface. Yet, not much research has been done on the effects of other geometries of olefin fibres in concrete slabs, such as crimped fibres. It is worth noting that a threshold volume fraction exists in which the compressive strength becomes less than that of typical unreinforced concrete (Alberti, et al., 2018).

2.8.2.4 Polyamides Fibre Reinforced Concrete

Polyamide (PA) fibres have the superior tensile strength to most synthetic fibres, including polypropylene and polyolefin fibres which is commonly used in concrete (Khajuria, et al., 1991; Song, et al., 2005; Jeon, et al., 2014). The use of micro-PA in concrete gives concrete superior properties, which resists early age shrinkage cracks. Macro PA fibres effectively enhance the axial load capacity and post-peak behaviour of concrete (Guler, 2018). PA fibre reinforced concrete is durable, resistant to corrosion effects, and has good workability. PA is commonly called nylons and contains the amide group [-CO-NH-] in their main chain.

Research carried out by Guler (2018) concluded that the ductility and toughness of concrete reinforced with PA increased significantly. However, there was only a marginal improvement in the compressive strength. PA fibres can be used successfully at volumes fractions $> 0.5\%$ as an alternative to steel fibre reinforced concrete (Guler, 2018).

Walton & Majumdar (1978) study showed that PA fibres in small amounts improved the impact resistance on concrete slabs substantially. However, PA fibres have only marginal improvement on the tensile or flexural strength. The high impact strength is attributed to the stretching and pulling out of the fibres, which occurs at large strains after the failure of the cement matrix at a lower load. On the contrary, not much research has been done using specific PA fibres such as nylon and nylon 6,6 to determine the effects of varying volume fraction and fibre length on the properties of a concrete slab.

2.8.3 Failure mechanisms of fibre reinforced concrete slabs

Characterisation of the failure mechanisms of composite material is difficult due to the complexity of their failure modes (Okoli & Smith, 1998). Failure of a composite can be defined as when it ceases to perform satisfactorily for the specific end-use. For FRCC, the main benefit obtained from the inclusion of fibres occurs after matrix cracking. The predominant mechanism of energy dissipation during composite fracture with fibres is in the pull-out of the fibres, which increases the fracture toughness of the composite (Ferreirra, et al., 2016). Some of the failure mechanisms of FRCC are discussed in the following subheadings.

2.8.3.1 Fibre effects

Fibres such as steel wire, polyester fibres or aromatic fibres can be classified as tough as they undergo non-elastic deformation after yielding. Deformation mechanisms include plastic necking and inter fibrillary splitting in polymer fibres. These fibres show high resistance to surface damage compared to brittle fibres. Figure 2-18 shows the different failure methods of fibres in fibre reinforced composites.

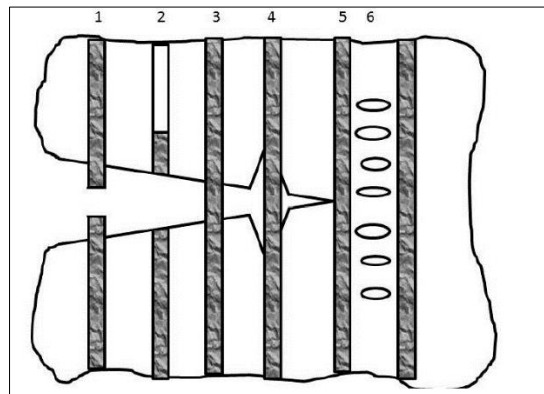


Figure 2-18 – Failure mechanisms in FRCC. 1 – Fibre rupture; 2 – Fibre pull out; 3 – Fibre bridging; 4 – Fibre/matrix debonding; 5 – Fibre preventing crack propagating; 6 – Matrix cracking (Zollo, 1997)

When the localised load in a fibre reaches the failure, stress the fibre break at its weak point, and the load is transferred into the neighbouring matrix regions. As the load is increased, other fibres may break. However, each fibre can break numerous times without having any significant impact on the overall

load-bearing ability of the composite material. This analogy is due to the ineffective length, the short distance with the tensile load supported rapidly building up again to its original level.

Catastrophic brittle failure can occur when the fibres are closely spaced, and the extra tensile load is transferred to a neighbouring fibre resulting in it breaking. The local stress concentration is then even higher. If this process is repeated several times, the cross-sectional area where the fibre breaks are occurring becomes weak, resulting in catastrophic brittle failure.

There is a need to optimize the fibre bond within the concrete matrix. If the fibres form a weak bond with the matrix, the dominant failure mode is fibre slippage. This slippage of fibres lowers the toughness of the fibre reinforced concrete slab as the fibres do not have much effect on increasing the toughness of the concrete. However, if the bond formed between the fibres and the concrete matrix is too strong, then the failure mode is dominated by fibre breakage. This breakage of fibres is due to the fibres breaking before they dissipate energy through any fibre slippage. The fibres in such a case have a marginal effect on increasing the strength properties of the concrete slab.

When a crack travelling in the concrete matrix approaches an isolated fibre, the crack is halted by the fibre. This crack retardation is due to the fibre's stiffness, which inhibits further propagation of the crack. The strength of the fibre is higher than the stress level, which is concentrated at the tip of the matrix crack. Crack propagation may occur if the local shearing force acting at the fibre and matrix interface becomes adequately high to allow fibre debonding. During the fibre debonding process, the fibre will extend elastically, and subsequent crack propagation occurs while the matrix slides relative to the fibre, as shown in Figure 2-19. This process requires energy which contributes to the toughness of the reinforced concrete slab.

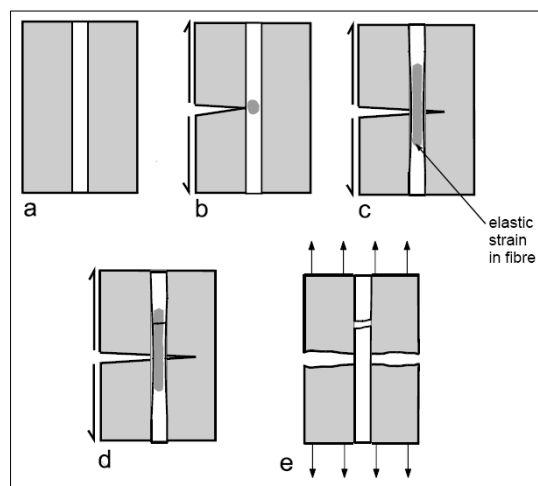


Figure 2-19 – Process of fibre debonding failure in concrete (Zollo, 1997)

2.8.3.2 Fibre length

The optimization of fibre length in composites results in improved mechanical properties. Shorter fibres are more evenly distributed in the concrete mixture, unlike longer fibres which tend to clump together, the interfacial bond strength can only be optimized if the fibre length is at its optimum value such that it provides resistance to fibre pull out and have enough fibre modulus of rupture to avoid fibre fracture.

The fibre length determines the failure mode of the composite. Fibre fracture is the most prevalent failure mode if the fibre length is longer than the critical length. If the fibre length is shorter than the critical length, then the fibre pullout is the likely failure mode.

Fibre critical length is dependent on the ultimate tensile strength of the fibre (σ_f), fibre diameter (d) and τ_c , which is either the matrix/bond strength or the matrix shear strength. Equation 2-8 shows the calculation of critical fibre length.

$$L_c = \frac{\sigma_f d}{2\tau_c} \quad 2-8$$

When the critical length L_c is equal to the length of the fibre, the optimal fibre load is achieved at the centre of the fibre if the $L > L_c$, then the optimal fibre load is carried by most of the fibre and is usually the case with continuous filaments. When $L < L_c$, the fibre is below a critical length, and the optimal fibre load cannot be reached. This results in a weaker composite material. The critical length is affected by the diameter of the fibre. As the diameter of the fibre becomes smaller, the critical length of the fibres decreases as well (Iuyenkimet, 2007).

Numerous short fibres effectively bridge numerous micro-cracks in the concrete slabs under load and avoid localised strain. On the other hand, long fibres are of great use in bridging macro cracks at higher loads. Nonetheless, long fibres reduce the workability of the concrete mix significantly. Furthermore, an increase in the fibre length reduces the bond strength between the fibre and concrete boundary. Fibres exceeding 12 mm in length are not suitable for optimum reinforcement of concrete slabs (Demyanova, et al., 2003). However, the addition of Mowilith Pulvet re-dispersible copolymeric powders increases the adhesion of long fibres between the fibre and cement matrix boundary (Demyanova, et al., 2003). There has not been much research done into the use of synthetic filament fibres and co-polymeric powders as reinforcement materials in concrete slabs. Despite co-polymeric powders, they are increasing the adhesion of fibres to concrete.

Mohd (2015) researched polypropylene fibres as reinforcement in concrete slabs. The study established a relationship between fibre length and the maximum nominal size of the aggregate in the concrete mixture. In addition, the study recommended that the fibre length be at least twice the diameter of the aggregate.

2.8.3.3 Fibre Aspect Ratio

One of the most important parameters describing a fibre is its aspect ratio. Aspect ratio is defined as the length of a fibre divided by an equivalent diameter of the fibre (Saxena & Saxena, 2015). The energy absorption of a concrete composite material increases when the fibre aspect ratio increases. A higher aspect ratio gives a greater surface area by having a more significant number of fibres in the concrete slab (Sovjak, et al., 2016).

Sudhikumar (2014) study reported that the compressive strength of slurry infiltrated fibrous ferrocement with steel fibre reinforcement reduced as the aspect ratio increased. Compressive strength of 41.33 MPa was recorded for a fibre aspect ratio of 25. Whereas a compressive strength of 28.29 MPa was recorded for an aspect ratio of 50 (Sudhikumar, et al., 2014). The study showed that a low aspect ratio gives better compressive strength. In addition, the same author studied further the same experiment described in the preceding sentence using polypropylene fibres instead of steel fibres. The study reported a similar trend on the effect of aspect ratio between the two fibres.

On the other hand, results on flexural strength and toughness indices showed a consistent trend for both fibres, with the flexural strength decreasing with an increase in fibre aspect ratio. This decrease in flexural strength may be attributed to the low fibre aspect ratio fibres being able to fill voids producing a denser concrete that absorbs energy better.

In another study by Sovjak (2016), it was established that increase in the fibre aspect ratio in polymeric fibre reinforced concrete slabs leads to an increase of the effective fracture energy (Sovjak, et al., 2016). Further, the study established a linear relationship between fibre aspect ratio and effective fracture energy. Nevertheless, research on the effects of aspect ratio on strength properties of concrete slabs for different types of polymeric fibres is not exhaustive.

2.8.4 Composite fabrication techniques

There are several materials that are used in fabricating composite materials. The main methods include the hand lay-up process, filament winding, resin transfer moulding, injection moulding and pultrusion. However, the primary methods of concrete composites are hand layup moulding and additive manufacturing, discussed in the following subsections.

2.8.4.1 Hand Lay-up moulding

Reinforced or pre-stressed concrete can only be manufactured in a limited number of ways. Generally, a prefabricated mould is used in which the reinforcement material has been positioned before fabrication. The mould can then be reused to make other concrete samples; however, this is not the case all the time (Bos, et al., 2016). Shapes of different concrete blocks, including bricks, is moulded using moulding boxes as shown in Figure 2-21. Block moulding uses typically a mould with decorative

markings running along its surfaces in accordance with the desired pattern. Wood and plastic moulding are common concrete block moulding materials. The concrete mixture is packed into the mould and compacted. Figure 2-20 (a) shows the mould used by Auna (2014) in fabricating a sisal fibre reinforced cement slab. Aruna (2014) used a metal mould and used the hand lay-up method to fabricate the slabs. Henderson (2005) made a wooden mould shown in Figure 2-21 for fabricating concrete slabs. This type of mould is faster and cheaper to fabricate. This design makes it suitable for making bespoke slabs.



(a)



(b)

Figure 2-20 – (a) Hand lay up of sisal fibre/cement composite slab (b) Fabricated slab (Aruna, 2014)



Figure 2-21 – Concrete slab moulds (Henderson, 2005)

2.8.4.2 Additive Manufacture

The use of moulds to fabricate reinforced concrete slabs is labour intensive process. The erection of the moulds and the placement of the reinforcements requires manual labour, more so in bespoke slab manufacture. Moulds, due to their nature, limit the geometries that can be produced. Additive manufacture has been explored for the fabrication of concrete slabs and structures. Some examples of 3D printed concrete structures are office buildings in Dubai, UAE, which was 3D printed in 2016. The

building measures 250 m². A series of 10 houses in China, Suzhou were 3D printed with a printer of dimensions 150 X 10 X 6.6 m (Wu, et al., 2016).

Concrete 3D printing machines work by mixing concrete with water, then pumping through a hose connected to the printer head. The printer head is positioned at the tip of a vertical arm with 4 degrees of freedom. The printer head allows concrete deposition at the required locations at the desired speed and angle. Figure 2-22 shows how a 3D printer head for concrete looks like with the hose feeding in the concrete.

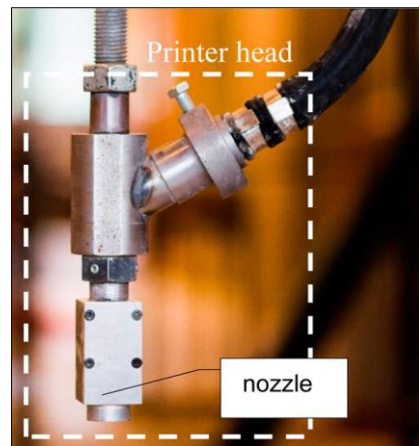


Figure 2-22 -3D printer head for concrete (Bos, et al., 2016)

However, 3D concrete printing is still in its infancy stage with a lot of potentials. The cost of the machinery involved in 3D printing is one of the current major hindrances to the technology. Furthermore, 3D printing fibre reinforced concrete tends to clog the printer nozzle.

2.8.5 Effect of fibre addition on concrete workability

Concrete workability can be defined as the effort required to manipulate and place a freshly mixed concrete paste, with minimum loss of homogeneity (Yeh, 2007). Workability directly bears the consistency, flowability, pumpability, compactability, and harshness of the concrete paste (Hoang & Pham, 2016).

There exist intricate and non-linear interactions between the mechanical characteristics of the concrete slabs and constituent ingredient properties that make up the concrete paste (Yeh, 1998; Chou, et al., 2014; Hoang, et al., 2016). The workability of the concrete paste containing fibre reinforcement is dependent on the fibre loading percentage and fibre aspect ratio. Aruna (2014) study reported that with an increase in fibre volume fraction and fibre length, there is a reduction in the workability of concrete. The author established that the concrete paste could be manually compacted without balling for fibre volume fractions of < 3% and fibre length < 50 mm, (Aruna, 2014). On the contrary, research carried out by Wilinki et al. (2016) reported that for fibre loading > 0.3%, there are severe problems in concrete paste homogeneity and workability. The variances between the findings of the two authors (Aruna,

2014; Wilinski, et al., 2016) may be attributed to the different aspect ratios of the fibres used in their studies.

Ismail et Hashmi (2008) claimed the addition of Polyethylene Terephthalate (PET) fibres in concrete increased the workability of concrete. Though, studies by Wilinski et al. (2016) and Aruna (2014) claimed that the addition of PET fibres improved the slump of concrete but decreased its workability. Wilinski et al. (2016) study concluded that the concrete slump is dependent on the fibre volume fraction. As the fibre volume fraction increases, the slump decreases significantly. According to a study by Wilincki et al. (2016), the use of 0.1% PET fibre in concrete gives a slump value of 50 mm, whereas 0.3% PET fibre gives a slump value of 10 mm.

Thirumurugan & Sivakumar (2013) study reported that the workability of concrete decreases with an increase in the fibre volume fraction of polypropylene fibres. Though, this can be overcome by the addition of water-reducing admixtures. Yet, the use of admixtures leads to a reduction in the compressive strength of the concrete slab (Thurumurugan & Sivakumar, 2013). Saadun et al. (2016) research concluded that adding 1 kg/m³ of polypropylene fibre gave a slump value of 60 mm.

Preti et al. (2012) study reported that higher volume fractions of polypropylene fibres in concrete slabs reduced the consistency of the concrete paste. For 0.5% fibre content, the workability was reported as high on the workability scale. However, at 1% fibre content, the workability is medium. Generally, polypropylene fibres are used in concrete as secondary reinforcement at low fibre fraction levels ranging from 0.1 to 0.2%. As a result, the effect on workability is low due to the low fibre loading. However, the slump is significantly improved (Zollo, 1982). Yet, not much research has been done to determine the effect of varying polypropylene aspect ratios on the workability of the concrete paste.

A study by Balaguru & Shah (1992) reported that if a high volume fraction of synthetic fibres are used in concrete slabs, there is a reduction in concrete paste consistency. However, the workability can be improved by increasing the water ratio (Balaguru & Shah, 1992). Though, this tends to reduce the compressive strength of the concrete slab. This reduction in compressive strength is attributed to increased entrapped air within the concrete mixture creating voids. However, not much research has been carried out to find the optimum amount of water to high fibre loading that can be added to concrete slabs to give optimum flexural and compressive strength.

The general trend in research (Patel, et al., 2012; Dharan & Lal, 2016; Balaguru & Shah, 1992; Zollo, 1997) shows that there is a decrease in the ease of placement and consistency of concrete paste containing polymeric fibre reinforcement. This phenomenon is attributed to an increase in the amount of entrapped air voids due to the presence of fibres. The increase in air voids has an adverse effect on the workability of the concrete (Dharan & Lal, 2016). Though, the slump value improves with the addition of fibres into the concrete paste.

2.8.6 Water-cement ratio

The quality of concrete is dependent on the water/cement ratio. The addition of water increases the water-cement ratio, adversely affecting the strength parameters and durability of the concrete. Decreasing the water content has several advantages, including Furthermore, there is a better bond between successive layers, better concrete and reinforcement bond and less volume change from wetting and drying. However, a balance must be struck between these properties and the workability of the concrete. Fresh concrete should be semi-fluid and mouldable. Each aggregate particle must be coated with paste, and the spaces between the aggregate materials filled. Semi-fluid concrete should not crumble but flow sluggishly.

2.8.7 Compressive strength

Ataei et al. (2017) studied the compressive strength effect of particles of recycled PET particles in cement composites. The research reported a decrease in compressive strength after the addition of PET particles, and this decrease was attributed to the weak cohesion between the particles and the cement resin. Rahmani et al. (2013) reported similar findings showing a decrease in compressive strength with the addition of PET particles to the cement composite. The results showed that compressive strength had an increase of 8.86% at 5% particle mass fraction and decreased by 5.14% at PET mass fraction of 15%. At a 10% mass fraction of PET particles, the compressive strength was found to remain the same as the unreinforced concrete (Rahmani, et al., 2013).

Choi et al. (2005) studied increasing the mass fraction of PET to establish the effect it has on the compressive strength. The results were consistent with the other researchers. There was a decline in compressive strength with an increase in mass fraction of PET particles. At 50% mass fraction mixture of PET particles, the loss in compressive strength was found to be 14.52%, and at 75% mass fraction of PET particles, the compressive loss in strength was found to be 33.06% (Choi, et al., 2005).

Bagherzadeh (2011) studied the compressive strength in cement composite reinforced with polypropylene fibres. Bagherzadeh used a universal testing machine at a loading rate of 14 N/mm²/min and tested the samples according to ASTM C39. The results from the test were interpreted as stress per unit load area on the sample (Bagherzadeh, et al., 2011).

2.8.8 Flexural strength

Ismail et al. (2008) studied the flexural strength of waste PET reinforced cement. The results showed that with a 20% PET particles mass fraction, there was a decrease of 30.5% in flexural strength. Ismail et al. (2008) attributed this decrease in flexural strength to a decrease in adhesive strength due to the hydrophobic nature of PET. Hannwai et al. (2010) attributed the decrease in flexural strength to the plastic aggregate's elastic nature and non-brittle loading characteristics. The decrease in flexural

strength using particulate reinforcement of PET shows a need for the use of fibres with a high aspect ratio to increase the flexural strength, a gap that this research seeks to fill.

The flexural toughness of FRCC is the ability to dissipate energy in the rupture process and is characterised by the area under the stress-strain curve for flexural strength. Figure 2-23 shows three-point testing of a concrete slab by Ferreirra (2016). The flexural strength is obtained through loading of the slabs in three- and four-point configurations (Ferreirra, et al., 2016).

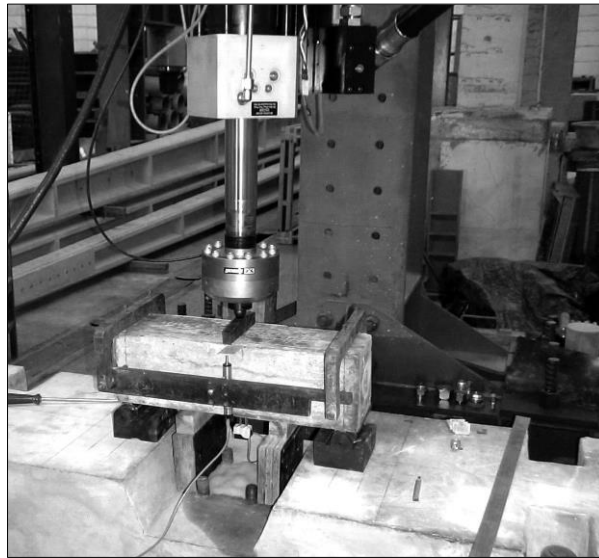


Figure 2-23 – Three-point bending test for a hybrid concrete slab (Ferreirra, et al., 2016)

2.8.9 Short duration dynamic loads

Concrete structures are subjected to static load and short-term dynamic loads. Short term dynamic loads can be from projectiles, wind gusts, earthquakes, and vibrations. The most common method to improve the impact load resistance of concrete is randomly oriented fibres. Research has shown that the incorporation of fibres in concrete improves the energy absorption and cracking resistance of concrete (Anand & Dutta, 2013).

2.9 Materials Testing

Composites are designed in a manner to maximise the strength of their individual materials while minimizing to some extent their deficiencies. This phenomenon allows manufacturers to optimize and overcome the deficiencies associated with conventional materials (Anand & Dutta, 2013). A complete understanding of the composite properties is essential for determining its suitability to specific end uses.

Composite material testing is carried out to simulate real-life application conditions and investigate variables that may impact the mechanical properties and damage tolerance of the composite. Testing gives data that can be used for modelling and finite element analysis. A complete and thorough understanding of material properties is of utmost importance in determining its suitability for specific

end-use. Engineers understand that no one testing method is superior without any faults. Therefore, it is important to review the different testing methods to come up with one that is most suitable for the hybrid concrete composite being developed in this research.

Furthermore, material testing is also carried out to investigate the effect of variables on the material. Properties of the constituent materials such as fibre volume fraction, fibre orientation, particle volume fraction, laminate thickness, and processing parameters such as the fabrication method and curing temperatures can significantly affect the composite properties (Anand & Dutta, 2013). Material testing is essential to study variables that influence the compound's properties and provide information to use in optimization and modelling.

2.9.1 Mechanical testing

Mechanical testing gives the properties of any material under dynamic or static force. Mechanical testing is carried out to assess the suitability of a particular material to a specific end-use. The results obtained from mechanical testing provide the information to identify suitable materials, designs and compositions suitable for specific end-use. Mechanical tests include tests such as flexural strength, compressive strength, tensile strength, hardness strength, water absorption and density (Narganti, et al., 2015).

2.9.1.1 Flexural strength

A flexural strength test measures the ability of a slab of material to withstand failure in bending. There are two main types of flexural strength tests: four-point bending (ASTM C78) and three-point load testing (ASTM C293). Vinodsinh et al. (2013) used a sample of size 500 mm X 100 mm X 100 mm cast in a metal mould for the flexural strength test. The rollers were cleaned to ensure no debris was present from previous specimens before running the flexural strength test on a Universal flexural testing machine shown in Figure 2-24 (Solanki & Pitroda, 2013). Figure 2-24a shows the schematic diagram of a four-point flexural strength with the important parameters for calculating the flexural strength.

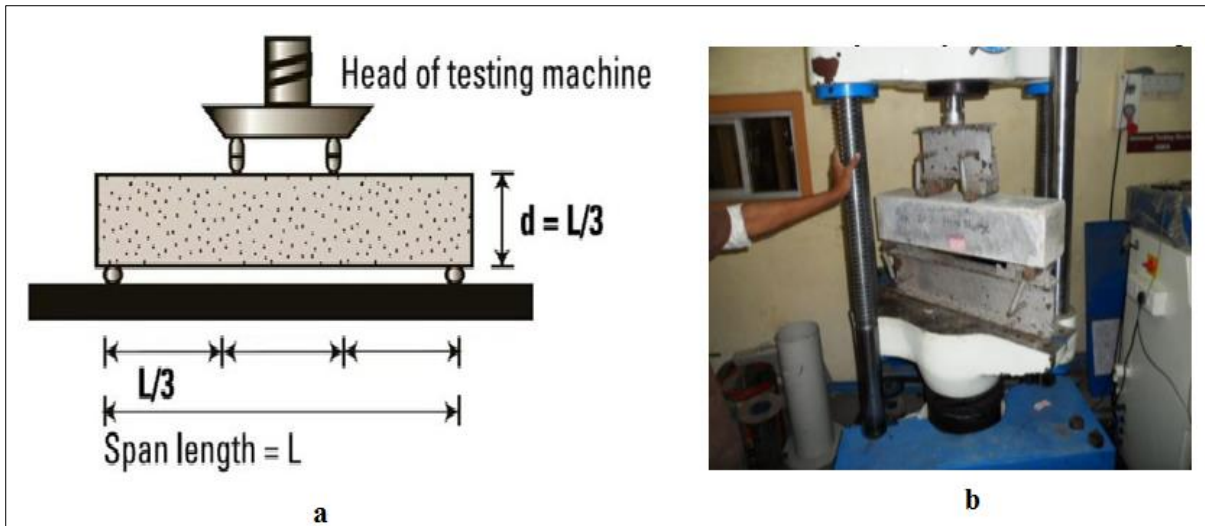


Figure 2-24 – (a) Showing Flexural strength test on a concrete sample using four-point loading (b) Test carried out on a fly ash/bamboo fibre reinforced concrete sample (Solanki & Pitroda, 2013)

2.9.1.2 Compressive strength

Concrete's compressive strength is defined as the strength of 28 days old specimen tested under monotonic uniaxial compressive load. This test can be carried out by making a mould of concrete in the shape of a cylinder with 16 cm diameter and 30 cm height or using a cube specimen with dimensions 15 cm X 15 cm X 15 cm. Figure 2-25 shows cube samples being prepared for compressive strength testing.



Figure 2-25 – Concrete cubes for compressive strength tests (Neyestani, 2011)

Saha (2018) tested a cement composite with fly ash reinforcement by using cylindrical specimens consisting of 100 mm diameter and having a height of 200 mm. The curing time of concrete was taken into effect in this study, and testing was done at 7, 28, 56, 90, 180 and 360 days following the Australian Standard AS 1012.9 (Australian, 2014). Figure 2-26 shows the compressive strength testing of the cylindrical test specimen.

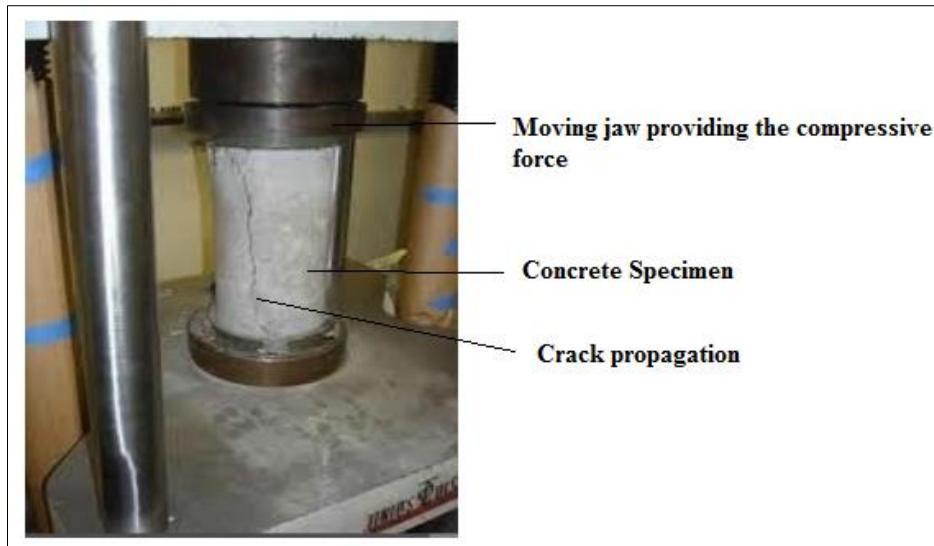


Figure 2-26 – Compressive testing of a concrete cylindrical specimen using a universal compressive tester (Tandon, 2017)

2.9.1.3 Tensile strength

The tensile strength of any material is defined as the maximum amount of stress that the material can endure before failure (Sathish, et al., 2014). A uni-axial load is applied to the test specimen from both ends of the material during the tensile strength test. The tensile strength test is typically performed using a universal tensile tester machine. Concrete materials have greater strength in compression and are generally weak under tensile load. Tensile load is normally avoided in concrete structures. However, it is impossible to completely avoid the propagation of tensile stress, which may not be negligible in the concrete material (Madandoust, et al., 2017). A concrete direct tensile test is the method that directly gives the tensile strength for concrete. Modulus of rupture and Brazilian splitting tests are methods of indirect testing of tensile strength of concrete in accordance with ASTM C78 (ASTM Standard C78, 2009) and ASTM C496 (ASTM Standard C469, 2002), respectively. Splitting tensile strength is defined as a measure of the concrete's tensile strength, which is measured by splitting a concrete cylinder across its diameter (Ayub, et al., 2014).

The tensile strength of concrete can be calculated from the compressive strength. The tensile strength is proportional to the square root of the compressive strength (f_c) in MPa. Equations 2-9 and 2-10 show how to direct tensile strength and split tensile strength can be calculated indirectly from the compressive strength of concrete, respectively.

$$\text{Direct tensile strength } f_{ct} = 0.35\sqrt{f_c} \quad 2-9$$

$$\text{Split tensile strength } f_{cts} = 0.50\sqrt{f_c} \quad 2-10$$

Most properties of concrete can be related to its compressive strength. Compressive strength testing for concrete is generally the most economical, accurate and easiest test to perform.

2.9.1.4 Water absorption

Water absorption is the rate of water uptake of concrete through the capillary porosity of concrete. Absorption test results are also known as the volume of permeable voids (VPV) and measure the total weight of concrete after being immersed in water for a specific amount of time. Sorptivity tests measure the water absorption rate, which is not considered in water absorption tests, which are mainly interested in the quantity of water absorbed only. Sorptivity value is obtained by immersing concrete in water with no pressure head and then measuring with time the weight gain. The sorptivity value is computed as the volume absorbed per unit surface related to the square root of time. Water absorption tests, however are not suitable for concrete that have water repellent additives within their mixture (Australia, 2007).

2.9.1.5 Density

The density of composite material can be measured by taking their dimensions using Vernier callipers or other such equipment with high tolerance levels and low error values. The composite density can then be calculated using equation 2-11.

$$p_{exp} = \frac{mass}{volume} \quad 2-11$$

The void content can be calculated once the density has been ascertained. Equation 2-12 shows the formula for calculating void content.

$$Void\ content\ (\%) = \frac{p_{th} - p_{exp}}{p_{th}} \times 100 \quad 2-12$$

Where p_{th} is the theoretical density calculated using Rule of Mixture (ROM)

2.9.2 Thermal properties

Thermal properties, which include the coefficient of thermal expansion, specific heat and thermal conductivity of concrete, are essential parameters for evaluating the use of concrete for specific end uses.

2.9.2.1 Coefficient of thermal expansion

Unreinforced concrete has a positive coefficient of thermal expansion that varies between 7×10^{-6} and 14×10^{-6} degrees Celsius (Sinha, 2014). Calculating and establishing the coefficient of thermal expansion of concrete is important as the expansion of the concrete slabs can induce stress in the adjacent slabs resulting in buckling. Differences between the thermal expansion potential of cement and

the aggregates used and any admixtures can produce internal stress. These stresses can cause cracks to develop, which further exasperate the refractory effects of the damaged surface layer due to the air contained in the crack voids (Sinha, 2014). The thermal expansion of concrete is affected by the type of aggregate used, cement content, water content and concrete age (Sinha, 2014).

2.9.2.2 Thermal diffusivity

Thermal diffusivity is defined as a measure of the rate at which temperature changes within a given mass. The thermal diffusivity is affected by the cement's aggregate type, moisture content, and degree of hydration. Equation 2-13 shows the equation to calculate the thermal diffusivity of concrete (Talebi, et al., 2020).

$$\text{Thermal Diffusivity } (D) = \frac{\text{Thermal conductivity } (K)}{\text{Specific heat } (S) \times \text{Density of the concrete } (d)} \quad 2-13$$

2.9.2.3 Thermal conductivity

Thermal conductivity measures the ability of a material to conduct heat and is defined as the ratio of the flux of heat to a temperature gradient. The conductivity of concrete is affected by moisture content and the type of aggregate and mixture of the concrete. Lightweight and calcareous aggregate concrete has low thermal conductivity compared to siliceous aggregate concrete (Talebi, et al., 2020).

2.9.2.4 Fire resistance test

Fire resistance characteristics and performance under fire exposure are of major concern to engineers in their choice of reinforced slab material to use (Sadek, et al., 2006). There has not been much research on the fire resistance of polymer reinforced concrete. Sadek et al. (2006) researched fire resistance of glass fibre reinforced concrete. Sadek et al. (2016) used beams loaded to 40 kN and 60 kN, which was approximately 60% of the ultimate load of the beam. The experiment was conducted in accordance with ASTM E119 and ISO 834. The temperature was measured underneath the tested specimens. There was a challenge with measuring the deflection of the test specimens due to the high temperatures, which tended to melt the dial gauges. Figure 2-27 shows the test specimen that Sadek et al (2006) used to test concrete slabs' fire resistance.

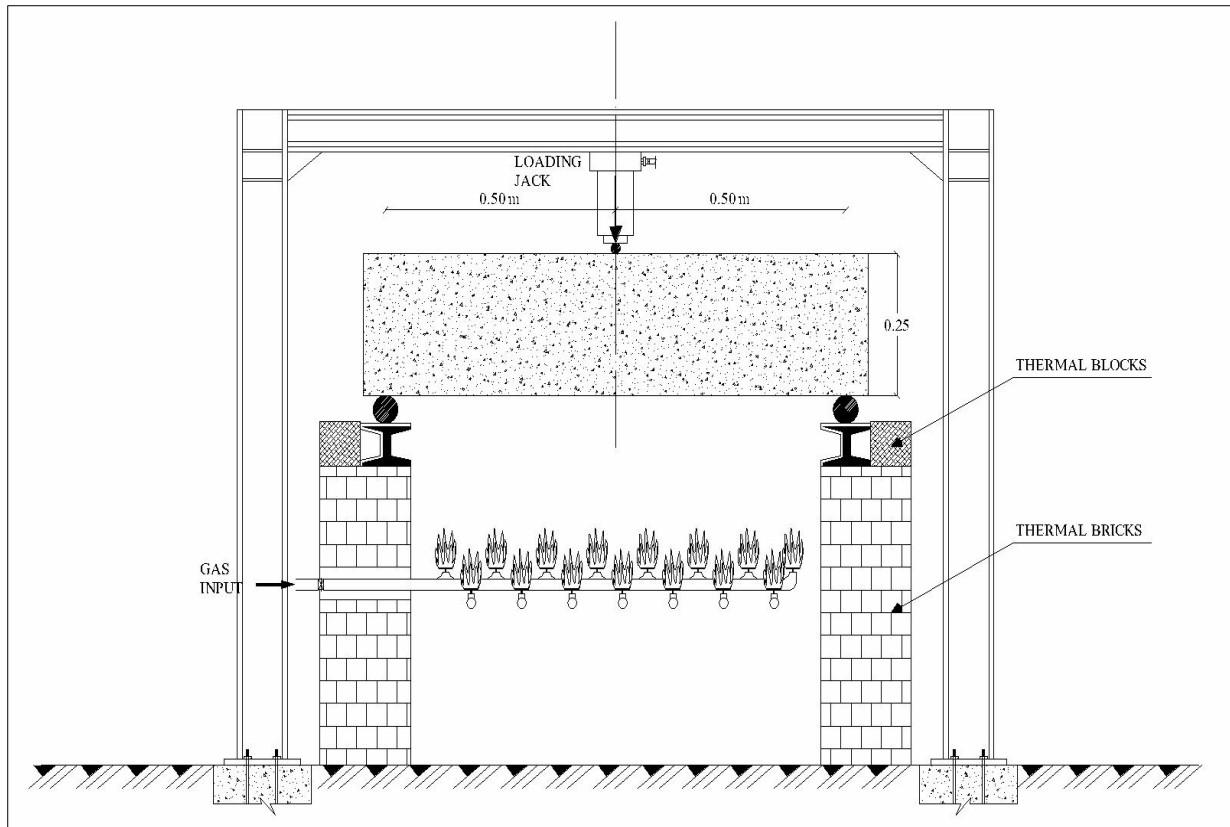


Figure 2-27 – Test setup for measuring resistance to fire of slabs made from glass-reinforced concrete (Sadek, et al., 2006)

Failure of polymer reinforced concrete is mainly due to fire penetration through the wide cracks developed, and this destroys the polymer fibres. The fire penetration then causes interface cracking and deboning bars, leading to global failure. There is a need to protect the polymeric material within the concrete by using denser concrete covers or use special materials to increase the fire resistance (Sadek, et al., 2006).

2.9.3 Non-destructive tests

Non-destructive tests (NDT) are tests carried out on materials to evaluate their material integrity and check for any internal flaws without affecting the suitability of the material for use in its intended application (Kumar & Mahto, 2013). Non-destructive testing is also defined as the inspection of material for flaws or characterisation and comparison with some set standard without affecting any of the material's properties (Dwivedi, et al., 2018). Non-destructive tests can be invasive in their nature, such as coring for concrete structures. In coring, a test specimen is extracted from concrete, and alters the visual appearance of the concrete but only marginally affects the mechanical properties of the concrete sample (Helal, et al., 2015). Non-destructive testing seeks to study the materials failure mechanisms and properties without reaching component failure.

2.9.3.1 Visual inspection

One of the most effective methods of detecting macroscopic flaws is to use visual inspection. With a visual inspection, bad welds, joints, improper finishing, cracks, dents, and cavities can be identified (Kumar & Mahto, 2013). However, a disadvantage with this method in concrete testing is that some flaws are difficult to detect with the human eye. Furthermore, this test is subjective, making it unreliable if used as the only source of testing.

2.9.3.2 Acoustic emission testing

Acoustic emission (AE) is the modification of sound waves created when a material is subjected to stress due to an external load. Acoustic emission results are detected with piezoelectric sensors (Dwivedi, et al., 2018). Through acoustic testing, it is possible to detect internal flaws within the concrete slab and measure the extent of the damage.

2.9.3.3 Surface hardness test methods

There are two main testing methods to determine the surface hardness of concrete. These two are indentation methods and rebound methods. The rebound method is the most used for concrete based on set standards. A rebound hammer is used, which gets a recording from the hammer as a rebound number. This number indicates the hardness by correlating the concrete's rebound number and strength properties. The Schmidt rebound hammer is the most used test method. This is a simple method requiring minimum mechanical skill. The Schmidt rebound hammer is pressed against the surface of the test specimen, and a spring-loaded mass is released, causing the plunger to impact against the surface. The rebound distance is then measured, which correlates with the strength properties of the concrete using standard charts. Furthermore, the rebound test can be used to estimate the compressive strength of concrete. Figure 2-28 shows the operation of the Schmidt rebound hammer and the movement of the plunger from A to D as it completes its cycle for measurement of rebound distance.

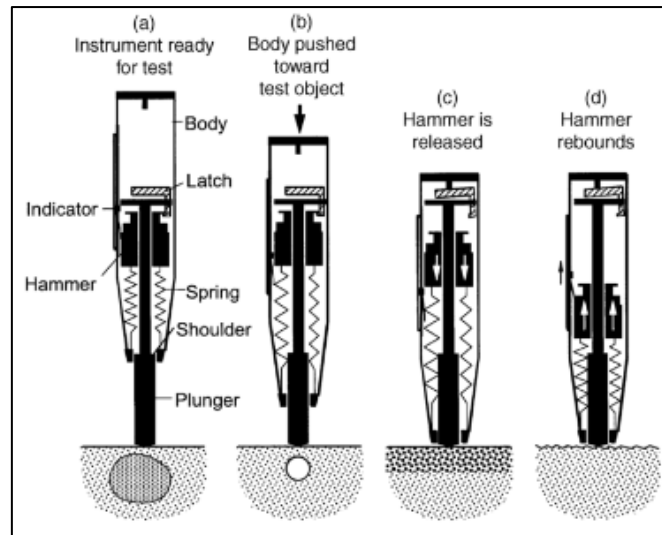


Figure 2-28 – Schematic diagram of a Schmidt rebound hammer test process (Alyamac, et al., 2017)

The rebound tests have a few disadvantages, such as being affected by the smoothness of the surface, geometric properties, age of specimen, moisture conditions, and carbonation of the concrete surface (Maholtra & Carette, 2004). Therefore, it is a good practice to carry out the standard compression testing and not rely entirely on the rebound test results for compressive strength.

2.9.3.4 Maturity test

The maturity test is defined as the test for ascertaining the strength gain of concrete based on the measured temperature history during curing. The maturity factor is cross-referenced to established correlations to establish the maturity of the concrete sample. The maturity test apparatus uses thermocouples that are put into fresh concrete, and the thermocouples measure the time versus temperature to compute a maturity index. The standard used for this test is ASTM C1074-11. Figure 2-29 shows a typical maturity tester with the probes attached.



Figure 2-29 – Maturity test apparatus (Helal, et al., 2015)

2.10 Optimization and modelling

Concrete is a classic example of a ceramic composite with sand and aggregate particles in a cement matrix. Material scientists have researched this mixture extensively, and the idea of mixing with another type of reinforcements is a natural extension of this idea. The properties of materials must be investigated extensively for reproducibility and accuracy. Composite material properties are dependent on the design of the combination of the materials to suit particular end-use. There is a need to be able to predict the resultant properties correctly.

Rohman et al. (2014) showed that multiple linear regression could be used to obtain an empirical formula between the compressive strength of concrete as a dependent variable and percentage recycled coarse aggregate, percentage fly ash and water/cement ratio as independent variables. The empirical formula could be used with 96.6% accuracy to determine the compressive strength of concrete. (Rohman & Aji, 2014).

Optimization of a concrete mixture is defined by Ahmad et al (2014) as a pursuit of a concrete mixture that has the lowest possible cost yet meets all the requirements for concrete use, such as strength and durability. In most previous research, the optimisation of the concrete mixture has been done using entirely experimental methods, fully analytical methods or semi-experimental methods or statistical methods. Experimental methods involve carrying out a lot of practical work and might involve a lot of hit and miss in the approach. This type of optimization has the downfall of being limited to a specific range of raw materials used during the study (Domone & Soutsos, 1994; Ahmad, 2007).

Analytical methods use known information and formulae from previous research to optimize the concrete mixture (Yeh, 2007; Kasperkiewicz, 1994). The main advantage of using analytical methods is that they are less costly and don't require experimental work. Fully analytical methods tend to be less accurate due to variations in the characteristics of the raw materials, which may not be factored into the model.

Semi experimental methods combine analytical and experimental methods in optimizing concrete mixtures. Analytical methods such as artificial neural networks, genetic algorithms and mathematical programming may be used (Lee, et al., 2009; Yeh, 2009; Jayaram, et al., 2009).

Statistical analytical methods use selected trial batches over a chosen range statistically. Trial batches are then fabricated and tested; the experimental results are then analysed using various statistical methods. These methods may include coming up with an empirical model to the data for each performance parameter. In these statistical models, each output response such as tensile strength, compressive strength and slump is expressed as a function of the factors, which may be fibre content, fly ash quantity. From these results, it is possible to build a model that would allow the determination of the effect of changing one of the factors.

2.11 Economic implications of fibre reinforced composites

Cost analysis and estimation are of paramount importance to the performance and sustainability of a business enterprise. Overestimation of the cost of the product can result in low sales and a loss of goodwill for the company. On the other hand, underestimation can result in financial losses for the company. Therefore, it is of great importance to do correct product cost analysis (Niazi, et al., 2006).

Fly ash as a waste by-product is cheaper than Portland cement, resulting in cost savings in the manufacture of concrete. Utilising of fly ash for a value-added product in concrete also lowers the cost incurred by power utility companies such as Eskom in the disposal of this waste.

The use of waste and recycled PET fibre waste lowers the cost of the fabricated slab significantly. Product cost includes the summation of direct material, direct labour, and manufacturing overhead costs.

2.11.1 Direct material costs

Direct material costs are the raw materials used in manufacturing the product. These include the cost of the sand, fly ash, fibres, water, admixtures, and Portland cement in the manufacture of slabs.

2.11.2 Direct labour

Direct labour costs are the cost of labour that goes into making the concrete slabs, and it is limited to only the labour costs that go into the product itself.

2.11.3 Manufacturing overhead

These costs are divided into three: indirect materials, indirect labour, and any other costs. Indirect material costs include those costs of material used that are not directly linked to the slabs being produced. These costs can include measuring instruments and mould fabrication and design.

Indirect labour costs are the costs of labour that is not directly in the making of the concrete slabs but any other labour used in the production of the slabs. This may include the labour used to check the quality of the concrete slabs.

Other costs are those which cannot be classified into any of the above and can include lease and rental costs for the laboratory space. These costs assist in determining the product cost and the product cost per unit.

2.12 Existing knowledge gaps

The following knowledge gaps have been identified based on the review of the literature.

- Literature shows that there is variability in the properties of fly ash from various geographical locations. The variation of properties of ash has a bearing on the mechanical properties of the

developed composite. Hence this study seeks to characterise local fly ash from South African power stations before use to establish its properties.

- There is a contradiction in the literature on the effect of adding PET fibres into concrete on the workability of the mixture. There is a need to further research to clarify this contradiction between various research. Prior studies show that the incorporation of fibres in concrete improves the energy absorption and cracking resistance of concrete (Anand & Dutta, 2013). This improvement demonstrates the feasibility of incorporating PET fibres in enhancing the ultimate strength of concrete.
- Literature has shown that incorporating PET particles tends to lower the compression strength of concrete regardless of the shape of the particles. This decrease is attributed to the weak cohesion between the PET particles and the cement matrix. PET replacement of less than 25% mass fraction is acceptable beyond it lowers the compressive strength rendering the composite unusable for load-bearing applications (Ataei, et al., 2017). The use of PET fibres instead of particles is expected to significantly improve the composite's strength.
- Optimization of a concrete mixture can be carried out through fully experimental methods, fully analytical methods, semi experimental methods, or statistical methods. Experimental methods involve carrying out a lot of practical work and is limited to specific properties of the raw materials that have been used in conducting the experiments (Domone & Soutsos, 1994; Ahmad, 2007). Research that has been done has not given reliable optimised compressive and flexural strength properties for PET and fly ash hybrid composites. This study seeks to address this gap in research by developing a model that can satisfactorily predict and optimise the mechanical properties of PET fibre reinforced hybrid composite in slabs.

CHAPTER 3: RESEARCH DESIGN AND METHODOLOGY

3.1 Introduction

The chapter comprises two main broad sections which are the experimental work and numerical modelling. The first sub-section of the methodology under the experimental work section, 3.4.1 deals with characterisation of the raw materials. The next section, 3.4.2 deals with the fabrication process and experimental design of the FRCC. Thereafter, material characterisation tests of the FRCC are outlined in section, 3.4.3 and 3.4.4. Section, 3.4.5 gives a description of the methods of costing of the FRCC to ascertain its feasibility for industrial production.

The second main section is numerical modelling. Under the section development of numerical modelling is discussed under sub heading 3.5.1. thereafter, model validation method is shown in section, 3.5.2. Response of optimization is outlined in the section, 3.5.3. Lastly, under section 3.5.4 the method of determination of the applications of the developed FRCC slabs is outlined.

3.2 Conceptual framework

This study involves the fabrication of a Fibre Reinforced Concrete (FRC), also known as Textile Reinforced Concrete (TRC), in some instances. The study characterized the raw materials used in the fabrication and shows the fabrication process according to the experimental design. Thereafter, the fabricated FRCC specimens were characterized for mechanical properties. Finally, a model was designed to optimise and predict the properties of the FRCC from the raw materials addressed by this study. Figure 3-1 shows a flow chart of the methodology of this study.

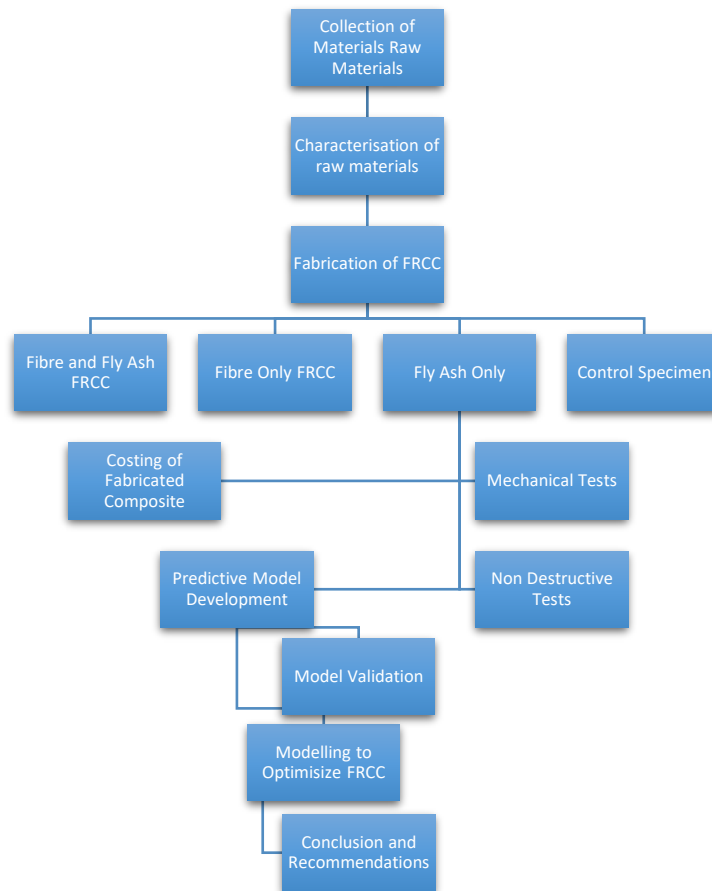


Figure 3-1 – Flow Diagram of Research Design

3.3 Raw materials

Locally available water, cement, fly ash, river sand, and coarse aggregates were used to produce the composite slabs. The fly ash was sourced from the Lethabo thermal power station, Vanderbijlpark, a subsidiary of Eskom. The fly ash was transported in an environmentally friendly method without any spillages or contamination to the environment. The fly ash was transported in double-bagged heavy duty refuse bags of 35 microns with dimensions of 750 mm X 950 mm with a carrying capacity of 80 litres. The cement and aggregates were bought from local hardware shops. The waste PET fibres were sourced readily made from a local fibre extruding company Eco Ace Pvt Ltd.

3.3.1 Cement

The Portland cement used in this study was the locally obtained Suretech Portland cement CEM I 52,5N manufactured by PPC. This cement is of strength class SANS 50197-1 (PPC, 2019). The Suretech

cement is suitable for precast, ready mix, civil speciality, and proprietary products (PPC, 2019). Furthermore, Suretech cement is formulated to allow blending with extenders such as fly ash, and it is ideal for high-performance precast and speciality concrete. Table 3-1 shows the specification sheet of the Suretech PPC cement that was used in this study.

Table 3-1 – Product specifications for Suretech Cement from PPC (PPC, 2018)

Parameter	Physical properties	Result
<i>Setting time:</i>	Initial (mins)	125
	Final (hours)	2.5
	Specific Area (Blaine): m ² /kg	400
<i>Compressive strength (mortar prism EN 196-1)</i>	At 2 days (MPa)	28
	At 28 days (MPa)	52.5
<i>Soundness</i>	Le Chatelier Expansion (mm)	1
<i>Densities</i>	Relative density	3.14
	Bulk density, aerated, kg/m ³	1100 - 1300
	Bulk density, as packed, kg/m ³	1500
	Approximate volume: 50kg bag, 1	33

The cement bags were stored in the lab under a plastic tapeline cover to prevent moisture from contaminating the bags.

3.3.2 Water

Clean tap water from the municipality treatment facilities was used in this study. Approximately 22% by weight of the concrete samples contain water. This necessitated approximately 636 litres of water for the concrete samples and 600 litres for cleaning tools and maintaining the samples wet during the curing period.

3.3.3 PET fibres

Waste PET fibres were sourced from a local recycling company, and the fibres were manufactured from recycled PET bottle material. The specification sheet of the fibres is as shown in Table 3-2.

Table 3-2 – Properties of PET fibres (Eco Ace, 2020)

Property	Specification
Appearance	White staple fibre
Chemical Name	Polyethylene terephthalate
Description	Thermoplastic fibre, round and uncrimped
Fibre diameter	18µm
Fibre count per gram	231.4 for 12mm fibre and 462.9 for 6mm fibre
Specific density	1.34 – 1.4
Melting point	254 °C
Autoignition temperature	515 °C
Physical state	Solid
Moisture regain	0.5%
Solubility in water	Not soluble
Solvents	None
Tenacity at break	45 cN/Tex (+/-5)
Elongation at break	40% (+/-)
Fibre tenacity at 10% elongation	>10 cN/Tex

According to the experimental design, the fibres used in this study were 12 mm in length.

3.3.3.1 Fibre length

The fibre length used in the FRCC slabs was above the critical length. The critical length was calculated using the Cox model (Lacroix, et al., 1992). The critical aspect ratio is the point where the central axial stress in the fibre equals the ultimate tensile strength of the fibre. Use of fibres above critical length ensured that the fibres were of optimum length. Thus, the matrix and fibre failed simultaneously. The fibre should experience its fracture stress at the midpoint, with the average stress carried in the fibre being one half of that value. The critical length was calculated using the formula shown in equation 3-1. The critical length is dependent on the fibre diameter (d) and its ultimate tensile strength (σ_f) and on the fibre matrix bond strength (τ_c).

$$l_c = \frac{\sigma_f d}{2\tau_c} \quad 3-1$$

3.3.4 Fly ash

Fly ash used in this research was obtained from the Lethabo thermal power station. Lethabo power station is located between Vereeniging and Sasolburg in the Free State. The daily production of fly ash at the Lethabo power station is approximately 20 000 tons per day (Eskom, 2019). The coal burnt in the Lethabo power plant has a caloric value of approximately 16 MJ/kg, which is considerably low compared to coal used in other power plants around the world.

3.3.5 Aggregates

The river sand fine aggregate and coarse aggregate used in this study were sourced from local hardware suppliers.

3.4 Experimental work

Experimental work was carried out in this study, which included characterisation of fly ash's mechanical properties and coarse and fine aggregates. Fabrication of the FRCC specimens was then carried out. Thereafter destructive and non-destructive testing of the specimens was carried out.

3.4.1 Characterisation of raw materials

Characterisation of fly ash's physicochemical properties and the aggregates' physical properties were carried out. The characterisation of the raw materials was of utmost importance in order to give scope to the model that was to be developed and understand the limitations of the model.

3.4.1.1.1 Physicochemical characterisation of Fly ash

The fly ash was characterised prior to its use to ascertain its physical and chemical properties. The following 6 properties were investigated.

3.4.1.1.2 True Density

True density is the weight per unit volume of the fine fly ash powder sample. To determine the true density, the fly ash sample was dispersed in water. The amount of water dispersed per gram of fly ash gives the true density of the fly ash. The test was carried out in accordance with ASTM C188 (ASTM C188-14, 2014) test method. The true density was obtained by use of a measuring jar filled with water to a predetermined level which was noted. Thereafter, 20 g of fly ash was added to the jar, and the new water level was noted. This test was repeated with four samples to obtain an average of the true density. The true density was then be calculated using equation 3-2.

$$Density = \frac{Mass}{Volume} \quad 3-2$$

3.4.1.1.3 Moisture regain

The moisture regains of the fly ash was measured by heating the fly ash to remove moisture using a hot air oven shown in Figure 3-2 in accordance with ASTM D2974 (ASTM, 2019). Thereafter, the fly ash was cooled in a desiccator and then weighed. The loss in weight was then reported as moisture (on a % basis). About 2 g of air-dried fly ash sample was weighed in an electronic balance of accuracy of 0.001 g and then placed in an electrically heated oven at $75\text{ }^{\circ}\text{C} \pm 2$. The fly ash sample was allowed to remain in the oven for 2 hours intervals and thereafter, taken out of the oven and weighed. The weight was recorded over 24 hours, and the final oven-dry weight was taken when three similar consecutive weights were recorded.

The loss in weight was reported as the moisture regain and recorded as a percentage. The moisture regain was calculated using equation 3-3.

$$\text{Moisture Regain (\%)} = \frac{\text{Initial weight} - \text{Oven dry weight}}{\text{Initial weight}} \times 100$$

3-3



Figure 3-2 – Oven used for drying out fly samples

3.4.1.1.4 Morphology analysis

The morphology of the fly ash particles obtained from the Eskom thermal power station was studied using an SEM with an EDS attachment. This analysis indicated the fly ash morphology, composition, and electrical conductivity.

3.4.1.1.4.1 Coating of sample

The fly ash sample was laid on the stage plate and blown with compressed air to ensure it was of the correct fineness. The fly ash sample was then gold coated with 5 nm gold using Quorum Q150R ES Plus Machine shown in Figure 3-3. The terminate thickness used was 5 nm, and the sputter current was set as 20 mA.



Figure 3-3 – Quorum coating machine

3.4.1.1.4.2 Morphology and chemical composition

The JSM IT500LA JEOL SEM shown in Figure 3-4 was used to analyse the morphology of the fly ash particles. Back Scattered Electron imaging (BSE) and Energy Dispersive Spectroscopy (EDS) were used to characterise the fly ash particles' morphology and constituent. Furthermore, the EDS technique was used to determine the different elements and oxides present in the fly ash sample.



Figure 3-4 – JEOL SEM Machine

3.4.1.1.5 Particle size distribution

The particle size distribution (PSD) of particles dispersed in a fluid is a list of values or a mathematical function that defines the relative amounts of particles present according to size. The particle size distribution was measured by the use of laser light scattering using the Malvern 2000G instrument shown in Figure 3-5 in accordance with ASTM D6941-19 (ASTM, 2019). The testing instrument measures particle sizes in the range of 0.02-2000 μm by use of the laser light scattering principle. For particle sizes greater than 0.4 μm the instrument uses Fraunhofer theory of laser diffraction and for the particle size $< 0.4 \mu\text{m}$ the Mie-theory of light scatter.



Figure 3-5 – Malvern 2000G PSD analyser

The particle size distribution and surface area values were determined using a PSD analyser. The sample was passed three times through the PSD to validate the results. Thereafter, using the obtained data points, a plot of the size distribution was obtained by using the weighted average of particles at certain intervals obtained from the PSD analyser.

3.4.1.1.6 Determination of active phases

X-ray diffraction (XRD) analysis was carried out on the fly ash sample to determine the ash's active phases, structure, and crystallinity. A Shimadzu XRD-7000 X-ray diffractometer machine shown in Figure 3-6, was used in accordance with ASTM C1365-18 standard. The diffraction patterns obtained were used to show the degree of disorder in the fly ash.

The source of radiation in the XRD machine was Copper $K\alpha$. The fly ash sample specimen was placed in a cylindrical holder with a diameter of 10 mm and a depth of 3 mm. The sample was then placed in the XRD machine and analysed from 20° to 80° at a speed of one degree per minute.



Figure 3-6 – XRD Diffraction analysis of fly ash sample on XRD-7000 Shimadzu

The sample preparation used in this setup was the randomly oriented powder mount technique. The aluminium holder with a circular hole was covered with sticky pad paper. The stick pad paper was then covered with a glass slide which was tapered into place and the mount inverted. The fly ash powder was then placed into the exposed well and compacted with a spatula, and slight excess was added then a second glass slide was taped to the aluminium frame. After that, the sample was turned around, and the original glass slide and paper were removed, leaving the plane face of fly ash particles ready to be tested in the XRD machine. Interpretation of the patterns for the presence of crystalline components was carried out by use of software assigning the different peaks to the matching crystalline substances that might be present.

3.4.1.2 Aggregate characterisation

Mechanical characterisation tests were conducted on both the fine and coarse aggregates.

3.4.1.2.1 Fine aggregate characterisation

The fine aggregate consisted of river sand sourced from a local hardware shop and supplied in polypropylene bags. Tests carried out on the river sand included specific gravity analysis, particle size distribution and water absorption tests as outlined in the following subsections.

3.4.1.2.1.1 Specific gravity analysis

Sieve analysis of aggregates was carried out in accordance with ASTM C136-96a, which governs the minimum and maximum percentage passing standard sieves (ASTM C136-96a, 2004). The weight of

the pycnometer was taken and recorded as W_1 . The pycnometer was then filled with sand up to approximately a quarter of the way up, and the weight was taken and recorded as W_2 . This arrangement is shown in Figure 3-7. The pycnometer was then filled with distilled water on top of the sand and shaken to remove any air voids. The weight of the assembly was then recorded as W_3 . After that, the sample and water were completely removed, and the pycnometer was cleaned. The pycnometer was then filled to the top with water and weighed and the weight was recorded as W_4 .

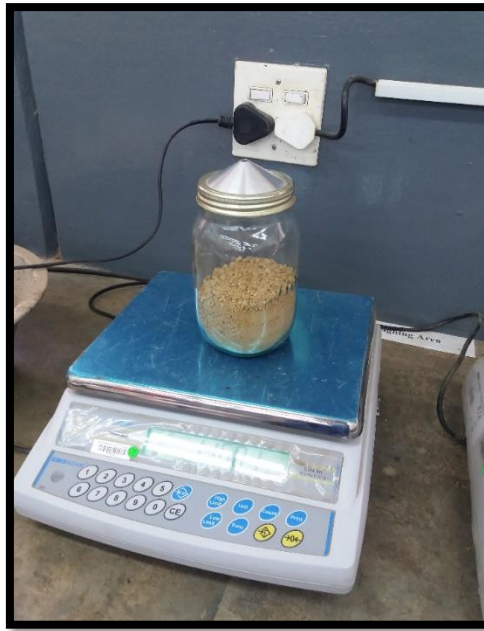


Figure 3-7 – Specific Gravity Test for Fine Aggregates

The specific gravity was then calculated using equation 3-4.

$$\text{Specific Gravity} = \frac{(W_2 - W_1)}{(W_4 - W_1) - (W_3 - W_2)} \quad 3-4$$

3.4.1.2.1.2 Particle Size Distribution

Particle size distribution was carried out through dry sieving in accordance with SANS 3001-AG1– Part AG1. A pre-weighed 1 kg sample of sand was poured onto sieves arranged in order of decreasing size from the top to the bottom, as shown in Figure 3-8. The sieves were arranged as follows 4.75 mm, 2.00 mm, 1.18 mm, 600 μm , 425 μm , 150 μm and a pan.



Figure 3-8– Sieving Apparatus Set Up

The sand was poured onto the sieves and put on a sieve-shaker where it was shaken for approximately 2 minutes. Thereafter, the quantity retained by each sieve was weighed and recorded on an observation sheet. The weight of aggregate captured in the pan was also recorded.

3.4.1.2.2 Coarse aggregate characterisation

The coarse aggregate consisted of 13 mm dolomite stone purchased from a local hardware supplier. This aggregate was characterised to determine particle size distribution, shape, texture, and specific gravity analysis.

3.4.1.2.2.1 Particle Size Distribution

Particle size distribution was carried out through sieving in accordance with SANS 3001-AG1 – Part AG1. A pre-weighed 1kg aggregate sample was poured onto sieves arranged in order of decreasing size from top to bottom. The sieves were arranged as follows 20 mm, 16 mm, 12.5 mm, 10 mm, 4.75 mm, and pan. The aggregate was poured onto the sieves and gently shaken for approximately 2 minutes in a sieve shaker shown in Figure 3-9. Thereafter, the quantity retained by each sieve was weighed and recorded on an observation sheet. The weight in the pan was also recorded.

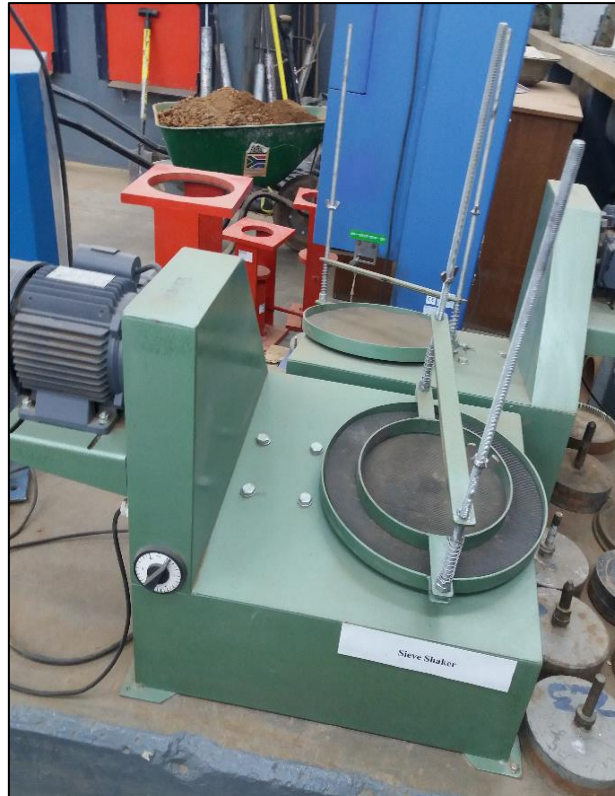


Figure 3-9 – Sieve shaker

3.4.1.2.2.2 Particle shape and texture

The particle shapes were graded according to ASTM D3398, which governs the maximum percentage of flat and elongated particles.

3.4.1.2.2.2.1 Flakiness index test

Flakiness Index test was carried out in accordance with ASTM 4791-10. The flakiness test was carried out to ascertain the suitability of the coarse aggregate for use in slabs. The sample of aggregate taken randomly was sieved and thus separated into a specific range of sizes. A minimum of 200 pieces were used from each size fraction and weighed using a scale to the accuracy of 0.01 g. The weighed aggregates were then passed through the appropriately sized slot on the thickness gauge, as shown in Figure 3-10. The flaky material that passed through the appropriately sized slot range was added and weighed. The weight obtained was then divided by the total weight of sample taken from different range of sizes and the ratio expressed as a percentage which is the flakiness index as shown in equation 3-5.

$$\text{Flakiness Index} = \frac{\text{Total weight retained on elongation gauge}}{\text{Total weight of test sample}} \times 100 \quad 3-5$$



Figure 3-10 – Coarse Aggregate Flakiness Test

3.4.1.2.2.2.2 Coarse aggregate elongation test

The sample taken was oven-dried at $100\pm 5^{\circ}\text{C}$ to constant mass. The material was then sieved in sieve sizes 19 mm, 16 mm, 13.20 mm, 9.50 mm, 4.75 mm. Each of the aggregate in each size fraction was tested and segregated into four groups, namely:

- (i) flat particles,
- (ii) elongated aggregates,
- (iii) aggregates that meet the criteria of (i) and (ii),
- (iv) neither flat nor elongated particles that do not fall into either (i) or (ii).

Each particle was subjected to a flat particle test and elongated particle test. The particles found to be flat but not elongated were placed in a designed flat group, and those particles found not to be flat but elongated were placed in the elongated group. Those flat and elongated particles were placed in a group for particles that met both (i) and (ii) criteria. Particles that were not flat and not elongated were grouped into particles that did not meet the criteria of either group (i) or (ii).

By use of an elongation device, the particles were tested and separated, as shown in Figure 3-11. Thereafter, the mass of each group was determined.



Figure 3-11 – Coarse Aggregate Elongation Test

The aggregate elongation was then determined using equation 3-6.

$$\text{The elongation Index} = \frac{\text{Total weight retained on elongation gauge}}{\text{total weight of test sample}} \times 100 \quad 3-6$$

3.4.1.2.2.3 Specific gravity and absorption of coarse aggregate

This test was carried out in accordance with SANS 5843:2008, which is the standard test method for specific gravity and absorption of coarse aggregates. A constant sample was taken with a weight of 1 kg and dried at a temperature of $110 \pm 5^\circ\text{C}$. Thereafter the aggregate sample was cooled at room temperature for 1 to 3 hours. The aggregate was then immersed in water at room temperature for 24 hours \pm 4 hours. The test sample was then removed and rolled on a mutton cloth until all surface water had been removed, as shown in Figure 3-12. The test sample was then weighed in the saturated surface dry condition. This reading was taken to the nearest 0.05% of the sample weight. After weighing the surface, the dry test specimen was placed in a container and determined its weight in water at $23 \pm 1.7^\circ\text{C}$, having a density of $997 \pm 2 \text{ kg/m}^3$. Care was taken to remove all trapped air before weighing through the shaking container while immersed to remove air. The sample was then dried to constant mass at a temperature of $110 \pm 5^\circ\text{C}$, then cooled at room temperature for 1 to 3 hours and then weighed again. Constant mass was determined by successive weighing performed at least 1 hour apart and not differing by $>0.1\%$.

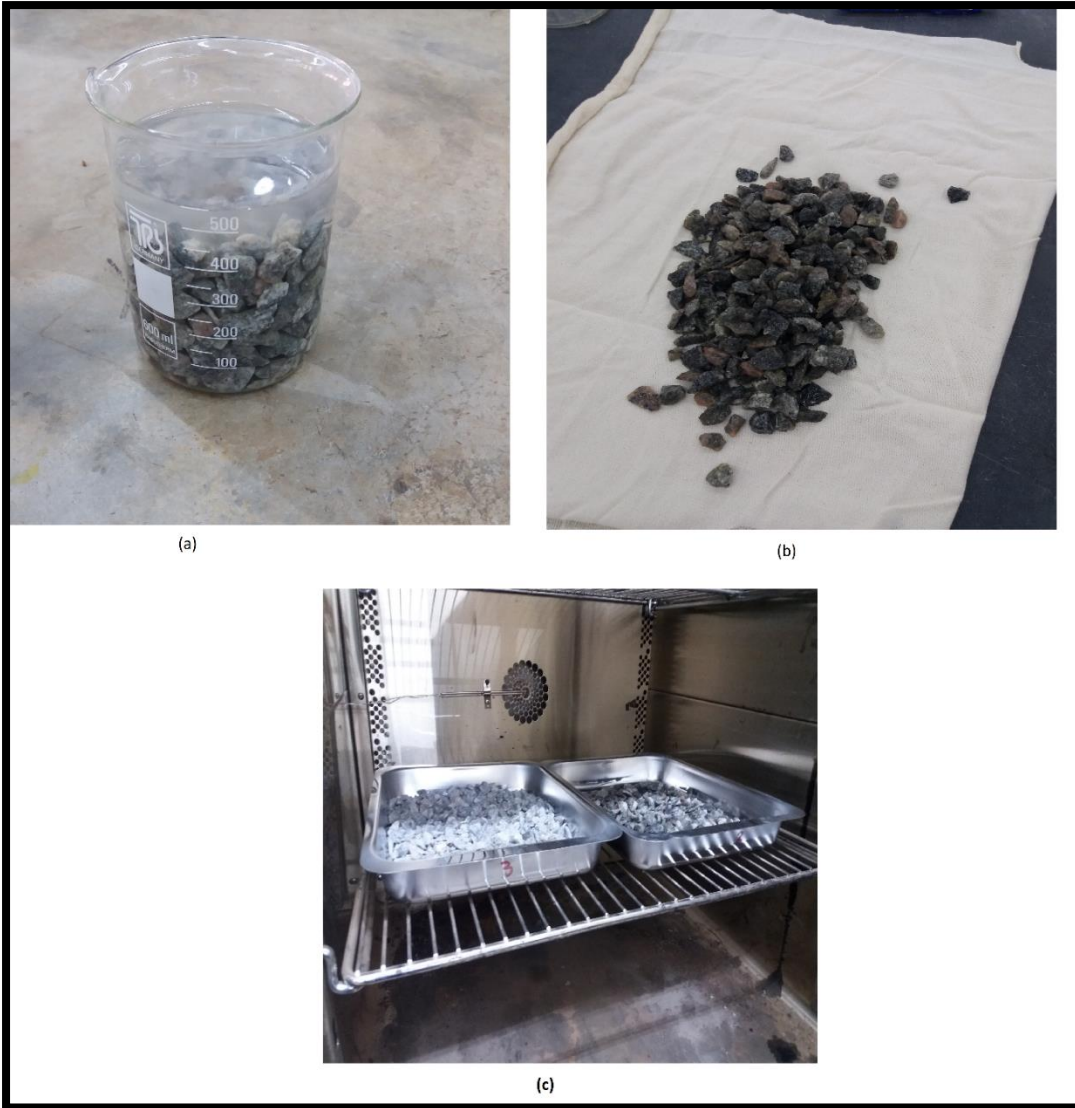


Figure 3-12 – (a) Aggregate immersed in water for 24 hrs (b) Removal of excess moisture (c) Oven drying for 24 hrs

The bulk specific gravity was calculated using equation 3-7.

$$\text{Bulk specific gravity} = A / (B - C) \quad 3-7$$

Where:

A – The weight of oven-dry test sample in grams

B – Weight of saturated surface dry test sample in the air in grams

C – Weight of saturated test sample in water in grams

The apparent specific gravity was calculated using equation 3-8.

$$\text{Apparent Specific Gravity} = A/(A - C) \quad 3-8$$

The specific gravity was calculated using equation 3-9.

$$\text{Specific Gravity} = \frac{D}{C - (A - B)} \quad 3-9$$

The percentage absorption was calculated using equation 3-10.

$$\text{Water Absorption (\%)} = \left[\frac{C - D}{D} \right] X 100 \quad 3-10$$

3.4.2 Fabrication of fibre reinforced cement composite

A full factorial experimental design was used, and the concrete was mixed in accordance with SANS5861-1, as outlined in the subsequent sections.

3.4.2.1 Design of experiments

A 2 factor and five levels full factorial experimental design was used to ascertain the effect of mass fraction of the PET fibres, fly ash and aggregates on the properties of the concrete composite slab. A total of 25 experimental runs were generated using the full factorial experimental design of response surface methodology. The full factorial experimental design can be used to predict dependent variables, also known as responses by using a small number of experimental data points, with all the parameters varied within a preferred and set range. 5 level experimental design with two factors, namely mass fraction of the PET fibres and fly ash, was developed using Minitab Software Version 17, Figure 3-13. Each factor was varied over five levels. The dependent variables included the slump value, compressive strength, flexural strength, split tensile strength and total cost.

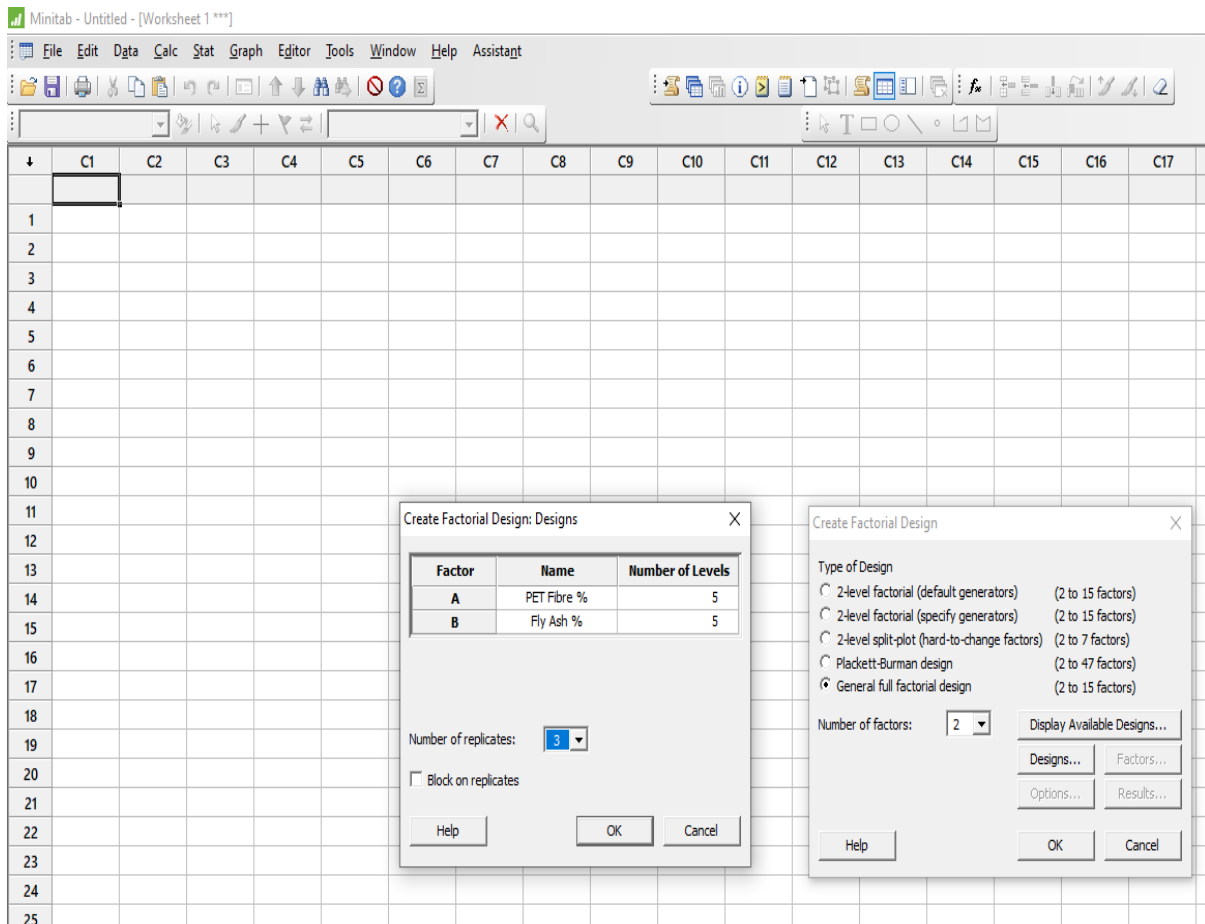


Figure 3-13 – Creation of general full factorial experimental design

Thereafter, the levels used in the experimental design shown in Table 3-3 were programmed.

Table 3-3 - Composite experimental design with values X_f of the independent variables

Variable	Parameters	Levels				
		1	2	3	4	5
X_1	PET Fibre Mass Fraction (%)	0.0%	0.5%	1%	1.5%	2.0%
X_2	Fly ash Mass Fraction (%)	0.0%	15%	20%	25%	30%

Minitab software was then used to generate the multilevel full factorial experimental design followed in generating the test samples, as shown in Figure 3-14.

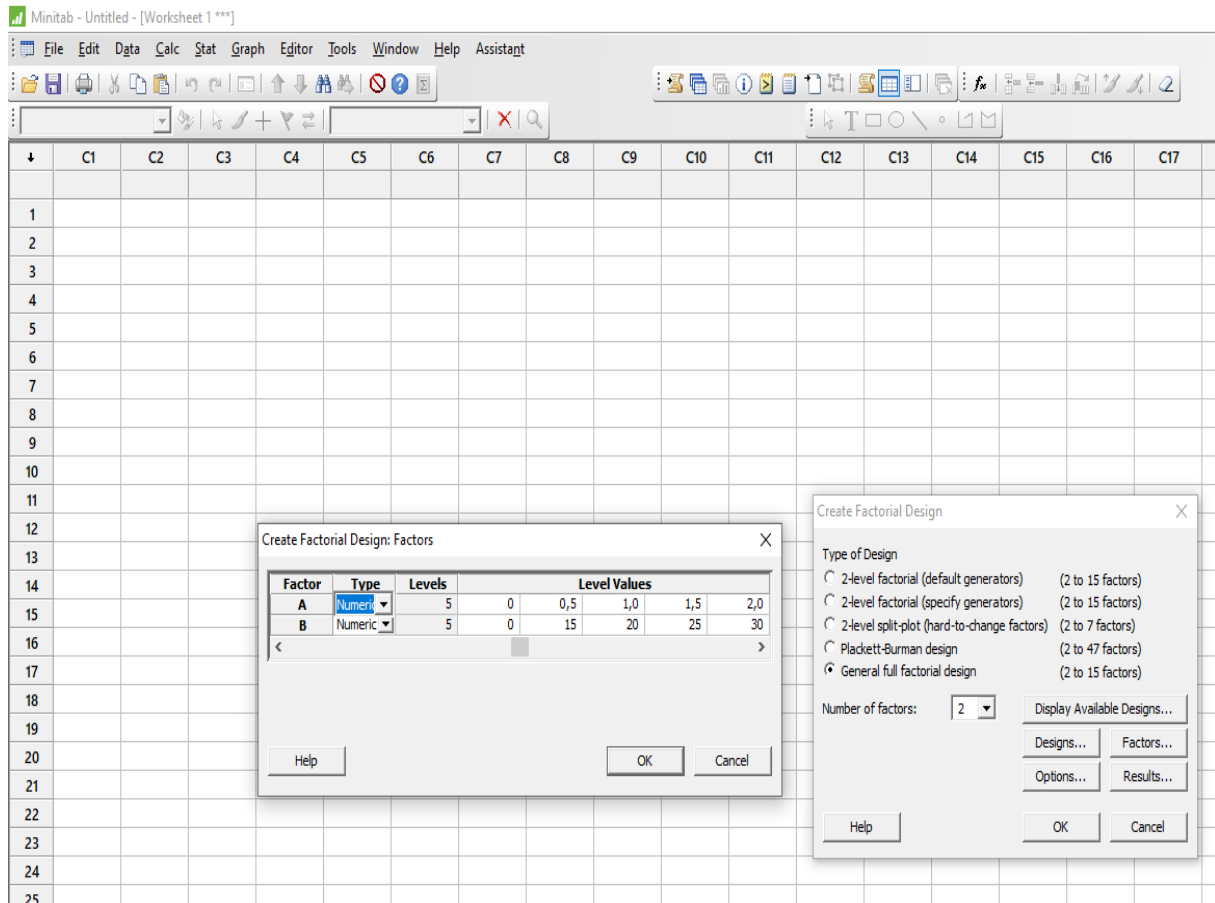


Figure 3-14 – Selection of the level values

The generated full experimental design that was followed in this study is outlined in Table 3-4. Table 3-4 also shows the details of all mix proportions in kilograms per cubic metre.

Table 3-4 – Multilevel full factorial experimental design mix

Code	PET Fibre Mass Fraction (%)	Fly Ash Mass Fraction (%)	Design Materials for FRCC					
			Cement	Fine Aggregate	Coarse Aggregate	Fly ash	Fibre	Water
			Kg/m ³	kg/m ³	kg/m ³	kg/m ³	kg/m ³	kg/m ³
S3	0	0	346,50	519,75	1093,50	0,00	0,00	207,90
S20	0	15	294,53	546,75	1093,50	51,98	0,00	176,72
S21	0	20	277,20	546,75	1093,50	69,30	0,00	166,32
S22	0	25	259,88	546,75	1093,50	86,63	0,00	155,93
S23	0	30	242,55	546,75	1093,50	103,95	0,00	145,53
S24	0,5	0	346,50	546,75	1093,50	0,00	9,93	207,90
S4	0,5	15	294,53	546,75	1093,50	51,98	9,93	176,72
S8	0,5	20	277,20	546,75	1093,50	69,30	9,93	166,32
S12	0,5	25	259,88	546,75	1093,50	86,63	9,93	155,93
S16	0,5	30	242,55	546,75	1093,50	103,95	9,93	145,53
S25	1	0	346,50	546,75	1093,50	0,00	19,87	207,90
S5	1	15	294,53	546,75	1093,50	51,98	19,87	176,72
S9	1	20	277,20	546,75	1093,50	69,30	19,87	166,32
S13	1	25	259,88	546,75	1093,50	86,63	19,87	155,93
S17	1	30	242,55	546,75	1093,50	103,95	19,87	145,53
S26	1,5	0	346,50	546,75	1093,50	0,00	29,80	207,90
S6	1,5	15	294,53	546,75	1093,50	51,98	29,80	176,72
S10	1,5	20	277,20	546,75	1093,50	69,30	29,80	166,32
S14	1,5	25	259,88	546,75	1093,50	86,63	29,80	155,93
S18	1,5	30	242,55	546,75	1093,50	103,95	29,80	145,53
S27	2	0	346,50	546,75	1093,50	0,00	39,74	207,90
S7	2	15	294,53	546,75	1093,50	51,98	39,74	176,72
S11	2	20	277,20	546,75	1093,50	69,30	39,74	166,32
S15	2	25	259,88	546,75	1093,50	86,63	39,74	155,93
S19	2	30	242,55	546,75	1093,50	103,95	39,74	145,53

Factors: 2 Replicates: 3
Base runs: 25 Total runs: 25
Base blocks: 1 Total blocks: 1

Number of levels: 5, 5

The water to cementitious materials ratio was held constant throughout the mix design at 0.6 in order to ensure acceptable workability of the concrete mixture with fibre addition.

3.4.3 Fresh concrete mixture

Concrete was mixed in accordance with SANS5861-1 using a hand mixing technique. The ambient temperature was recorded and maintained between 22°C and 25°C for storage of the materials. The concrete was mixed in a laboratory with a shovel inside a wheelbarrow, as shown in Figure 3-15. The

cement and fine aggregate were mixed first in accordance with SANS5861-1, then the coarse aggregate and fibres were added and mixed thoroughly until the coarse aggregate was uniformly distributed in the mixture. The fibres were sprinkled over the mixture while mixing to avoid clumping of the fibres. Water was then added slowly until the batch appeared homogeneous and of uniform consistency.

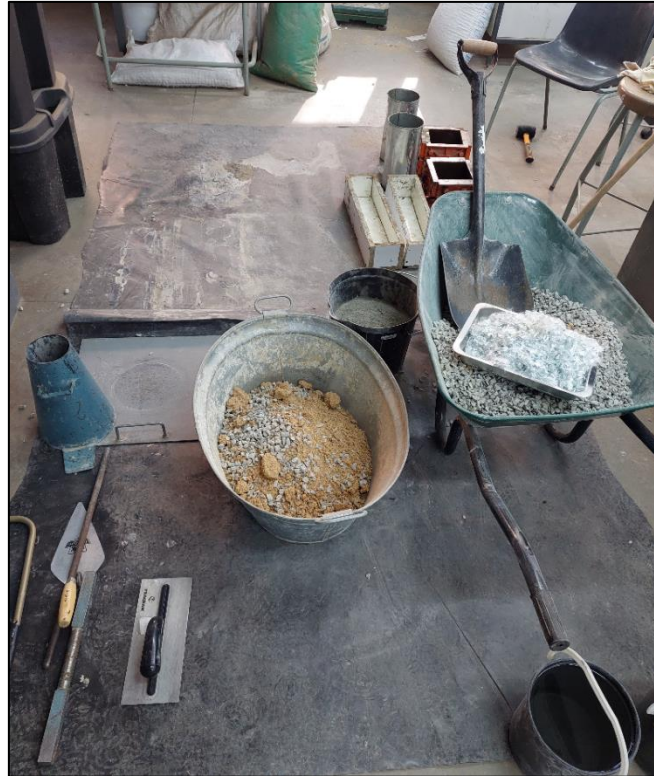


Figure 3-15– Showing Concrete Hand mixture

The Portland cement and sand were measured and blended for 3 minutes to obtain a homogeneous mixture. The fly ash and weighed PET fibres were then added to the mixture. Water was constantly added to the mixture until there was equal distribution. The concrete mix was then placed in a lubricated mould of dimensions consistent with the test to be carried out. The samples were covered with a damp hessian sack for 24 hrs and then demoulded and put into temperature-controlled water tanks as shown in Figure 3-16 at $23^{\circ}\text{C} \pm 2^{\circ}\text{C}$ for 28 days.



Figure 3-16 – Curing Tank

3.4.3.1 Workability of concrete mixture

Slump tests were done in accordance with SANS 5862-1:2006 to check the consistence of the concrete and indirectly give the workability of the concrete mixture.

3.4.3.1.1 Slump test

A representative composite sample was obtained in line with SANS 5861-2 from the freshly mixed concrete sample. The mould for the slump test was cleaned and placed on a horizontal surface. This test equipment that was used included a mould, base plate, 16 mm diameter steel tamping rod and steel ruler. To minimise the variations of surface friction on the slump test, the inside of the mould was moistened before each test. This moisturization was necessary to reduce the surface friction. The area surrounding the cone base was cleaned from any concrete that may have accidentally been spilt.

The mould was then filled with the fresh concrete in three layers, with each layer being about a third of the height of the mould. Each layer tampered with the metal rod. After the final layer had been done, excess concrete was removed from the surface using a sawing and rolling motion of the tampering rod. Thereafter, demoulding was done by raising the mould upwards and slowly. The lifting time of the cone took 3 to 7 seconds. The time between the filling of the cone and the lifting did not exceed 2 ½ minutes in accordance with the standard. The slump was measured after placing the cone beside the concrete slump, and the tampering rod was placed over the cone such that it comes over the area of the concrete slump, as shown in Figure 3-17. The difference in height (h), as shown in Figure 3-17 of the concrete to the mould, was noted to the nearest 5 mm. The slump after demoulding was measured to the nearest 5 mm in accordance with the SANS standard.

The slump was calculated using equation 3-11 (Hoang & Pham, 2016).

$$\text{Slump} = h_m - h_s \quad 3-11$$

Where:

h_m – Height of the mould in mm

h_s – Height of the slumped test specimen in mm



Figure 3-17 – Concrete slump test

3.4.4 Testing of specimens

Mechanical tests and non-destructive tests were carried out on the fabricated composite slabs in accordance with ASTM and SANS standards.

3.4.4.1 Mechanical Testing

The mechanical tests that were carried out include flexural, compressive, tensile strength, water absorption and rebound hammer test. These tests are outlined in the following subsections.

3.4.4.1.1 Flexural Strength Test

The FRCC flexural strength and modulus were determined on model number 1887B0001 ELE machine shown in Figure 3-18. in accordance with ASTM C78. This test uses a simple beam with four point loading (ASTM C78-00, 2004).

The mould used for this flexural test was of dimensions 150 mm X 150 mm X 510 mm. After placing the concrete in the mould, it was spaded with a trowel along the perimeter of the mould. The concrete beams were rodded 60 times evenly across the beam. It was also necessary to tap the sides of the mould using a mallet to close any holes left in the beam from the tampering rod. Any holes left by the tampering rod could be potential sites for the ingress of air and the development of voids within the concrete. The beam was then levelled off with a trowel. The mould was then removed, and the sample saturated in water. Thereafter, the test sample was weighed and measured to calculate the specific weight and the area. The flexural strength of the fibre reinforced concrete sample was then ascertained by subjecting the sample to flexure under transverse load, as shown in Figure 3-19. The modulus of rupture is a theoretical maximum tensile strength reached in the bottom fibre of the test sample. The flexural strength machine had two steel rollers that support the frame at 40 cm apart. The rate of loading was set at 180 kg/min.



Figure 3-18 – Flexural Strength set up

The load in the four-point testing is distributed evenly between the two top-loading rollers. The load was increased at a 6.3 kN/min rate until the sample failed (Alotaibi & Galal, 2018). If the concrete

fracture initiated in the tension surface within the middle third of the span length, the modulus of rupture was calculated as shown in equation 3-12.

$$R = \frac{PL}{bd^2} \quad 3-12$$

Where:

R - The modulus of rupture (MPa)

P – The maximum applied load indicated by the testing machine (N)

L – Span length (mm)

b – The width of the specimen in millimetres (mm)

d – The depth of the specimen in millimetres (mm)



Figure 3-19 – Four Point flexural strength test setup

However, if the fracture of the fibre reinforced concrete occurred in the tension surface outside the middle third of the span length by not more than 5% of the span length, then the modulus of rupture was calculated as shown in equation 3-13.

$$R = \frac{3Pa}{bd^2} \quad 3-13$$

Where:

a - Average distance between the line of fracture and the nearest support (mm)

3.4.4.1.2 Compressive Strength Test

A compressive test was carried out on the FRCC to determine the yield stress and compressive strength. The standard used for the compressive tests on the concrete was SANS 5836:2006.

A steel cube mould (150 mm X 150 mm X 150 mm) was used for casting cubes within 15 minutes of mixing the concrete. The samples were cured for 28 days in the water tank and thereafter tested. The samples were removed from the water and excess water was wiped off. The weight of each cube was then taken and recorded. Testing was carried out on an Ele 1887B0001 compressive testing machine. The samples were placed in the machine with the sample faces that were in contact with the true plane surfaces of the mould. The compression load rate was applied at a 6.8 MPa until the specimen failure. The ultimate load at failure and stress were recorded, and the compressive strength was calculated as shown in equation 3-14.

$$f_m = P/A \quad 3-14$$

Where:

f_m – Compressive strength (MPa)

P – Total maximum load (N)

A – Area of loaded surface (mm²)

Figure 3-20 shows the cube compressive strength tester (Model number 1887B0001 ELE machine) that was used.



Figure 3-20 - ELE 1887B0001 Compressive strength tester machine

$$T = \frac{2P}{\pi ld}$$

Where:

T – Splitting tensile strength

P – Maximum applied load indicated by the testing machine (kN)

l – Length in (m)

d – Diameter in (m)

3.4.4.2 Non-destructive test

As part of the non-destructive test, a visual and rebound hammer test (ASTM C806-02) were carried out as outlined in the subsections hereafter.

3.4.4.2.1 Visual inspection

The surface of the composite was inspected visually for any signs of crazing, cracking or delamination. These imperfections were noted, and further investigation was carried out to ascertain the effect on the mechanical properties of the composite.

3.4.4.2.2 Rebound hammer Test

A rebound hammer test was carried out on the fabricated FRCC using a Rebound Hammer tester shown in Figure 3-22. The hardness test gave an indication of the quality and strength of concrete. This test ascertains the in-plane uniformity of concrete to delineate regions of poor quality. The test was done in accordance with ASTM C806-02 (ASTM C806-02, 2004).



Figure 3-22 – Rebound Hammer Test

The test area was prepared prior to testing by grinding the concrete surface until it was flat and did not contain any loose mortar. The concrete surface was wiped free of excess moisture. The test was carried out by placing the plunger perpendicular to the test surface. The rebound number was recorded to the nearest whole number. Ten readings were taken from each test area on two opposite faces in the non-casting direction. The average of the ten readings was then calculated and taken as the rebound number for the sample. Furthermore, no two tests were carried out within 25 mm of each other.

3.4.5 Costing of the fabricated composite

The costing of the fabricated FRCC was done, factoring in the cost of all the raw materials, time and labour involved in the process. The costing indicated the cost of a kilogramme per cubic metre (kg/m^3). The cost depends significantly on the cost of cement. However, when it is replaced by waste PET fibres and fly ash, there can be significant cost savings. The lower cost of polymeric waste and fly ash provides an impetus towards greener construction materials.

3.4.5.1 Direct materials

The cost of the raw materials, which include the sand, fly ash, fibre, water, admixtures, and Portland cement, was calculated under direct material costs. This cost was directly influenced by the experimental design and the quantities of each material incorporated into each slab. The cost of transport was not factored in for the various mix designs for all the raw materials as these costs are dependent on the location of the manufacturing plant. The indirect costs were not considered in this study as it is assumed that these costs are not affected by the current study (Babaie, et al., 2019)

3.5 Numerical modelling

Modelling was carried out in order to develop a multi objective functions composite slab predictive model that was also able to optimise the response parameters. Modelling was done using Minitab software as outlined in the following subsequent sub-sections.

3.5.1 Development of model

Modelling and statistical analysis were carried out using Minitab software. The experimental data was entered thereafter, factorial response optimization was carried out. Optimization was carried out on the major strength parameters of the slabs, which includes the split tensile, compressive, and flexural strength.

The response surface design was first carried out through the Stat>DOE>Response Surface> Analyse response surface. This procedure was carried out to create the design model. The continuous optimised factors were selected, as shown in Figure 3-23. The continuous factors to be optimized are the fibre and the fly ash mass fraction.

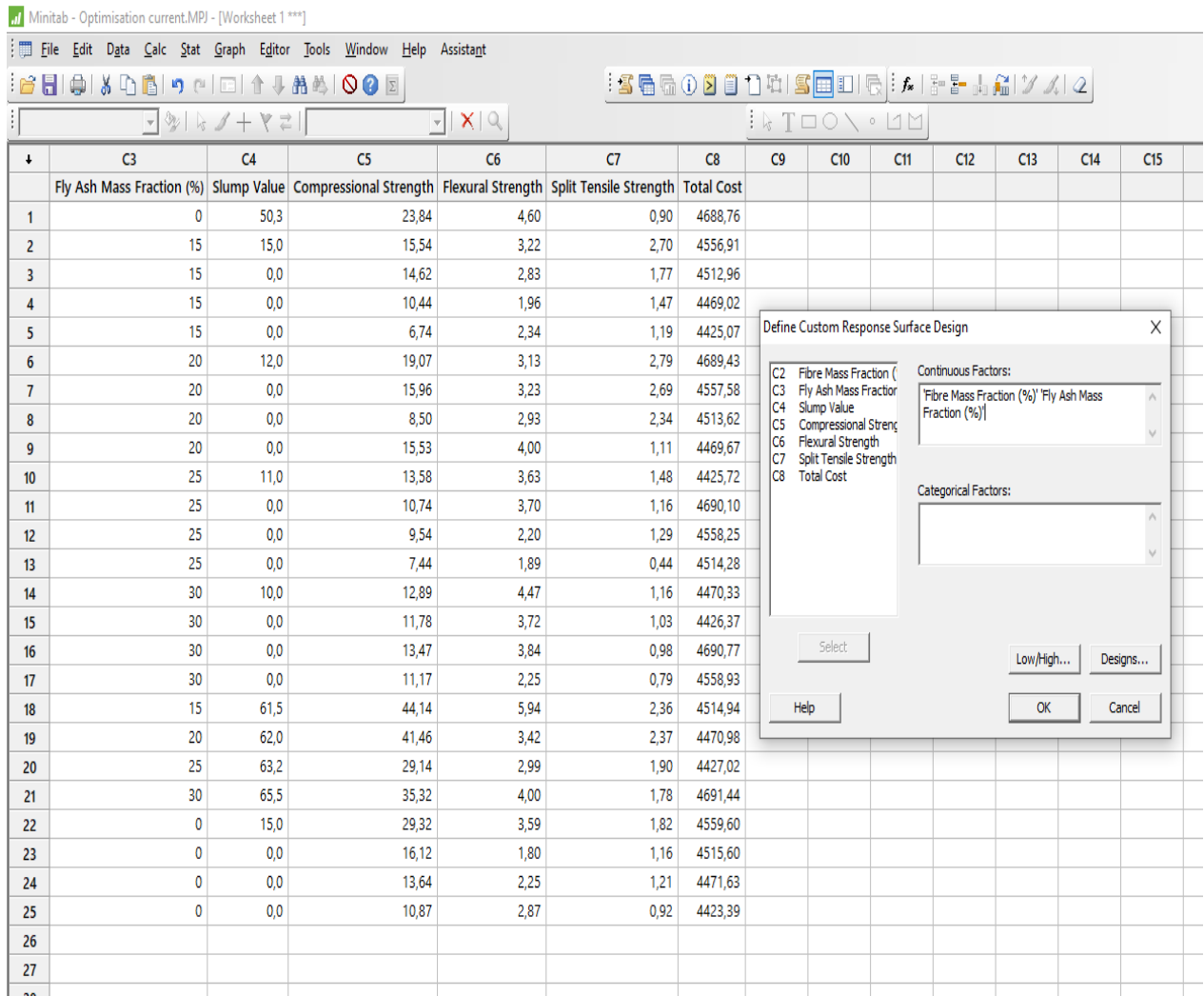


Figure 3-23 – Defining Response Surface Design

The responses to be analysed were then selected to create the response surface design. The responses to be considered in the optimization were the slump value, total cost, compressive, flexural, and split tensile strength, as shown in Figure 3-24.

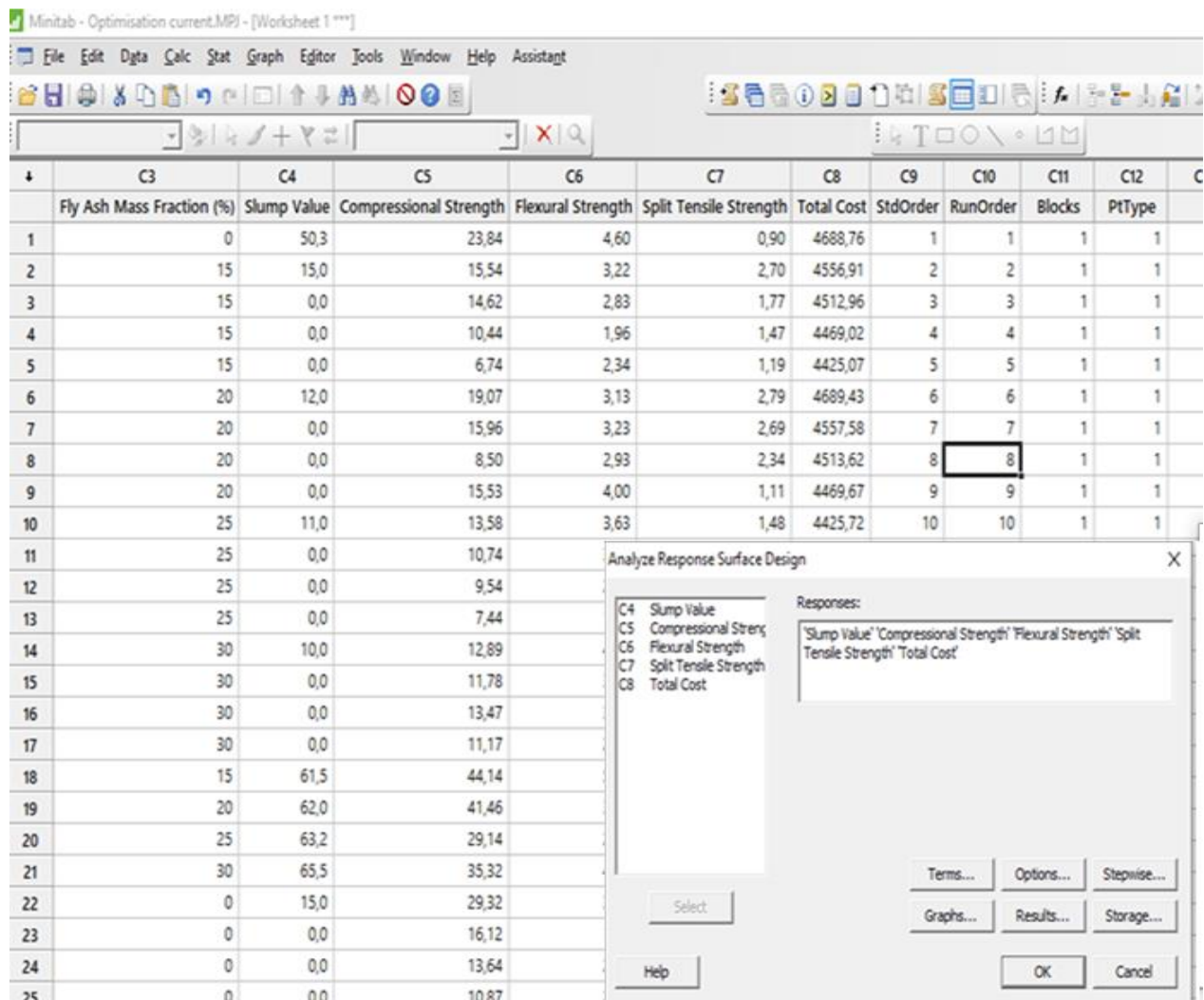


Figure 3-24 – Responses used to analyse response surface design

Thereafter, response surface regression analysis was carried for each of the responses against the continuous factors individually.

3.5.1.1 ANOVA and response surface regression analysis

ANOVA response surface design analysis was carried out for each of the responses that were analysed in this study. The ANOVA gave valuable information such as the coefficient of determination which determined the fit of the model. Furthermore, the statistical significance was tested through the t-test.

3.5.1.2 Overlaid contour plot

An overlaid contour plot was constructed with the specified governing parameters for the acceptable low and high values for the responses, as shown in Figure 3-25.

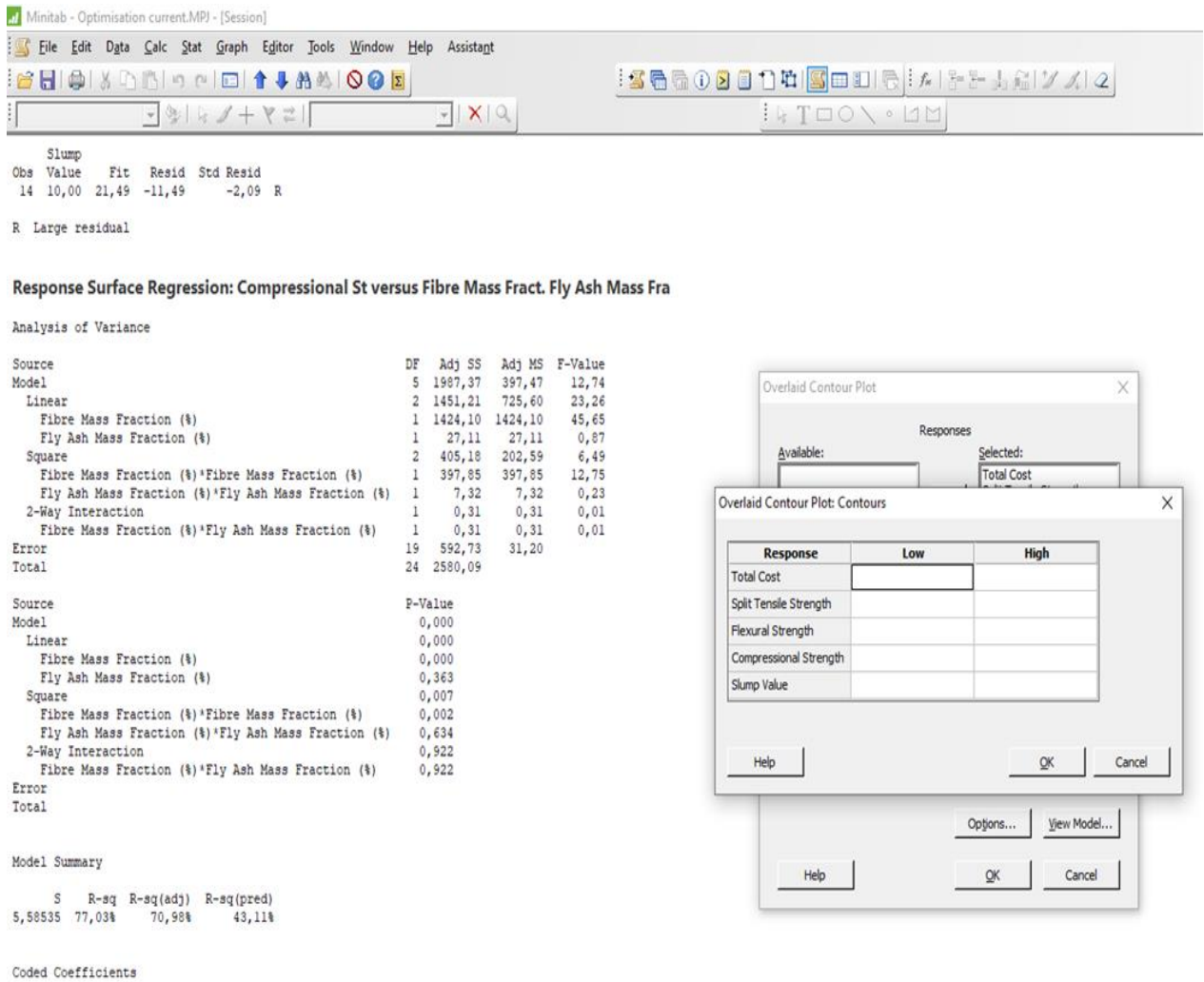


Figure 3-25 – Overlaid Contour plot counters

3.5.1.3 Development of prediction modelling

The developed model on Minitab software was tested for the prediction of response output based on the input parameters. The input values to the model were taken as the fibre and fly ash mass fraction, as shown in Figure 3-26.

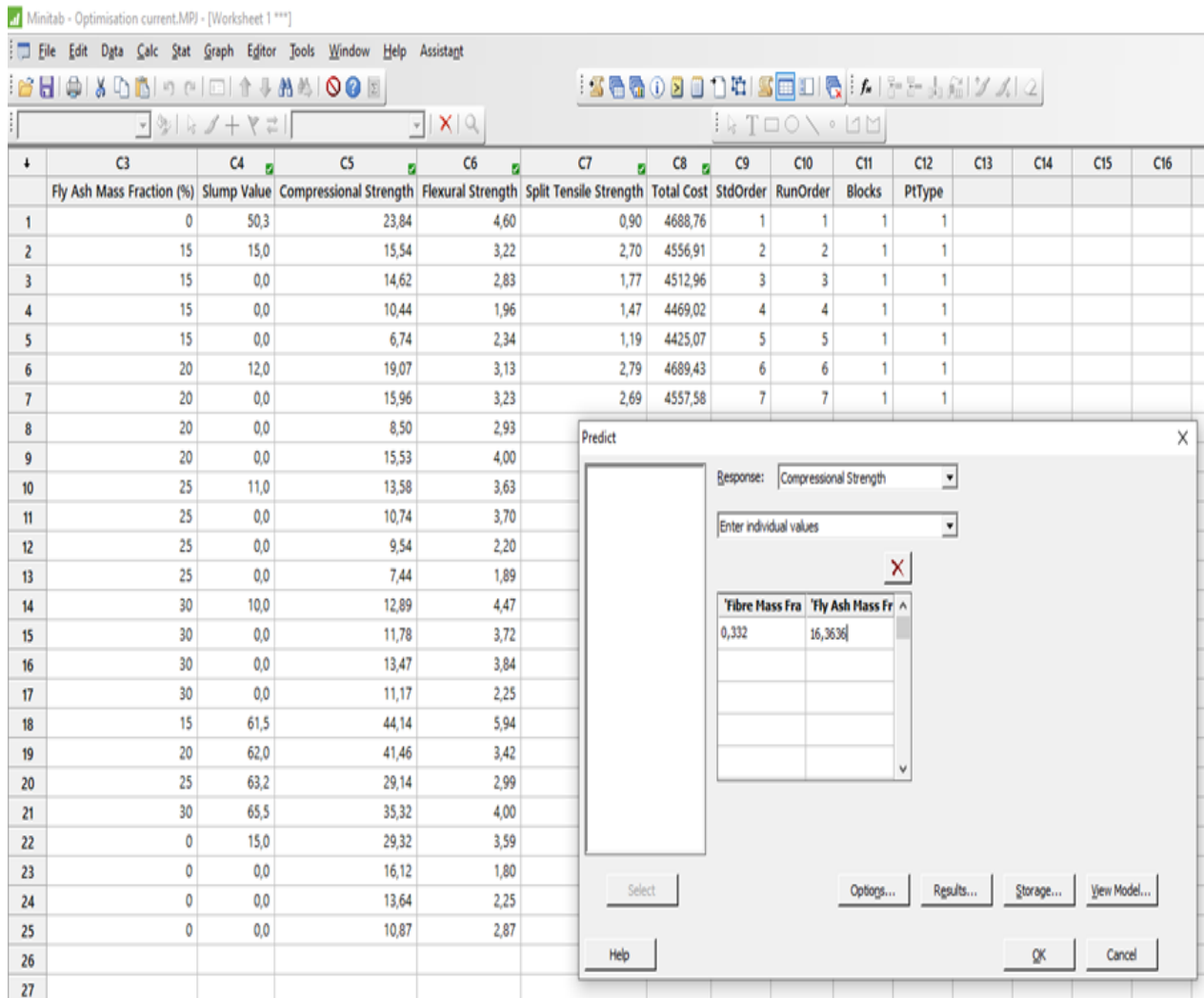


Figure 3-26 – Model Response Predictor

3.5.2 Model validation

The model was validated by entering factor input data and comparing the model response outputs with the experimental results. These results were then tested for the extent of deviations of the model output from the actual response outputs obtained experimentally.

Further, validation was carried out after running the optimising model to compare the model optimum response outputs to actual response outputs obtained through experiments. The variation between the optimum model responses and actual experimental responses was compared statistically to validate the model.

3.5.3 Response optimizer

The response optimizer was a multi-objective function statistical optimiser. To obtain the optimum values for the continuous factors, which are the fly ash and fibre mass fraction, the responses were optimized as shown in **Error! Reference source not found.**

Table 3-5 – Showing Optimization targets for model

Factor	Target
Total Cost	Minimize
Split Tensile Strength	Maximize
Compressive Strength	Maximize
Flexural Strength	Maximize
Slump Value	Target of 8 mm

For increased workability, the slump value was set at target of 8 mm according to study by Hoang et al (2016) study.

3.6 Applications of fibre reinforced composite in slabs

The predictive model developed was used to determine the optimum mixture design for the fabricated reinforced slabs' various applications. The values given in Table 3-6 give the target values for the suitable end uses of the slabs.

Table 3-6 – Target values used for various applications

Parameter	Paving Slabs	Floor Slabs	Foundation Slabs	Suspended Slabs	References
Total Cost (R)	Minimum	Minimum	Minimum	Minimum	
Split Tensile Strength (N/mm ²)	1.01	1.01	1.83	2.30	(Roesler, et al., 2004; Buitrago, et al., 2020)
Flexural Strength (N/mm ²)	2.09	3.70	2.09	3.70	(Roesler, et al., 2004; Namarak, et al., 2018)
Compressive Strength (N/mm ²)	20	25	20	30.5	(Stawiski, 2012; Buitrago, et al., 2020)
Slump Value (mm)	8	8	8	8	(Hoang & Pham, 2016)

The values shown in Table 3-6 were input into the Minitab predictive model and the mechanical and cost responses acquired.

CHAPTER FOUR: RESULTS AND DISCUSSION

4.1 Introduction

This chapter consists of two main broad sections which are the discussion of the experimental and numerical modelling results. The first sub-section under experimental results section, 4.2.1 deals with analysis of the characterization results of the raw materials. The next section 4.2.2 analyses the results from fabrication and concrete workability. The following section 4.2.3 discusses the results from the testing of the fabricated specimens. The last section under experimental work analyses the results from the analysis of material cost.

The second main section in this chapter is numerical modelling. The first sub-section 4.3.1 deals with optimization of mechanical strength and cost of the composite. The following section 4.3.2 analyses the response countour and surface plots. Model validation discussion is under section 4.3.3. Lastly, the application of the fibre reinforced composite slabs is discussed in section 4.4.

4.2 Experimental results

This experimental results section discusses results obtained from the experimental work in this study. The characterisation of raw materials is reported and discussed. Thereafter, the specimens' fabrication and testing results, inclusive of both the destructive and non-destructive tests, are analysed.

4.2.1 Characterisation of raw materials

The results for characterisation of the fly ash, fine and coarse aggregate are presented in the following subsections.

4.2.1.1 Fly Ash physiochemical characterisation

The moisture regains, colour, morphology, particle size distribution and chemical composition of the fly ash was studied, and the results are discussed in the subsequent subsections.

4.2.1.1.1 Moisture regain

The fly ash moisture regain (MR) was measured and the results obtained are as shown in Table 4-1.

Table 4-1 – Showing the moisture regain test on the fly ash sample

Time	1 Hour	2 Hours	4Hours	24 Hours	28 Hours	30 Hours	
Test No.	W ₁ (%)	W ₂ (%)	W ₃ (%)	W ₄ (%)	W ₅ (%)	W ₆ (%)	% MR
1	5,0873	5,063	5,0632	5,0631	5,0643	5,0631	0,4757
2	4,0613	4,0299	4,0293	4,0288	4,0371	4,0288	0,8002
3	4,0115	3,9956	3,995	3,9935	3,9942	3,9935	0,4487
4	2,5568	2,5441	2,5443	2,5429	2,541	2,543	0,5397
5	6,6416	6,6414	6,6321	6,6219	6,6219	6,6219	0,2966
6	4,4226	4,4126	4,4101	4,4069	4,4076	4,4068	0,3573
7	3,2503	3,2416	3,2301	3,2197	3,2209	3,2209	0,9045
8	3,9263	3,9103	3,8997	3,8992	3,8975	3,8975	0,7335
<i>Mean</i>							<i>0,57</i>

The average moisture regain obtained from the test was 0.57%. This moisture regain is relatively low for Class F fly ash which is normally approximately 2.71%, as reported in a study by Shreya et al. (2014). The low moisture can be attributed to the high combustion temperature and efficiency of the thermal power station. The fly ash was sourced from Lethabo Power Station, which has furnaces that reach high temperatures of 1200 °C at full load giving high-efficiency combustion (Eskom, 2019). Combustion at elevated temperatures results in the breakdown of oxygen-containing groups, which lowers the moisture regain of the fly ash. Moisture regains of fly ash is an important parameter with a direct bearing on the durability of the fabricated FRCC slab. This phenomenon is attributed to the fact that the movement of water through concrete pores significantly compromises its durability due to the water eroding and weakening the interfacial bonds within the concrete. The lower the amount of water absorbed by the fly ash, the greater the resistance to water penetration of the concrete slab and hence the environmental damage on the FRCC.

A similar observation was made by Pitroda et al. (2013) study which concluded that the movement of water through concrete is a significant factor that can compromise its durability. Concrete permeability is related to the characteristics of its pore structure and the number of microcracks present at the cement paste and aggregate interface. Moreover, the pore structure involves the volume and size of the interconnected capillary pores, including fly ash particles. The pore structure provides transport of fluid into the concrete and subsequently affects its development and strength. However, other factors besides the constituent materials influence the water absorption of concrete, such as initial curing condition and its duration and the climatic condition during drying and condition of the concrete.

Fly ash with a high-water holding capacity and moisture regain is not suitable for use as cement replacement. However, such fly ash may find use as a substitute for soil and gravel road embankments, as shown by a study carried out by Asokana et al. (2005). The fly ash used in this study has acceptable moisture regain of < 3 %, making it suitable for use in FRCC as it is considered acceptable by ASTM

C618. Not much research has been done on the moisture regain of fly ash and its effect on subsequent mechanical properties of the fabricated FRCC.

4.2.1.1.2 Colour

Figure 4-1 shows the dark grey colour of the fly ash used in the present study.



Figure 4-1 – Dark grey fly ash sample

The colour of the fly ash used in this study is dark grey. In general, fly ash colours vary from tan to dark grey. The colour is influenced by the chemical and mineral constituents of the ash. The observed dark grey colour is characteristic of elevated unburned carbon content within the fly ash, confirmed with the EDS analysis test, which recorded carbon content of greater than 20 %. Furthermore, the colour of fly ash is also controlled largely by the iron content. The higher the iron content, the darker the shade. The fly ash in this present study was observed to be dark grey, implying a high amount of calcium oxides, and this was confirmed to be indeed the case by the XRD and EDS results. Figure 4-2 shows a colour scale for fly ash. The effect of chemical composition has an effect on the colour of fly ash from various geographical regions. Study by Alterary et al (2020) (Alterary & Marei, 2020) reported a darker brown colour for similar class F fly ash. The colour variation is attributed to lower quantity of carbon and higher quantity of sulphur in study by Alterary et al (2020) compared to the current study.

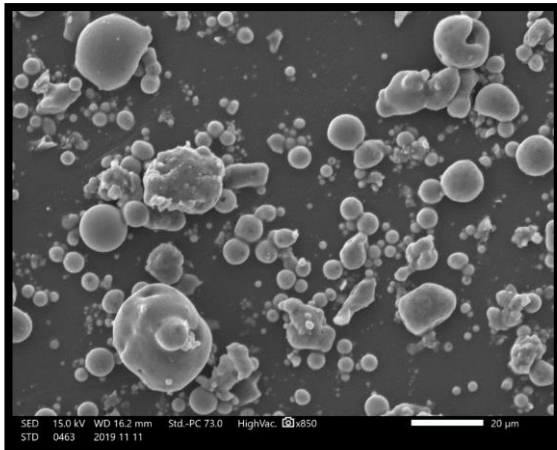


Figure 4-2 – Fly ash colour scale (Vishnu, 2016)

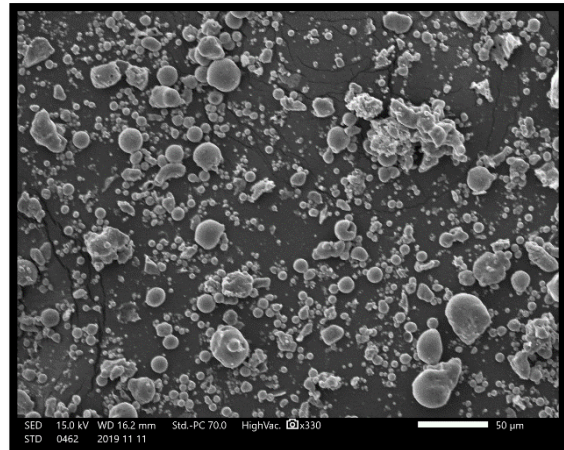
Figure 4-2 indicates that the fly ash used in this study is of intermediate lime content and may belong to either Class F or C, depending on the mineral constituents. However, upon further tests on EDS and XRD, it was ascertained that the fly ash used in this study belongs to Class F. The particle size of the fly ash was measured by PSD, and the results shown in sub-section 4.2.1.1.4.1 gave fly ash of medium fineness which was consistent with the dark grey fly ash colour. The particle size and shape determine the colour of fly ash. Fine-grained fly ash has a grey colour that becomes darker as particle size and amount of carbon increases. Furthermore, fly ash colour is also indicative of the lime content. Yet, not much research has been done on the dominant parameter that affects the fly ash's colour and the relationship between the mineral constituents and the particle size on the colour of fly ash. It is assumed that the mineralogical makeup of the fly ash has the most significant impact on the colour of the fly ash.

4.2.1.1.3 Surface morphology of the fly ash

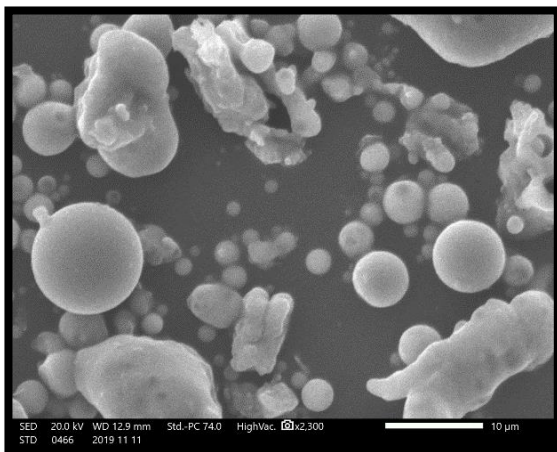
Figure 4-3 shows the surface morphology of fly ash as observed under SEM.



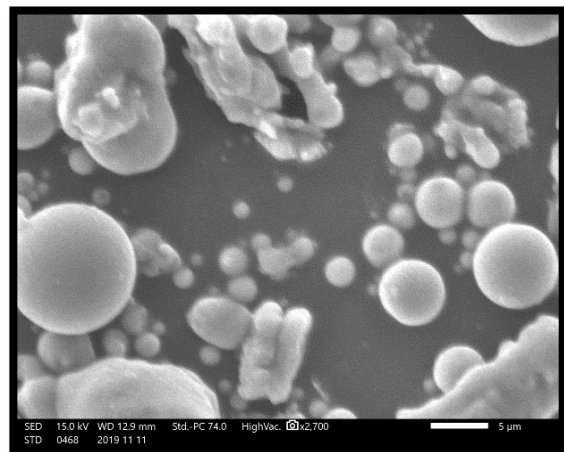
(a)



(b)



(c)



(d)

Figure 4-3 – Showing the SEM Images of fly ash

When observed under SEM, the fly ash in the present study is seen to consist of vitreous spherical shaped particles with few irregularly shaped particles, as can be seen in Figure 4-3a. The SEM images also show that the fly ash particles are generally spherical in shape. Between the spherical fly ash particles, there are some elongated and angular shaped particles, as can be seen, more clearly in Figure 4-3c. These are carbonaceous materials. The vesicular shaped fly ash particles had limited exposure to the high temperatures during combustion; thus, their shape is like that of the pre-combustion particle form. The spherical shape of the fly ash particles can be attributed to the rapid cooling that takes place in the post-combustion zone. This rapid cooling encourages the formation of spherical, amorphous particles. The study by Kutchko & Kim (2006) and Sciubidlo et al. (2015) showed that the morphology of fly ash particles is largely influenced by the combustion temperature and the cooling rate.

The formation of the larger size irregular shaped particles can be attributed to the collision of the flame borne particles of silica ash and sulphate fume in pulverized coal-fired boilers, as observed by Aaron Fuller et al. (2018).

As shown in Figure 4-3c, large irregular-shaped fly ash particles tend to lead to non-uniform compaction in FRCC, resulting in reduced FRCC slab compressive strength. The greater the regularity in the shape of fly ash, the higher the observed compressive strength, as observed in the study by Saha (2018). This increase in compressive strength can be attributed to the lower interparticle voids when regular-shaped fly ash particles are used. When the fly ash sample used in this study is critically examined, it is apparent that most of the particles are of a uniform spherical shape. Therefore, the compressive strength is expected to be high for FRCC made from this ash. Furthermore, due to the fly ash particles being predominantly spherical, it is expected that the fly ash reported giving very good workability with concrete, as reported in a study by Saha (2018). The spherical shape of the fly ash particle has a positive impact on the workability of concrete. The fly ash particles act like small ball bearings, increasing the workability of the concrete paste, making it easier to place, handle and finish. Furthermore, an increase in workability translates to a reduction in the amount of water required in the concrete mixture, as Jiang et al. (2000) reported. On the other hand, larger irregular shaped fly ash particles do not have a smooth texture, and it is expected that these would give poor workability to the concrete paste. The particle morphology and size, as observed by Jiang et al. (2000), influences the water requirement of the concrete and the rate of strength development in hardened concrete. Finer and regular fly ash particles as used in the present study would be expected to give concrete a higher rate of strength development.

This observation of fly ash morphology is consistent with research carried out by Rohilla et al. (2018). Rohilla et al. (2018) studied fly ash from Electrostatic Precipitator Heater (ESP) hoppers of the same power plant unit. They observed spherical shaped particles and a few angular shaped particles as shown in Figure 4-4 for Class F fly ash.

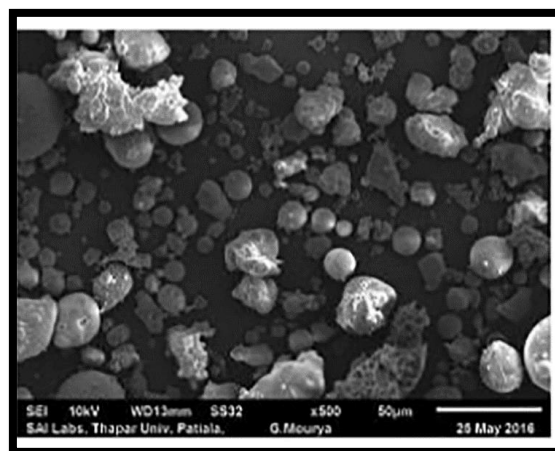


Figure 4-4 – Fly ash particles from ESP hopper (Rohilla, et al., 2018)

4.2.1.1.4 Particle size distribution

The fly ash particle size distribution (PSD) is presented under the following two subheadings.

4.2.1.1.4.1 Particle size distribution using particle size distribution analyser

The graph in Figure 4-5 shows the fly ash particle size distribution in this study.

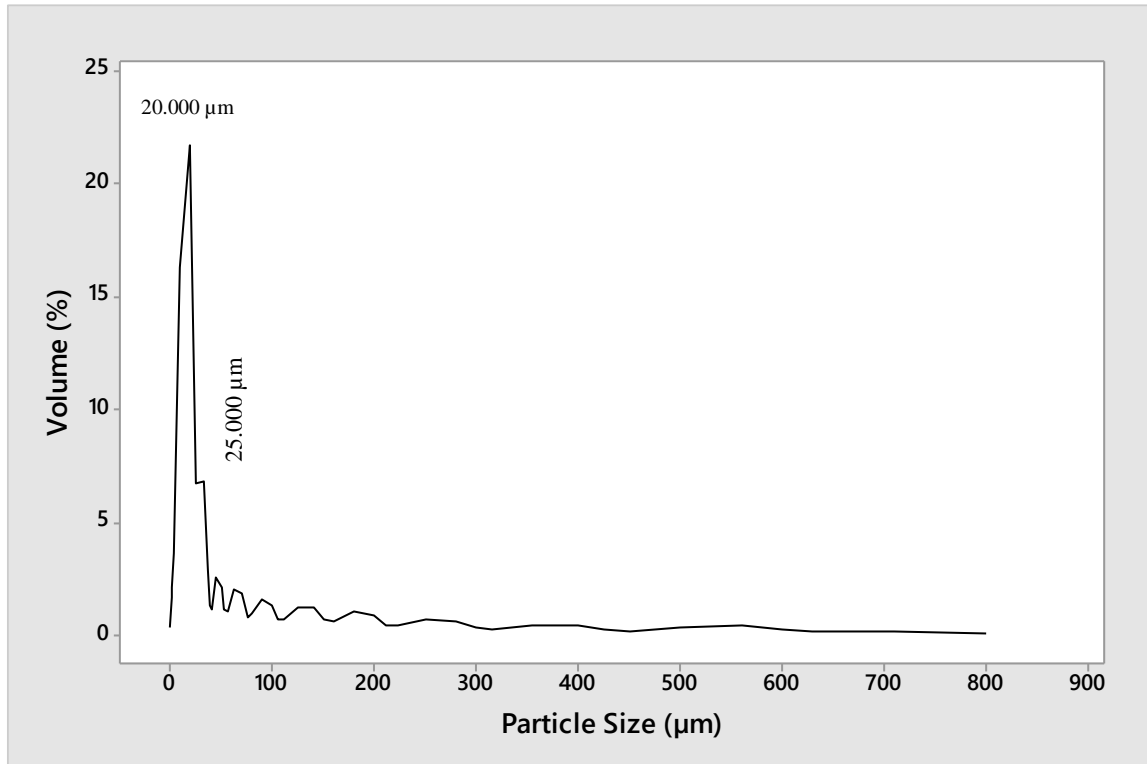


Figure 4-5 – Particle size distribution of fly ash

The fly ash particle sizes range from 0.31 µm to 800 µm. However, the largest volume of fly ash particles have specific sizes ranging from 5 µm to 32 µm. The highest volume of fly ash of specific particle size is seen at 20 µm, with a volume of 21.75% falling within this particle size. After 32 µm, there is a sharp decline in the volume of particles with any specific size exceeding 32 µm.

The fly ash used in this study has over 50% of the particles having a particle size of < 20 µm, as shown in Figure 4-5. This distribution implies that the ash has high pozzolanic activity, and hence these particles are suited for use in concrete to increase the strength. In addition, the smaller particle size of fly ash generally indicates high-efficiency combustion and less amount of carbon content. On the other hand, larger particle size fly ash generally indicates lower combustion of coal and hence higher quantity of carbon content in the fly ash. This observation is supported by the SEM images, which show few large and irregular shaped particles implying high efficiency of combustion.

Fly ash particles sizes < 10 µm are present in this fly ash sample and are expected to give better compaction of concrete and reduce the water requirement in concrete. Furthermore, these particles were

shown in a study by Masao et al. (1993) to strengthen the transition zone, give lower bleed quantity and increase the long-term compressive strength.

Fly ash particles > 45 µm are inferior compared to particles < 10 µm. These particles serve a major function of being fillers. Furthermore, there is a noticeable difference in tricalcium aluminate (C₃A), and mullite content which tends to be higher in particles with < 10 µm than the particles > 40 µm. The higher content of these mineral elements imparts greater pozzolanic activity to the fly ash particles, giving concrete better mechanical properties.

The fly ash used in this study constitutes the bulk of the particle sizes being < 45 µm, indicating small presence of unburnt carbon. A large percentage of unburnt carbon in the fly ash is undesirable as shown by study carried out by Kearsley & Wainwright (2003). It increases the water requirement for a given concrete paste consistency and the admixture requirement entrainment per given air volume. Fly ash containing moderate or low carbon content and moderately high fineness is considered more suited for a partial replacement for Portland cement. The particle size of the fly ash obtained in this research is in the mild to fine size range, making it suitable for use as a pozzolanic partial replacement of cement.

The distance between two points equally spaced from the median is the span. The span is a critical parameter that governs the suitability of fly ash for use in concrete. The formula for Span is as shown in equation (4-1).

$$Span = d_{0.9} - d_{0.1} / d_{0.5} \tag{4-1}$$

The fly ash particle size distribution is shown in Table 4-2.

Table 4-2 – PSD fly ash analysis results

Parameter	Value
Span	6.635 µm
Vol Weighted Mean D [4.3]	48.174
d (0.1)	3.183 µm
d (0.5)	17.610 µm
d (0.9)	120.029 µm

*D (0.1), D (0.5) and D (0.9) are percentiles from particle size distribution curve

The obtained Span value for the fly ash in the present study, as shown in Table 4-2, was 6.635 µm which signified that the sample was homogeneous. Span value indicates the homogeneity or inhomogeneity of the fly ash sample. A small value of Span indicates that the sample is homogenous, whereas a high span value indicates that the sample is inhomogeneous. However, the value of Span

obtained in this study is higher than that of similar grade fly ash studied by Sarkar et al. (2012) from Indian power stations with a Span value of less than 3.13 μm . The difference between this current study and Sarkar et al. (2012) could be attributed to the higher combustion efficiency in the South African Lethabo power plant.

The average particle size is 17.610 μm and is indicated by d (0.5) size as shown in Table 4-2. Furthermore, these results are consistent with research work by Mardon et al. [2008], Vassilev et al. [2005] and Dai et al. [2015] on similar grade fly ash. Table 4-3 shows a comparison of Class F fly ash particle size distribution with research carried out in various geographic areas.

Table 4-3 – Comparison of PSD distribution of fly ash

Particle size distribution	Present study [South Africa]	Chandrapura (Shreya, et al., 2014) [India]	(Bentz, et al., 2011) [USA]	(Joaquin, et al., 2021) [Spain]
d (0.1)	3.183 μm	2.02 μm	2.7 μm	2.8 μm
d (0.5)	17.610 μm	11.89 μm	15 μm	30 μm
d (0.9)	120.029 μm	117.70 μm	114 μm	98 μm

The fly ash consists of submicron size particles which are respirable hence, poses a significant health risk as the particles are small enough to penetrate to various organs in the human body. There is, therefore, a need for the fly ash to be handled with appropriate care, and suitable masks must be worn when dealing with the dry fly ash.

4.2.1.1.4.2 Particle size distribution using SEM

The fly ash particle size was obtained by use of direct measurement with the software on the SEM images, as shown in Figure 4-6.

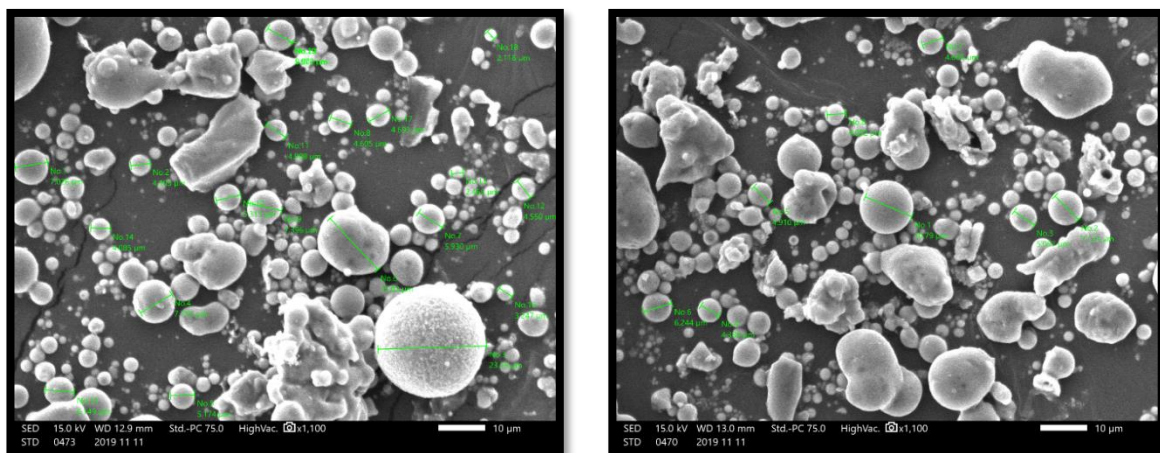


Figure 4-6 – Size measurement of fly ash particles

Most of the fly ash particle sizes range from 4 μm to 45 μm , as shown in Figure 4-6, which is consistent with the results obtained from the PSD analysis shown in section 4.2.1.1.4.1. Ramswamy & Sharma (2011) study concluded that the finer the fly ash particles used in a concrete mixture, the less the amount of water required for the paste. Therefore, the finer the fly ash, the greater the cost-saving in reducing water demand in the concrete paste. These results imply that the fly ash would be suitable for partial cement replacement in concrete. Furthermore, using this type of fly ash could lower the cost of fabrication of the FRCC due to the lower water requirement in concrete paste formulation.

4.2.1.1.5 Chemical composition characterisation

The chemical composition was characterised using EDS, and the results are as shown in Table 4-4.

Table 4-4 – Data from energy dispersive X-Ray spectrometer (EDS) elementary analysis of fly ash sample

Detection spot	Elements (at %) as detected by EDS								
	O	Al	Si	P	K	Ca	Ti	Mg	C
1	43.05	22.73	30.29	-	-	3.92	-	-	-
2	52.60	21.14	26.26	-	-	-	-	-	-
3	47.47	11.52	24.02	-	-	14.52	-	2.47	-
4	50.70	15.10	17.44	-	-	-	-	-	16.76
5	39.39	15.88	17.09	-	-	-	-	-	27.64
6	44.61	16.16	18.09	-	-	-	-	-	21.14
7	52.25	9.65	15.83	-	1.52	-	-	-	20.76
8	48.66	2.75	9.93	1.63	-	37.03	-	-	-
9	59.03	23.76	27.21	-	-	-	-	-	-
10	54.17	13.47	29.34	-	-	-	3.02	-	-
11	38.36	3.50	32.21	-	-	-	-	-	25.93
12	34.20	9.25	9.54	-	-	-	-	-	47.01

Table 4-4 shows the elements found within the fly ash sample as observed by EDS analyses. Different samples of fly ash were tested from the same batch. These were labelled the detection spots the results from EDS analysis showed the predominant elements in the fly ash samples to contain Calcium (Ca), Aluminium (Al), Phosphorus (P), Silicon (Si) and trace amounts of Titanium (Ti) and Magnesium (Mg). These results indicated that the fly ash is Grade F due to the high silica and alumina content which was observed to exceed 70%. The results showed homogeneity in the formulation of the fly ash sample with minor deviations due to the presence of trace elements such as Titanium. The EDS results are shown in Figure 4-7.

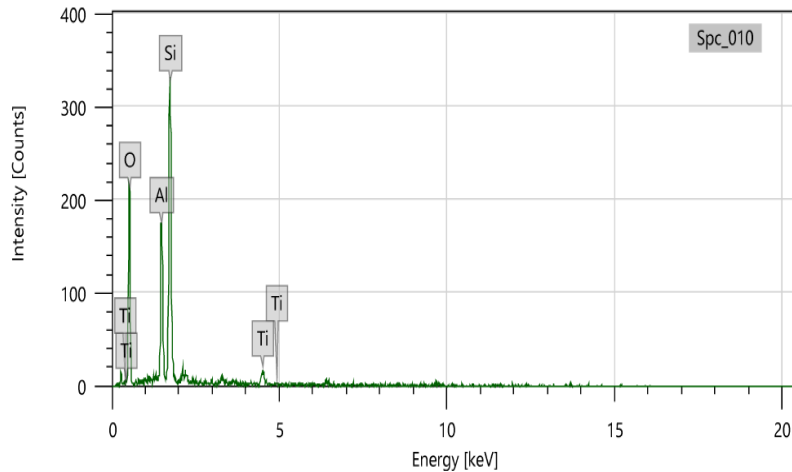


Figure 4-7 – EDS Test results showing trace amounts of Titanium element

In general, the elements with a high concentration in the coal are also expected to have a high concentration in the fly ash as well. The results obtained here are consistent with the XRD results, which showed a high percentage of Calcium Aluminium oxide and Silicon oxide. These results show that the fly ash contains a low quantity of unburned carbon, which makes the ash suitable for use in concrete applications. Low carbon content in fly ash has minimum effect on the air entrapment in concrete.

4.2.1.1.6 Chemical and mineralogical characterisation

X-ray diffraction is a necessary analytical tool to identify and determine the constituent minerals in fly ash. The experimental results obtained from the XRD analysis are shown in Table 4-5.

The combined content of silicon, aluminium and iron oxides exceeded 70%. In accordance with ASTM C618, fly ash with the combined quantity of silicon, aluminium and iron oxides exceeding 70% is classified as Class F. The XRD results show the presence of trace elements of heavy metals such as Magnesium (Mg), Titanium (Ti), Iron (Fe) which could lead to ground pollution if the fly ash is not properly disposed of.

Table 4-5 – XRD based mineralogy of fly ash sample

Mineral	Formula	L	d	R
Potassium Graphite	C16K	0.545	0.610	0.333
Calcium Phosphide	CAP	0.571	0.579	0.331
Silicon Oxide (Tridymite-O)	SiO ₂	0.500	0.657	0.328
Calcium Aluminium Oxide	Ca12Al14O33	0.548	0.582	0.319
Sodium Sulfide	NaS ₂	0.472	0.668	0.315
Silicon Oxide	SiO ₂	0.490	0.618	0.311
Phosphorus	P	0.565	0.545	0.309
Aluminum Oxide	Al ₂ O ₃	0.556	0.552	0.308
Silicon Carbide (Moissanite-5H)	SiC	0.619	0.494	0.307
Magnesium Silicon	Mg ₂ Si	0.556	0.539	0.306
Sodium Calcium Phosphate (Buchwaldite)	NaCa(PO ₄)	0.529	0.565	0.300
Calcium Iron Oxide	CaFeO ₃	0.412	0.726	0.299
Iron Aluminum silicate (Almandine)	Fe ₂ +2Al ₂ (SiO ₄) ₃	0.563	0.519	0.299
Titanium Silicon	TiSi	0.565	0.517	0.292
Sodium Carbon	C32Na	0.500	0.574	0.287
Titanium Oxide	TiO ₂	0.600	0.478	0.287
Sodium Magnesium Iron Titanium oxide silican	Na ₃ (Mg ₃ Fe+3Ti+4)Si ₈₀ 2202	0.455	0.628	0.286
Aluminium Titanium	Al ₂ Ti	0.500	0.569	0.285
Silicon Oxide (Tridymite-M. syn)	SiO ₂	0.411	0.685	0.281

Figure 4-8 shows the XRD pattern for the fly ash particles. The high quantity of aluminosilicates in the fly ash contributes to its pozzolanic activity and makes it suitable for partial cement replacement in concrete.

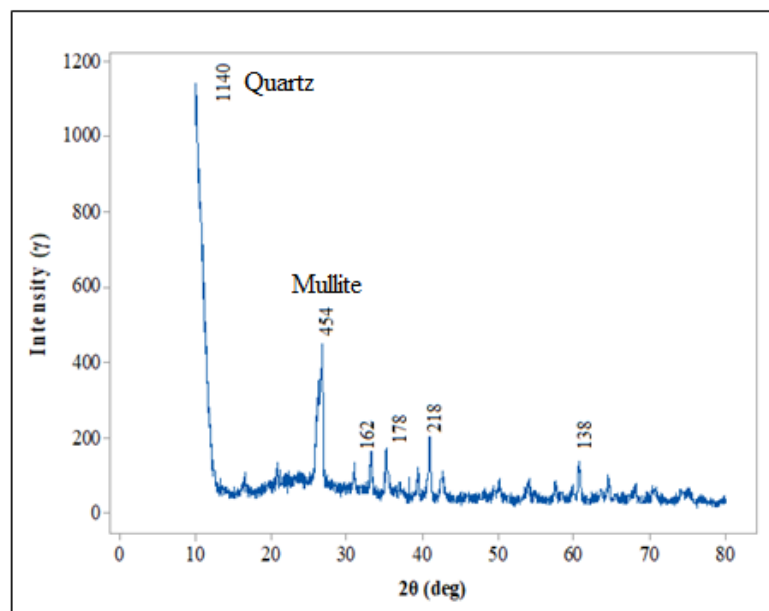


Figure 4-8 – XRD Pattern for fly ash particles

The XRD pattern in Figure 4-8 shows a large number of crystalline minerals like mullite ($\text{Al}_6\text{Si}_2\text{O}_{13}$) and quartz (SiO_2). These results are consistent with Ayanda (2012) results on fly ash from Matla Power station in South Africa. There is a higher metal concentration in the fly ash than in the coal fed into the thermal power station due to the loss of organic components during volatilization and enrichment of heavy inorganic metals. Cao et al. (2008) research concluded that due to fly ash's high surface area of fly ash condensation trace elements tend to occur. The XRD pattern shows the presence of amorphous or non-crystalline content. The non-crystalline state can be seen by broad diffraction x-ray rather than sharp diffraction peaks. From Figure 4-8, the broad diffraction peaks represent the amorphous structure that can be observed from 25° 2θ . The diffraction pattern shows that the major components include mullite, quartz and magnetite. During combustion in the coal furnaces in power plants, the minerals in coal include kaolinite, illite-montmorillonite mixed layer, pyrite, calcite, siderite, and even anatase and quartz would have melted to some extent. Newly formed minerals as shown in Figure 4-8 such as mullite, hematite, maghemite, anhydrite and a proportion of quartz form by recrystallization as the molten mass cools down.

The chemical composition of fly ash from various geographical locations has some variations. A study by Kumar et al (2012) showed that fly ash from Gorakhpur, India had a high SiO_2 compared to the current study. Furthermore, the fly ash from Gorakhpur contained some minerals such as MgO (Magnesium Oxide), and SO_4^- (Sulphate) which were not present in the fly ash studied in the current study. The chemical composition of fly ash can have significant effects on the reaction it has and can ultimately affect the mechanical properties of the concrete composite.

4.2.1.2 Aggregate characterisation

Several aggregate characterisation tests were carried out on fine and coarse aggregates, which are discussed in the subsequent sub-sections.

4.2.1.2.1 Fine aggregate characterisation

The tests carried out on the fine aggregates included particle size characterization, specific gravity, and moisture absorption tests.

4.2.1.2.1.1 Fine particle size characterisation

Fine particle size characterization of the river sand used in the study was carried out using sieve analysis, and the results obtained are as shown in Table 4-6.

Table 4-6 – Sieve Analysis of fine aggregates

Sieve Size	Weight of Fine Aggregate (gms) Determination				% Retained	Cumulative % Retained	% Passing
	I	II	III	Average			
4.75 mm	64.90	69.70	63.20	65.93	6.59	6.59	93.41
2.00 mm	242.60	225.80	299.70	256.03	25.60	32.20	67.80
1.18 mm	280.90	248.70	254.20	261.27	26.13	58.32	41.68
600.00 µm	254.20	256.50	222.60	244.43	24.44	82.77	17.23
425.00 µm	75.00	85.60	73.60	78.07	7.81	90.57	9.43
150.00 µm	75.00	101.10	74.50	83.53	8.35	98.93	1.07
Pan	6.10	10.30	9.20	8.53	0.85	99.78	0.22

The gradation of the river sand is uniformly graded distribution, as seen in Table 4-6. The fineness modulus refers to the fineness or coarseness of the aggregate. The sand's fineness modulus (FM) was calculated using equation 4-2 based on the sieve analysis results shown in Table 4-6.

$$\text{Fineness modulus of Sand} = \frac{\text{Cumulative \% Retained}}{100} \quad 4-2$$

$$\text{Fineness modulus of River Sand used} = \frac{369.33}{100} \quad 4-3$$

$$\text{Fineness modulus of River Sand used} = 3.69 \quad 4-4$$

The calculated FM of the sand was 3.69. This value is considered as high and coarse sand. The FM is an index number that gives an indication of the mean size of the river sand particles. Thus, in accordance with the ASTM standard shown in Table 4-7, the river sand is classified as coarse sand.

Table 4-7– Showing Classification of Sand based on Fineness Modulus (Amey, et al., 2014; Kagonbe, et al., 2020)

Type of Sand	Fineness Modulus
Over fine sand	< 2.12
Slightly over fine sand	2.1 to 2.5
Medium sand	2.5 to 3.1
Slightly medium-coarse sand	3.1 to 3.5
Over coarse sand	> 3.5

A higher FM has an adverse effect on the concrete properties both in plastic and hardened concrete. The concrete mixture was inadvertently harsher and more prone to segregation, and in addition, a higher FM makes it more difficult to place and finish the concrete. However, as shown in a study by Backus (2021), higher FM in the fine aggregate has been noted to produce concrete with good strength properties and workability in concrete mixes that contain a higher cement content. Kagonbe et al. (2020)

research showed that it is possible to modify the fineness of sand by incorporating and blending with finer sand.

Due to its higher FM, the sand in this study has a lower surface area, which lowered the cement requirement. This has a bearing on the economy of the concrete mixture. However, more water is required with a higher FM.

Aggregate grading is an important characteristic in concrete mixture as it affects the workability and packing density of the concrete mix among other properties. The graph in Figure 4-9 shows the particle size distribution of the river sand.

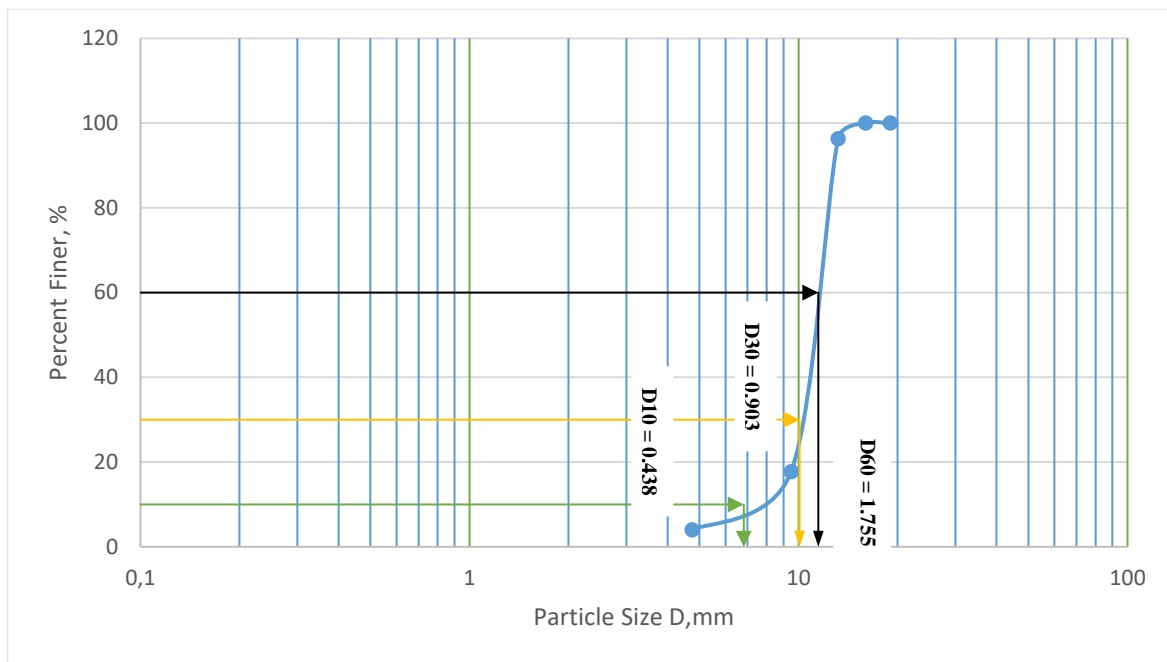


Figure 4-9 – Fine Aggregate Particle Size Distribution Curve

From the grading curve presented in Figure 4-9, the coefficient of gradation of D_{10} , D_{30} and D_{60} diameters are 0.438, 0.903, and 1.755, respectively. The uniformity index was calculated as shown in equation 4-5.

$$\text{Uniformity Coefficient } (C_u) = \frac{D_{60}}{D_{10}} \quad 4-5$$

$$C_u = \frac{1.755}{0.438}$$

$$C_u = 4.007$$

The uniformity coefficient gives the variation in particle sizes in the river sand represented as a ratio of D_{60} to D_{10} . D_{60} is the particle size where 60% of the river sand particles are finer and 40% are coarse.

At the same time, D_{10} is the sand particle size where 10% of the sand particles are finer, and 90% are coarser. The calculated uniformity coefficient for the river sand used in this study was 4.007, which puts it into the category of well-graded particles. Uniformly distributed river sand particles observed in the current study, have numerous advantages, as shown in research by Glavind et al. (1993) and Goltermann et al. (1997), that uniformly distributed mixtures tend to have better workability compared to gap graded mixtures. Gap graded mixtures have a high percentage of the particle at specific sizes. However, Gap graded mixtures achieve better slump values than uniformly distributed mixtures.

4.2.1.2.1.2 Specific gravity of fine aggregates

The specific gravity of fine aggregates was measured, and the results are shown in Table 4-8.

Table 4-8 – Specific gravity of fine aggregates

No.	Description	Average
1	Weight of Empty Pycnometer, (W1) grams	558.20
2	Weight of Pycnometer + Sample, (W2) grams	1168.00
3	Weight of Pycnometer + Sample + Water (W3) grams	1941.90
4	Weight of Pycnometer + Water, (W4) grams	1616.00
5	Specific Gravity	2.15

The specific gravity of the river sand was calculated according to equation 3-4 and found to be 2.15, which is on the lower end of the range for normal fine aggregate. The specific gravity for the most natural and normal river sand aggregates, as reported in a study by Siddiquee (2021) ranges between 2.65 and 2.67. The specific gravity of the river sand is less than the normal this can be attributed to either large amounts of organic matter or porous particles within the sand. Ajao et al. (2018) characterised river sand from Ogun State in Nigeria and obtained river sand specific gravity of 2.67. Further, research by Orozco et al. (2018), Tebbal & Rahmouni (2016), and Nkengue et al. (2019) showed that the geographical location influences the quality of the sand.

4.2.1.2.2 Coarse aggregate characterisation

The coarse aggregate tests, including particle size analysis, flakiness test, elongation test, and water absorption tests, are discussed in the following subsections.

4.2.1.2.2.1 Coarse aggregate particle size characterisation

Sieve analysis of coarse aggregate was carried out, and the results are shown in Table 4-9.

Table 4-9 – Sieve analysis results for coarse aggregate

Sieve Size (mm)	Weight of Coarse Aggregate (gms) Determination				% Retained	Cumulative % Retained	% Passing
	I	II	III	Average			
19.00	0	0	0	0.00	0.00	0.00	100.00
16.00	0	0	0	0.00	0.00	0.00	100.00
13.20	27.70	39.60	43.70	37.00	3.70	3.70	96.30
9.50	792.60	769.70	793.90	785.40	78.54	82.24	17.76
4.75	177.30	188.60	157.70	174.53	17.45	95.99	4.01
Pan	2.40	2.10	2.30	2.27	0.23	17.68	82.32

The coarse aggregate was classified as 13 mm dolomite stone by the supplier. As shown in Table 4-9, Sieve analysis showed that most of the particles did indeed fall into this category between 9.5 mm and 13.2 mm. No coarse aggregate particles were greater than 13.2 mm in size, as shown in Table 4-9. All coarse aggregate particles passed through the 19 mm and 16 mm sieves. The use of an aggregate of less than 13 mm in size has some advantages and disadvantages. Larger aggregate particles generally require less mixing water in comparison to smaller aggregates, and this observation is attributed to the lower specific surface area.

Furthermore, a reduction in the water quantity increases the strength of the concrete and reduces the cement quantity required. Reduction in cement needed lowers the cost of production of the concrete. However, Oritola et al. (2014) showed that coarser aggregate tends to form weaker transition zones that contain a more significant number of microcracks.

The graph shown in Figure 4-10 shows the coarse aggregate particle size distribution curve.

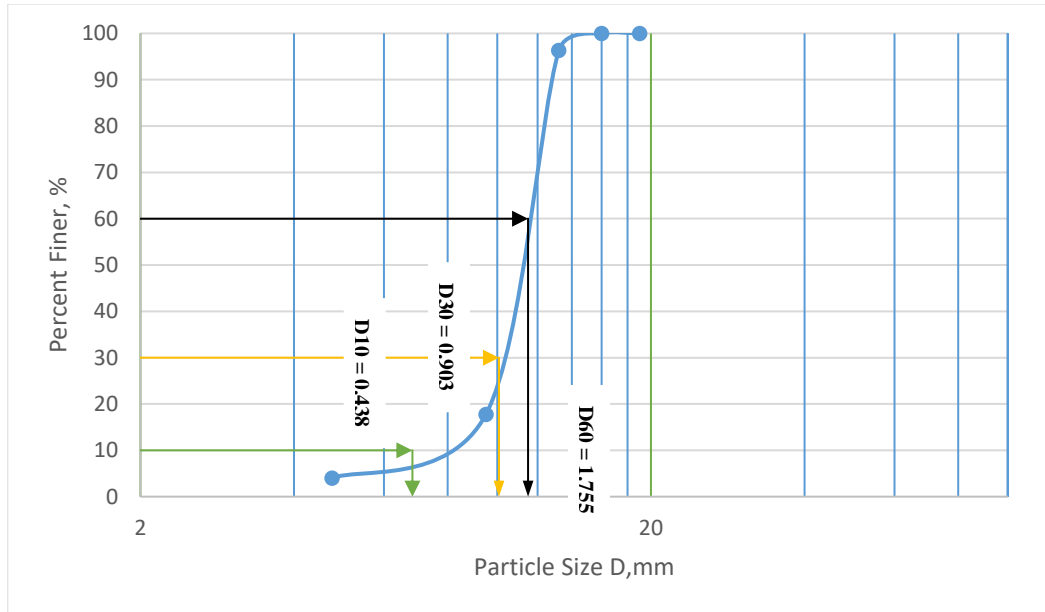


Figure 4-10 – Coarse Aggregate Particle Size Distribution Curve

From the grading curve presented in Figure 4-10, the coefficient of gradation of D_{10} , D_{30} and D_{60} diameters are 0.438, 0.903 and 1.755, respectively. The uniformity coefficient was calculated using equation 4-6.

$$\text{Uniformity Coefficient } (C_u) = \frac{D_{60}}{D_{10}} \quad 4-6$$

$$C_u = \frac{1.755}{0.438}$$

$$C_u = 4.007$$

The uniformity coefficient gives the variation in particle sizes in the river sand represented as a ratio of D_{60} to D_{10} . D_{60} is the particle size where 60% of the coarse aggregate particles are finer and 40% are coarse. At the same time, D_{10} is the coarse aggregate particle size where 10% of the aggregate are finer, and 90% of the particles are coarser. The calculated uniformity coefficient was 4.007. In research by Oritola S (2018), it was reported that for well-graded coarse aggregate, the uniformity coefficient must be greater than 4. Hence the uniformity coefficient obtained in this study for the coarse aggregate is well graded. Uniformly graded aggregate indicates particles of almost the same size in the aggregate. Aggregate gradation has a significant effect on the properties of concrete. Uniform coarse aggregates allow ease of compaction of the concrete as the smaller particles fill the voids created by the larger particles. This results in concrete which is dense and has fewer voids, as shown in research by Alsayed & Amjad (1996).

4.2.1.2.2.2 Particle shape and texture

The flakiness and elongation of the coarse aggregate were tested, and the results are as shown in Table 4-10.

Table 4-10– Flakiness and Elongation of Coarse aggregate

Retained	Sieve size (mm)	Sample Weight (g)	Weight of Aggregate Passing Thickness Gauge (g)	Weight of non-flaki agg. Retained on Thickness Gauge (g)	Weight of Aggregate Retained on Elongation Gauge (g)
A	19	0	0	0	0
	13.2	45.9	45.9	0	4.2
	9.5	700.6	567.4	133.2	443.4
	6.7	232.6	148.7	83.9	80.8
	4.75	19.5	14.1	5.4	5.5
	3.35	0.1	0	0.1	0
	Pan	1.3	0	0	0
B	19	0	0	0	0
	13.2	70.2	67.3	2.7	6.3
	9.5	623.5	499.8	123.4	392.6
	6.7	263.2	183.1	80	68.8
	4.75	36.5	22.3	14.2	4
	3.35	3.4	1.3	2.1	0
	Pan	2.8	0	0	0
C	19	0	0	0	0
	13.2	30.8	30.8	0	11.7
	9.5	607.9	444.3	163.3	308.2
	6.7	265.8	175.9	89.9	72.4
	4.75	69.5	40.9	27.4	3.8
	3.35	6	2.9	3.1	0
	Pan	19.1	0	0	0
Average	19	0.0	0.0	0.0	0.0
	13.2	49.0	48.0	0.9	7.4
	9.5	644.0	503.8	140.0	381.4
	6.7	253.9	169.2	84.6	74.0
	4.75	41.8	25.8	15.7	4.4
	3.35	3.2	1.4	1.8	0.0
	Pan	7.7	0.0	0.0	0.0

Most of the coarse aggregate particles were caught in the 9.5 mm sieve during sieve analysis as the aggregate was graded as 13 mm. Hence most of the aggregate passed the 13.2 mm sieve and was caught in the 9.5 mm sieve. The flakiness index was calculated as shown in equation 4-7.

$$Flakiness\ Index = \frac{\Sigma X}{\Sigma Y} \times 100 \quad 4-7$$

Where:

ΣX - The weight of material passing through the various thickness gauges

ΣY - The weight of aggregate passing and retained on the specified sieves

$$Flakiness\ Index = \frac{748.2}{1000} \times 100 \quad 4-8$$

$$Flakiness\ Index = 74.82\% \quad 4-9$$

The flakiness index for the coarse aggregate used was 74.82%. The flakiness index is defined as the percentage by mass of coarse aggregate particles whose least dimension is less than $\frac{2}{3}$ of their average dimension. The flakiness index was considered high, and it was necessary to take mitigation factors in the concrete fabrication. The high flakiness index influences the degree of packing of aggregates. Furthermore, high flakiness has an adverse effect on the workability of the concrete mixture. The elongation index was calculated using equation 4-10.

$$Elongation\ Index = \frac{Total\ weight\ retained\ on\ various\ length\ gauges}{Total\ weight\ of\ test\ sample\ taken} \times 100 \quad 4-10$$

$$Elongation\ Index = \frac{467.2}{1000} \quad 4-11$$

$$Elongation\ Index = 46.72\% \quad 4-12$$

Elongation index is defined as the percentage by weight of aggregate particles whose greatest dimension is greater than 1.8 of its mean dimensions. The elongation index for the coarse aggregate was 46.72%. This elongation index was considered acceptable to produce concrete, and however, the elongation index was on the higher side. The highly elongated particles improve the interfacial bond strength between the cement paste and the aggregate compared to the rounded and smooth aggregate. However, the elongation of the coarse aggregate has a bigger impact during the mixing of concrete compared to the final properties of the hardened concrete. The high elongated particles in this study require the addition of more water to the mixture to have good workability. This increase in water content required then necessitates the addition of more cementitious material to maintain a good cement to water ratio.

4.2.1.2.2.3 Specific gravity and absorption of aggregates

The specific gravity and absorption of coarse aggregates were determined, and the results obtained are as shown in Table 4-11.

Table 4-11 –Water absorption test for coarse aggregate

Description	A	B	C	Average
Weight of sample (g)	1000	1000	1000	
Weight of vessel + sample + water [A]	1582.1	1084.7	1565.0	
Weight of Vessel + Water [B]	1027.5	724.0	1016.5	
Weight of saturated and surface dry sample [C]	893.8	581.6	887.4	
Weight of Oven Dry Sample [D]	885.5	578.0	880.2	
Water Absorption (%)	0.94	0.63	0.82	0.80
Specific Gravity	2.6106	2.6166	2.5972	2.608
Apparent Specific Gravity	2.6760	2.6599	2.6536	2.663
Bulk Specific gravity	11.8332	7.6173	12.1224	10.5243

The water absorption was calculated in accordance with equation 3-10. The specific gravity and apparent specific gravity were calculated in accordance with equations 3-9 and 3-8, respectively. The bulk specific density was calculated according to equation 3-7. The mean water absorption of the coarse dolomite aggregate was calculated to be 0.80%. The water absorption obtained was vital information in developing the proper water/cementitious mix ratio. The value obtained for water absorption is within the range obtained in the study by Ibearugbulem & Igwilo (2019), which showed suitable water absorption for coarse aggregate. Coarse aggregate water absorption, as shown in research by Galloway (1994) is generally in the range of 0.2% to 4%.

4.2.2 Concrete workability

The workability of the fresh concrete mixture was measured and analysed through the slump test for all the specimens produced according to the full factorial experimental design. The results from the slump tests are discussed in the following subsections.

4.2.2.1 Effects of fly ash on concrete workability

The graph shown in Figure 4-11 shows the effect on slump value with an incremental percentage of fly ash replacement of cement.

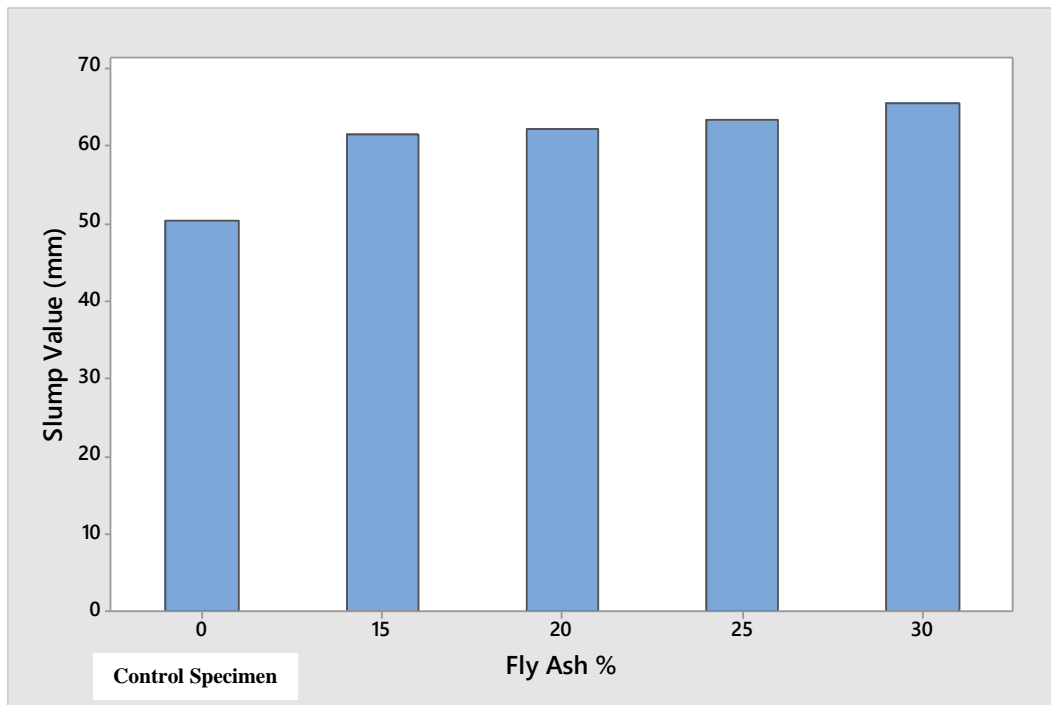


Figure 4-11 – Showing slump values with fly ash replacement of cement

The results indicated that an increase in fly ash content increased the slump value of the concrete. The control specimen without any fly ash had a slump value of 50.30 mm. The slump increases sharply with the addition of 15% fly ash to 61.50 mm after that. A marginal increase was realised with an increase in fly ash content. The trend observed in Figure 4-11 showed that the higher the fly ash content, the greater the workability of the concrete paste. The increase in slump value could be attributed to the flowability of the concrete containing fly ash. The fly ash particle morphology was shown in section 4.2.1.1.3 to be pre-dominantly spherical in shape and hence act as miniature ball bearings in the concrete paste, increasing its flowability. Concrete containing fly ash flowed better and consolidated better than conventional concrete. Furthermore, the use of fly ash also reduced the amount of water required in the concrete mixture.

Research by Shaikuthali et al. (2019) agreed with the trend observed in the current study. Shaikuthali et al. (2019) reported an increase in slump value from 155.00 mm for 10% fly ash replacement to 175.00 mm for 30% fly ash replacement. The high values observed by Shaikuthali et al. (2019) could be attributed to the slump measurement being observed and recorded after 120 mins, unlike in the current study where the slump value was taken within 5 minutes of removing the cone in accordance with SANS 5861-2. However, another research by Akmal et al. (2003) showed an inverse trend with an increase in fly ash content replacing cement, giving a decrease in the slump values. This could be attributed to the fact that the researcher used additives such as a superplasticizer in their research which was not used in this study.

4.2.2.2 Effects of PET fibre on concrete workability

The graph shown in Figure 4-12 shows the effect of PET fibre addition on the slump value of the fresh concrete.

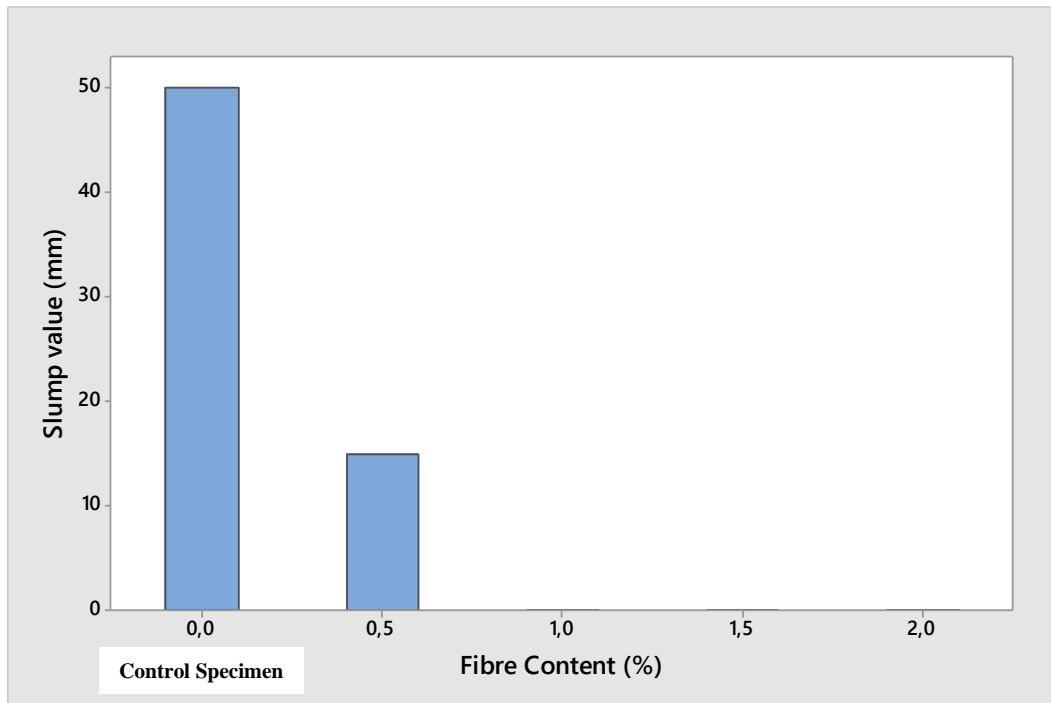


Figure 4-12 – Showing slump values with PET fibre in FRCC

The slump value dropped sharply from 50.30 mm for the control specimen without any reinforcement to 15.00 mm for the FRCC containing 0.5% PET fibre. As PET fibre content was increased to 1.0%, the slump value dropped from 15.00 mm to 0 mm. Any further increase in fibre content yielded a zero-slump value. This drop could be attributed to the decrease in workability that results from an increase in fibre content. The decrease in workability is due to frictional resistance between the PET fibres and the concrete particles. Research carried out by Hasan A et al. (2019) reported a similar trend, with the slump value at 0.48% polypropylene fibre being 15.00 mm and the slump for 0.72% polypropylene fibre content dropping to 8.00 mm. Thereafter, any additional increase in polypropylene fibre beyond 0.72% fibre content resulted in an insignificant slump value as observed in this present study.

McWhannel (1994) and Govindasami et al. (2018) reported that increasing the fibre content tends to increase the frictional resistance between the fibres and the concrete particles resulting in obstruction to the free flow of concrete. This frictional resistance ultimately reduces the slump value of the concrete. A lower slump value makes it more difficult to pump and place the concrete, Although the workability can be increased by the use of super plasticisers as admixtures in the concrete. Further, research is needed to improve the slump value of PET FRCC beyond 1.0 % fibre addition.

4.2.2.3 Effects of PET fibre and fly ash on concrete workability

The graph in Figure 4-13 shows the combined effect of PET fibre and fly ash on the slump value in fresh FRCC.

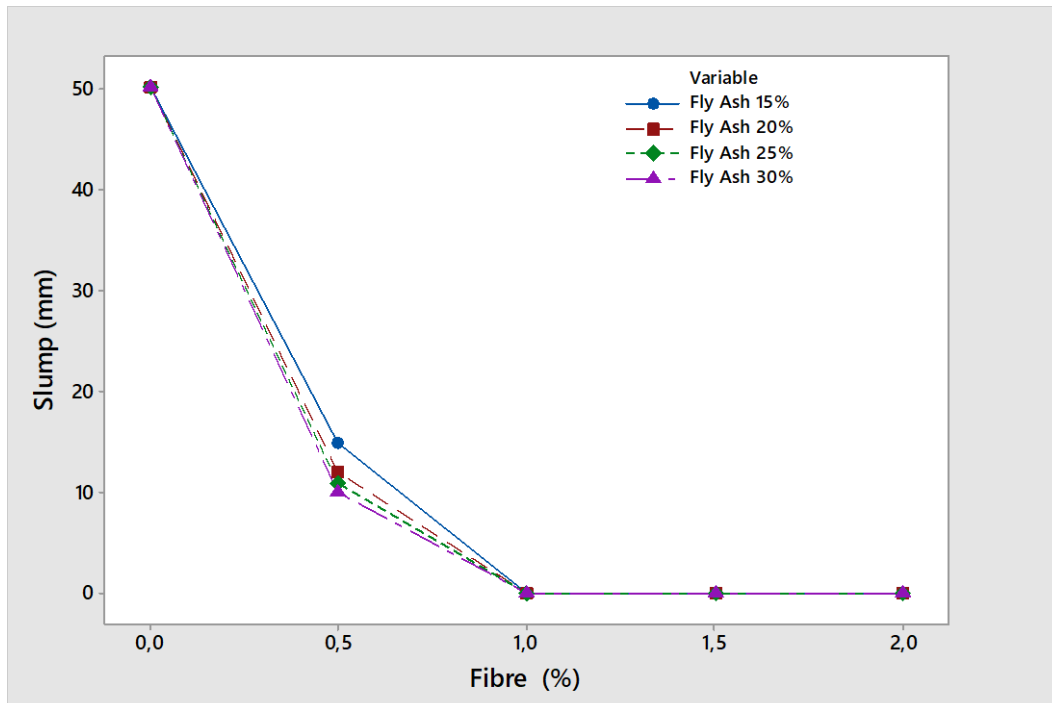


Figure 4-13 – Showing Combined Slump Value of Fly Ash and PET Fibre on Concrete

As observed in Figure 4-13 the slump value dropped drastically from the control specimen with an increase in fibre content regardless of the quantity of fly ash added to the concrete mixture. However, the mixture containing a lower fly ash content had a slightly higher slump value compared to corresponding higher fly ash content for 0.5% fibre content. The mixture containing 15% fly ash content recorded a slump value of 15.00 mm. The mixtures containing 20%, 25% and 30% fly ash recorded slump values of 12.00 mm, 11.00 mm, 10 mm respectively for 0.5% PET fibre content. However, upon the addition of 1% fibre content regardless of the fly ash content, the slump value dropped to zero. Any further addition of fibre beyond 1% resulted in an insignificant slump value.

As expected, the lower slump values realised with the addition of fibre resulted in reduced workability of the concrete mixture and made placing of the concrete increasingly difficult with higher fibre content. From 1% addition of PET fibre, the workability became a significant problem. The FRCC containing 2% fibre addition gave a very harsh concrete mixture that was extremely difficult to work with coupled with significant fibre clumping. Fibre clumping started being a significant problem from 1.5% fibre addition. Slump value could be increased by adding more water or other additives. However, the addition of more water compromises the ultimate strength properties of the concrete.

Furthermore, the addition of more water into the mixture tends to result in aggregate separation. The study by Wang et al. (2019) reported a similar trend of decreased slump value with more fibre. Furthermore, the study by Wang et al. (2019) reported that workability decreased drastically from 0.40 % fibre addition. However, their study considered Basalt fibre at 12 mm fibre length only.

4.2.3 Testing of the fabricated specimens

Mechanical and non-destructive tests were carried out on the FRCC. These results will be discussed in the following subsections.

4.2.3.1 Mechanical testing

This section discusses the concrete composite results obtained for the compressive strength, split tensile strength and flexural strength.

4.2.3.1.1 Compressive strength properties

The compressive strength of concrete was analysed according to the design of the experiment to model a relationship between the factors and the ultimate 28-day compressive strength. The results for the compressive strength test are presented in the following subsections.

4.2.3.1.1.1 Effects of PET fibre addition on composite compressive strength

The graph in Figure 4-14 shows the effect of fibre addition without any fly ash on the 28-day compressive strength of concrete.

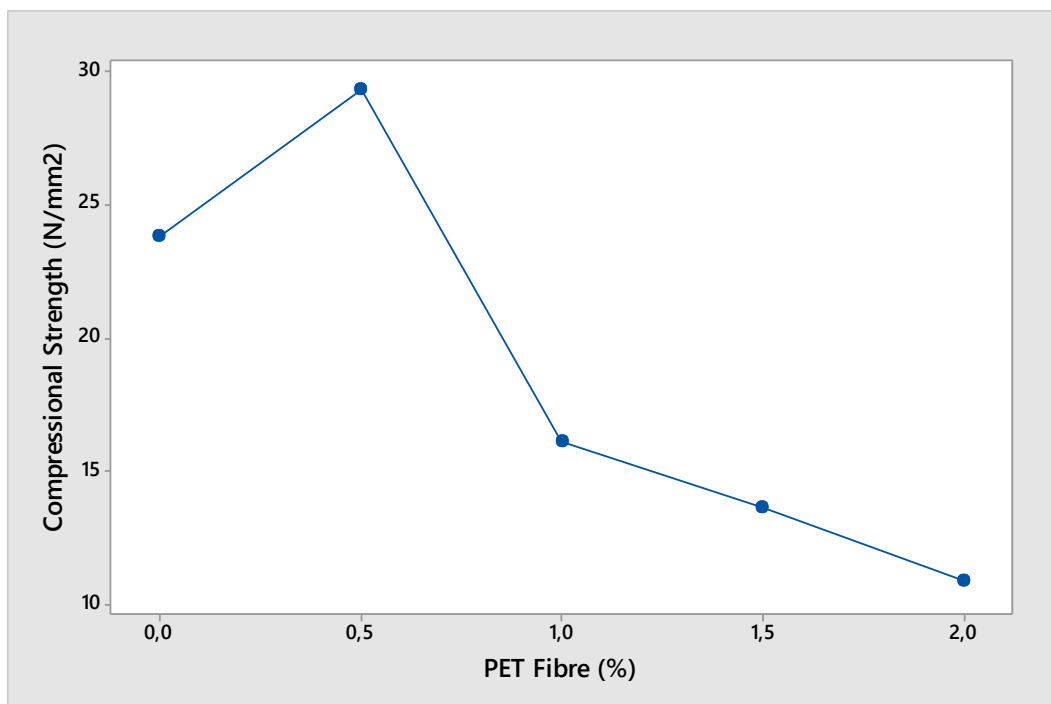


Figure 4-14 – Effects of Fibre Addition on Compressive strength

Figure 4-14 shows that duan increase in compression strength of concrete occurs up to 0.5% PET fibre addition. Thereafter, there is a 45% decline in compressive strength from 0.5% up to 1% fibre addition. The strength of FRCC is significantly less than the strength of unreinforced concrete at 1.0% fibre addition. Thereafter, there is a moderate decline in compressive strength with increased fibre content up to 2%. The maximum compressive strength recorded was at 0.5% fibre addition, which gave compressive strength of 29.32 N/mm², an increase of 23% in compressive strength over the control specimen. The stress on the FRCC followed a similar trend to the compressive strength, as shown in Figure 4-15.

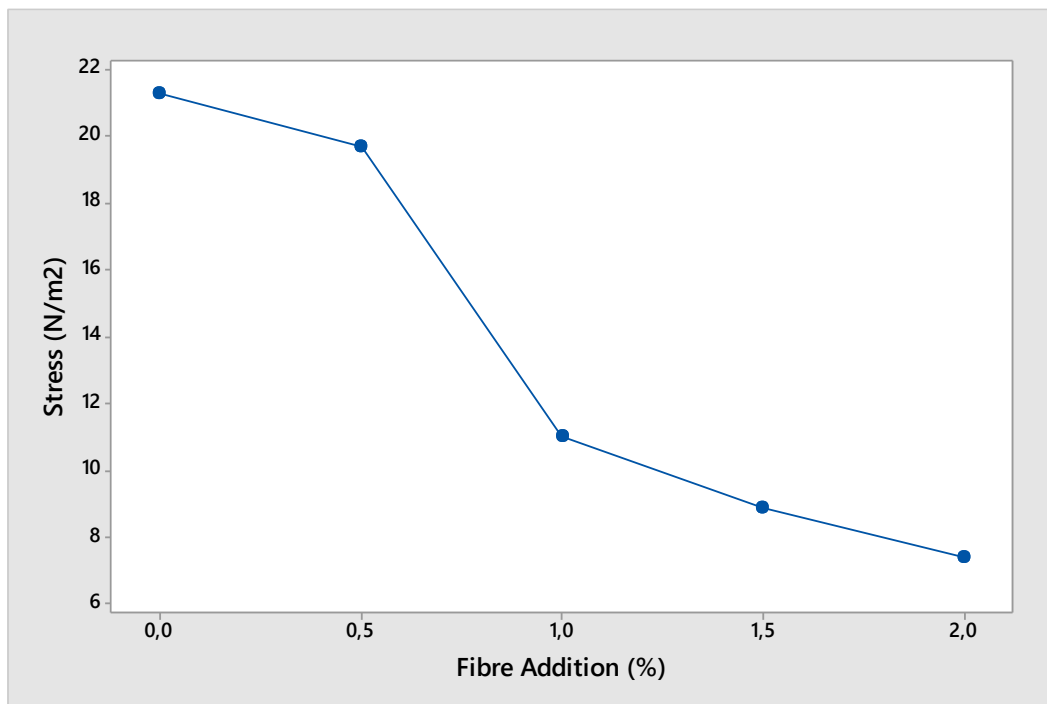


Figure 4-15 – Effects of Fibre Addition on Compressive Stress of Concrete

The compressive stress was reduced with the addition of PET Fibre in a gradual trend. The failure of the specimens under compressive test for the PET reinforced concrete cubes was not catastrophic as realised for the control specimen. It was a gradual failure. On the other hand, the failure for the control specimen of concrete without any fibre reinforcement was a sudden and explosive global failure. The addition of 0.5% PET fibres has a modest increase in the compressive strength of the FRCC. However, the addition of PET fibres significantly alters and increases the ductility of the concrete and impacts the post cracking ductility of the FRCC. Ductility and deformability are interrelated concepts and is the ability of concrete to undergo considerable deflection prior to failure (Raghucharan & Prasad, 2015). Unreinforced concrete is normally considered as a brittle material however, PET fibre concrete in this study has some ductility as was observed during the mechanical tests. The strain observed in the fibre reinforced concrete increased with increase in fibre loading

The increase in the compressive strength between 0% and 0.5% can be attributed to an increase in the bonding that occurs between the concrete mixture contents due to the fibre addition. Similar results were observed by Mashrei et al. (2018), who reported a sharp increase in the compressive strength of concrete reinforced with polypropylene fibres from 0% to 0.2% and thereafter a moderate increase to 0.5%. Another research carried out by Nuruddin (2015) indicated that PVA fibres have a small effect in increasing the compressive strength of FRCC. The author further reported that the optimum results for PVA addition were at 0.5%, which is consistent with the results obtained in the present study. Govindasami et al. (2018) studied the effect of polypropylene fibre on the compressive strength of concrete and reported an initial increase in strength up to 1.0% fibre addition. Thereafter, there was a significant decrease in compressive strength.

There is a sharp decrease in compressive strength between 0.5% and 1.0% fibre addition due to fibres having a negative effect on the hydration of cement. Furthermore, high fibre percentages tend to encourage fibre clumping during fabrication. Fibre clumping creates nucleus sites for crack formation under a compression load, leading to lower compressive strength. The use of a high percentage of fibre in FRCC > 0.5% significantly affects the workability of the concrete. The finish of the concrete is not smooth and may have some voids, which are the origin of the failure cracks of the concrete under compressional load. It was concluded that the best range of PET fibre addition is between 0.1% and 0.5% for optimal compressive strength of the FRCC.

4.2.3.1.1.2 Effects of fly ash addition on composite compressive strength

The graph shown in Figure 4-16 shows the effect of varying fly ash mass fractions on the 28-day concrete compressive strength.

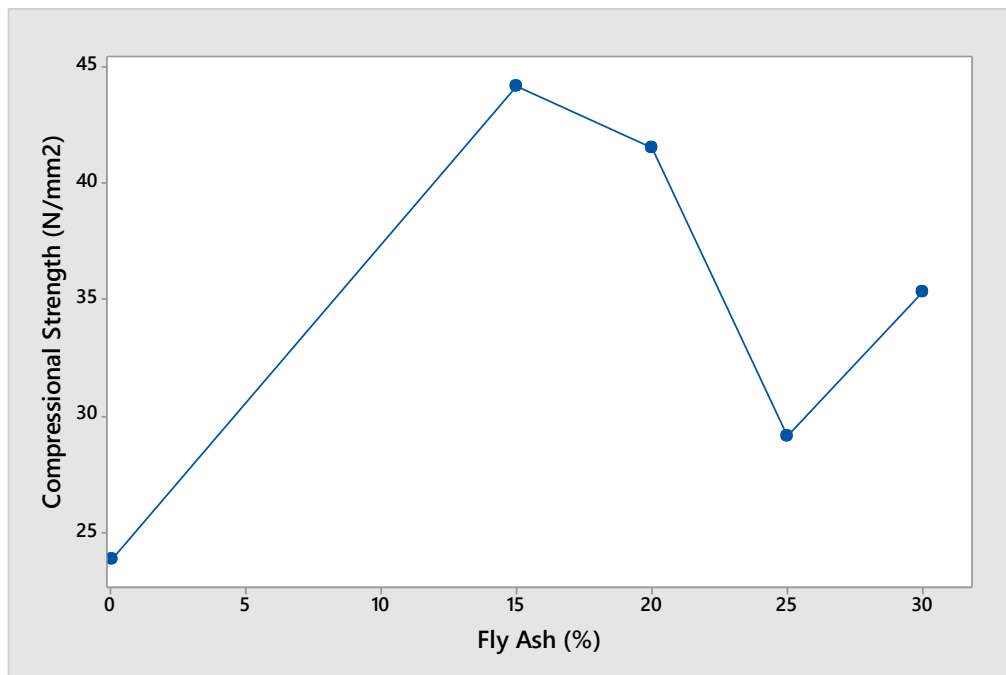


Figure 4-16 – Effects of Fly Ash Addition on Compressive strength

The compressive strength of concrete increases sharply with cement replacement with fly ash up to 15%, as shown in Figure 4-16. The control specimen has a compressive strength of 23 N/mm² this strength rises sharply to 43 N/mm² with 15% replacement with fly ash. Thereafter, there is a slight decline with any further replacement of cement with fly ash, as can be seen with the 20% fly ash replacement having a compressive strength of 41 N/mm². There is a further significant decline in the compressive strength with 25% replacement of cement with fly ash, giving compressive strength of 28 N/mm². Thereafter, there is an increase in compressive strength with a further increase in fly ash, as shown by the strength of 30% fly ash replacement of cement, giving a strength of 36 N/mm². The compressive stress on the concrete followed a similar trend to the compressive strength, as shown in Figure 4-17.

The maximum compressive stress was obtained at 15% fly ash addition and thereafter a decline in stress up to 25%. However, 30% fly ash added gave a moderate increase in compressive stress, as shown in Figure 4-17.

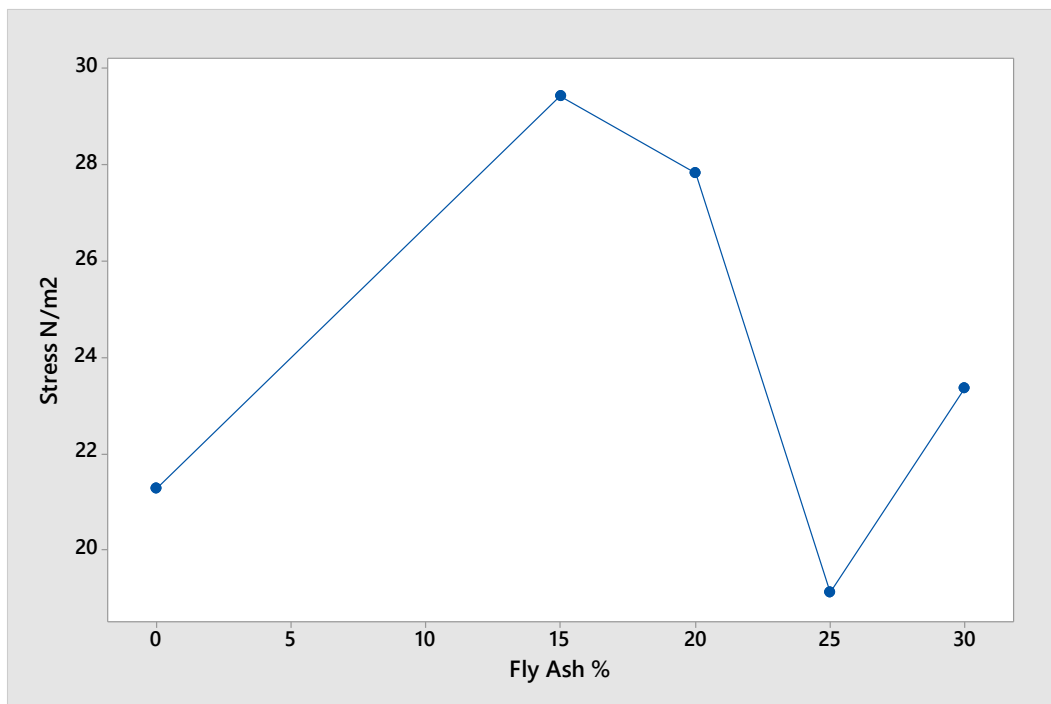


Figure 4-17 - Effects of Fly Ash Addition on Compressive Stress of Concrete

The results obtained in this study were consistent with results obtained by Yerramala et al. (2012) and George et al. (2018), who both reported that an increase in fly ash content up to 15% had a significant increase in compressive strength. The study by Yerramala et al. (2012) reported a significant drop in compressive strength with the addition of 25%, which was consistent with the trend obtained in the present study. However, the research by Yerramala et al. (2012) focused on M10 concrete mix design; hence the obtained compressive strength values were lower than those observed in the current study.

Patel et al. (2012) reported a decrease in compressive strength of concrete beyond 15% fly ash addition. This agreed with the results obtained in the current study. A study by Chethan et al. (2015) and Sivakumar et al. (2015) reported a similar trend to that observed in the current study, as shown in Figure 4-18 for compressive strength.

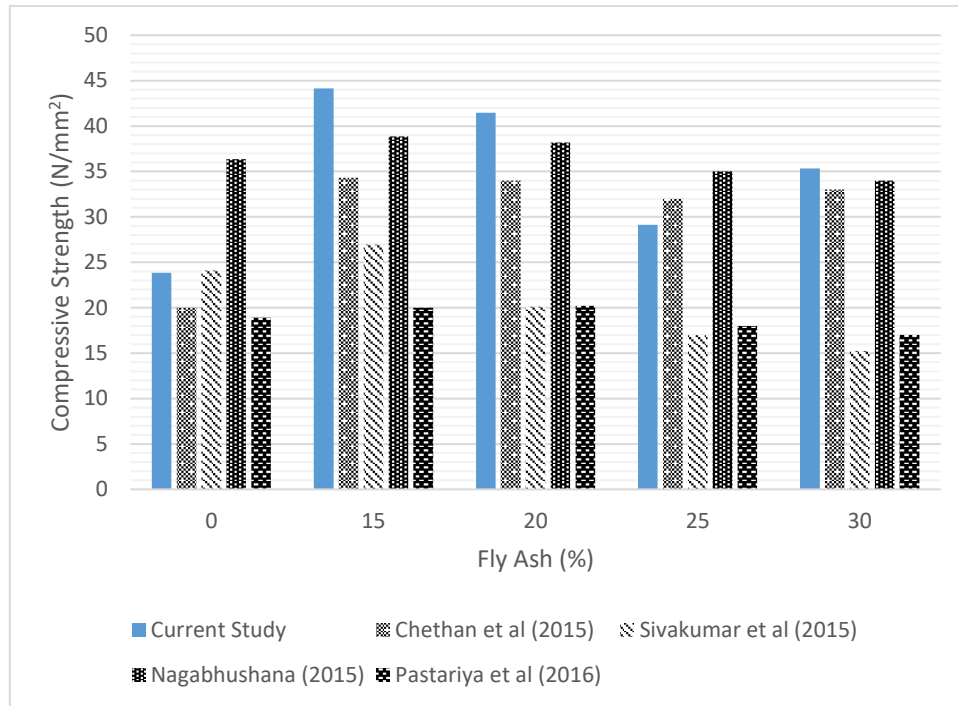


Figure 4-18 – Compressive Strength Comparison

From Figure 4-18, the highest compressive strength as reported by Chethan et al. (2015), Sivakumar et al. (2015), Pastariya & Keswani (2016) and Nagabhushana (2015) was at 15% fly ash addition which was consistent with the results obtained in the current study.

However, the results obtained contrasted with a study by Joshi (2017), who reported a decrease in compressive strength with an increase in fly ash content. The study reported compressive strength of 19.64 N/mm² for 10% fly ash replacement and 18.07 N/mm² for 20% replacement. However, in the current study, the compression strength increased with an increase in fly ash replacement with 20% replacement giving a compressive strength of 41 N/mm², which was greater than that observed on the control specimen, which had the strength of 23 N/mm². The difference in these results could be attributed to the type of fly ash used in the study.

4.2.3.1.1.3 Effects of a combination of PET fibre addition and fly ash on composite compressive Strength

The graph in Figure 4-19 shows the effect of PET fibre addition on various fixed percentages of fly ash and the relationship with the 28-day compressive strength.

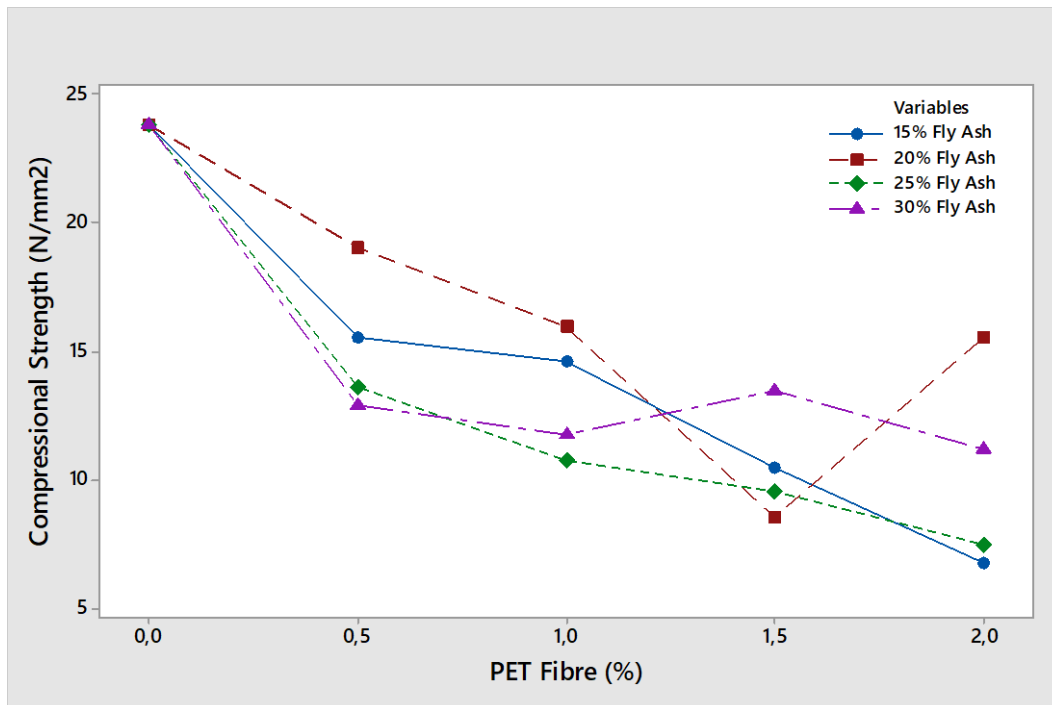


Figure 4-19 – Combined Effect of Fibre and Fly Ash Addition on Compressive strength

The addition of both fibre and fly ash in the FRCC had an adverse effect on the compressive strength. For all samples in the experimental design, the combined addition of fly ash and PET fibre decreased the ultimate compressive strength.

The FRCC containing 15% fly ash had a sharp decline in compressive strength of 34.8% within the first 0.5% fibre addition, with strength dropping from the control of 23.84 N/mm² to 15.54 N/mm². After that, there was a marginal 5.9% drop in compressive strength between 0.5% and 1.0%. There was a constant decline in compressive strength from 1.0% to 2%.

The FRCC containing 20% fly ash had an almost constant decline in compressive strength up to 1.0% fibre addition. However, this composition had the best overall compressive strength compared to the other samples with different fly ash content. There was a drastic decrease in compressive strength between 1.0% and 1.5% from 15.96 N/mm² to 8.50 N/mm², respectively. However, the compressive strength picked up with the addition of more fibre with 2.0% fibre addition having a strength of 15.53 N/mm².

The FRCC containing 25% ash exhibited a similar trend to that containing 20% up to 1.0% fibre content. This was the third strongest mix design containing fly ash. From 1.0% to 2.0% fibre addition, there was an almost constant and marginal decrease in compressive strength.

The FRCC containing 30% exhibited the lowest compressive strength at 0.5% fibre addition of all the specimens. However, from 0.5% to 1.5%, there was an increase in compressive strength, which

surpassed that of mix design with 25% at 0.5% and was greater than all other mix designs at 1.5%. But, from 1.5%, there was a decline in compressive strength to 7.44 N/mm².

The graph in Figure 4-20 shows the combined effect of fibre and fly ash on the compressive material stress of the specimens.

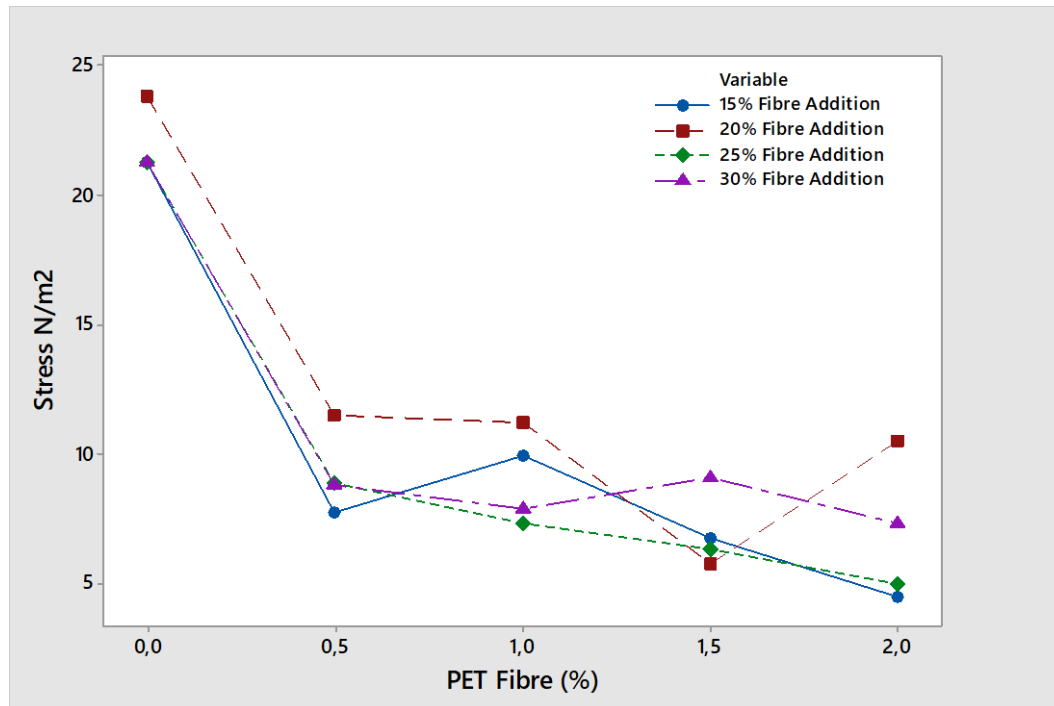


Figure 4-20 – Combined Effect of Fibre and Fly ash addition on FRCC compressive stress

The trend observed for the stress on the FRCC was like that of the compressive strength in Figure 4-19. The results show that the addition of PET fibres has an adverse effect on the compressive strength regardless of the fly ash quantity used. This conclusion is reasonable as several researchers (Exeldin & Balaguru, 1992; Fanella & Naaman, 1985; Shaikh & Taweel, 2015) have reported a similar decrease or lack of improved compressive strength concrete with the addition of polymeric and natural fibres. The poor compressive strength with PET fibre reinforced concrete can be attributed to a poor interfacial bond between the fibre and cement matrix. Furthermore, the increase in porosity in the concrete mixture can be a significant contributing factor, as stated in Jiang et al. (2014) study. However, the addition of steel fibres into the concrete slightly increases the compression strength. This increase in strength can be attributed to the stiffness of the steel fibres compared to flexible polymeric fibres. Another study by Prahallada and Prakash (2013) investigated the effect of waste fibre reinforced concrete and fly ash on the compressive strength of concrete. The study reported that there was a decrease in compressive strength with all combinations, and this agreed with the results obtained in this study. There is a need to study the effect of a hybrid FRCC containing both steel fibres and PET fibres to ascertain the improvement, if any, in the compressive strength of the composite.

4.2.3.1.2 Split tensile strength test

The influence of fly ash and PET fibre on the split tensile strength of concrete was studied according to the design of the experiment at the ultimate 28-day compressive strength. The split tensile strength test results are presented in the following subheadings.

4.2.3.1.2.1 Effects of PET fibre addition on composite split tensile strength

The graph in Figure 4-21 shows the effect of fibre addition on the split tensile strength of FRCC.

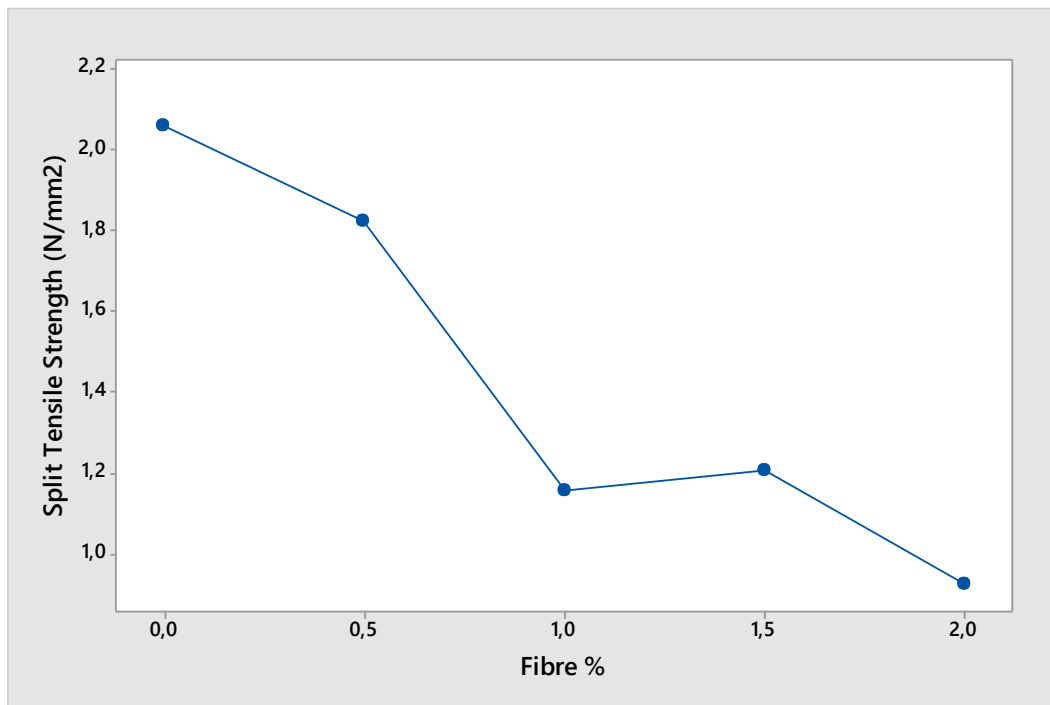


Figure 4-21 – Effect of Fibre Addition on Split Tensile Strength of FRCC

The addition of fibre decreased the split tensile strength of the FRCC. Unreinforced concrete had a split tensile strength of 2.06 N/mm² which dropped marginally to 1.82 N/mm² with 0.5 % PET fibre. However, the further addition of PET fibre resulted in a drastic drop in the split tensile strength. The addition of 1.0 % PET fibre gave a split tensile strength of 1.16 N/mm². This was a drop of 44% from the split tensile strength of unreinforced concrete. After that, there was a slight increase in the split tensile strength with a 1.5 % addition of PET fibre, giving a strength of 1.21 N/mm².

Further addition of PET fibre to 2.0 % resulted in a reduction of split tensile strength to 0.92 N/mm². The splitting strength of the FRCC was negatively affected by the addition of fibres. However, the fibres helped delay the development and propagation of cracks during the testing.

The low splitting strength with an increase in fibre content could be attributed to the effect of high air voids due to fibre clumping. These results were consistent with the study carried out by Irwan et al. (2013), who reported a decrease in split tensile strength with PET filaments. The author reported that

the split tensile strength dropped from 3.65 N/mm², the control specimen, to 3.57 N/mm² with 0.5 % PET filament reinforced concrete. Irwan et al. (2013) reported a steady reduction of split tensile strength up to 1.5% PET fibre addition with various water to cement ratios the trend remained the same. In contrast, Govindasami et al. (2018) reported a marginal 19 % increase in split tensile strength of FRCC containing polypropylene fibre up to 1.0 % fibre addition. The increase in strength, which contrasts with the current study, can be attributed to polypropylene's significantly higher fibre tensile strength properties over PET.

4.2.3.1.2.2 Effects of fly ash addition on composite split tensile strength

The graph in Figure 4-22 shows the effect of fly ash on the split tensile strength of concrete.

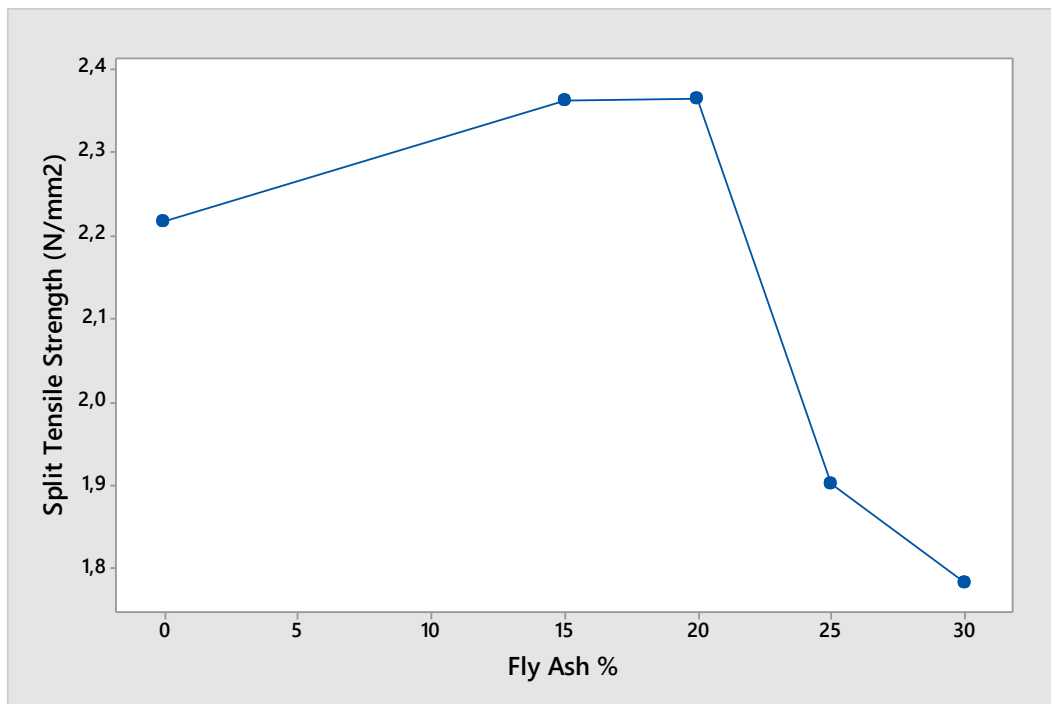


Figure 4-22 – Effect of fly Ash on the Split Tensile Strength of the FRCC

The concrete's split tensile strength increased with the addition of 15% fly ash from the control, which had the strength of 2.06 N/mm² to 2.36 N/mm². There was a further moderate increase in split tensile strength with further addition of fly ash of 20%, which gave a strength of 2.37 N/mm². After that, any further fly ash addition beyond 20 % resulted in a drop in the split tensile strength. The addition of 25% fly ash gave a drastic drop in split tensile strength to 1.98 N/mm². Further addition of fly ash to 30% reduced the split tensile strength further to 1.78 N/mm². It was concluded from these results that 20% addition of fly ash gives the highest split tensile strength of the DOE.

The results obtained are consistent with those reported in the literature by Yerramala et al. (2012), who reported an increase in split tensile strength with the addition of up to 15% fly ash and a decrease in strength after that. The initial increase in split tensile strength with the addition of fly ash up to 20%

can be attributed to an increase in the cohesiveness of the matrix. The use of fly ash in concrete can increase durability through a reduction in permeability hence, its use in the construction of dams (Patel, et al., 2012). A comparison with a study by Sivakumar et al. (2015), Singh et al. (2017) and Nagabhushana (2015) showed a similar trend with the current study, as shown in Figure 4-23.

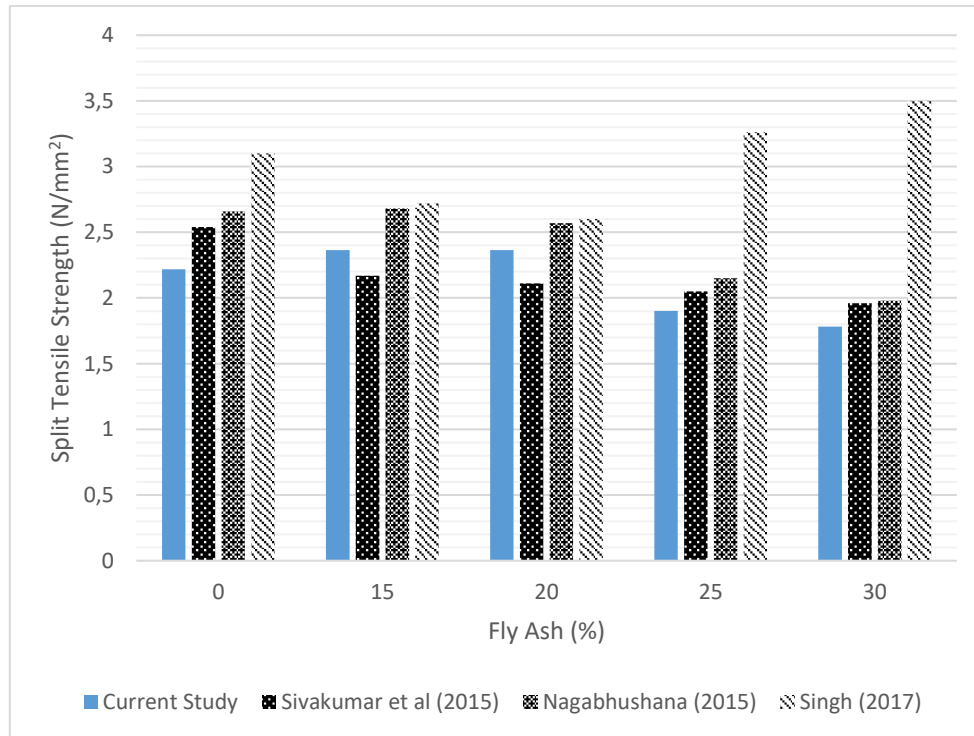


Figure 4-23 – Split Tensile Strength Comparison

The comparative results in Figure 4-23 show that the optimum fly ash addition is a 15% cement replacement. It can also be concluded that the addition of fly ash of > 25% has an adverse effect on the split tensile strength of concrete. The study by Singh et al. (2017) showed a sharp increase in split tensile strength with 25% fly ash. This sharp increase could be attributed to the type of fly ash, which was bottom ash used by the researcher. The variation in the results shows that there is potential for better results at higher fly ash percentages with the use of bottom fly ash.

There has been a lot of research supporting using fly ash to increase the split tensile strength of concrete due to its ability to increase the workability of concrete. Furthermore, the spherical shape of the fly ash particles improves the cohesiveness of the concrete mixture with minimum bleeding and segregation, according to a study by Nagabhushana (2015), Nale et al. (2012) and Mullick (2005).

4.2.3.1.2.3 Combined effects of fibre and fly ash on composite split tensile strength

The graph in Figure 4-24 shows the combined effects of fibre and fly ash addition on the split tensile strength of the FRCC.

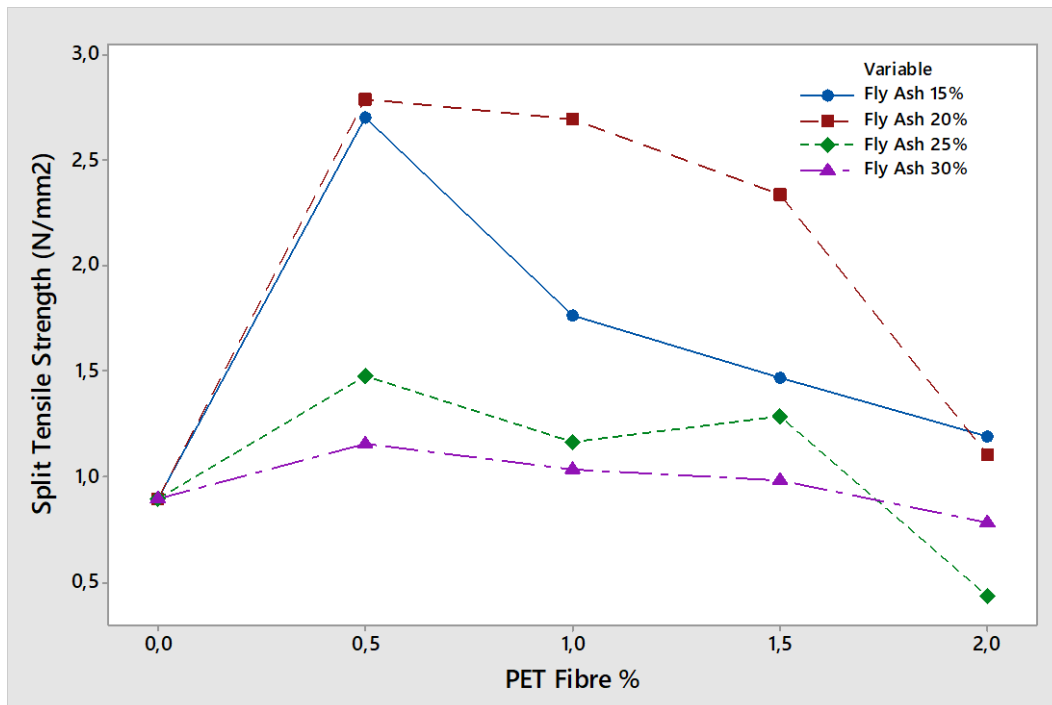


Figure 4-24 – Combined Effects of Fibre and Fly Ash on Split Tensile Strength

The FRCC containing 20% fly ash had the highest flexural strength at 0.5% PET fibre addition with a splitting tensile strength of 2.79 N/mm² compared to the control specimen with the strength of 0.90 N/mm². However, there was a gradual reduction in the split tensile strength with the further addition of PET fibre. The addition of 1.0% PET fibre gave a split tensile strength of 2.69 N/mm². Further, the addition of PET fibre reduced the split tensile strength even further, with 1.5% PET fibre addition giving the strength of 2.34 N/mm² and 2.0% PET fibre giving a strength of 1.11 N/mm².

The FRCC containing 15% fly ash had a significantly high split tensile strength of 2.70 N/mm² at 0.5% addition of PET fibre. This FRCC exhibited a similar trend for 0.5% PET fibre addition with the FRCC containing 30% fly ash. Further PET fibre addition to 1.0% resulted in a sharp decrease in the split tensile strength to 1.77 N/mm². After that, there was a slight decrease in split tensile strength with increased PET fibre content with 2.0% PET fibre content having a split tensile strength of 1.19 N/mm². However, this split tensile strength was still higher than that observed on the control specimen, which was 0.90 N/mm².

The FRCC containing 25% fly ash content had a marginal increase in split tensile strength with the addition of 0.5% PET fibre giving a strength of 1.48 N/mm². After that, a decrease in strength was observed with 1.0% PET fibre content giving a strength of 1.29 N/mm². There was a sharp decline in strength with 2.0% PET fibre content which gave the strength of 0.44 N/mm², which was way less than the control specimen split tensile strength of 0.90 N/mm².

The FRCC containing 30% fly ash had the lowest split tensile strength at PET fibre content of between 1.0% and 1.5%. PET fibre addition of 0.5% yielded the highest strength for the fly ash ratio giving a strength of 1.16 N/mm². After that, the trend was indicative of a steady decline in the split tensile strength with 1.0% PET fibre yielding 1.03 N/mm² and 1.5% PET fibre content giving the strength of 0.98 N/mm². PET fibre addition of 2% gave the lowest split tensile strength of 0.89 N/mm².

The addition of fibres significantly altered the failure pattern of the concrete. The concrete containing fibres had a complex crack propagation due to the bridging and retardation effect of the fibres, as shown in Figure 4-25. This phenomenon made the concrete, despite being weaker to be able to withstand load for longer before failure. This analogy agrees with a study by Truong (2012) and Vu et al. (2020), who reported that fibre content is mainly used for crack control and used in percentages less than 0.3.



Figure 4-25 – Split Tensile Failure of Concrete Cylinder a) Unreinforced concrete b) FRCC

4.2.3.1.3 Flexural strength test

The flexural strength of concrete was measured according to the experimental design at 28 days. The results for the flexural strength test are presented in the following subheadings.

4.2.3.1.3.1 Effects of fly ash addition on composite flexural strength

The graph in Figure 4-26 shows the effects of cement replacement with fly ash on the flexural strength of concrete.

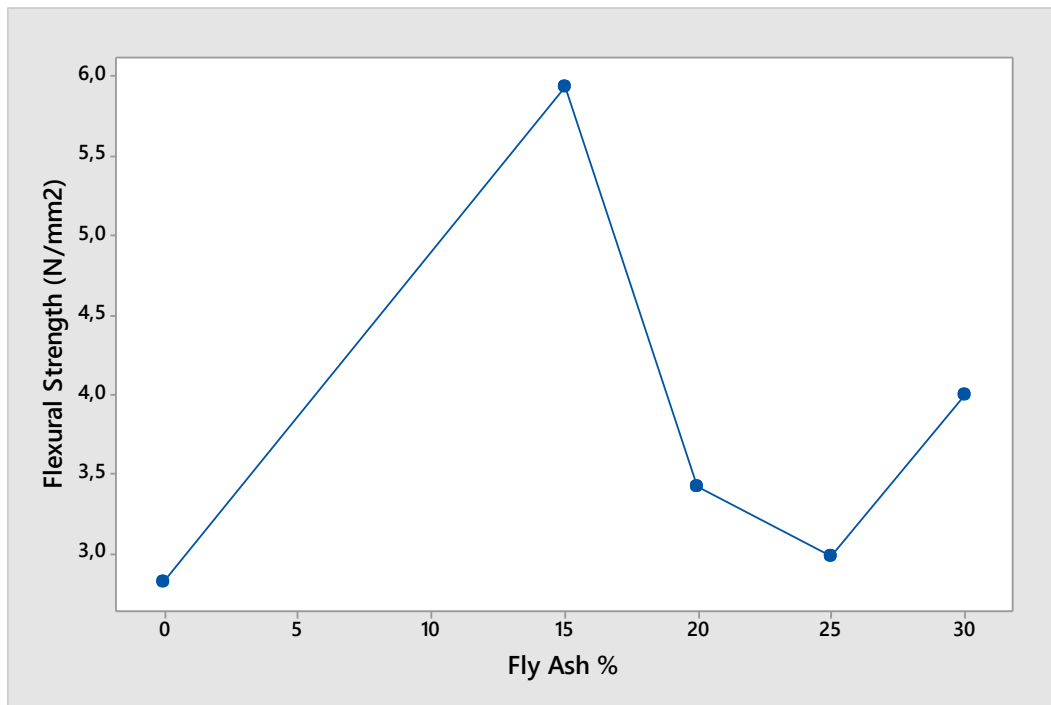


Figure 4-26 – Effect of fly ash on flexural strength

The addition of 15% fly ash has a significant impact on the flexural strength of concrete. The strength of concrete increases from the control value of 2.82 N/mm² to 5.94 N/mm² for 15% fly ash addition.. This is a 52.5% increase in strength. Thereafter, any addition of fly ash resulted in a reduction in flexural strength. There was a drastic decrease in the flexural strength with 20% fly ash addition giving a flexural strength of 3.42 N/mm². This decrease was still above the flexural strength of the control specimen.

Further, the addition of fly ash to 25% resulted in a further decrease in flexural strength to 2.99 N/mm². However, adding 30% fly ash increased the flexural strength marginally to 4.00 N/mm² which was greater than that of both 25% and 20% fly ash addition. The addition of 15% fly ash gave the highest flexural strength.

The results obtained following a similar trend to a study by Vinodsinh & Pitroda (2013) and Upadhyay et al. (2014), who reported an increase in flexural strength with the addition of fly ash up to 15%. The authors thereafter observed a significant decrease in flexural strength to less than that of the control specimen. The study by Nagabhushana (2015) and Upadhyay (2014) showed a similar trend with an increase in flexural strength with 15% fly ash, as shown in Figure 4-27.

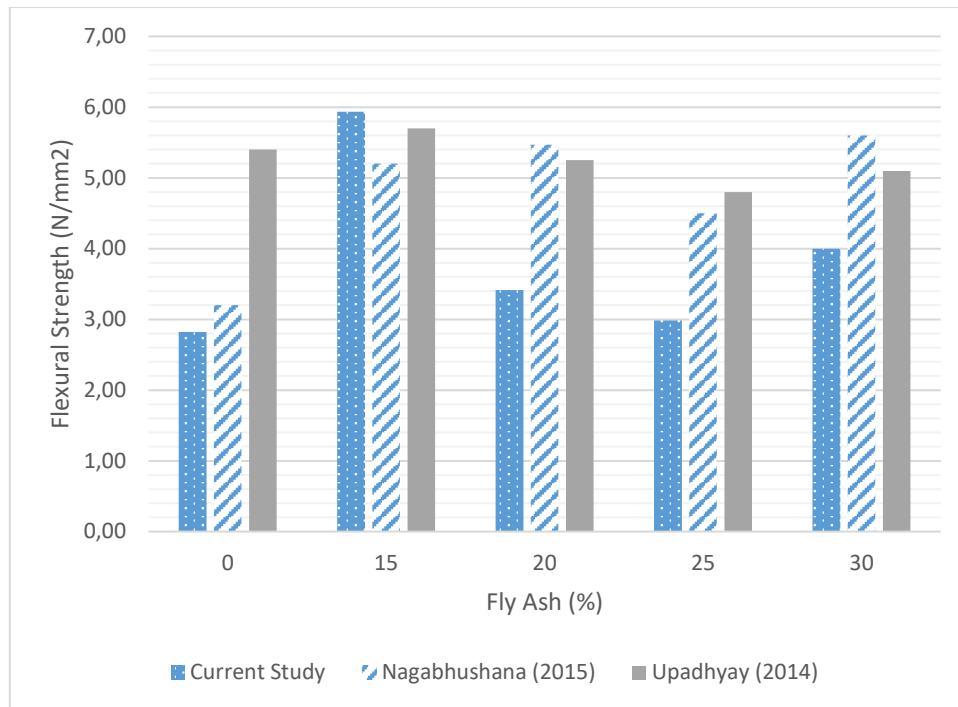


Figure 4-27 – Flexural Strength Comparison

Beyond 20% fly ash, an additional study by Nagabhushana (2015) and Upadhyay (2014) showed a marginal drop in flexural strength, contrasted with the present study. The reason for the low flexural strength in the present study could be attributed to the poor compaction of the concrete.

Jayeshkumar et al. (2012) reported that fly ash reduced the strength of the concrete with an increase in the percentage of fly ash added, and this reduction agreed with the results obtained in this study. A study by Kazberuk & Lelusz (2007) highlighted that the strength gain of concrete containing fly ash is slower than control specimens without fly ash. This implies that there is a possibility of a further increase in strength properties between 28 and 180 days.

4.2.3.1.3.2 Effects of fibre addition on flexural strength of composite

The graph in Figure 4-28 shows the effects of fibre addition on the flexural strength of the FRCC.

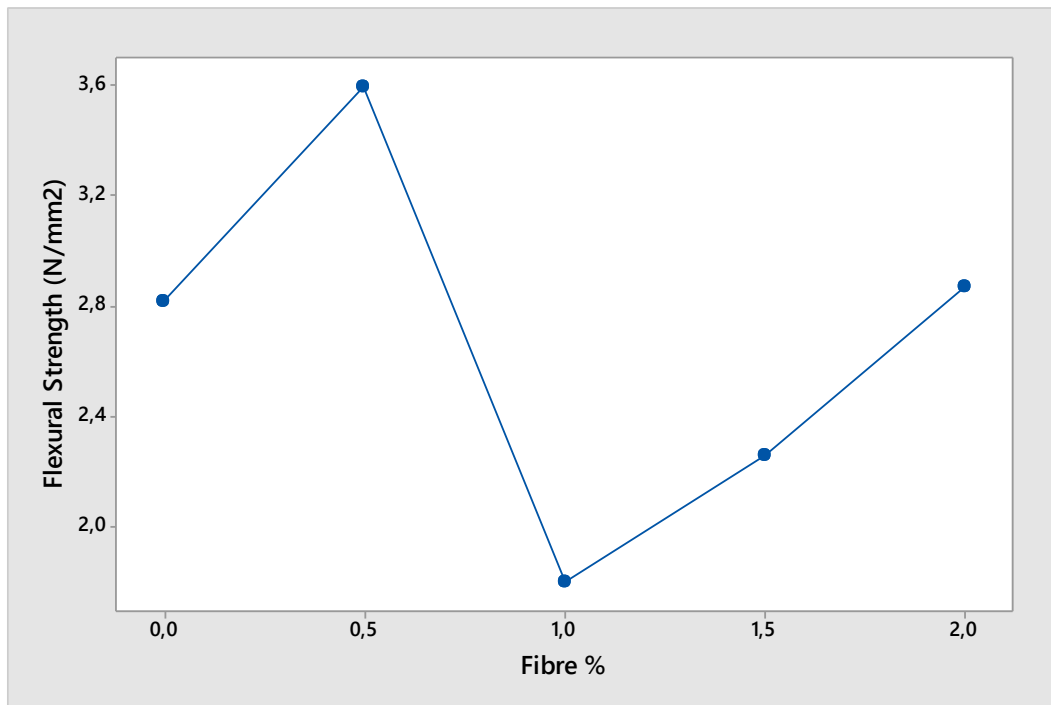


Figure 4-28 – Effect of Fibre Addition on Flexural Strength

The addition of 0.5% PET fibre increased the flexural strength of the FRCC significantly from the control specimen of 2.82 N/mm² to 3.59 N/mm². Adding a further quantity of PET fibre to 1% resulted in a drastic drop in the flexural strength to less than that observed for the control specimen giving a flexural strength of 1.80 N/mm². Further, the addition of fibre gave a steady increase in flexural strength. In addition, 1.5% PET fibre gave flexural strength of 2.25 N/mm². Further, the addition of PET fibre to 2.0% gave flexural strength of 2.87 N/mm². The highest flexural strength was obtained with 0.5% PET fibre addition.

The results are consistent with Govindasami (2018) results, who also reported a significant increase in flexural strength with the addition of polypropylene fibre up to 0.5% after that, a drastic reduction in flexural strength with the addition of 2.0% fibre.

4.2.3.1.3.3 Effects of combined fibre and fly ash addition on flexural strength of composite

The graph in Figure 4-29 shows the combined effects of fly ash and PET fibre on the FRCC flexural strength.

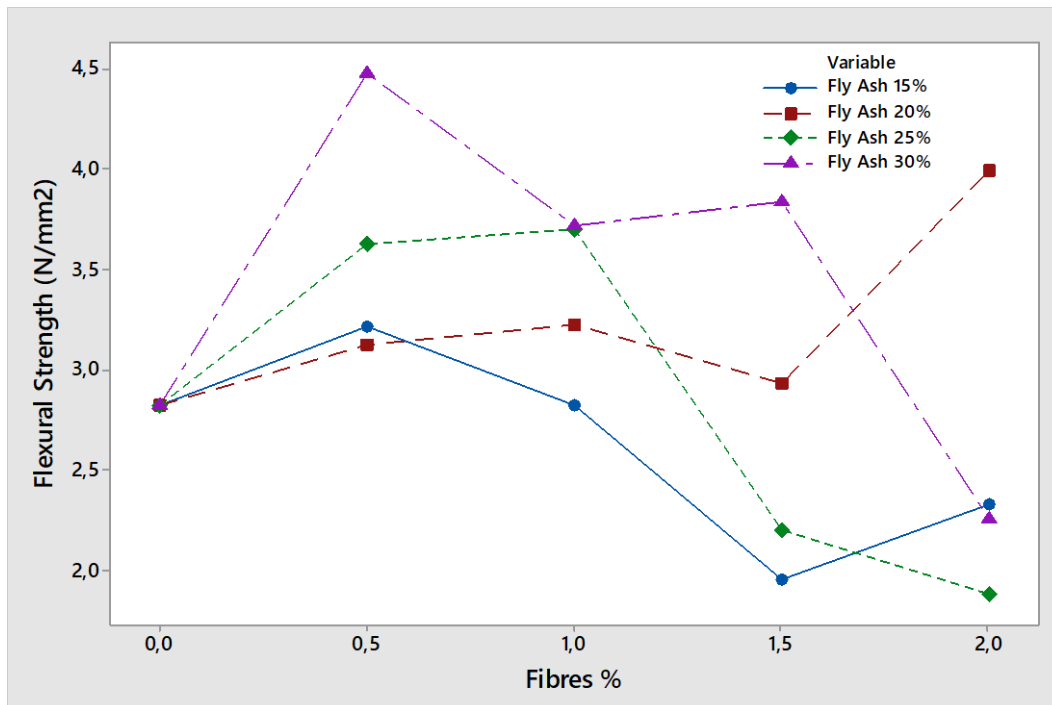


Figure 4-29 – Effects of combined fibre and fly ash addition on FRCC

The FRCC containing 15% cement replacement with fly ash showed the highest flexural strength at 0.5% PET fibre addition of 3.220 N/mm². Further addition of PET fibre decreased flexural strength with 1% PET fibre addition giving 2.825 N/mm². This strength was still greater than the control specimen flexural strength of 2.820 N/mm². Further addition of PET fibre to 1.5% resulted in a slight increase in flexural strength to 1.960 N/mm². The addition of PET fibre to 2.0% resulted in a drastic decrease in flexural strength to 2.335 N/mm² which was less than observed in the control specimen.

PET fibre addition of 0.5% and 20% fly ash content resulted in all the specimens' lowest flexural strength. However, the flexural strength obtained of 3.125 N/mm² was still greater than that of the control specimen of 2.820 N/mm². There was a slight increase in flexural strength with 1.0% PET fibre. The addition of 1.5% PET fibre resulted in a slight decrease in flexural strength to 2.930 N/mm². However, the addition of 2.0% PET fibre resulted in a significant increase in flexural strength to 3.995 N/mm². This magnitude was the highest flexural strength realised for the 20% fly ash composite.

The specimen containing 25% fly ash had the second-highest flexural strength at 0.5% PET fibre addition of 3.625 N/mm². There was a slight increase in flexural strength with 1.0% PET fibre to 3.70 N/mm². After that, any further addition of PET fibre resulted in a decline in flexural strength with 1.5% PET fibre addition giving flexural strength of 2.20 N/mm². This magnitude was less than the control specimen, which had a flexural strength of 2.820 N/mm². Besides, the addition of 2.0% PET fibre gave flexural strength of 1.885 N/mm².

The FRCC containing 30% fly ash had the highest flexural strength of 4.47 N/mm² with 0.5% PET fibre addition. Further addition of PET fibre resulted in a decrease in flexural strength with 1.0% PET fibre addition giving flexural strength of 3.72 N/mm². In contrast, the addition of 1.5% fibre gave a moderate increase in flexural strength to 3.84 N/mm². Further addition of 2.0% fibre content drastically decreased flexural strength to 2.25 N/mm².

The overall optimum flexural strength was obtained with the specimen containing 30% fly ash at 0.5% PET fibre addition which had a strength of 4.47 N/mm². This optimum increased 37% in flexural strength over the control specimen.

4.2.3.2 Non-destructive composite test

A rebound hammer non-destructive test was carried out on the FRCC. The results are discussed in the following subsequent subsections as well as a comparison with the destructive test results.

4.2.3.2.1 Rebound hammer test

The following subsections report and discuss the rebound hammer test results. The fully detailed rebound hammer measurement table is shown in Appendix E. The Rebound hammer test gives an estimation of the mechanical properties of the FRCC. The guideline for rebound numbers is as reported by Divvala & Rani (2020) in Table 4-12.

Table 4-12 – Concrete guideline for Rebound Hammer Test (Divvala & Rani, 2020)

Rebound number	Concrete quality
>40	Very good
30-40	Good
20-30	Fair
<20	Poor

4.2.3.2.1.1 Effects of fly ash on rebound number

The graph in Figure 4-30 shows the effects of fly ash on the rebound number.

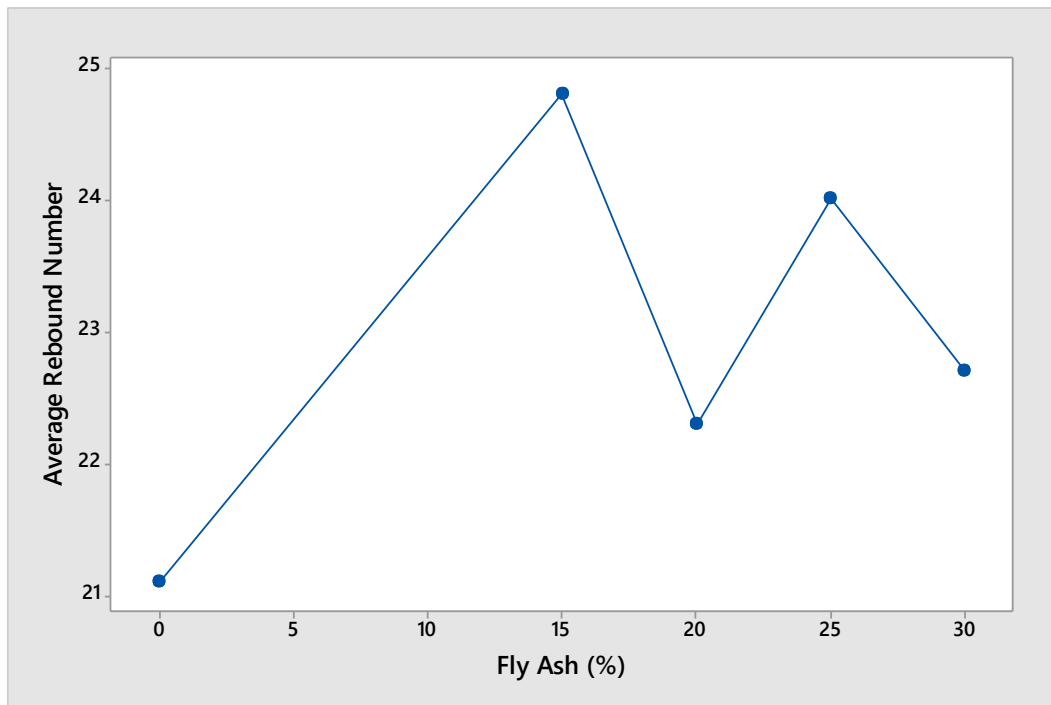


Figure 4-30 – Effect of fly ash addition on rebound number

The addition of 15% fly ash resulted in a drastic increase in the Schmidt rebound number from the control rebound number of 21.1 to 24.8. Thereafter, there was a decline in the rebound number with the addition of 20% fly ash to 22.3. The addition of 25% fly ash resulted in a marginal increase in the rebound number to 24.0. Further, the addition to 30% of fly ash resulted in a drop in the rebound number to 22.7. The rebound number obtained for all the fly ash specimens was higher than the control specimen.

The rebound number obtained for all fly ash containing samples in the study fell into the fair region of concrete quality based on the rebound number as shown in Table 4-12. A comparison between the non-destructive rebound hammer compressive strength and the destructive cube test was made to establish a relationship between the two measurement techniques. This relationship was plotted on a graph, as shown in Figure 4-31. Table 4-13 shows a comparison between the current study and the rebound number obtained in a study by Reddy (2014).

Table 4-13 – Comparison of Rebound Number

Fly Ash (%)	Current Study	Reddy V (2014)
0	21,10	20,00
15	24,80	21,00
20	22,30	20,00
25	24,00	18,00
30	22,70	17,00

The trend obtained by Reddy (2014) agrees with the current study. There is an increase in the rebound number up to 15% fly ash addition thereafter, and there is a steady decline in the rebound number.

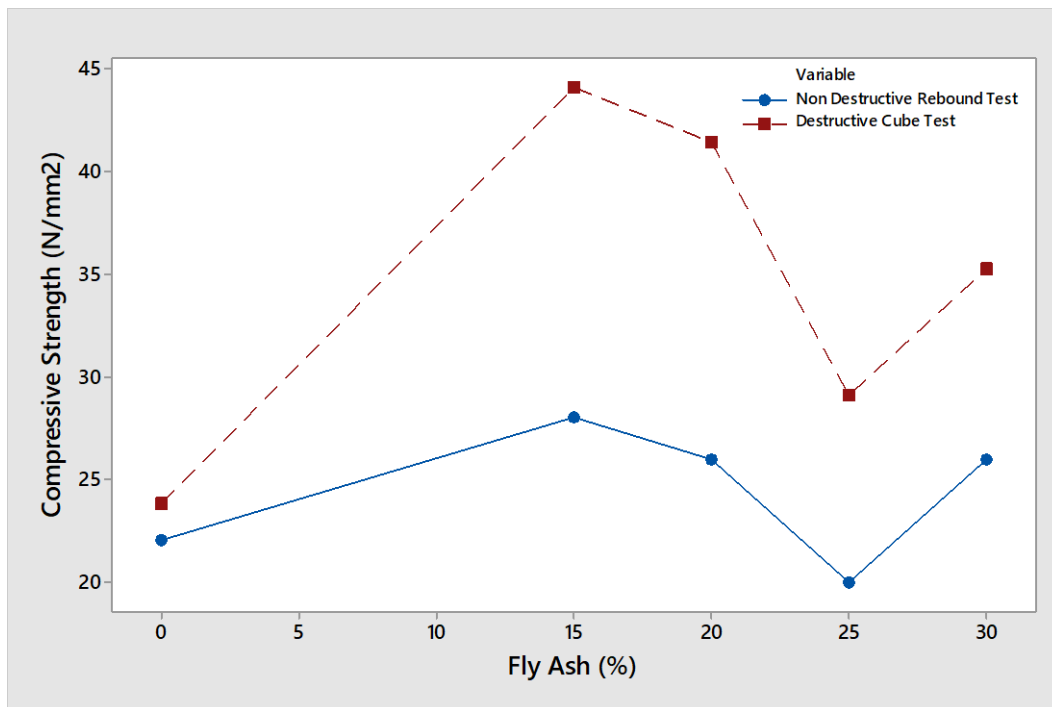


Figure 4-31 – Comparison between non-destructive and destructive cube test results

Figure 4-31 shows that the measurement of concrete compressive strength using the NDT rebound hammer method gives a significantly lower compressive value to the actual value obtained through compressive strength. The rebound hammer test is about 20–45% of the actual compressive strength, and this range is similar to a report given by Shaikuthali S (2019). The study reported that the NDT method gives 20-40% of the actual concrete compressive strength. From the results, it might seem there is no direct correlation between the strength of the concrete and the rebound number. However, the similarity of the trend of the destructive and non-destructive test in Figure 4-31 clearly show that within certain constraints, there exists an empirical correlation between the compressive strength and the derived rebound hammer compressive strength. As shown in this study, this correlation requires calibration to suit the type of concrete being tested to give accurate results.

4.2.3.2.1.2 Effects of fibre on rebound number

The graph in Figure 4-32 shows the average rebound number with an increase in PET fibre addition.

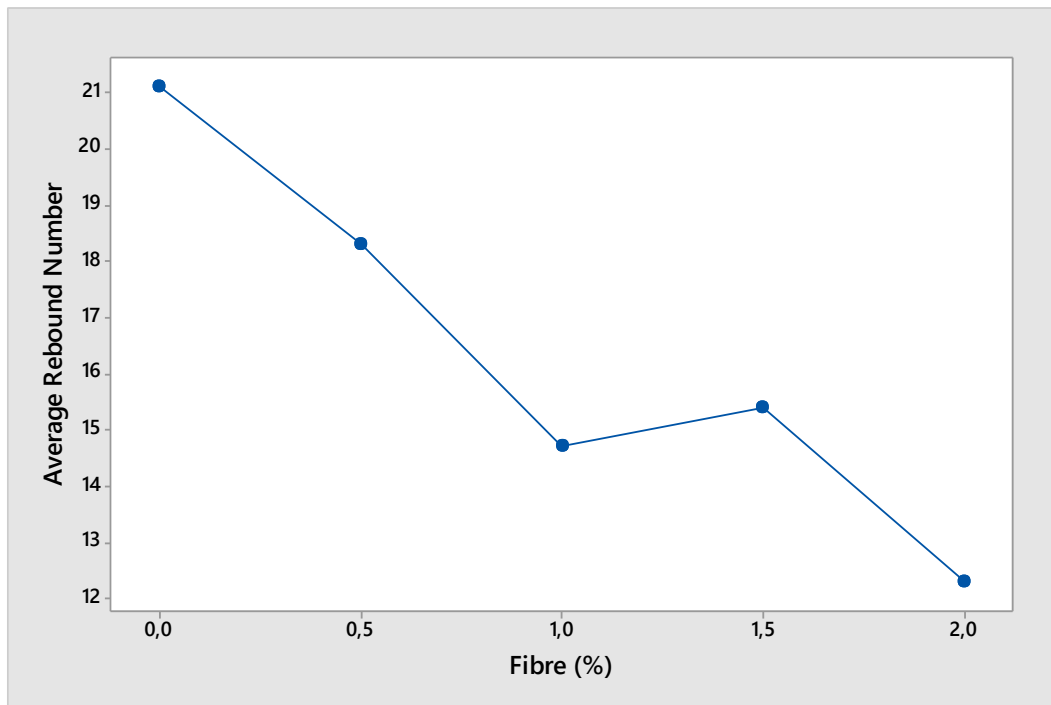


Figure 4-32 – Average Rebound number for FRCC with PET fibre addition

The addition of PET fibres lowered the rebound number as the percentage of fibres increased. The addition of 0.5% PET fibre resulted in a reduction of 13.27% from the control specimen. Further addition of PET fibre to 1.0% resulted in a decrease in rebound number of 19.67% from that of 0.5% fibre content. However, the addition of 1.5% fibre content resulted in a slight increase in the rebound number. Further addition of 2.0% fibre resulted in a drop in rebound hammer number to 12.3. Figure 4-33 shows a comparison between the compressive strength obtained from the destructive cube test and the results of the rebound compressive test.

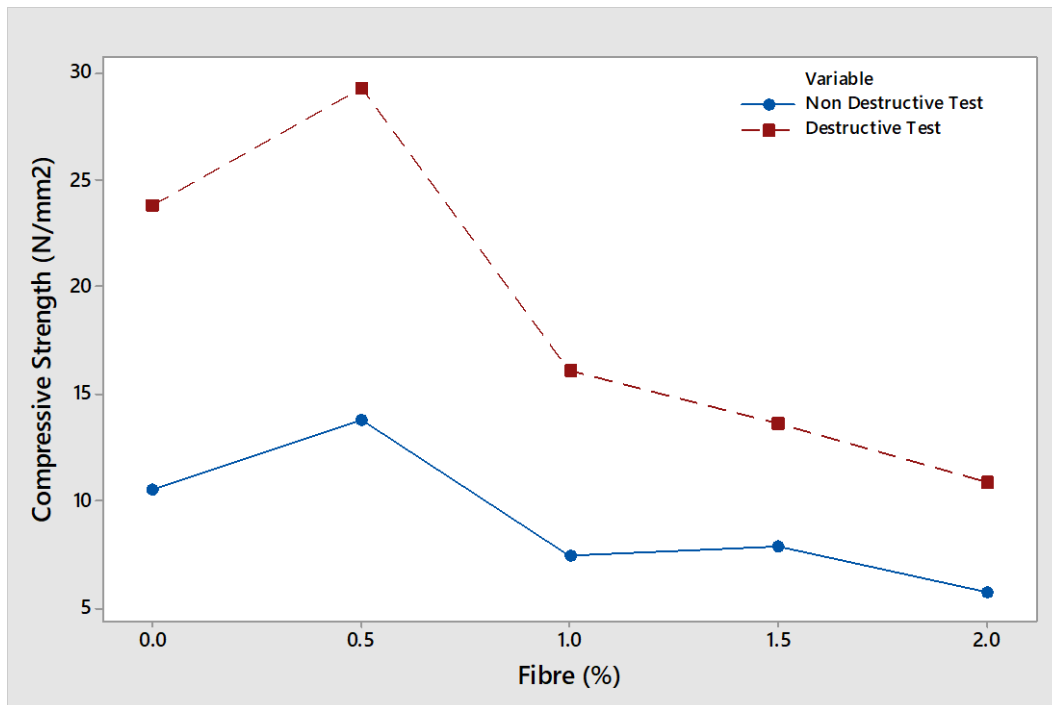


Figure 4-33 - Comparison between non-destructive and destructive cube test results for PET fibre

The non-destructive test results follow the same trend as that of the destructive tests, which indicated a decrease in compressive strength with an increase in PET fibre content. The trend observed was like that reported by Ede and Ige (2014), who reported a decrease in the rebound number of concretes containing polypropylene fibre.

4.2.3.2.1.3 Combined effects of fibre and fly ash on rebound number

The graph in Figure 4-34 shows the effects of PET fibre and fly ash on the FRCC rebound number.

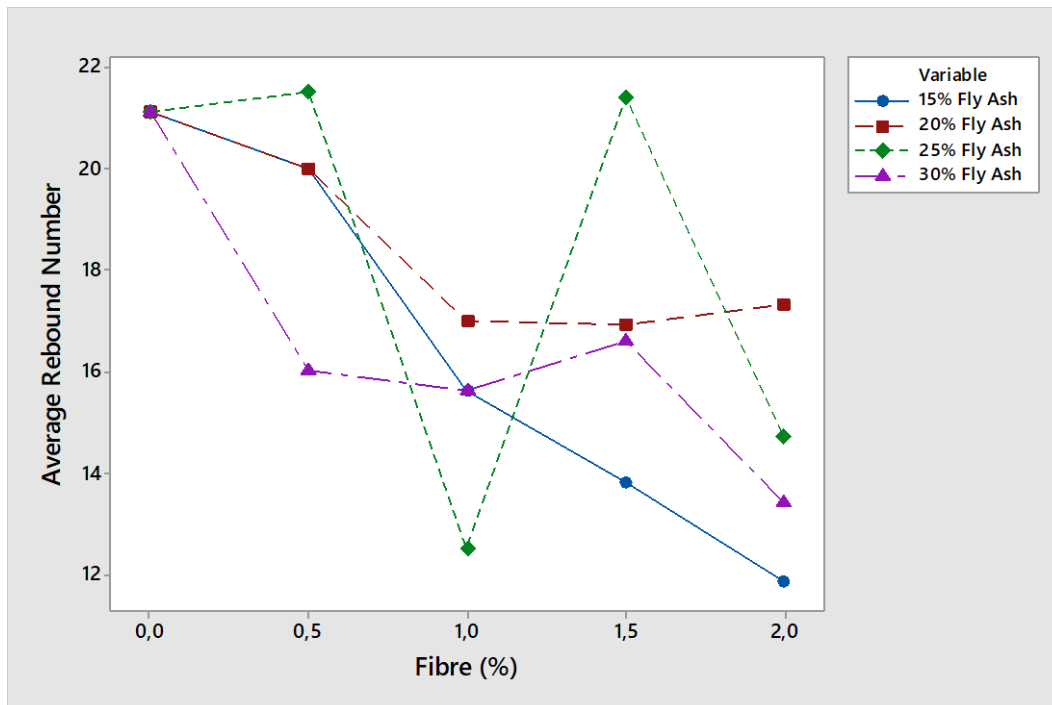


Figure 4-34 – Average Rebound Number of combined fibre and fly ash FRCC

The rebound number for the FRCC containing 25% fly ash has the highest rebound number of 21.5 at 0.5% PET fibre addition which is marginally higher than that of the control specimen, which had a rebound number of 21.1. Thereafter, there is a sharp drop in the rebound number with 1.0% fibre addition to the lowest rebound number for 25% fly ash content of 12.5. Further addition of PET fibre results in a drastic increase in the rebound number to 21.4 at 1.5% fibre addition. Addition of 2.0% fibre results in another drop in the rebound number to 14.7.

The specimen containing 20% fly ash had a steady drop in the rebound number with the addition of fibre up to 1.0%. Further addition of fibre content to 1.5% resulted in a drop in rebound number from 17.0 to 16.9. On the other hand, the addition of fibre to 2.0% resulted in a slight increase in rebound number to 17.3.

The specimen containing 30% fly ash had a similar trend to the sample with 20% fly ash. The rebound number dropped with the addition of fibre to 16.0 for 0.5% fibre content. Thereafter, the addition of 1.0% fibre content slightly decreased the rebound number to 15.6. In contrast, further addition of fibre gave an increase in rebound number to 16.6 and thereafter a decrease with further addition of fibre.

The specimen containing 15% had a decreasing trend with an increase in fibre content. This trend was different to that observed in other specimens containing higher quantities of fly ash which had a fluctuation in the trend at 1.5% fibre addition. The specimen containing 15% fly ash had a decrease in rebound number to 20.0 for 0.5% fibre content which was identical to the rebound number obtained for 0.5% fibre addition with 30% fly ash content. Thereafter, the rebound number dropped to 15.6 for 1.0% fibre content, which was lower than the rebound number realised for 1.0% fibre addition for 30% fly

ash content FRCC. Further, the addition of PET fibre resulted in a steady decline in rebound numbers to 13.8 and 11.9 for PET fibre content 1.5% and 2.0%, respectively.

4.2.4 Analysis of material cost

The costing of the FRCC was carried out to ascertain the feasibility of the product. The basic market prices of the raw materials are given in Table 4-14.

Table 4-14 – Cost of Raw Materials

Sr No.	Materials	Rate [R/(kg/m ³)]
1	Cement	2.18
2	Fly Ash	0.00
3	Fine aggregate	1.29
4	Coarse aggregate	1.29
5	PET Fibres	0.04
6	Water Municipality Rate	7.14

The fly ash was sourced as waste material from Power generation plants at no cost. Table 4-14 shows the cost per square metre of concrete for the full experimental design used in this study. Cost breakdown analysis is an essential process in product development as it allows a holistic view of the financial feasibility of the product. The chart in Figure 4-35 shows the bill of materials that are needed in the manufacture of reinforced concrete slabs.



Figure 4-35 – Bill of Materials in Manufacture of FRCC

Only the direct raw material cost analysis has been carried out in this study. Indirect expenses were neglected. These indirect costs were neglected as they are standard costs in all types of concrete manufacture and are not unique to the current study. Figure 4-36 shows a comparison of the cost of manufacturing the FRCCC.

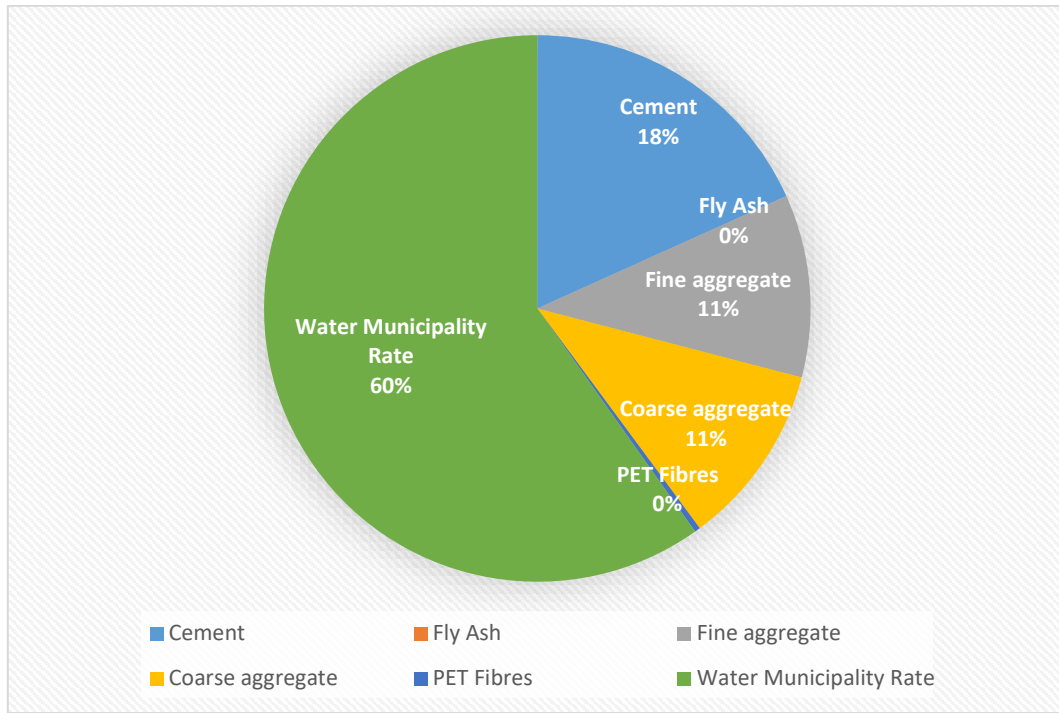


Figure 4-36 – Raw Materials Cost Comparison

From Figure 4-36, the cost of water and cement are the two major costs based on the cost of each of the items per kilogramme per cubic metre. This costing shows the importance of producing FRCC with a minimum quantity of cement and water to manage the cost of production. The quantity of raw materials used per kg/m^3 was calculated using densities' characterisation results. The water ratio to cementitious material was 0.6, and the air entrainment was assumed to be 2.0%.

Table 4-15 – Materials costing for the FRCC

Code	PET Fibre Mass Fraction (%)	Fly Ash Mass Fraction (%)	Design Materials for FRCC						Total Cost [R]
			Cement	Fine	Coarse	Fly ash	Fibre	Water	
			[Kg/m3]	Aggregate	Aggregate	[kg/m3]	[kg/m3]	[kg/m3]	
			[kg/m3]	[kg/m3]					
S3	0	0	346,50	519,75	1093,50	0,00	0,00	207,90	2 840,75
S20	0	15	294,53	546,75	1093,50	51,98	0,00	176,72	2 762,27
S21	0	20	277,20	546,75	1093,50	69,30	0,00	166,32	2 724,50
S22	0	25	259,88	546,75	1093,50	86,63	0,00	155,93	2 686,73
S23	0	30	242,55	546,75	1093,50	103,95	0,00	145,53	2 648,97
S24	0,5	0	346,50	546,75	1093,50	0,00	9,93	207,90	2 875,97
S4	0,5	15	294,53	546,75	1093,50	51,98	9,93	176,72	2 762,67
S8	0,5	20	277,20	546,75	1093,50	69,30	9,93	166,32	2 724,90
S12	0,5	25	259,88	546,75	1093,50	86,63	9,93	155,93	2 687,13
S16	0,5	30	242,55	546,75	1093,50	103,95	9,93	145,53	2 649,36
S25	1	0	346,50	546,75	1093,50	0,00	19,87	207,90	2 876,37
S5	1	15	294,53	546,75	1093,50	51,98	19,87	176,72	2 763,07
S9	1	20	277,20	546,75	1093,50	69,30	19,87	166,32	2 725,30
S13	1	25	259,88	546,75	1093,50	86,63	19,87	155,93	2 687,53
S17	1	30	242,55	546,75	1093,50	103,95	19,87	145,53	2 649,76
S26	1,5	0	346,50	546,75	1093,50	0,00	29,80	207,90	2 876,77
S6	1,5	15	294,53	546,75	1093,50	51,98	29,80	176,72	2 763,46
S10	1,5	20	277,20	546,75	1093,50	69,30	29,80	166,32	2 725,69
S14	1,5	25	259,88	546,75	1093,50	86,63	29,80	155,93	2 687,93
S18	1,5	30	242,55	546,75	1093,50	103,95	29,80	145,53	2 650,16
S27	2	0	346,50	546,75	1093,50	0,00	39,74	207,90	2 877,17
S7	2	15	294,53	546,75	1093,50	51,98	39,74	176,72	2 763,86
S11	2	20	277,20	546,75	1093,50	69,30	39,74	166,32	2 726,09
S15	2	25	259,88	546,75	1093,50	86,63	39,74	155,93	2 688,32
S19	2	30	242,55	546,75	1093,50	103,95	39,74	145,53	2 646,27

The addition of fly ash reduces the cost of the FRCC. The cost of cement is a significant cost in the production of concrete, with the cost of cement being R 2,18/m³ compared to the coarse and fine aggregate, which both cost R 1,29/m³. The cost of cement is 40% more than the cost of either the fine or coarse aggregate. Therefore, the cost of the concrete mixture is reduced with the addition of fly ash in incremental amounts. Concrete containing no fibre and no-fly ash costs R 2840,75 to manufacture. However, with the incorporation of just 15% fly ash replacement of cement, the cost per cubic metre drops by R 78,48 to R 2762,27, which is a 2.80% decrease. Further addition of fly ash results in significant cost savings with 30% fly ash replacement concrete costing just R 2648,97 to produce compared to the control sample with no-fly ash costing R 2840,75. This is a saving of 6.80%, a total saving of R 191,78/m³, with the incorporation of 30% fly ash. Table 4-16 shows a comparison of cost-

saving between this study and research by Upadhyay (2014). It indicates a trend of cost-saving with the incremental quantity of fly ash replacement. However, Upadhyay (2014) realised a higher cost saving percentage compared to the current study, which could be attributed to the higher cost of cement in the region of the author's study compared to the current study.

Table 4-16 – Cost Comparison

Fly Ash	Percentage Decrease in Cost	
	Current Study	Upadhyay (2014)
0	-	-
15%	2.80	5.40%
20%	4.10	10.62%
25%	5.42	14.80%
30%	6.80	15.93%

The addition of PET fibres into the concrete increases the cost of the FRCC due to the cost of the PET fibres of R 0,04/m³. FRCC containing 0.5% PET fibre and no fly ash costs R 2875,97 which is an increase in cost from unreinforced concrete of R 35.22. Further addition of PET fibre has an incremental effect on the cost of the FRCC. The FRCC contained the maximum quantity of fibre used in this study of 2.0% costs R 2877,17, which is R 36,42 more expensive than unreinforced concrete. This translates to a 1.28% increase in cost.

However, the addition of fly ash to make a hybrid FRCC reduces the cost of the reinforced concrete significantly. The FRCC containing 15% fly ash and 0.5% fibre content costs R 2 762,67/m³, cheaper than the control specimen by R78.08/m³. The specimen is containing 2.0% PET fibre and 15% fly ash costs R 2 763,86/m³ to produce, which is still considerably cheaper than the control specimen by R 76,85/m³.

The addition of fly ash reduces the cost of concrete production significantly, as shown in Table 4-15. The reduction in concrete cost with the addition of fly ash is a cost-effective alternative to cement. The use of PET fibres is a cost-effective way to increase the strength of the concrete while mitigating against crack propagation. Beyond the significant improvement in the performance of concrete, the use of PET fibres has a positive impact on the cost of the concrete to attain the required ultimate strength.

4.3 Numerical modelling

Numerical modelling was carried out, and the results are presented and discussed in the following subsections. Optimization of the composite parameters was carried out to obtain the optimum design mix that gave the best response mechanical properties at the lowest possible cost.

4.3.1 Optimization of mechanical strength and cost of composite

The optimization process was considered for all the responses simultaneously to build an appropriate model that could ascertain the optimum fibre and fly ash values for the FRCC. The parameters considered in the optimization are as shown in Table 4-17, including slump value, compressive strength, flexural strength, split tensile strength, and the total cost of the composite. The optimization model was programmed through Minitab software.

Table 4-17 – Response Analysis of FRCC

Code	Fibre Mass Fraction (%)	Fly Ash Mass Fraction (%)	Slump Value (mm)	Compressive strength (N/mm ²)	Flexural Strength (N/mm ²)	Split Tensile Strength (N/mm ²)	Total Cost (R)
S3	0,0	0	50,3	23,84	4,60	0,90	2 840,75
S4	0,5	15	15,0	15,54	3,22	2,70	2 762,27
S5	1,0	15	0,0	14,62	2,83	1,77	2 724,50
S6	1,5	15	0,0	10,44	1,96	1,47	2 686,73
S7	2,0	15	0,0	6,74	2,34	1,19	2 648,97
S8	0,5	20	12,0	19,07	3,13	2,79	2 875,97
S9	1,0	20	0,0	15,96	3,23	2,69	2 762,67
S10	1,5	20	0,0	8,50	2,93	2,34	2 724,90
S11	2,0	20	0,0	15,53	4,00	1,11	2 687,13
S12	0,5	25	11,0	13,58	3,63	1,48	2 649,36
S13	1,0	25	0,0	10,74	3,70	1,16	2 876,37
S14	1,5	25	0,0	9,54	2,20	1,29	2 763,07
S15	2,0	25	0,0	7,44	1,89	0,44	2 725,30
S16	0,5	30	10,0	12,89	4,47	1,16	2 687,53
S17	1,0	30	0,0	11,78	3,72	1,03	2 649,76
S18	1,5	30	0,0	13,47	3,84	0,98	2 876,77
S19	2,0	30	0,0	11,17	2,25	0,79	2 763,46
S20	0,0	15	61,5	44,14	5,94	2,36	2 725,69
S21	0,0	20	62,0	41,46	3,42	2,37	2 687,93
S22	0,0	25	63,2	29,14	2,99	1,90	2 650,16
S23	0,0	30	65,5	35,32	4,00	1,78	2 877,17
S24	0,5	0	15,0	29,32	3,59	1,82	2 763,86
S25	1,0	0	0,0	16,12	1,80	1,16	2 726,09
S26	1,5	0	0,0	13,64	2,25	1,21	2 688,32
S27	2,0	0	0,0	10,87	2,87	0,92	2 646,27

4.3.1.1 Analysis of variance and response surface regression models

The analysis of variance (ANOVA) was carried out for all the response surfaces investigated and presented in the following subsections.

4.3.1.2 Slump value

The ANOVA response surface design analysis for slump value is reported in Table 4-18.

Table 4-18 – ANOVA for slump (Minitab 17 output)

Source	DF	Adj SS	Adj MS	F value	P value	Comment
Model	5	13170.4	2634.08	67.47	0.000	S = 6.2845
Linear	2	7937.5	3968.74	101.65	0.000	R ² = 0.9467
A	1	9.1	9.12	0.23	0.634	Adj. R ² = 0.9326
B	1	7928.4	7928.36	203.07	0.000	Pred R ² = 0.9074
Square	2	4200.2	2100.08	53.79	0.000	
AB	1	3.5	3.53	0.09	0.767	
BA	1	4196.6	4196.63	107.49	0.000	
2-Way interaction	1	35.0	35.05	0.90	0.3555	
AB	1	35.0	35.05	0.90	0.3555	
Error	19	741.8	39.04			
Total	24	13912.2				

SS: Sum of squares; MS: Mean square; DF: Degree of freedom; R²: Coefficient of determination; Adj R²: Adjusted coefficient of determination; A = Fly Ash Mass Fraction (%); B = Fibre Mass Fraction (%)

From Table 4-18, it was observed that for the linear terms, the Fibre Mass Fraction (%) was statistically insignificant according to the t-test having a p-value < 0.05. However, the Fly Ash Mass Fraction (%) was statistically significant, having a p-value of 0.634. The effects of the interaction between the square of AB were statistically significant. However, the interaction between the square off BA was insignificant for the slump. The model for the slump was insignificant at a 95% confidence level, F-value of 67.47 and a p-value of 0.000.

By applying multiple regression analysis, the regression equation 4-13 was obtained for slump value

$$\text{Slump value} = 52.40 + 0.340A - 85.74B - 0.0040A^2 + 30.97B^2 - 0.163AB \quad 4-13$$

4.3.1.3 Compressive strength

The ANOVA response surface design analysis for compressive strength is reported in Table 4-19.

Table 4-19 – ANOVA for Compressive Strength (Minitab 17 output)

Source	DF	Adj SS	Adj MS	F value	P-value	Comment
Model	5	1987.37	397.47	12.74	0.000	S = 5.58535
Linear	2	1451.21	725.60	23.26	0.000	R ² = 0.7703
A	1	27.11	27.11	0.87	0.363	Adj. R ² = 0.7098
B	1	1424.10	1424.10	45.65	0.000	Pred R ² = 0.4311
Square	2	405.18	202.59	6.49	0.007	
AB	1	7.32	7.32	0.23	0.634	
BA	1	397.85	397.85	12.75	0.002	
2-Way interaction	1	0.31	0.31	0.01	0.922	
AB	1	0.31	0.31	0.01	0.922	
Error	19	592.73	31.20			
Total	24	2580.09				

SS: Sum of squares; MS: Mean square; DF: Degree of freedom; R²: Coefficient of determination; Adj R²: Adjusted coefficient of determination; A = Fly Ash Mass Fraction (%); B = Fibre Mass Fraction (%)

From Table 4-19, it was observed that the linear terms for both A and B were statistically significant in accordance with the t-test as the p-value > 0.05. The interaction between the two factors AB was statistically insignificant with a p-value of 0.634. However, the square interaction between BA was statistically insignificant with a p-value of 0.002. The two-way interaction between AB was statistically significant with a p-value of 0.922. The two-way interaction between AB was significant with a p-value of 0.922. The model for compressive strength was not significant at a 95% confidence level with F-value of 12.74 and a p-value of 0.0000.

By applying multiple regression analysis, regression equation 4-14 was obtained for compressive strength.

$$\begin{aligned} \text{Compressive Strength} & \qquad \qquad \qquad 4-14 \\ & = 34.50 + 0.084A - 29.96B - 0.0057A^2 + 9.54B^2 - 0.015AB \end{aligned}$$

4.3.1.4 Flexural strength

The ANOVA response surface design analysis for compressive strength is reported in Table 4-20.

Table 4-20 – ANOVA for Flexural Strength

Source	DF	Adj SS	Adj MS	F value	P-value	Comment
Model	5	9.4466	1.88931	2.70	0.053	S = 0.836999
Linear	2	8.6792	4.33961	6.19	0.008	R ² = 0.4151
A	1	0.4350	0.43496	0.62	0.440	Adj. R ² = 0.2612
B	1	8.2443	8.24427	11.77	0.003	Pred R ² = 0.00
Square	2	0.7220	0.36102	0.52	0.605	
AB	1	0.0653	0.06534	0.09	0.763	
BA	1	0.6567	0.65669	0.94	0.345	
2-Way interaction	1	0.2837	0.28368	0.40	0.532	
AB	1	0.2837	0.28368	0.40	0.532	
Error	19	13.3108	0.70057			
Total	24	22.7573				

SS: Sum of squares; MS: Mean square; DF: Degree of freedom; R²: Coefficient of determination; Adj R²: Adjusted coefficient of determination; A = Fly Ash Mass Fraction (%); B = Fibre Mass Fraction (%)

From Table 4-20, it was observed that the linear terms of A relation to the flexural strength were statistically significant in accordance with the t-test as their p-value > 0.005. However, B was statistically insignificant with a p-value of 0.003. The square interaction between AB and BA was statistically significant according to the t-test with a p-value > 0.005. the two-way interaction between AB was statistically significant with a p-value of 0.532. The model for flexural strength was significant at a 95% confidence level with an F-value of 2.70 and a p-value > 0.05.

By applying multiple regression analysis, regression equation 4-15 was obtained for flexural strength.

Flexural Strength

$$= 4.317 - 0.0179A - 1.840B + 0.00054A^2 + 0.387B^2 + 0.0144AB \quad 4-15$$

4.3.1.5 Split tensile strength

The ANOVA response surface design analysis for split tensile strength is reported in Table 4-21.

Table 4-21 – ANOVA for Split Tensile Strength

Source	DF	Adj SS	Adj MS	F value	P value	Comment
Model	5	7.3720	1.47439	8.63	0.000	S = 0.413387
Linear	2	2.4902	1.24512	7.29	0.004	R ² = 0.6942
A	1	0.0666	0.06657	0.39	0.540	Adj. R ² = 0.6138
B	1	2.4237	2.42367	14.18	0.001	Pred R ² = 0.4419
Square	2	4.0966	2.04823	11.99	0.000	
AB	1	3.6888	3.68876	21.59	0.000	
BA	1	0.4078	0.40782	2.39	0.139	
2-Way interaction	1	0.2027	0.20269	1.19	0.290	
AB	1	0.2027	0.20269	1.19	0.290	
Error	19	3.2469	0.17089			
Total	24	10.6188				

SS: Sum of squares; MS: Mean square; DF: Degree of freedom; R²: Coefficient of determination; Adj R²: Adjusted coefficient of determination; A = Fly Ash Mass Fraction (%); B = Fibre Mass Fraction (%)

From Table 4-21, it was observed that the linear terms of A relation to the split tensile strength were statistically significant in accordance with the t-test as their p-value > 0.005. However, B was statistically insignificant with a p-value of 0.001. The square interaction between AB and BA was statistically insignificant according to the t-test with a p-value < 0.005. The two-way interaction between AB was statistically significant with a p-value of 0.290. The model for flexural strength was insignificant at a 95% confidence level with an F-value of 8.63 and a p-value of 0.00. By applying multiple regression analysis, regression equation 4-16 was obtained for split tensile strength.

Split Tensile Strength

$$= 1.319 + 0.1287A - 0.337B - 0.004046A^2 + 0.305B^2 + 0.0124AB$$

4-16

4.3.1.6 Total cost

The ANOVA response surface design analysis for total FRCC cost is reported in Table 4-22.

Table 4-22 – ANOVA for Total Cost

Source	DF	Adj SS	Adj MS	F value	P value	Comment
Model	5	37089	7418	1.32	0.297	S = 74.9201
Linear	2	18914	9457	1.68	0.212	R ² = 0.2580
A	1	3745	3745	0.67	0.424	Adj. R ² = 0.628
B	1	15169	15169	2.70	0.117	Pred R ² = 0.00
Square	2	7141	3570	0.64	0.540	
AB	1	4223	4223	0.75	0.397	
BA	1	2918	2918	0.52	0.480	
2-Way interaction	1	19371	19371	3.45	0.079	
AB	1	19371	19371	3.45	0.079	
Error	19	106647	5613			
Total	24	143737				

SS: Sum of squares; MS: Mean square; DF: Degree of freedom; R²: Coefficient of determination; Adj R²: Adjusted coefficient of determination; A = Fly Ash Mass Fraction (%); B = Fibre Mass Fraction (%)

From Table 4-22, it was observed that the linear terms of A and B in relation to the total cost were statistically significant in accordance with the t-test as their p-value > 0.005. The square interaction between AB and BA was statistically significant with a p-value > 0.005. The two-way interaction between AB was statistically significant with a p-value of 0.079. The model for total cost was significant at a 95% confidence level with an F-value of 1.32 and a p-value > 0.05. The regression equation 4-17 was obtained for total cost by applying multiple regression analysis.

$$\mathbf{Total\ Cost} = 2813.1 - 6.73A - 42.0B + 0.137A^2 - 25.8B^2 + 3.82AB \quad 4-17$$

4.3.2 Response contour and surface plots

The response contour and surface plots discussed in this section show the optimal, comfort and adverse zones of the analysed responses, including the compressional, split tensile, flexural strength, total cost, and slump values. The contour plots present the strength responses with the dark green area, and light green and dark coloured areas indicate high strength and low strength, respectively.

4.3.2.1 Compressive strength

Figure 4-37 shows the contour plot of the relationship between the compressive strength versus fibre mass fraction and fly ash mass fraction in the FRCC.

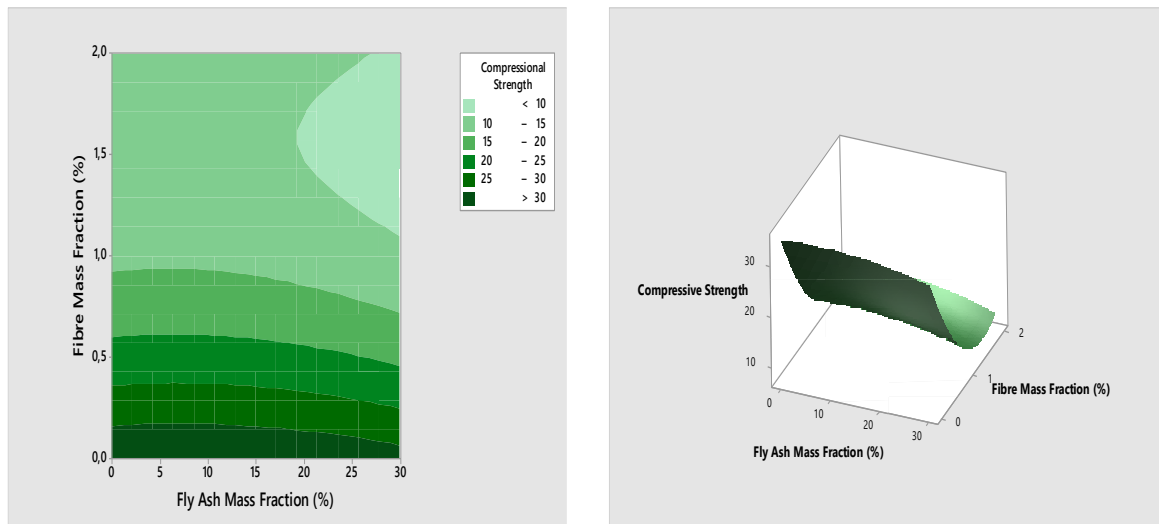


Figure 4-37 - Contour plot and a 3D surface plot showing the effect fibre mass fraction (%) and fly Ash mass fraction (%) on compressive strength

The contour plot shows that the compressive strength between 10 N/mm² and 15 N/mm² covers the greatest area and is bounded by 1.0% to 2.0% fibre mass fraction, mainly as shown in Figure 4-37. The area with the greatest compressive strength is shown at the bottom of the contour plot and is within the region underneath 0.3% fibre content. The contour plot clearly shows a decrease in compressive strength with an increase in fibre content. This decrease can be attributed to the flexibility of PET fibres and their inability to withstand compressive forces without buckling. The compressive strength of the composite is then realised at low fibre percentages. The 3D plot in Figure 4-37 clearly shows the effect of the interaction between the factors and the compressive strength.

4.3.2.2 Split tensile strength

Figure 4-38 shows the contour plot of the relationship between the split tensile strength versus fibre mass fraction and fly ash mass fraction in the FRCC.

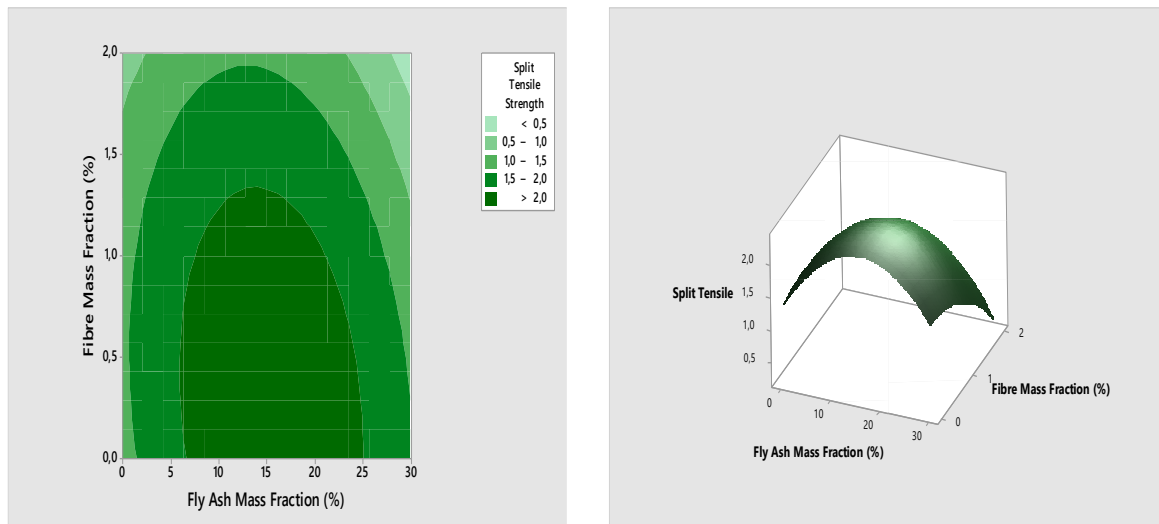


Figure 4-38 – Contour plot and a 3D surface plot showing the effect of fibre mass fraction (%) and fly ash mass fraction (%) on the slit tensile strength

The contour plot in Figure 4-38 shows that the highest split tensile strength region of greater than 2 N/mm² falls between 7 and 23% fly ash and is bounded by 0 to 1.2% PET fibre content. The region with the lowest split tensile strength of less than 0.5N/mm² is found in the region on top of 1.8% PET fibre content between 0 to 3% fly ash content as well as between 28 to 30% fly ash content. Split tensile strength between 1.5 to 2.0 N/mm² is found when fly ash mass fraction is between 2 and 6%, and when the PET fibre mass fraction is between 0 to 1.6%, the same strength is realised when the fly ash mass fraction is between 25 and 30%. The 3D surface plot shown in Figure 4-38 shows much clearer the effect of the interaction between fibre and fly ash mass fraction with the split tensile strength.

4.3.2.3 Flexural strength

Figure 4-39 shows the contour plot of the relationship between the flexural versus fibre mass fraction and fly ash mass fraction in the FRCC.

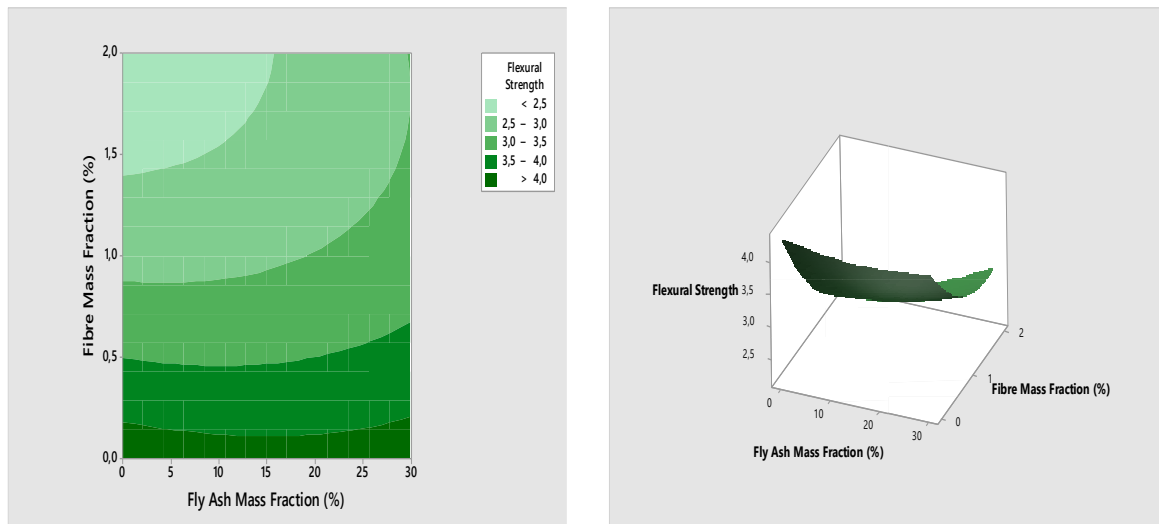


Figure 4-39 - Contour plot and 3D surface plot showing the effect fibre mass fraction (%) and fly ash mass fraction (%) on the flexural strength

The contour plot in Figure 4-39 shows that the highest flexural strength of greater than 4 N/mm² is realised at a very low PET fibre mass fraction of less than 0.25% for all ranges of fly ash content from 0 to 30%. However, marginally higher flexural strength is reported between 25 to 30% fly ash content. Addition of between 0.25% to 0.5% PET fibre content gives flexural strength of between 2.5 to 4.0 N/mm². However, the flexural strength for that range is slightly higher, with fly ash content of between 25 to 30%. Flexural strength of between 3.0 to 3.5 is reported at fibre mass fraction of between 0.5 to 0.8% for all fly ash mass fractions up to 30%. On the other hand, between 25 to 30% fly ash content, the strength is between 3.0 to 3.5 N/mm² for up to 1.4% fibre content. The lowest flexural strength of less than 2.5 N/mm² is between 1.4 to 2.0% fibre content and between 0 to 15% fly ash content. From these results, it can be concluded that the flexural strength is at its highest with lower fibre content. Further addition of fibres beyond 0.3% results in a decrease in flexural strength with all percentages of fly ash. Figure 4-39 gives the 3D surface plot clearly showing the interaction between the fibre content, fly ash content and flexural strength.

4.3.2.4 Total cost

Figure 4-40 shows the contour plot of the relationship between the total cost versus fibre mass fraction and fly ash mass fraction in the FRCC.

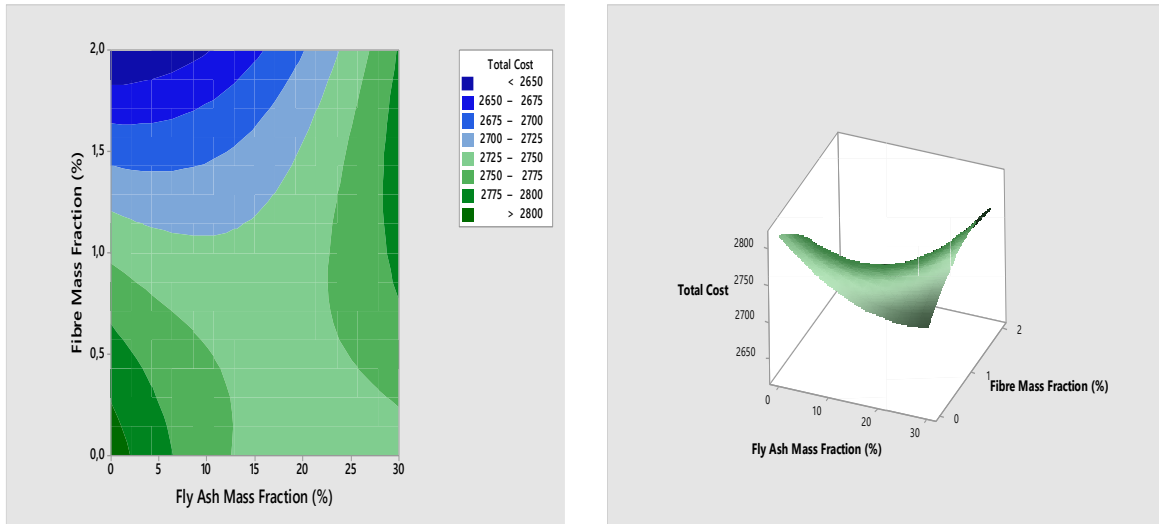


Figure 4-40 – Contour plot and a 3D surface plot showing the effect fibre mass fraction (%) and fly ash mass fraction (%) on the total cost

The contour plot shows that the highest composite cost of more than R 2650 per m³ occurred in the region of the highest fibre mass fraction of 1.8- 2.0% with fly ash mass fraction of between 0% and 12%. The lowest cost was realised with the control containing 0% fibre and 0% fly ash content. The bulk of the cost of between R 2725 – R 2750 per m³ fell in the region of between 0% -1.2% fibre content with fly ash mass fraction of between 12% and 25%. The 3D surface plot shown in Figure 4-40 shows much clearer the interaction of the fibre mass fraction, fly ash mass fraction and total cost.

4.3.2.5 Slump value

Figure 4-41 shows the contour plot of the relationship between the slump value versus fibre mass fraction and fly ash mass fraction in the FRCC.

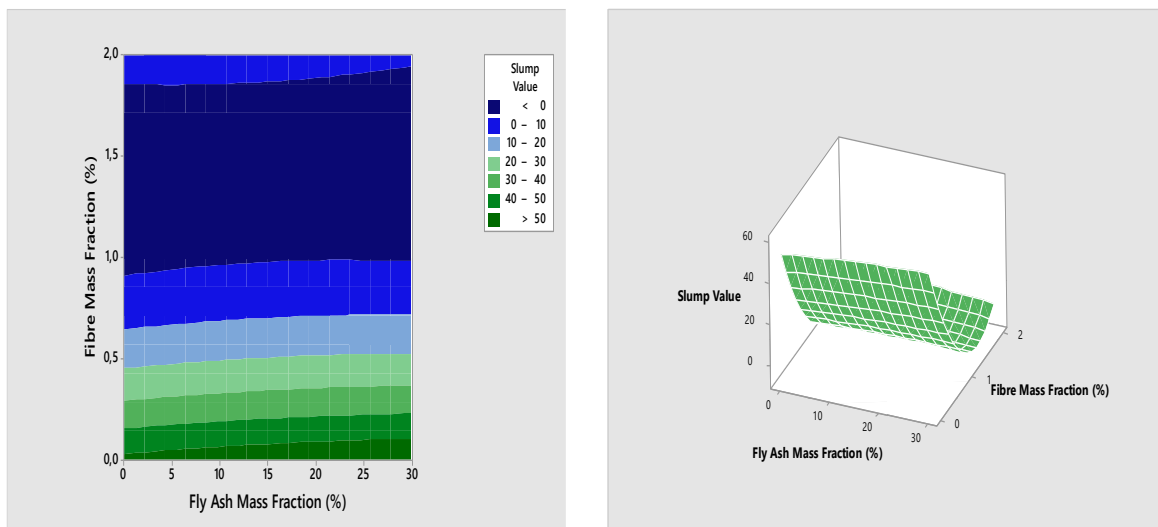


Figure 4-41 - Contour plot and 3D surface plot showing the effect fibre mass fraction (%) and fly ash mass fraction (%) on the slump value

Workability is a measure of how easy or difficult to place and handle fresh concrete mixture and is measured from the slump value. The effect of fibre mass fraction and fly ash mass fraction on slump value is illustrated with the help of a response contour plot shown in Figure 4-41. This figure shows that a gradual increase in slump value is realised with an increase in fly ash content. However, an increase in fibre content has a negative impact on the slump value. For fibre mass fraction less than 0.3, the slump value is at its highest value and increases with an increase in fly ash content. The increase in slump value with an increase in fly ash content can be attributed to the predominantly spherical shape of the fly ash particles, as shown in Figure 4-3, which induce a roller effect encouraging the flow of the fresh concrete mixture. In this study, the maximum slump was realised at 0% fibre addition and 30% fly ash replacement of cement. The lowest slump value is indicated by the upper region bounded by 0.9 % and 1.8% fibre mass fraction on the contour plot and is predominantly in the region with fibre addition above 1%.

The 3D surface plot in Figure 4-41 shows more clearly the effect of the interaction between the factors. Furthermore, it is clearer that at 0% fibre content, the slump value is at its highest point for all addition of fly ash with higher fly ash content giving a higher slump value compared to the control specimen.

4.3.3 Model validation

The model developed is restricted to the initial raw material composition, which includes the water, cement, river sand, dolomite stone, fly ash and PET fibre content. The model's predictive capabilities were tested, with input for the numerical simulation being independent of those used to construct the model. In this manner, the model was rigorously assessed, and its predictive capabilities were confirmed through actual experimental data. The input parameters are the fibre and fly ash mass fraction.

4.3.3.1 Comparison of predictive and actual normality plots

The effectiveness and acceptability of prediction models have based on the premise that the model is able to predict the output accurately. In this study, the model was designed to predict the mechanical behaviour of the FRCC based on the two-factor input parameters. This subsection validated the prediction model through the coefficient of determination (R^2), adjusted coefficient of determination (R^2 adj) and S value. This information is consolidated and summarised in Table 4-23. Data were checked for the actual versus predicted plots for all the tested responses in this study.

Table 4-23 – Statistical conducted on Predictive Model

Predicted Parameters	S	R²	R² (adj)
Slump Value	4.22051	0.965	0.965
Compressive Strength	3.62398	0.824	0.816
Flexural Strength	0.490019	0.415	0.390
Split Tensile Strength	0.313243	0.694	0.681
Total Cost	34.6682	0.254	0.222

S - Standard Deviation; R²- Coefficient of determination; R² adj -Adjusted Coefficient of determination

Figure 4-42 to Figure 4-46 show the predicted versus actual plot for all the responses in the study. From these plots, it was observed that the plotted points fell very close to the distribution fitted line for compressive strength, slump value, and split tensile strength. However, for the total cost and flexural strength, the plotted points were not as strong a fit to the distribution fitted line.

The prediction of slump value has an acceptable standard deviation of 4.22051 and a coefficient of determination R² of 0.965. This indicates high accuracy and a strong co-relationship between the predicted and the actual values. The prediction plot for compressive strength with respect to its actual value is shown in Figure 4-42. The statistical validation of the compressive strength model shows that the R² and standard deviation are within acceptable limits, and the model exhibits high accuracy.

From Figure 4-44, it was observed that the flexural strength model predicts high accuracy until actual flexural strength is 4 N/mm² thereafter, the scatter plots deviate from the trend line. Hence the model has an R² value of 0.415. Therefore, the model for flexural strength can only be used with confidence up to 4 N/mm² strength. Figure 4-45 shows the prediction against the actual plot for split tensile strength to have high accuracy with an R² value of 0.694, which is acceptable. Figure 4-46 shows the plot for actual total cost versus the predicted total cost, which has the lowest R² value of 0.254. This made the model unreliable for estimating the total cost with great accuracy.

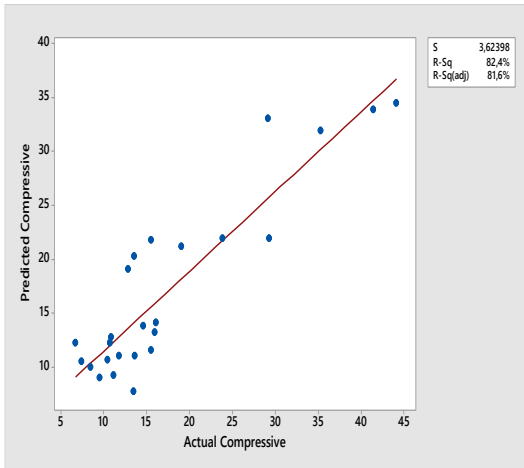


Figure 4-42 – Predicted vs Actual for Compressive Strength

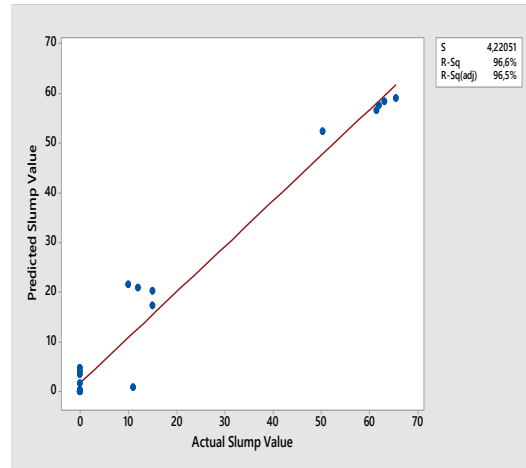


Figure 4-43 – Predictive vs Actual for Slump Value

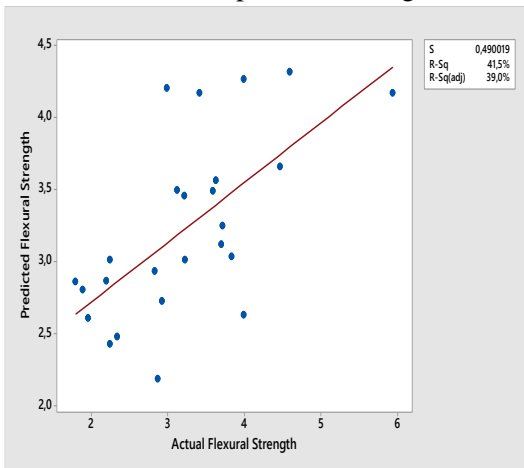


Figure 4-44 – Predictive vs Actual for Flexural Strength

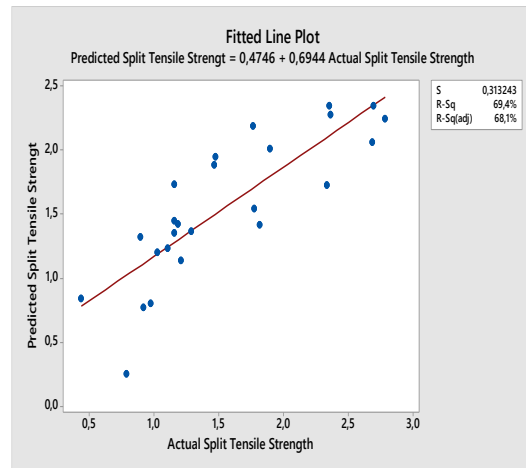


Figure 4-45 – Predictive vs Actual for Split Tensile Strength

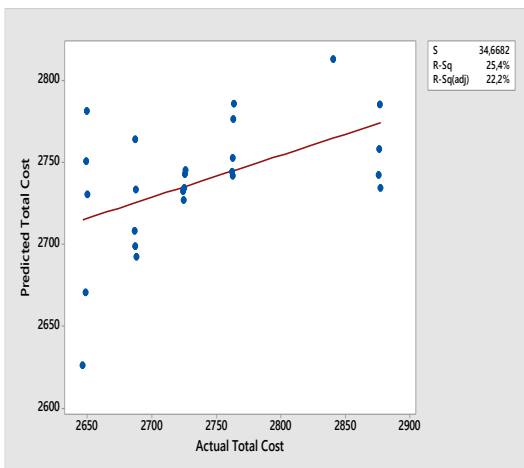


Figure 4-46 – Predictive vs Actual for Total Cost

The developed model performed generally well and had a good fit between the actual and predicted values except for the total cost model. Other generated models in studies by Zain et al (2002) and

Karthiyaini et al. (2019) used input properties such as cement, admixtures, fine and coarse aggregate. They did not provide adequate reliability for tensile flexural properties. However, this current study provided a model that generated a good fit for flexural and tensile properties. Karthiyaini (2019) study used Artificial Neural Network (ANN) to build a predictive model for fibre reinforced concrete; however, the model failed to predict the compressive strength with reliable accuracy. This limitation has been overcome in this study.

4.3.4 Response optimizer for the mix design

The optimisation of the design considered all the responses simultaneously to achieve an optimum mix design favourable to all the reported responses. The optimisation was carried out to determine the optimum fibre and fly ash mass fraction taking into consideration the responses, which included the compressive strength, flexural strength, split tensile strength, slump value and total cost. The maximum goal was set for split tensile strength, flexural strength and compressive strength, as shown in Table 4-24. However, the total cost was set at the lowest goal to manage the cost of the product. The slump value was set at a target value of 9 cm, which was a compromise on the workability of the concrete paste.

Table 4-24 – Response surface Optimizer

Response	Units	Goal	Lower	Target	Upper	Weight	Importance
Total Cost	Rands	Minimum		2646.27	2877.17	1	1
Split Tensile Strength	N/mm ²	Maximum	0.44020	2.79	-	1	1
Flexural Strength	N/mm ²	Maximum	1.80000	5.93	-	1	1
Compressive Strength	N/mm ²	Maximum	6.73778	44.14	-	1	1
Slump Value		Target	0.00000	9.00	65.50	1	1

Table 4-25 was generated from the variable settings in Table 4-25 to calculate all the responses included in the optimization. The fit gives the mean responses for the continuous measurements. From Table 4-25, the mean for a total cost, split tensile strength, flexural strength and compressive strength and slump value were 2744.2, 2.356, 3.689, 25.65 and 31.48, respectively.

The standard error of the fit gives an estimation of the variation in the estimated mean responses for the specified variable settings. Split tensile strength and flexural strength have a low standard error of fit, showing that with 95 % confidence, the mean is within range. The total cost has a high standard error of fit.

Table 4-25 – Multiple Response Prediction

Response	Fit	SE Fit	95% CI	95% PI
Total Cost	2744.2	28.2	(2685.2;2803.1)	(2576.6; 2911.7)
Split Tensile Strength	2.356	0.155	(2.031;2.682)	(1.432; 3.281)
Flexural Strength	3.689	0.315	(3.030;4.348)	(1.817; 5.561)
Compressive strength	25.65	2.10	(21.25;30.04)	(13.16;38.14)
Slump Value	31.48	2.35	(26.56;36.39)	(17.50; 45.45)

SE Fit- Standard Error of the Fit; CI – Confidence Interval; PI – Prediction Interval

The 95 % confidence interval for all the responses is within range for all the experimental data carried out. The Confidence intervals are for all responses relatively narrow, implying that there is strong confidence in the mean of future values.

The 95 % prediction interval assesses the prediction precision. The prediction intervals are all within acceptable boundaries for the responses except the slump value. The low precision interval for slump value could be attributed to the low slump for most of the experiments, which did not give sufficient data precision. The prediction interval has a wider range than the confidence interval due to the uncertainty in predicting a single response compared to a mean response.

Figure 4-47 shows the overlaid contour-plot for all the composite responses. The overlaid contour plot gives a visual representation of the area where the predicted means of the responses are in the acceptable region.

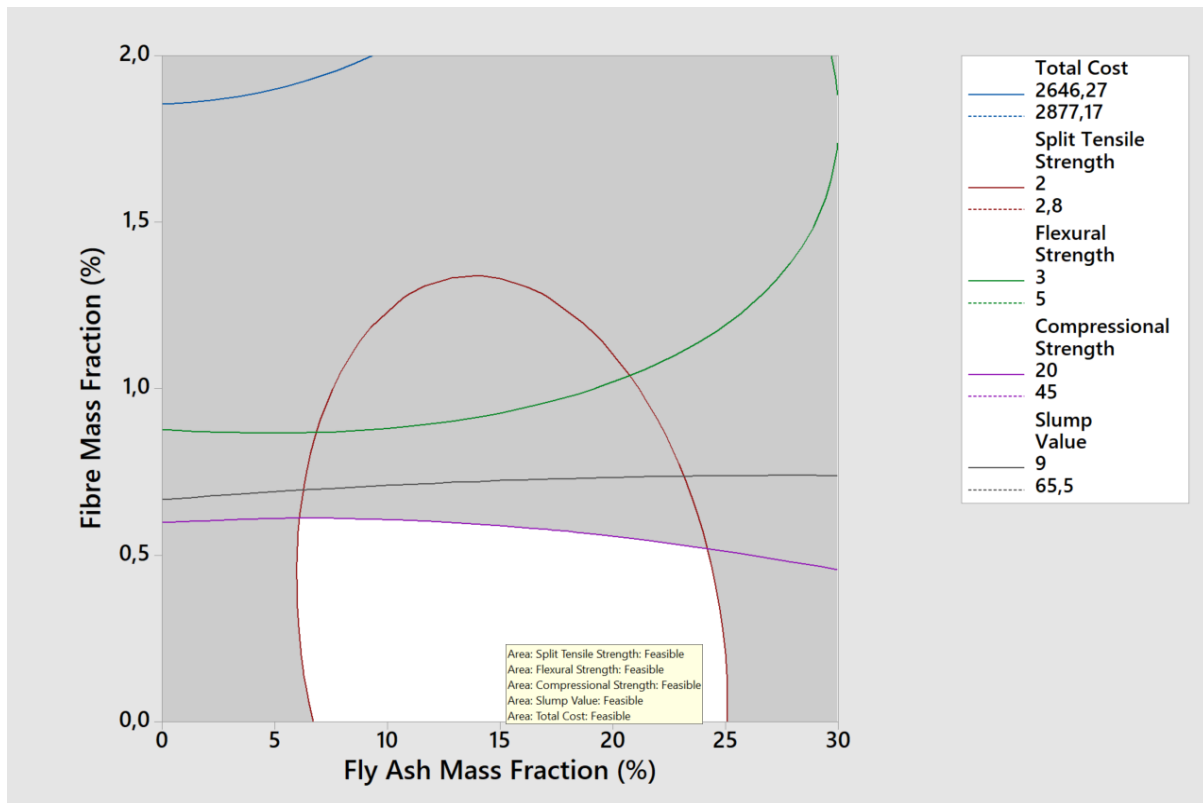


Figure 4-47 – Overlaid Contour Plot

The overlaid contour plot shows that the optimum and feasible region is within 6 to 25 % fly ash content and within 0 to 0.5 % fibre mass fraction content. The optimum was calculated using the response optimizer, as shown in Figure 4-48.

The region bounded by the compressional strength, slump line and split tensile strength line has feasible split tensile strength, flexural strength, slump value and total cost. However, the compressive strength is low. The region bounded by the flexural strength, slump value and split tensile strength line has acceptable flexural strength, total cost and split tensile strength. Although, that region has low compressional strength and low slump. The region of the contour plot bounded by the split tensile strength and flexural strength line has acceptable split tensile strength and total cost. Despite, that the compressional strength, slump value and flexural strength are low. The area bounded by the flexural strength, split tensile strength and total cost has only the total cost feasible. The upper most portion of the graph bounded by total cost has unacceptably low all the parameters. This is in line with the previous discussions whereby high levels of fibre content exceeding 1.8% do not yield favourable strength properties due to the formation of voids and clumping of fibres.

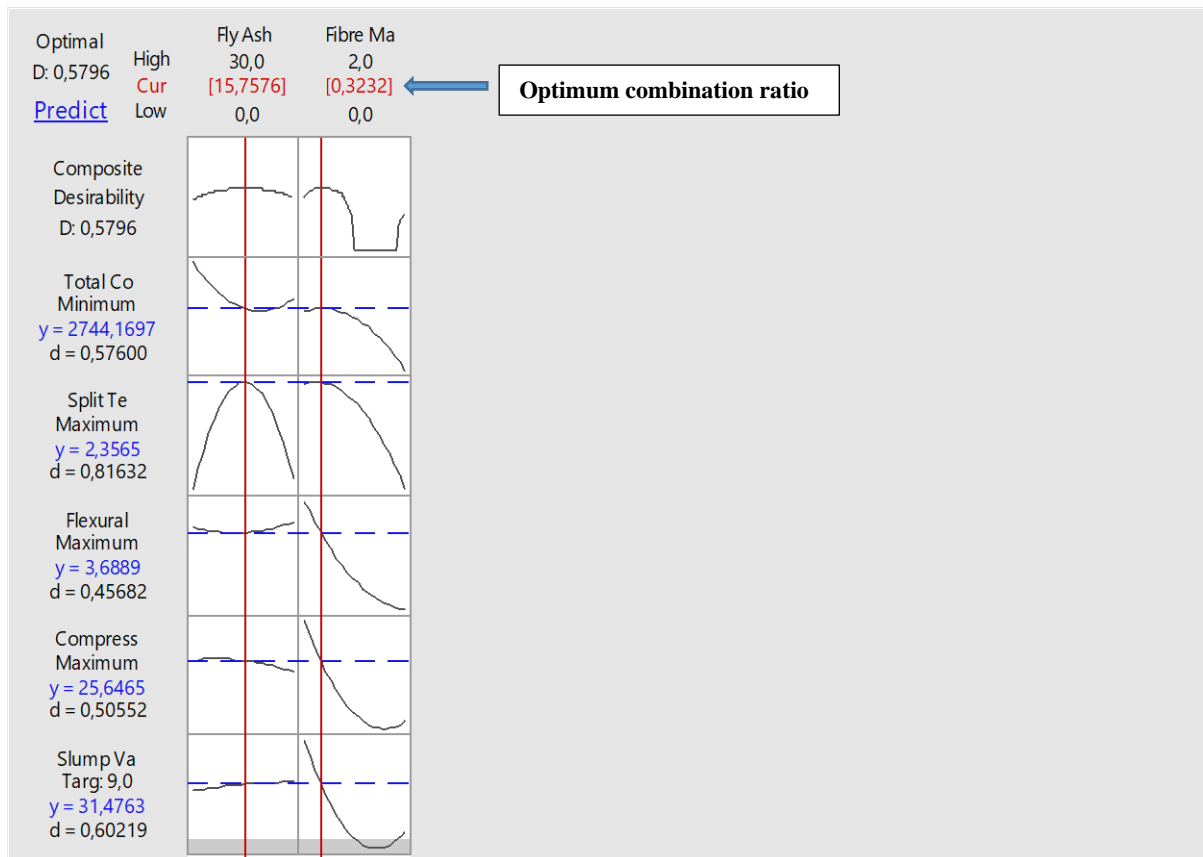


Figure 4-48 – Numerical Response Optimiser

For the FRRC, the composite desirability is 0.5796, which is considered acceptable for the model. Low composite desirability less than 0.5 would indicate that the model does not optimise the overall responses well. From Figure 4-48, increasing the fly ash mass fraction decreases the total cost with decreasing gradient. On the other hand, the split tensile strength increases with a steep gradient to a certain point and then starts to decline with a steep gradient. The addition of fly ash content has a marginal increment in the flexural strength of the composite. Fly ash has a small increase in flexural strength. However, the addition of higher quantities of fly ash decreases the compressional strength. Besides, the addition of fly ash increases the slump value of the composite moderately.

Fibre content gives the FRCC high flexural strength, split tensile strength, compressive strength, and slump value at very low fibre percentages. Further, the addition of fibre content tends to decrease the strength properties, as shown in Figure 4-48. However, the addition of fibre tends to increase the composite cost gradually.

4.3.4.1 Comparison of Model Prediction with Experimental Data

Numerical simulations of three data points were carried out experimental, and the same data points were fed into the predictive model. The output results for a compressive, flexural, slump, split tensile strength and cost were then assessed for statistical significance to validate the model, as shown in Table 4-26.

Table 4-26 – Validation of the Optimal Results Generated from Minitab

Parameter	Units	Goal	Optimum	Experimental	SD	PE
Fly Ash Mass Fraction (%)		Optimum	15.7576	15.7576		
Fibre Mass Fraction (%)		Optimum	0.3232	0.3232		
Total Cost	Rands	Minimum	2744.17	2744.19	±0.02	
Split Tensile Strength	N/mm ²	Maximum	2.3565	2.3570	±0.005	0.02121
Flexural Strength	N/mm ²	Maximum	3.6889	3.7200	±0.031	0.8360
Compressive Strength	N/mm ²	Maximum	25.6465	25.7800	±0.1335	0.5178
Slump Value		Target	31.4763	30.80	±0.676	2.20

SD- Standard deviation; PE – Absolute relative percent error

The absolute relative percent error was calculated according to equation 4-8.

$$\text{Absolute relative percent error (PE)} = \left(1 - \frac{\text{Predicted value}}{\text{Experimental value}}\right) \times 100 \quad 4-18$$

The standard deviation was very low for the total cost with a magnitude of 0.02, as shown in Table 4-26. This low standard deviation showed a good fit between the experimental and predicted optimum data. The standard deviation for split tensile and flexural strength was also very low showing that the model was representative and valid. On the other hand, the slump value had a slightly higher standard deviation of 0.676. However, this higher deviation was still within the acceptable limits. The results shown in Table 4-26 show that the model is valid. However, it is necessary for further research into the use of varied raw material properties in order to develop a model suited for other raw materials outside the scope of this study.

4.4 Applications of fibre reinforced composite in slabs

The optimum compositions and responses for the various end uses of the fabricated composite slabs are shown in Table 4-27.

Table 4-27 – Optimum composition and strength properties for various applications

Parameter	Paving Slabs	Floor Slabs	Ceiling Slabs	Foundation Slabs	Suspended Slabs
<i>Fly Ash Mass Fraction (%)</i>	0.0000	30.0000	0.0000	3.9394	19.0909
<i>Fibre Mass Fraction (%)</i>	0.6465	0.1818	0.4040	0.6465	0.3434
Total Cost (R/kg/m ³)	2775.13	2746.66	2791.88	2760.47	2742.03
Split Tensile Strength (N/mm ²)	1.4096	1.5223	1.4055	1.8223	2.3001
Flexural Strength (N/mm ²)	3.2891	4.0231	3.6365	3.2642	3.6814
Compressive Strength (N/mm ²)	19.1149	26.6830	23.9497	19.3200	24.7664
Slump Value (mm)	9.9176	43.00	22.8145	10.7832	30.5986

The response optimiser showed that the mix design, as shown in Table 4-27 gave the optimum strength and cost responses for reinforced paving, floor, ceiling, foundation, and suspended slabs. The use of waste material significantly reduces total cost, as seen with suspended slabs total cost of R2742.03 /kg/m³. Despite the higher strength required for suspended slabs, the cost is lower than slabs requiring lower strength. This is attributed to the increased use of fly ash, which lowers the cost of the composite.

CHAPTER FIVE: CONCLUSIONS AND RECOMMENDATIONS

5.1 Introduction

This chapter presents a summary of the present study for both the experimental and numerical results from optimization. The major conclusions reached and recommendations for future research are also presented.

5.2 Conclusions

- i. The fly ash had a dark grey colour, with moisture regain of 0.5695%, which was considered low for Class F fly ash. The SEM morphology study showed that the fly ash had predominantly spherically shaped particles. This was expected to improve the workability of the concrete. The fly ash particle sizes analysed by the particle size distribution machine (PSD) had sizes that ranged from 0.31 μm to 800 μm . Chemical analysis using EDS showed that the fly ash contained Ca, Al, P, Si, and trace amounts of Ti and Mg. The XRD pattern showed the presence of a large number of crystalline minerals like mullite ($\text{Al}_6\text{Si}_2\text{O}_{13}$) and quartz (SiO_2).
- ii. The fine aggregate characterisation showed that the river sand had an FM of 3.69, considered coarse sand. The fine aggregate showed uniform particle size distribution with a uniformity coefficient of 4.007. The specific gravity of the river sand was calculated as 2.15, which was considered a bit low for fine aggregate.
- iii. Coarse aggregate characterisation revealed that the size of the aggregate particle was between 9.5 mm and 13 mm. The coarse aggregate had a uniformity coefficient of 4.007, which implied the aggregate was well graded. The coarse aggregate had a high flakiness index of 74.82% and an acceptable elongation index of 46.72%. The water absorption of the coarse aggregate used was 0.80% with a specific gravity of 2.609, which is typical for coarse aggregates.
- iv. The slump value was observed to increase with the addition of fly ash, and however, the addition of PET fibre decreased the slump value with incremental amounts of fibre. The combined effect of fibre addition and fly ash showed a general decreasing slump value for all amounts of fly ash content. The use of lower amounts of fibres less than 0.5% gave acceptable workability of the FRCC. Therefore, it is recommended to maintain less than 0.5% fibre content to have acceptable concrete workability.
- v. The addition of 0.5 % PET fibre alone to the FRCC increased the compressive strength to 28 N/mm^2 . However, further fibre addition above this percentage resulted in a decrease in compressive strength.

- vi. The initial addition of fly ash alone increased the compressive strength significantly, with the highest strength being realized with the addition of 15 % Fly ash. Further addition of fly ash beyond this percentage up to 30 % resulted in a decrease in compressive strength. However, for all percentages of fly ash added, the compressive strength was above that of the control specimen.
- vii. The combined addition of PET fibre and fly ash gave the highest compressive strength at 20 % fly ash and 0.5 % PET fibre addition.
- viii. The addition of PET fibre only decreased the split tensile strength of the FRCC. Unreinforced concrete had a split tensile strength of 2.06 N/mm² which dropped marginally to 1.82 N/mm² with the addition of 0.5 % PET fibre. The addition of 1.0 % PET fibre gave a split tensile strength of 1.16 N/mm². This was a drop of 44% from the split tensile strength of unreinforced concrete. Further addition of PET fibre to 2.0 % resulted in a reduction of split tensile strength to 0.92 N/mm².
- ix. The addition of fly ash alone increased the split tensile strength gradually to the peak of 2.35 N/mm² for 20 % fly ash addition. Thereafter, there was a sharp decrease in split tensile strength with the further addition of fly ash. The specimen containing 30 % fly ash content had the lowest flexural strength of 1.7 N/mm² which was lower than that of the control specimen.
- x. The combined addition of 0.5 % PET fibre addition and 20 % fly ash gave the highest split tensile strength of 2.7 N/mm². The mix ratio containing 30 % fly ash had the lowest split tensile strength at all PET fibre additions.
- xi. The addition of fly ash alone had a positive effect on the flexural strength, with 15 % addition of fly ash giving a strength of 5.94 N/mm² which was almost double that of the control specimen. However, further addition of fly ash beyond 15 % yielded a negative effect on the flexural strength.
- xii. The addition of 0.5 % PET fibre alone gave the highest flexural strength. However, further addition above 0.5 % gave a decreasing trend and unsatisfactory flexural strength.
- xiii. The combined addition of 0.5 % PET fibre and 30 % fly ash gave the highest flexural strength. However, all the other specimens containing fly ash ranging from 15 % to 25 % gave satisfactory flexural strength at 0.5 % fibre addition. Thereafter, there was a drop in the flexural strength with increased PET fibre addition beyond 0.5 %. There is need for further investigative study into the cause of the increase in flexural strength with 30% fly ash whereas 15 – 25% gave unsatisfactory strength values.
- xiv. The rebound number was highest for concrete containing 15% fly ash alone. Further rebound number tests beyond 15 % fly ash content showed a decreasing rebound number trend. This agreed with the destructive compressive strength test. Though the rebound number gave calculated compressive strength, which followed the destructive test trend, the results were significantly lower at all fly ash addition levels in relation to the destructive test.

- xv. The addition of PET fibre only to the FRCC gave a decreasing rebound number with an increase in fibre content. This was in line with the trend observed for the destructive test.
- xvi. A comparison between the destructive and non-destructive rebound hammer test was done and showed that the non-destructive test gave significantly lower strength of between 20 - 40 %. This showed the need to accurately map a relationship between the destructive and non-destructive test to use the rebound hammer test for compressive strength approximation. The rebound number for the FRCC containing both fibre and fly ash followed a similar trend to that of the compressive strength test.
- xvii. 15% fly ash only had the effect of decreasing the cost per cubic metre of concrete by R 78.48 to R 2762.27. Further addition of fly ash results in significant cost savings, with 30% fly ash replacement concrete costing just R 2648.97 to produce compared to the control sample with no-fly ash costing R2840.75. This is a total saving of R191.78/m³ with the incorporation of 30 % fly ash. FRCC specimens containing fly ash and PET fibres were cheaper than the control specimen.
- xviii. ANOVA test for all the responses indicated that the model was able to predict the slump value and mechanical properties of the fibre reinforced concrete correctly and effectively with a coefficient of determination, R², in the range of 0.4151 to 0.9467.
- xix. An overlaid contour plot was drawn, which showed that the optimum region was between 6% and 25 % fly ash content and between 0 % and 0.5 % PET fibre content. The optimum constituent combination for maximum mechanical strength at the lowest possible cost was found to be 15.7576 % Fly ash and 0.3232 % PET fibre. These values corresponded to responses of 25.6465 N/mm², 3,6889 N/mm², 2.3565 N/mm², 31.4763 mm, R 2744.17 for compressive strength, flexural strength, tensile strength, slump value and total cost, respectively. These predictions were validated experimentally, and a good correlation was observed between the actual and predicted values based on the observed standard deviations of 0.1335, 0.031, 0.005, 0.676, 0.02 for compressive strength, flexural strength, tensile strength, slump value and cost, respectively.
- xx. The optimum combination for suspended slabs was 19.0909% for fly ash and 0.3434% PET fibre. These values corresponded to responses of R 2742.03/kg/m³, 2.3001 N/mm², 3.6814 N/mm², 24.7664 N/mm², 30.5986 mm for a total cost, split tensile, flexural, compressive strength and slump value. For foundation slabs, the optimum combination was 3.9394% fly ash and 0.6465 % PET fibre, and the corresponding response values are R 2760.47 /kg/m³, 1.8223 N/mm², 3.2642 N/mm², 19.3200 N/mm² and 10.7832 mm for a total cost, split tensile, flexural, compressive strength and slump value, respectively. For paving slabs, the optimum combination was 0.6465% PET fibre giving a response of R 2775.13 kg/m³, 1.4096 N/mm², 3.2891 N/mm², 19.1149 N/mm² and 9.9176 mm for a total cost, split tensile, flexural, compressive strength and slump value, respectively.

5.3 Recommendations for Future Work

Given the scope of the thesis, there are still some areas that need to be addressed of great complexity and perplexity in the current work.

- i. To increase the sustainability of the FRCC slab, it is necessary for further research to be carried out in the use of recycled aggregates to lower the cost further and increase sustainability.
- ii. The PET fibre used in the current study had a fibre length of 12 mm there is a need to expand the study and test the possibilities of using varying fibre lengths. There is also a possibility of using varying fibre lengths within the same mix design. This can improve the strength properties of the long fibres. The short fibres can improve the ease of finishing the slabs.
- iii. The PET fibres used in the study were untreated and used as they were. There is a need to explore the possibility of treating the PET fibres to increase the interfacial bond strength between the fibre and the matrix.

REFERENCES

- Abdulkarim, I. & Abiodun, A. O., 2012. A study of problems associated with PET bottles generation and disposal in Kano Metropolis. *Natural & Applied Sciences*, 3(2), pp. 56-65.
- Abuakrous, Y., Panesar, D., Hooton, D. R. & Singh, B., 2016. Particle size analysis as a means to better understand the influence of fly ash variability in concrete. *Resilient infrastructure*, pp. 759-1 - 759-8.
- ACI Committee-544, 1996. *State of the art report on fibre reinforced concrete*, Michigan: Farmington Hills.
- Aguado, J. & Serrano, D., 1999. Feedstock recycling of plastic wastes. *RSC clean technology monographs*, p. 1992.
- Ahmad, S., 2007. Optimum concrete mixture design using locally available ingredients. *The Arabian journal for science and engineering*, 32(1), pp. 27-33.
- Ahmad, S. & Alghamdi, S. A., 2014. A statistical approach to optimizing concrete mixture design. *The scientific world journal*, Volume 1, pp. 1-7.
- Ahmaruzzaman, M., 2010. A Review on the utilization of fly ash. *Prog Energy Combust*, Volume 36, pp. 327-63.
- Ajao, A. M. et al., 2018. Experimental datasets on properties of river sand as an aggregate in replacement of crushed rock for interlocking stones production. *Data Brief*, Volume 20, pp. 602-608.
- Akbar, H., Krishan, G., Prajapati, S. D. & Saini, R., 2016. Determination of reactive silica (SIO₂) of fly ash. *Rasayan journal of chemistry*, 9(1), pp. 27-30.
- Akcaozoglu, S., Atis, C. D. & Akcaozoglu, K., 2010. An investigation on the use of shredded waste PET bottles as aggregate in lightweight concrete. *Waste Management*, Volume 30, pp. 285-290.
- Akinola, A. A., Adeyemi, A. & Adetinka, F. M., 2014. A proposal for the management of plastic packaging waste. *IOSR Journal of Environmental Science, Toxicology and Food Technology*, 8(1), pp. 71-78.
- Albano, V. et al., 2009. Influence of content and particle size of waste PET bottles on concrete behaviour at different w/c ratios. *Waste Management*, Volume 29, pp. 2707-2716.
- Alberti, M. G., Enfedaque, A. & Glavez, J. C., 2018. Polyolefin fibres for the reinforcement of concrete. In: *Polyolefin fibres for the reinforcement of concrete*. Madrid: IntechOpen, pp. 145-167.
- Alegbe, J. et al., 2018. Chemical, Mineralogical and Morphological Investigation of Coal Fly Ash Obtained from Mpumalanga Province, South Africa. *Research Journal of Environmental Sciences*, 12(3), pp. 98-105.
- Alhozaimy, A. M., Soroushian, P. & Mirza, F., 1996. Mechanical properties of polypropylene fibre reinforced concrete and the effects of pozzolanic materials. *Cement & Concrete Composites*, Volume 18, pp. 85-92.
- Alhozaimy, A. M., Soroushian, P. & Mirza, F., 1996. MEchanical properties of polypropylene fibre reinforced concrete and the effects of pozzolanic materials. *Cement Concrete Composites*, Volume 18, pp. 85-92.
- Alhozaimy, A. & soroushian, P., 1996. Mechanical properties of polypropylene fibre reinforced concrete and effects of pozzolanic materials. *Cement and Concrete Composites*, 18(2), pp. 85-92.

- Ali, T. & Yehia, S., 2016. Study on strengthening of RC slabs with different innovative techniques. *Open journal of civil engineering*, 6(1), pp. 516-525.
- Alomar, C., Estarellas, F. & Deudero, S., 2016. Microplastics in the Mediterranean Sea: Deposition in coastal shallow sediments, spatial variation and preferential grain size. *Marine Environmental Research*, Volume 115, pp. 1-10.
- Alotaibi, K. S. & Galal, K., 2018. Experimental study of CFRP-confined reinforced concrete masonry columns tested under concentric and eccentric loading. *Elsevier*, Volume 155, pp. 257-271.
- Al-Salem, S. M., Lettieri, P. & Baeyens, J., 2009. Recycling of recovery routes of plastic solid waste. *Waste management*, Volume 29, pp. 2625-2643.
- Alsayed, S. H. & Amjad, M. A., 1996. Strength, Water Absorption and Porosity of Concrete Incorporating Natural and Crushed Aggregate. *Eng Sci*, 8(1), pp. 109-120.
- Alyamac, K. E., Tas, Y., Ulas, M. A. & Ghafari, E., 2017. *Feasibility analysis of NDT methods using to estimate the concrete strength as part of urban regeneration*. Turkey, International Conference on Advances and Innovations in Engineering.
- Amey, K. B. et al., 2014. Caractérisation physique de sables silteux au Togo. *AfriqueScience*, 10(2), pp. 53-69.
- Annadnua, K., Tangchirapat, W. & Jatuparitakkul, C., 2013. Strength, water permeability and heat evolution of high strength concrete made from the mixture of calcium carbide residue and fly ash. *Materials and Design*, 51(5), pp. 894-901.
- Anand, Y. & Dutta, V., 2013. Testing of composites: A Review. *Advanced Materials and Manufacturing & Characterization*, 3(1), pp. 359-364.
- Anand, Y. & Dutta, V., 2013. Testing of composites: A Review. *Advanced Materials Manufacturing & Characterization*, 3(1), pp. 359-364.
- Andrady, A. L., 2011. Microplastics in the marine environment. *Marine Pollution Bulletin*, Volume 62, pp. 1596-1605.
- Andrady, A. L., 2011. Microplastics in the marine environment. *Marine pollution bulletin*, 62(8), pp. 1569-1605.
- Andredi, C., 2004. *Man-made fibres*. 1st Edition ed. Milano: Italian Association of Textile Machinery Producers.
- Anon., 2007. Characterisation of fly ash and bottom ash from a coal-fired power plant. *International journal of surface mining, reclamation and environment*, 10(4), pp. 181-186.
- Arum, C. & Alhassan, Y. A., 2005. Combined effect of aggregate shape, texture and size on concrete strength. *Journal of science, Engineering and technology*, 13(2).
- Aruna, M., 2014. Mechanical Behaviour of Sisal Fibre Reinforced Cement Composites. *International Journal of Materials and Metallurgical Engineering*, 8(4), pp. 650-654.
- Asokana, P., Saxena, M. & Asolekar, S. R., 2005. Coal combustion residues - Environmental implications and recycling potentials. *Resources Conservation and Recycling*, Volume 43, pp. 239-262.
- ASTM C128-01, 2004. *Standard test method for density, relative density (specific gravity), and absorption of fine aggregate*, West Conshohocken: ASTM International.

ASTM C136-96a, 2004. *Standard test method for sieve analysis of fine and coarse aggregates*, West Conshohocken: ASTM International.

ASTM C146-21, 2021. *ASTM C146 - 21: Standard Test Methods for Chemical Analysis of Glass Sand*, West Conshohocken: ASTM International.

ASTM C1585-04, 2004. *Standard test method for measurement of rate of absorption of water by hydraulic cement concretes*, West Conshohocken: ASTM International.

ASTM C188-14, 2014. *ASTM C188-14: Standard Test Method for Density of Hydraulic Cement*, West Conshohocken: ASTM International.

ASTM C535-01, 2004. *Standard test method for resistance to degradation of large size coarse aggregate by abrasion and impact in the Los Angeles Machine*, West Conshohocken: ASTM International.

ASTM C78-00, 2004. *Standard test method for flexural strength of concrete (using simple beam with third point loading)*, West Conshohocken: ASTM.

ASTM C806-02, 2004. *Standard test method for rebound number of hardened concrete*, West Conshohocken: ASTM International.

ASTM C940-98a, 2004. *Standard test method for expansion and bleeding of freshly mixed grouts for preplaced aggregate concrete in the laboratory*, West Conshohocken: ASTM International.

ASTM D3822-01, 2004. *Standard Test Method for Tensile properties of single textile fibres*, West Conshohocken: ASTM International.

ASTM International, 2004. *Standard test method for slump of hydraulic cement concrete ASTM C143/C143 M-00*, West Conshohocken: ASTM.

ASTM Standard C469, ., 2002. *Standard test method for splitting tensile strength of cylindrical concrete specimens*, West Conshohocken: Annual Book of ASTM Standards, American Society for Testing and Materials.

ASTM Standard C78, 2009. *Standard test method for flexural strength of concrete (using simple beam with third point loading)*, West Conshohocken: Annual book of ASTM standards, American Society for Testing and Materials.

ASTM, 2019. *ASTM D2974-84 Standard Test Methods for Moisture, Ash and Organic Matter of Peat and Other Organic Soils*, Philadelphia: American Society for Testing and Materials.

ASTM, 2019. *ASTM International*. [Online] Available at: <https://www.astm.org/Standards/D6941.htm> [Accessed 6 June 2020].

Ataei, H., Anakari, K. K. & Ma, R., 2017. *Mechanical properties of polyethylene terephthalate particle based concrete: A Review*. Philadelphia, s.n.

Ataei, H., Anaraki, K. K. & Ma, R., 2017. Mechanical properties of polyethylene terephthalate particle based concrete: A review. *Airfield and Highway*, Volume 1, pp. 57-68.

Australia, C. I. o., 2007. *Performance tests to assess concrete durability*, North Sydney: Engineers Media.

Australian, S. 1., 2014. *Methods of Testing concrete - Compressive Strength Tests-Concrete, Mortar and Grout Specimens*, Sydney: Australia : Standards Australia.

Auta, H. S., Emenike, C. U. & Fauziah, S. H., 2017. Distribution and importance of microplastics in the marine environment: a review of the sources, fate, effects and potential solutions. *Environ Int*, Volume 102, p. 165176.

Avaze, A., 2018. *What is the procedure for elongation index of coarse aggregates*. [Online] Available at: <https://www.quora.com/What-is-the-procedure-for-elongation-index-of-coarse-aggregates> [Accessed 13 October 2021].

Avio, C. G., Gorbi, S. & Regoli, F., 2015. Experimental development of a new protocol for extraction and characterization of microplastics in fish tissues. *First observation in commercial species from Adriatic Sea*, p. Marine Environmental Research.

Awaja, F. & Pavel, D., 2005. Recycling of PET. *European Polymer Journal*, Volume 41, pp. 1453-1477.

Ayub, T., Khan, S. U. & Memon, F. A., 2014. Mechanical characteristics of hardened concrete with different mineral admixtures: A review. *The scientific world journal*, pp. 1 - 15.

Azevedo, N. M. & Lemon, J. V., 2006. Aggregate shape influence on the fracture behaviour of concrete. *Journal of structural engineering and mechanics*, 24(4), pp. 411-427.

Azmi, N. B. et al., 2018. Performance of composite sand cement brick containing recycle concrete aggregate and waste polyethylene terephthalate with different mix design ratio. *Earth and Environmental Science*, Volume 140, pp. 1-8.

Babaie, R., Abolfazli, M. & Fahimifar, A., 2019. Mechanical properties of steel and polymer fiber reinforced concrete. *Journal of the Mechanical Behaviour of Materials*, Volume 28, pp. 119-134.

Backus, B., 2021. *Fineness Modulus of Concrete Aggregates*. [Online] Available at: <https://www.globalgilson.com/blog/fineness-modulus-of-concrete-aggregates> [Accessed 07 October 2021].

Badave, N. S. & Pise, C., 2018. Study on effect of waste polyethylene terephthalate bottle fibers on silica fume concrete - A Review. *International Journal of Scientific & Engineering Research*, 9(2), pp. 2046-2049.

Badave, N. S. & Pise, C., 2018. Study on effect of waste polyethylene terephthalate bottle fibres on silica fume concrete - A review. *International Journal of Scientific & Engineering Research*, 9(2), pp. 2046-2049.

Bagherzadeh, R., Sadeghi, A. H. & Latifi, M., 2011. Utilizing polypropylene fibres to improve physical and mechanical properties of concrete. *Textile Research Journal*, 82(1), pp. 88-96.

Balaguru, P. N. & Shah, S. P., 1992. *Fiber-reinforced cement composites*. New York: McGraw-Hill Inc.

Bandyopadhyay, S. et al., 2010. Advanced utilization of as received and near whitened fly ash in polypropylene polymer to improve mechanical, notched impact and whiteness colour properties. *Int J Plast Technol*, Volume 14, pp. S52-S56.

Banthia, N. & Gupta, R., 2006. Influence of polypropylene fiber geometry on plastic shrinkage cracking in concrete. *Cem Concr Res*, 36(7), pp. 1263-7.

Banthia, N. & Gupta, R., 2006. Influence of polypropylene fibre geometry on plastic shrinkage in concrete. *Cement and Concrete Research*, 36(7), pp. 1263-1267.

- Banthia, N., Zanotti, C. & Sappakittipakorn, M., 2014. Sustainable fiber reinforced concrete for repair applications. *Construction and Building Materials*, Volume 67, pp. 405-412.
- Banthia, N., Zanotti, C. & Sappakittipakorn, M., 2014. Sustainable fiber reinforced concrete repair applications. *Construction and Building Materials*, Volume 67, pp. 405-412.
- Barbuta, M. et al., 2017. Combined effect of fly ash and fibers on properties of cement concrete. *Procedia Engineering*, Volume 1881, pp. 280-284.
- Barbuta, M. et al., 2017. Combines effect of fly ash and fibres on properties of cement concrete. *Procedia Engineering*, Volume 181, pp. 280-284.
- Barough, A. S., Shoubi, M. V., Kiani, I. & Amini, Z., 2012. *Advantages of using fly ash in concrete industry for achieving sustainable development*. Kuala Lumpur, Management in construction research association Postgraduate conference.
- Bederina, M., Khefer, M. M. & Dheilily, R. M., 2005. uéneudec, Reuse of local sand: effect of limestone filler proportion on the rheological and mechanical properties of different sand concretes. *Cement and Concrete Research*, Volume 35, pp. 1172-1179.
- Bediako, M. & Amankwah, E. O., 2015. Analysis of chemical composition of portland cement in Ghana: A key to understand the behavior of cement. *Advances in Materials Science and Engineering*, Volume 1, pp. 1-6.
- Belani, D. & Pitroda, J., 2013. Fly ash (F-Class): Opportunities for sustainable development of low cost rural roads. *International Journal of Engineering Trends and Technology (IJETT)*, Volume 4.
- Belardi, G., Massimilla, S. & Piga, L., 1998. Crystallization of K-L and K-W zeolites from fly ash. *Resour Conserv Recycl*, Volume 24, pp. 167-181.
- Bendapudi, S. C. & Saha, P., 2011. Contribution of fly ash to the properties of mortar and concrete. *International Journal of Earth Science and Engineering*, 4(6), pp. 1017-1023.
- Bentz, D. P., Hansen, A. S. & Guynn, J. M., 2011. Optimization of cement and fly ash particle sizes to produce sustainable concretes. *Cement and concrete composites*, 33(8), pp. 824-831.
- Besseling, E. et al., 2015. Microplastic in a macro filter feeder: humpback whale Megaptera novaeangliae. *Mar Pollut Bull*, Volume 1, pp. 248-252.
- Bilodeau, A. & Maholtra, V. M., 2000. High volume fly ash system: the concrete solution for sustainable development. *ACI Materials Journal*, 97(1), pp. 41-48.
- Bilodeau, A., Sivasundaram, V. K., Painter, K. E. & Malhotra, V. M., 1994. Durability of concrete incorporating high volumes of fly ash from sources in the USA. *ACI materials journal*, 91(1), pp. 3-12.
- Bos, F., Wolfs, R., Ahmed, Z. & Salet, T., 2016. Additive manufacturing of concrete in construction: potential challenges of 3D concrete printing. *Virtual and physical prototyping*, 11(3), pp. 209-225.
- Brandt, A. M., 2009. *Cement based composites: Materials, mechanical properties and performance*. Abingdon: Taylor & Francis.
- Brooks, J., 2000. Effect of admixture on the setting times of high strength concrete. *Cement and concrete composites*, 22(4), pp. 293-301.
- Brooks, J. J., 2000. Effect of admixture on the setting times of high strength concrete. *Cement and concrete composites*, 22(4), pp. 293-301.

- Brown, P., Pommersheim, J. & Frohnsdrff, G., 1985. kinetic model for the hydration of tricalcium silicate. *Cement and Concrete Research*, 15(1), pp. 35-41.
- Brydson, J. A., 1995. Plastics material. In: *Plastics material*. Oxford: Butter-worth-Heinemann.
- Buitrago, M. et al., 2020. A Parametric Computational Study of RC Building Structures under Corner-Column Removal Situations. *Applied Sciences*, 10(8911), pp. 1-27.
- Bullard, J. W. et al., 2011. Mechanisms of cement hydration. *Cem Concr Res*, 41(12), pp. 1208-1223.
- Callister, W. D., 2001. Introduction to Materials Science and Engineering. In: s.l.:s.n.
- Camoes, A. et al., 1998. *Low Cost High Performance Concrete Using Low Quality Fly Ash*. Lisboa, ERMCO98.
- Campolat, F. K. et al., 2004. Use of zeolite, coal bottom ash and fly ash as replacement materials in cement production. *Cement & Concrete Research*, Volume 34, pp. 731-736.
- Cauwenberghe, V. L. et al., 2015. Microplastics in sediments: A review of techniques, occurrence and effects. *Marine Environmental Research*, Volume 111, pp. 5-17.
- Celauro, C., Bernardo, C. & Gabriel, B., 2010. Production of innovative, recycled and high performance asphalt for road pavements. *Resources, Conservation & Recycling*, pp. 337-347.
- Celik, O., Damci, E. & Piskin, S., 2008. Characterization of fly ash and its effect on the compressive strength properties of Portland cement. *Indian journal of engineering & material sciences*, Volume 15, pp. 443-440.
- Cemix, 2018. *Advance polypropylene fibre concrete*, Warwickshire: CEMEX UK.
- CEP, 2018. *Civil Engineering Portal*. [Online] Available at: <https://www.engineeringcivil.com/what-are-the-differences-between-shear-slump-and-collapse-slump-in-slump-test.html> [Accessed 30 July 2019].
- Challal, O., Nollet, M. & Perraton, D., 1998. Strengthening of Reinforced Concrete Beams with Externally Bonded Reinforced Plastic Plates: Design Guidelines for Shear and Flexure. *Canadian Journal for Civil Engineering*, Volume 25, pp. 692-704.
- Chethan, C. & Chandrashekar, A., 2015. Experimental Study on effect of fibre addition on the properties of plastic fibers reinforced concrete. *International Journal of Engineering Research & Technology (IJERT)*, 4(8), pp. 1545-1552.
- Chindraprasirt, P., Chotithanorm, C., Cao, H. T. & Sirivivatnanon, V., 2007. Influence of fly ash fineness on the chloride penetration of concrete. *Construct Build Mater*, Volume 21, pp. 356-61.
- Choi, Y. W., Moon, D. J., Chung, J. S. & Cho, S. K., 2005. Effects of waste PET bottles aggregate on properties of concrete. *Cement and Concrete Research*, Volume 35, pp. 776-781.
- Choi, Y. W., Moon, D. J. & Chung, S. J., 2005. Effects of waste PET bottles aggregate on the properties of concrete. *Cement and Concrete Research*, Volume 35, pp. 776-781.
- Choudhary, V. & Luhar, S., 2017. Fly ash utilization: A review. *International Journal of Civil Engineering and Technology*, 8(4), pp. 301-312.
- Chou, J. S., Tsai, C. F., Pham, A. D. & Lu, Y. H., 2014. Machine learning in concrete strength simulations: multi-nation data analytics. *Construction and building materials*, Volume 73, pp. 771-780.

- Chou, M. M., 2012. Fly Ash. In: *Encyclopedia of Sustainability Science and Technology*. New York: Springer.
- CIP, 2014. *synthetic fibers for concrete*, Washington DC: National ready mixed concrete association.
- Concrete Society, 2017. *Concrete at your fingertips*. [Online] Available at: <http://www.concrete.org.uk/fingertips-nuggets.asp?cmd=display&id=559#> [Accessed 2 May 2019].
- Critchell, K. & Hoogenboom, M. O., 2018. Effects of microplastic exposure on the body condition and behaviour of planktivorous reef fish (*Acanthochromis polyacanthus*). *PLOS*, 13(3).
- Crouch, L. K., Hewitt, R. & Byard, B., 2007. *High volume fly ash concrete*. Northern Kentucky, World of Coal Ash.
- Crow, J. M., 2008. *The concrete conundrum*, Leeds: Chemistry World.
- Da costa, J. P., Santos, P. S., Duarte, A. C. & Rocha, S. T., 2016. Nano plastics in the environment - Sources, fate and effects. *Science of the Total Environment*, 566(567), pp. 15-26.
- De Schutter, G. & Audenaert, K., 2004. Evaluation of water absorption of concrete as a measure for resistance against carbonation and chloride migration. *Materials and Structures*, 37(273), pp. 59-596.
- Deepa, C., Sathiyakumar, K. & Sudha, P., 2010. Prediction of compressive strength of high performance concrete mix using tree based modeling. *International journal of computer applications*, 6(5), pp. 18-24.
- Demyanova, V. S., Kalashnikov, V. I. & Minenko, E. Y., 2003. Reinforcement of concrete with polyamide fibres. *International polymer science and technology*, 30(11), pp. 1-47.
- Derraik, J., 2002. The pollution of the marine environment by plastic debris: a review. *Marine pollution bulletin*, Volume 1, pp. 842-852.
- Derraik, J. G., 2002. The pollution of the marine environment by plastic debris: A review. *Marine Pollution Bulletin*, Volume 44, pp. 842-852.
- Dharan, D. S. & Lal, A., 2016. Study the effect of polypropylene fibre in concrete. *International Research Journal of Engineering and Technology*, 3(6), pp. 616-619.
- Diamond, S., 1988. *Rapid particle size analysis of fly ash with a commercial laser diffraction instrument*. s.l., s.n., pp. 119-127.
- Divvala, S. & Rani, S., 2020. Experimental Works on Geopolymer Concrete Composites: Destructive and Non-Destructive Testing. *International Journal of Recent Technology and Engineering (IJRTE)*, 9(1).
- Do Sul, I. J. & Costa, M. F., 2014. The present and future of microplastic pollution in marine environment. *Environmental Pollution*, Volume 185, pp. 352-364.
- Domone, P. L. & Soutsos, M. N., 1994. An approach to the proportioning of high strength concrete mixes. *Concrete International*, 16(10), pp. 26-31.
- Dora, F., 2011. Preliminary analysis of concrete reinforced with waste bottles PET fibres. *Construction and Building Materials*, Volume 25, pp. 1906-1915.
- Dris, R. et al., 2016. A first overview of textile fibres, including microplastics in indoor and outdoor environments. *Environ Pollut*, pp. 453-458.

Dunuweera, S. P. & Rajapakse, R. M., 2018. Cement types, composition, uses and advantages of nanocement, environmental impact on cement production, and possible solutions. *Advances in Materials Science and Engineering*, pp. 1-11.

Dwivedi, A. & Jain, M. K., 2014. Fly ash waste management and overview: A Review. *Recent Research in Science and Technology*, 6(1), pp. 30-35.

Dwivedi, S. K., Vishwakarma, M. & Son, A., 2018. Advances and researches on non destructive testing: A review. *Materials Today Proceedings*, Volume 5, pp. 3690-369.

Ebead, U. & Marzouk, H., 2004. Fiber-Reinforced Polymer Strengthening of Two-Way Slabs. *ACI Structural Journal*, Volume 101, pp. 650-659.

Ebnesajjad, S., 2014. Surface treatment of materials for adhesive bonding. In: *Surface and Material Characterization Techniques*. s.l.:s.n.

Eco Ace, 2020. *Fibre Plast Con*, Johannesburg: Eco Ace.

Edugreen, 2010. *Types of solid waste*. [Online] Available at: <http://edugreen.teri.res.in/explore/solwaste/types.htm> [Accessed 28 February 2019].

engineering, C., 2017. *Concrete slump test - step by step procedure*. [Online] Available at: <https://civiltoday.com/civil-engineering-materials/concrete/79-concrete-slump-test-standard-equipment-procedures-cautions> [Accessed 09 May 2019].

Erdogdu, K. & Turker, P., 1998. Effects of fly ash particle size on strength of Portland cement fly ash mortars. *Cem Concr Res*, 28(9), pp. 1217-1222.

ESKOM, 2013. *Ash management in Eskom. Factsheet CO 0004*, s.l.: Eskom.

Eskom, 2019. *Fact Sheet*. [Online] Available at: http://www.eskom.co.za/AboutElectricity/FactsFigures/Pages/Facts_Figures.aspx [Accessed 20 March 2019].

Eskom, 2019. *Lethabo Power Station*. [Online] Available at: http://www.eskom.co.za/Whatweredoing/ElectricityGeneration/PowerStations/Pages/Lethabo_Power_Station.aspx [Accessed 15 May 2019].

Eskom, 2019. *Lethabo Power Station*. [Online] Available at: http://www.eskom.co.za/Whatweredoing/ElectricityGeneration/PowerStations/Pages/Lethabo_Power_Station.aspx [Accessed 15 May 2019].

Exeldin, A. S. & Balaguru, P. N., 1992. Normal and high-strength fiber-reinforced concrete under compression. *J. Mater. Civil Eng.*, 4(4), pp. 415-529.

Fanella, D. A. & Naaman, A. E., 1985. Stress-strain properties of fiber reinforced mortar in compression". *ACI J*, 82(4), pp. 475-483.

Fang, G., Bahrami, H. & Zhang, M., 2018. Mechanisms of autogenous shrinkage of alkali-activated fly ash-slag pastes cured at ambient temperature within 24 h. *Constr. Build. Mater.*, Volume 171, pp. 377-387.

- Fanghui, H., Renguang, L., Dongming, W. & Peiyu, Y., 2014. Characteristics of the hydration heat evolution of composite binder at different hydration temperature. *Thermochimica Acta*, 586(8), pp. 52-57.
- Fanghui, L., Renguang, W., Dongming & Peiyu, Y., 2014. Characteristics of the hydration heat evolution of composite binder at different hydration temperature. *Thermochimica Acta*, 586(8), pp. 52-57.
- Farrell, P. & Nelson, K., 2013. Tropical level transfer of microplastic: *Mytilus edulis* (L) to *Carcinus maenas* (L). *Environmental pollution*, 177(1), pp. 1-3.
- Feng, J., Sun, J. & Yan, P., 2018. The Influence of ground fly ash on cement hydration and mechanical property of mortar. *Advances in civil engineering*, pp. 1-8.
- Feng, X. & Clark, B., 2011. *Evaluation of the Physical and Chemical Properties of Fly Ash Products for Use in Portland Cement Concrete*. Denver, World of Coal Ash Conference.
- Ferreira, L. E., de Hania, J. B. & Ferrari, V. J., 2016. Optimization of a hybrid fibre reinforced high strength concrete. *Mechanics of Composite Materials*, 52(3), pp. 295-304.
- Flower, R. J., 2006. Diatoms in ancient building materials: Application of diatom analysis to Egyptian mud bricks. *Nova Hedwigia*, pp. 245-263.
- Foley, C. J., Feiner, Z. S., Malinich, T. D. & Hook, T. O., 2018. A meta analysis of the effects of exposure to microplastics on fish and aquatic invertebrates. *Sci Total Environ*, pp. 550-559,631-632.
- Foti, D., 2013. Use of recycled waste pet bottle fibers for the reinforcement of concrete. *Composite structures*, Volume 96, pp. 396-404.
- Frigione, M., 2010. Recycling of PET bottles as fine aggregate in concrete. *Waste Management*, 30(6), pp. 1101-1106.
- Frigione, M., 2010. Recycling PET bottles as fine aggregate in concrete. *Waste Management*, Volume 30, pp. 1101-1106.
- Gaharwar, A. S. et al., 2016. A review article on manufacturing process of cement, environment attributes, topography and climatological data station:IMD. *Journal of medicinal plants studies*, 4(4), pp. 47-53.
- Galloway, J. E., 1994. Grading, Shape and Surface Properties. In: P. Klieger, ed. *Significance of Tests and Properties of Concrete and Concrete Making Materials*. Pennsylvania: West Conshohocken, pp. 401-410.
- Gamage, N., Liyanage, K. & Fragomeni, S., 2011. *Overview of different types of fly ash and their use as a building and construction material*. Sri Lanka, International Conference of Structural Engineering, Construction and Management.
- Gamage, N., Liyanage, K., Fragomeni, S. & Setunge, S., 2011. *Overview of different types of fly ash and their use as a building and construction material*. s.l., s.n.
- GangaRao, H. V. & Vijay, P. V., 1998. Bending Behavior of Concrete Beams Wrapped with Carbon Fabric. *Journal of Structural Engineering*, 124(1), pp. 3-10.
- Gao, Y. et al., 2017. Effects of nano-particles on improvement in wear resistance and drying shrinkage of road fly ash concrete. *Construction and building*, Volume 151, pp. 228-235.
- German, R. M., 1997. A comparison of powder particle size measuring instruments. *International journal of powder metallurgy*, 33(8), pp. 35-48.

- Geyer, R., Jambeck, J. R. & Law, K. L., 2017. Production, use and fate of all plastics ever made. *Sci Adv*.
- GE, Z., WANG, K., SANDBERG, P. J. & RUIZ, J. M., 2009. Characterization and performance prediction of cement based materials using a simple isothermal calorimeter. *J Adv Concr Technology*, 7(3), pp. 355-366.
- Giere, R., Carleton, L. E. & Lumpkin, G. R., 2003. Micro and nanochemistry of fly ash from a coal fired power plant. *American Mineralogist*, Volume 88, pp. 1853-1865.
- Glavind, M., Olsen, G. S. & Munch, P. C., 1993. Packing Calculations and Concrete Mix. *Nordic Concrete Research*, Volume 13, pp. 21-34.
- Gleick, P. H., 2004. The World's water. In: *The Biennial Report on Freshwater Resources*. Oakland: Island Press, pp. 17-43.
- Goltermann, P., Johansen, V. & Palbful, L., 1997. Packing of aggregates: An alternative tool to determine the optimal aggregate mix. *ACI Mater. J.*, Volume 94, pp. 435-443.
- Goodship, V., 2007. Introduction to plastic recycling. *Smithers rapra technology limited*, p. 174.
- Govindasami, S., Sakthivel, P. B. & Harish, R., 2018. Strength Assessment of Polypropylene Fibre Reinforced Concrete (PPFRC). *International Journal of Engineering & Technology*, 7(3.34), pp. 436-438.
- Guler, S., 2018. The effect of polyamide fibres on the strength and toughness properties of structural lightweight aggregate concrete. *Concrete and Building Materials*, Volume 173, pp. 394-402.
- Guneyisi, E., Gesoglu, M. & Mermerdas, K., 2008. Improving strength, drying shrinkage and pore structure of concrete using metakaolin. *Materials and Structures*, 41(5), pp. 937-949.
- Halder, B., Tandon, V., Tarquin, A. & Ramana, C., 2009. *Influence of coal fly ash on mechanical properties of mortar consisting of total dissolved solids*. s.l., Proceeding of World of Coal Ash Conference, pp. 22-25.
- Hamou, T. A., Vanhove, Y. & Petrov, N., 2005. Microstructural analysis of the bond mechanism between polyolefin fibers and cement pastes. *Cement and Concrete Research*, 35(2), pp. 364-370.
- Hansen, L. D. & Fisher, G. L., 1981. Crystalline components of stack collected size fractionated coal fly ash. *Environmental Science & Technology*, Volume 15, pp. 1057-1062.
- Han, S. H., Kim, J. K. & Park, Y. D., 2003. Prediction of compressive strength of fly ash concrete by new apparnt activation energy function. *Cement and Concrete Research*, 33(7), pp. 965-971.
- Hanson, C. M., 1995. The advanced industrial material of the 21st century. *Metallurgical & Materials Transactions*, pp. 1321-1341.
- Harris, B., 1999. *Engineering Composite Materials*. 1st ed. London: The Institute of Materials.
- Hegel, C. et al., 2014. Particle size characterization: comparison of laser diffraction (LD) and scanning electron microscopy (SEM). *Acta Microscopica*, 23(1), pp. 11-17.
- Helal, J., Sofi, M. & Mendis, P., 2015. Non-destructive testing of concrete: A review of methds. *Electronic journal of structural engineering*, 14(1), pp. 97-107.
- Henderson, G. L., 2005. *Design of continuously reinforced concrete pavements using glass fibre reinforced polymer rebars*, Georgetown: US Department of Transporation.

- Heniegal, A. M., El-Habiby, F. F. & Hafez, R. D., 2015. Physical and mechanical properties of concrete incorporating industrial and agricultural textile wastes. *International Journal of Research in Engineering and Technology*, 4(7), pp. 166-175.
- Hill, R. L. & Folliard, K. J., 2006. Fly ash on air-entrained concrete. *Concrete in focus*, pp. 71-72.
- Hiremath, M. P. & Shetty, S., 2014. Utilization of waste plastic in manufacturing of plastic-soil bricks. *International journal of technology enhancements and emerging engineering research*, 2(4), pp. 102-107.
- Hoang, N. D. & Pham, A. D., 2016. Estimating concrete workability based on slump test with least squares support vector regression. *Journal of construction engineering*, pp. 1-9.
- Hoang, N., Pham, A., Nguyen, Q. & Pham, Q., 2016. Estimating compressive strength of high performance concrete with gaussian process regression model. *Advances in civil engineering*, pp. 1-8.
- Hopewell, J., Dvorak, R. & Kosior, E., 2009. Plastics recycling: challenges and opportunities. *Philosophical transactions R Soc Biological Science*, 364(1526), pp. 2115-2126.
- Hourau, L., Ainley, L., Jean, C. & Ciccione, S., 2014. Ingestion and defecation of marine debris by loggerhead sea turtles, *Caretta caretta* from by-catches in the South West Indian Ocean. *Marine Pollution Bulletin*, Volume 84, pp. 90-96.
- However, J. C. et al., 1999. Petrology, mineralogy and chemistry of magnetically separated sized fly ash. *Fuel*, Volume 78, pp. 197-203.
- Hughes, B. P. & Fattuhi, N. I., 1976. Improving the toughness of high strength cement paste with fiber reinforcement. *Composite*, 7(4), pp. 185-188.
- Huidong, L. et al., 2016. Morphology and Composition of Microspheres in Fly Ash from the Luohuang Power Plant, Chongqing Southwestern China. *Minerals*, 6(30), pp. 1-10.
- Hui, K. S., Hui, K. N. & Lee, S. K., 2009. A novel and green approach to produce nanoporous materials zeolite A and MCM-41 from coal fly ash and their application in environmental protection. *Proc World Acad Sci Engine & Technol*, Volume 41, pp. 174-184.
- Ibearugbulem, O. M. & Igwilo, K. C., 2019. Physical and mechanical properties of river stone as coarse aggregate for concrete production. *Nigerian Journal of Technology (NIJOTECH)*, 38(4), pp. 856-862.
- Impacts, V. A., 2015. *Colcanic ash impacts & mitigation*. [Online] Available at: https://volcanoes.usgs.gov/volcanic_ash/respiratory_effects.html [Accessed 07 May 2020].
- Irwan, J. M. et al., 2013. Development of Mix Design Nomograph for Polyethylene Terephthalate Fiber Concrete. *Applied Mechanics and Materials*, Volume 253-255, pp. 408-416.
- Islam, M. M. & Islam, M. S., 2013. Strength and durability characteristics of concrete made with fly ash blended cement. *Australian journal of structural engineering*, 14(3), pp. 303-319.
- Ismail, K. N., Hussin, K. & Idris, M. S., 2007. Physical, Chemical & Mineralogical Properties of Fly Ash. *Journal of Nuclear and Related Technology*, Volume 4, pp. 47-51.
- Ismail, Z. Z. & Hashmi, A. L., 2008. Use of waste plastic in concrete mixture as aggregate replacement. *Waste Management*, Volume 28, pp. 2041-2047.
- Iuyenkimet, 2007. *Slideshare*. [Online] Available at: https://www.slideshare.net/luyenkimnet/lecture-11?next_slideshow=1 [Accessed 1 May 2019].

- Jamal, H., 2017. *Concrete slump test - theory and lab test*. [Online] Available at: <https://www.aboutcivil.org/concrete-slump-test.html> [Accessed 09 May 2019].
- Jassim, H. M. & Anwar, A. G., 2016. Experimental study of polypropylene fiber reinforced concrete. *International journal of R&D in engineering science and management*, 4(3), pp. 149-161.
- Jayaram, M. A., Nataraja, M. C. & Ravikumar, C. N., 2009. Enlist genetic algorithm models: optimization of high performance concrete mixes. *Materials and manufacturing processes*, 24(2), pp. 225-229.
- Jennings, H. M., 1986. Aqueous solubility relationships for two types of calcium silicate hydrate. *Journal of the American Ceramic Society*, Volume 69, pp. 614-618.
- Jeon, J. K., Kim, W., Jeon, C. K. & Kim, J. C., 2014. Processing and mechanical properties of macro polyamide fiber reinforced concrete. *Materials*, Volume 7, pp. 7634-7652.
- Jimenez, F. A. & Palomo, A., 2005. Composition and microstructure of alkali activated fly ash binder: effect of the activator. *Cement and concrete research*, 35(10), pp. 1984-1992.
- Joaquin, A. G., Torres-Castellanos, N., Fernandez, G. J. & Andres, N. L., 2021. Ultra-high-performance concrete with local high unburned carbon fly ash. *DYNA*, 88(216), pp. 38-47.
- Jo, B. W., Park, S. K. & Park, J. C., 2008. Mechanical properties of polymer concrete made with recycled PET and recycled concrete aggregates. *Construction and Building Materials*, Volume 22, pp. 2281-2291.
- Kagonbe, P. B. et al., 2020. Physical Characterization and Optimization of Fineness Moduli of Natural Sand from The North Region of Cameroon Used in Construction. *Journal of Sustainable Construction Materials and Technologies*, 5(1), pp. 407-419.
- Karthiyaini, S. et al., 2019. Prediction of Mechanical Strength of Fiber Admixed Concrete Using Multiple Regression Analysis and Artificial Neural Network. *Advances in Materials Sciences and Engineering*, pp. 1-9.
- Kasperkiewicz, J., 1994. Optimization of concrete mix using a spreadsheet package. *ACI Materials Journal*, 91(6), pp. 551-559.
- Kassa, R. B., Kanali, C. & Ambassah, N., 2019. Environmental and Cost Advantages of Using Polyethylene Terephthalate Fibre Reinforced Concrete with Fly Ash as a Partial Cement Replacement. *Open journal of Civil Engineering*, 9(4), pp. 1-7.
- Katja, O., Mirja, I. & Jouko, N., 2013. Effect of operational parameters and stress energies on the particle size distribution of TiO₂ pigment in stirred media milling. *Powder Technology*, Volume 234, pp. 91-96.
- Kazberuk, M. K. & Lelusz, M., 2007. STRENGTH DEVELOPMENT OF CONCRETE WITH FLY ASH ADDITION. *JOURNAL OF CIVIL ENGINEERING AND MANAGEMENT*, 13(2), pp. 115-122.
- Kearsley, E. P. & Wainwright, P. J., 2003. The effect of fly ash properties on concrete strength. *Journal of South Africa Institution of Civil Engineering*, 45(1), pp. 19-24.
- Kesharwani, K. C., Biswas, A. K., Chaurasiya, A. & Rabbani, A., 2017. Experimental study on use of fly ash in concrete. *International Research Journal of Engineering and Technology*, 4(9), pp. 1527-1530.

- Khajuria, A., Bohra, K. & Balaguru, P., 1991. Long term durability of synthetic fibres in concrete. *Concr Inst* 2, pp. 851-868.
- Kiattikomol, K., Jaturapitakkul, C., Songpiriyakij, S. & Chutubtim, S., 2001. A study of ground coarse fly ashes with different fineness from various sources as pozzolanic materials. *Cement and concrete composites*, Volume 23, pp. 335-343.
- Kiilaots, I., Hurt, R. H. & Suuberg, E. M., 2004. Size distribution of unburned carbon in coal fly ash and its implications. *Fuel*, Volume 83, pp. 223-30.
- Kim, D. J., Naaman, A. E. & El-Tawil, S., 2008. Comparative flexural behaviour of four fibre reinforced cementitious composites. *Cement Concrete Composites*, Volume 30, pp. 917-928.
- Kizinievic, O., Kizinievic, V., Pundiene, I. & Molotokas, D., 2018. Eco-friendly fired clay brick manufactured with agricultural solid waste. *Archives of civil and mechanical engineering*, Volume 18, pp. 1156-1165.
- Kobayashi, K. & Cho, R., 1982. Flexural characteristics of steel fibre and polyethylene fibre hybrid reinforced concrete. *Composites*, Volume 13, p. 164.
- Koushal, V. et al., 2014. Plastics: Issues Challenges and Remediation. *International Journal of waste resources*, 4(1), pp. 1-6.
- Kruger, J. E., 1998. An Overview, in : Guides on the use of South African fly ash as cement extender guide. *The South African Coal Ash Association (SACAA)*, p. 2.
- Kumar, D. P. & Sashidar, C. C., 2018. Effect of fineness modulus of manufactured sand on fresh properties of self-compacting concrete. *The Indian Concrete Journal*, pp. 77-81.
- Kumar, P. et al., 2001. Mesoporous materials prepared using coal fly ash as the silicon and aluminium source. *J Mater Chem*, Volume 11, pp. 3285-3290.
- Kumar, P. T., Sudheesh, C. & Kumar, S. S., 2015. Strength characteristics of saw dust ash based geopolymer concrete. *International journal of chemtech research*, 8(2), pp. 738-745.
- Kumar, S. & Mahto, G., 2013. Recent trends in industrial and other engineering applications of non destructive testing: a review. *International journal of scientific and engineering research*, 4(9).
- Kumruzzanman, M., Islam, S. M., Nizamudoulah, S. M. & Jingkaojai, S., 2003. *Performance of pulverized fuel ash in cement concrete*. Kharagpur, Proceedings of International Workshop and Conference on Construction Management and Materials, pp. 539-548.
- Kunthe, D. V., Manavendra, G. & Sondur, M. V., 2018. Effect of thermal properties on fly ash based concrete. *International Research Journal of Engineering and Technology (IRJET)*, 5(12), pp. 396-400.
- Kuroda, M., Watanabe, T. & Terashi, N., 1993. Increase of bond strength at interfacial transition zone by the use of fly ash. *Cem Concr Res*, Volume 30, pp. 253-358.
- Kutchko, B. G. & Kim, A. G., 2006. Fly ash characterization by SEM-EDS. *Fuel*, Volume 85, pp. 2537-2544.
- Kutchko, B. G. & Kim, A. G., 2006. Fly ash characterization by SEM-EDS. *Elsevier*, Volume 85, pp. 2537-2544.
- L. Andray, A., Andray, A. L. & Neal, M. a., 2009. Applications and societal benefits of plastics. *Philosophical transactions of the Royal Society of London, Series B, Biological sciences*, pp. 1977-1984.

- Labib, W. A., 2018. Fibre Reinforced Cement Composites. In: *Cement Based Materials*. Riyadh: IntechOpen, pp. 31-56.
- Lacroix, T. et al., 1992. Modelling of critical fibre length and interfacial debonding in the fragmentation testing of polymer composites. *Composites Science and Technology*, 43(1), pp. 379-387.
- Lambert, S., Christian, S. & Wagner, M., 2017. Ecotoxicity testing of microplastics: considering the heterogeneity of physico-chemical properties. *Integrated Environmental Assessment and Management*, 13(3), pp. 470-475.
- Landman, A. A., 2003. *Literature review of fly ash*, Pretoria: University of Pretoria.
- Lee, B. Y., Kim, J. H. & Kim, J. K., 2009. Optimum concrete mixture proportion based on a database considering regional characteristics. *Journal of computing in civil engineering*, 23(5), pp. 258-265.
- Lee, N. K. & Lee, H. K., 2013. Setting and mechanical properties of alkali-activated fly ash/slag concrete manufactured at room temperature. *Constr. Build. Mater*, Volume 47, pp. 1201-1209.
- Lepoittevin, B. & Roger, P., 2011. *Handbook of Engineering and Speciality Thermoplastics: Polyethers and Polyesters*. 3 ed. New Jersey: John Wiley & Sons.
- Li, G. Z., 2003. Properties of concrete incorporating fly ash and ground granulated blast furnace slag. *Cement Concr Compos*, Volume 25, pp. 293-9.
- Lin, W. T., Huang, R., Chen, C. Y. & Zhou, G. X., 2011. *Effect of polyolefin fibre on the engineered properties of cement based composites containing silica fume*. s.l., s.n.
- Li, V. C., 2003. On engineered cementitious composites - A Review of the Material and its Applications. *Journal of Advanced Concrete Technology*, 1(3), pp. 215-230.
- Li, X., Xu, W. & Chen, S., 2016. An experimental and numerical study on water permeability of concrete. *Construction and Building Materials*, Volume 105, pp. 503-510.
- Li, Y., Wang, J. & Xu, Z., 2016. Design optimization of a concrete face rock-fill dam using genetic algorithm. *Mathematical problems in engineering*, Volume 2016, pp. 1-11.
- Lumay, G. et al., 2012. Measuring the flowing properties of powders and grains. *Powder Technology*, Volume 224, pp. 19-27.
- Lura, P. & Terrasi, G. P., 2014. Reduction of fire spalling in high performance concrete by means of superabsorbent polymers and polypropylene fibres: Small scale fire tests of carbon fibre reinforced plastic prestressed self compacting concrete. *Cement and Concrete Composites*, Volume 49, pp. 36-42.
- Lusher, A., 2015. Microplastics in the marine environment distribution, interactions and effects. *Mar Anthropog Litter*, Volume 1, pp. 245-307.
- Machovik, V. et al., 2013. Microstructure of interfacial transition zone between PET fibres and cement paste. *Acta Geodynamica et Geomaterialia*, Volume 10, pp. 121-127.
- Madandoust, R., Kazemi, M. & Moghadam, S. Y., 2017. Analytical study on tensile strength of concrete. *Romanian Journal of Material*, 47(2), pp. 204-209.
- Madhavi, T. C., Raju, L. S. & Mathur, D., 2014. Polypropylene fibre reinforced concrete - A Review. *Internatinal journal of emerging technology and advanced engineering*, 4(4), pp. 114-120.
- Mahlaba, J. S., Kearsley, E. P. & Kruger, R. A., 2011. Physical, chemical and mineralogical characterisation of hydraulically disposed fine coal ash from SASAL Synfuels. *Fuel*, Volume 90, pp. 2491-2500.

- Maholtra, V. & Carette, G., 2004. Penetration resistance methods. In: *Handbook on non destructive testing of concrete*. New York: CRC Press, pp. 10-23.
- Makwara, C. & Magudu, S., 2013. Confronting the reckless gambling with people's health and lives: Urban solid waste management in Zimbabwe. *European Journal of Sustainable Development*, 2(1), pp. 67-98.
- Malegowski, V., 2016. *Making cordage from plastic bottles hack for survival*. [Online] Available at: <https://www.youtube.com/watch?v=5GbMjq75wpA> [Accessed 20 May 2019].
- Mancini, S. D. et al., 2009. Additional steps in mechanical recycling of PET. *Journal of cleaner production*, Volume 18, pp. 92-100.
- Mark, H. F., 1985. Encyclopedia of polymer science and engineering. In: *Encyclopedia of polymer science and engineering*. New York: John Wiley and Sons.
- Marthong, C. & Agrawal, T. P., 2012. Effect of fly ash additive on concrete properties. *International Journal of Engineering Research and Applications*, 2(4), pp. 1986-1999.
- Masao, K., Tomohida, W. & Nariaki, T., 1993. *Cement and concrete research*, Volume 30, pp. 253-258.
- Mashrei, M. A., Sultan, A. A. & Mahdi, A. M., 2018. Effects of polypropylene fibres on compressive and flexural strength of concrete material. *International Journal of Civil Engineering and Technology (IJCIET)*, 9(11), pp. 2208-2217.
- Matusaka, S. et al., 2012. Development of vibration shear tube method for powder flowability evaluation. *Powder Technology*, Volume 217, pp. 548-553.
- Mazaheripour, H., Ghanbarpour, S., Mirmoradi, S. H. & Hosseinpour, I., 2011. The effect of polypropylene fibers on the properties of fresh and hardened lightweight self compacting concrete. *Construction and building materials*, 25(1), p. 351358.
- Mehta, P. K., 1998. *Role of fly ash in sustainable development*. s.l., Concrete, Fly ash and the Environment Proceeding.
- Meszáros, L. & Turcsán, T., 2014. Development and mechanical properties of carbon fibre reinforced EP/VE hybrid composite systems. *Period Polytech Mech Eng*, 58(2), pp. 127-133.
- Mindess, S. & Vondran, G., 1988. Properties of concrete reinforced with fibrillated polypropylene fibers under impact loading. *Cement and concrete research*, Volume 18, pp. 109-115.
- Mindess, S., Young, J. & Darwin, D., 2003. *Concrete*. New Jersey: Pearson Education.
- Mishra, D. P. & Das, S. K., 2010. A study of physico-chemical and mineralogical properties of Talcher coal fly ash for stowing in underground coal mines. *Material characterisation*, Volume 61, pp. 1252-1259.
- Mohammed, B. S. & Fang, O. C., 2011. Assessing the properties of freshly mixed concrete containing paper-mill residuals and class F fly ash. *Journal of Civil Engineering and Construction Technology*, 2(2), pp. 17-26.
- Mohd, A., Mallick, J. & Hasan, M. A., 2016. A study of factors affecting the flexural tensile strength of concrete. *Journal of King Saud University - Engineering Sciences*, 28(2), pp. 147-156.
- Mohod, M. V., 2015. Performance of polypropylene fibre reinforced concrete. *Journal of Mechanical and Civil Engineering*, 12(1), pp. 28-36.

- Monzo, J., Paza, J. & Mora, E. P., 1994. The utilization of fly ash as cement replacement material in concrete. *Cem Concr Res*, Volume 24, pp. 791-796.
- Morton, W. E. & Hearle, J. W., 2008. *Physical properties of textile fibres*. Fourth Edition ed. New York: Woodhead Publishing Limited.
- Mukhopadhyay, S. & Khatana, S., 2015. A review on the use of fibers in reinforced cementitious concrete. *Journal of Industrial Textiles*, 45(2), pp. 239-264.
- Mullick, A. K., 2005. Use of fly ash in structural concrete. *Indian Concrete Journal*, 19(6).
- Nagabhushana, 2015. study on Properties of Concrete with Different Levels of Replacement of Cement by Fly Ash. *International Journal of Research in Engineering and Technology*, 4(8), pp. 158-161.
- Naik, T. R. & Ramme, B. W., 2002. *Influence of fly ash and chemical admixtures on the setting time of cement paste and concrete*. Berlin, International Conference on superplasticizers and other chemical admixtures in concrete.
- Naik, T. R. & Ramme, B. W., 2002. *Influence of fly ash and chemical admixtures on the setting time of cement paste and concrete*. Berlin, s.n.
- Naik, T. R. & Singh, S. S., 1997. Influence of fly ahs on setting and hardening characteristics of concrete systems. *ACI Materials Journal*, pp. 355-360.
- Nale, J. N., Patil, S. L. & Suman, S., 2012. Fly Ash concrete - A Technical analysis for Compressive Strength. *nternational journal of advanced engineering research and studies*, 2(1).
- Namarak, C., Bumrungsri, C., Tangchirapat, W. & Jaturapitakkul, C., 2018. Development of Concrete Paving Blocks Prepared from Waste Materials without Portland Cement. *Materials Science*, 24(1), pp. 92-99.
- NAPCOR, 2011. *National Association for PET Container Resources*. [Online] Available at: www.napcor.com
- Narganti, S. R., Rao, M. & Jagadeesh, P., 2015. Experimental evaluation of strength properties of steel fibre reinforced concrete. *Asian Journal of Civil Engineering*, 17(4), pp. 487-494.
- Nawaz, A., Julnipitawong, P., Krammart, P. & Tangtermsirikul, S., 2016. Effect and limitation of free lime content in cement-fly ash mixtures. *Construction and building materials*, 102(1), pp. 515-530.
- Nawaz, A., Julnipitawong, P., Krammart, P. & Tangtermsirikul, S., 2016. Effect and limitation of free lime content in cement-fly ash mixtures. *Construction and building materials*, 102(1), pp. 515-530.
- Nedunuri, A. S. & Muhammad, S., 2021. Fundamental understanding of the setting behaviour of the alkali activated binders based on ground granulated blast furnace slag and fly ash. *Constr. Build. Mater.*, Volume 291.
- Neeley, B. D. & O'Neil, E. F., 1996. *Polyolefin fibre reinforced concrete*. s.l., s.n., pp. 93-102.
- Nelms, S. E. et al., 2015. Plastic and marine turtles: a review and call for research. *ICES Journal of Marine Science*, pp. 1-17.
- Neville, A. M., 1996. *Properties of concrete*. London, UK: John Wiley and sons Inc.
- News, B., 2018. *BBC News*. [Online] Available at: <https://www.bbc.com/news/science-environment-45509822> [Accessed 29 April 2019].
- Neyestani, B., 2011. *Specified tests for concrete quality*, s.l.: De La Salle University.

- Niazi, A., Balabani, S. & Seneviratne, L., 2006. Product cost estimation: Technique classification and methodology review. *Journal of Manufacturing Science and Engineering*, 128(1), pp. 563-575.
- Nibudey, R. N., Nagarnaik, P. B., Parbat, D. K. & Pande, A. M., 2013. A model for compressive strength of PET fibre reinforced concrete. *American journal of engineering research*, 2(12), pp. 367-372.
- Nkengue, C. B., Malanda, N., Ganga, G. & Mouengue, G. R., 2019. Influence of Aggregate Grain Size on the Formulation of Sand Concrete in the Construction Industry in Congo. *Geomaterials*, 9(4), pp. 81-96.
- NRMCA, 2014. *Concrete in practice what, why and how*, s.l.: National Ready Mixed concrete association.
- Nziu, P. K., Masu, L. M., Mendonidis, P. & Alugongo, A. A., 2014. Characterization of titanium powder flow: A review on current status on flowability. *Materials Science*, 11(7), pp. 239-255.
- Odler, L., 1998. Hydration, setting and hardening of Portland cement. In: Lea, ed. *Chemistry of Cement and Concrete*. London: Hewlett.
- Oh, B. H. & Kim, J. C., 2007. Fracture behaviour of concrete members reinforced with structural synthetic fibres. *Engineering fracture mechanics*, 74(13), pp. 243-257.
- Oh, B. H. & Park, D. G., 2005. Experimental and theoretical investigation on the postcracking inelastic behaviour of synthetic fibre reinforced concrete beams. *Cement and Concrete Research*, 35(2), pp. 384-392.
- Okoli, O. I. & Smith, G. F., 1998. Failure modes of fibre reinforced composites: The effects of strain rate and fibre content. *Journal of Materials Science*, Volume 33, pp. 5415-5422.
- Oritola, S., Saleh, A. L. & Mohd.Sam, A. R., 2014. Comparison of different forms of gravel as aggregate in concrete. *Leonardo Electronic Journal of Practices and Technologies*, 13(25), pp. 135-144.
- Orozco, M., Avila, Y., Restrepo, S. & Parody, A., 2018. Factors influencing the concrete quality: a survey to relevant actors of the concrete industry. *Revista ingeniería de construcción*, 33(2), pp. 161-172.
- Oztas, A. et al., 2006. Predicting the compressive strength and slump of high strength concrete using neural networks. *Construction and building materials*, 20(9), pp. 769-775.
- Oztas, A. et al., 2006. Predicting the compressive strength and slump of high strength concrete using neural networks. *Construction and building materials*, 20(9), pp. 769-775.
- Pakravan, H. R., Jamshidi, M. & Latifi, M., 2010. Performance of fibres embedded in a cementitious matrix. *Journal of Applied Polymer Science*, Volume 116, pp. 1247-1253.
- Pandya, K. S., Veerraju, C. & Naik, N., 2011. Hybrid composites made of carbon and glass woven fabric under quasistatic loading. *Mater Des*, Volume 32, pp. 4094-4099.
- Pane, L. & Hansen, W., 2005. Investigation of blended cement hydration by isothermal calorimetry and thermal analysis. *Cem Concr Res*, 35(6), pp. 1155-1164.
- Parasivamurthy, P., 2007. Study of waste plastics as composites material in cement concrete construction. *Advanced Materials Research*, Volume 15-17, pp. 220-224.
- Park, J. & Gan, S. Y., 2014. Microplastic management for preventing risk of persistent/bioaccumulative substance. *J Environ Pol*, Volume 13, pp. 65-98.

- Parveen & Sharma, A., 2013. Structural behaviour of fibrous concrete using polypropylene fibres. *International journal of modern engineering research*, Volume 3, pp. 1279-1282.
- Pastariya, S. & Keswani, S., 2016. Experimental Investigation on Strength Characteristics of Fly Ash as Partial Replacement of Cement for M-20 grade of Concrete. *International Journal of Software & Hardware Research in Engineering*, 4(10), pp. 24-28.
- Patel, P. A., Desai, A. K. & Desai, J. A., 2012. Evaluation of engineering properties for polypropylene fibre reinforced concrete. *International journal of advanced engineering technology*, 3(1), pp. 42-45.
- Patil, V. & Shukla, V., 2017. Use of PET fibre as constituent of concrete. *IJARIE*, 3(2), pp. 280-284.
- Pitroda, J. & Umrigar, F. S., 2013. Stone waste: Effective replacement of cement for establishing green concrete. *International Journal of Innovative Technology and Exploring Engineering*, 2(2278-38075), pp. 24-27.
- Poondla, N., Srivatsan, T. s., Patnik, A. & Petraroli, M., 2009. A study of microstructure and hardness of two titanium alloys. Commercial pure and Ti-6Al-4V. *Journal of Alloys and Compounds*, Volume 486, pp. 167-167.
- Potgieter, J. H., 2012. An overview of cement production: How "green" and sustainable is the industry. *Environmental management and sustainable development*, 1(2), pp. 14-37.
- Powell, J. J., Thoree, V. & Pele, L. C., 2007. Dietary microplastics and their impact on tolerance and immune responsiveness of the gastrointestinal tract. *British journal of nutrition*, 98(1), pp. S59-S63.
- PPC, 2018. *Product datasheet PPC Suretech 55,5N Cement*, Johannesburg: PPC.
- PPC, 2019. *Suretech*. [Online] Available at: <https://ppc.co.za/za/products/cement/suretech4> [Accessed 13 May 2019].
- Pravallika, B. S. & Lakshmi, V., 2014. A study on fly ash concrete in marine environment. *International journal of innovative research in science engineering and technology*, 3(2319-8753), pp. 12395-12401.
- Pravallika, B. S. & Lakshmi, V., 2014. A study on fly ash concrete in marine environment. *International Journal of Innovative Research in Science, Engineering and Technology*, 3(5), pp. 12395-12401.
- Puertas, F., MartoAnez-RamoArez, S., Alonso, S. & VaAzquez, T., 2000. Alkali activated fly ash/slag cement strength behaviour and hydration products. *Cement and concrete research*, Volume 30, pp. 1625-1632.
- Quan, H. z. & Kasami, H., 2014. Experimental study on durability improvement of fly ash concrete with durability improving admixture. *The scientific world journal*, pp. 1-11.
- Rafieizonooz, M. et al., 2016. Investigation of coal bottom ash and fly ash in concrete as replacement for sand and cement. *Constr Build Mater*, Volume 116, pp. 15-24.
- Raghucharan, M. C. & Prasad, M. L., 2015. How to Make Concrete More Ductile - A State Of Art. *International Journal of Engineering and Technical Research (IJETR)*, 3(5), pp. 349-354.
- Rahmani, E., Dehestani, M. & Beygi, M., 2013. On the mechanical properties of concrete containing waste PET particles. *Construction and Building Materials*, Volume 47, pp. 1302-1308.
- Rahman, M. E. et al., 2018. Utilization of blended waste materials in bricks. *Technologies*, 6(1), pp. 20-32.

- Ramakrishnan, V., 1996. *Performance characteristics of polyolefin fibre reinforced concrete*. s.l., s.n., pp. 93-102.
- Ramaswamy, K. P., Muhammed, S. A. & Nazeer, M., 2011. *Workability and strength studies on fly ash modified masonry mortars*. s.l., s.n.
- Ramaswamy, K. P., Siddik, M. A. & Nazeer, M., 2011. *Workability and strength studies on fly ash modified masonry mortars*. s.l., s.n.
- Ramaswamy, V. & Sharma, H. R., 2011. Plastic bag threat to environment and cattle health: A retrospective study from Gndar city of Ethopia. *The IIOAB Journal*, 2(1), pp. 7-12.
- Ramujee, K., 2013. Strength properties of polypropylene fibre reinforced concrete. *International journal of innovative research in science, engineering and technology*, 2(8), pp. 3409-3413.
- Ramujee, K., 2013. Strength properties of polypropylene fibre reinforced concrete. *IJRSET*, 2(8), pp. 3409-3413.
- Rani, R. & Jain, M. K., 2015. Physiochemical and engineering characteristics of fly ash and its application in various field - a review. *Journal of Biodiversity and Environmental Sciences*, 6(2), pp. 167-174.
- Ravina, D., 1984. Slump loss of fly ash concrete. *Concrete International*, 6(4), pp. 35-39.
- Ravindrarahah, S. R., 2003. *Bleeding of fresh concrete containing cement supplementary materials*. Bali, Ninth east Asia-Pacific Conference on Structural Engineering and Construction.
- Rawal, A. & Mukhopadhyay, S., 2014. Melt spinning of synthetic polymeric filaments. In: D. Zhang, ed. *Advances in filament yarn spinning of textiles and polymers*. s.l.:Woodhead Publishing, pp. 75-99.
- Rebeiz, K. S., 1995. Time-temperature properties of polymer concrete using recycled PET. *Cement and Concrete Composites*, Volume 17, pp. 119-124.
- Rebeiz, K. S. & Craft, A. P., 1995. Plastic waste management in construction: technological and institutional issues. *Conservation and Recycling*, Volume 15, pp. 245-257.
- Reddy, R., 2014. Assessment of Strength of Concrete by Non-Destructive Testing Techniques. *International Journal of Engineering and Management Research*, 4(3), pp. 248-256.
- Reddy, S. A. & Reddy, C., 2013. Effect of fly ash on strength and durability parameters of concrete. *International journal of science and research*, 4(5), pp. 1368-1370.
- Revel, M., Chatel, A. & Mouneyrac, C., 2018. Micro(nano)plastics: A threat to human health?. *Current opinion in environmental science & health*, Volume 1, pp. 17-23.
- Richardson, I. G., 2008. The Calcium Silicate Hydrates. *Cement and Concrete Research*, 38(2), pp. 137-158.
- Ritchie, P. A., Thomas, D. A., Lu, L. W. & Connelly, G. M., 1991. External Reinforcement of Concrete Beams Using Fiber Reinforced Plastics. *ACI Structural Journal*, 88(4), pp. 490-500.
- Rochman, C. M., 2014. Early warning signs of endocrin disruption in adult fish from the ingestion of polyethylene with and without sorbed chemical pollutants from the marine environment. *Sci Total Environ*, Volume 493, pp. 656-661.
- Rodrigues, F. A. & Joekes, I., 2010. Cement industry: challenges and perspectives. *Environmental chemistry letters*.

- Roesler, J. R. et al., 2004. Fracture of Plain and Fiber-Reinforced Concrete Slabs under Monotonic Loading. *JOURNAL OF MATERIALS IN CIVIL ENGINEERING*, 16(5), pp. 452-460.
- Rohilla, L., Garg, V., Mallick, S. S. & Setia, G., 2018. An experimental investigation on the effect of particle size on the flowability of fly ash. *Powder Technology*, Volume 330, pp. 164-173.
- Rohman, R. K. & Aji, S., 2014. *Effect of fly ash on compressive strength of concrete containing recycled coarse aggregate*. s.l., AIP Conference Proceedings, p. 020097.
- Rohman, R. K. & Aji, S., 2018. *Effect of fly ash on compressive strength of concrete containing recycled coarse aggregate*. s.l., s.n.
- Saadun, A. et al., 2016. Behaviour of polypropylene fiber reinforced concrete under dynamic impact load. *Journal of Engineering Sciences and Technology*, 11(5), pp. 684-693.
- Sabih, G., Tarefder, R. A. & Jamil, S. M., 2016. Optimization of gradation and fineness modulus of naturally fine sands for improved performance as fine aggregate in concrete. *Procedia Engineering*, Volume 145, pp. 66-73.
- Sadeghi, G. M. & Sayaf, M., 2012. From PET Waste to Novel Polyurethanes. In: *Material Recycling - Trends and Perspectives*. Tehran: Intech.
- Sadek, A. W., El-Hawary, M. & El-Deeb, A. S., 2006. Fire resistance testing of concrete beams reinforced by GFRP rebars. *European Journal of Scientific Research*, 15(2), pp. 190-200.
- Saha, A. K., 2018. Effects of class F fly ash on the durability properties of concrete. *Sustainable Environme Research*, Volume 28, pp. 25-31.
- Saha, A. K. & Sarker, P. K., 2017. Sustainable use of ferronickel slag fine aggregate and fly ash in structural concrete: mechanical properties and leaching study. *Journal of Cleaner Production*, Volume 162, pp. 438-448.
- Saha, A. K. & Sarker, P. K., 2017. Sustainable use of ferronickel slag fine aggregate and fly ash in structural concrete: mechanical properties and leaching study. *J Clean Prod*, Volume 162, pp. 438-48.
- Sahu, K. M. & Singh, L., 2017. Critical review on types of bricks type 14: Plastic sand bricks. *International Journal of Mechanical and Production Engineering*, 5(11), pp. 2320-2092.
- Sahu, S. & Majling, J., 1994. Preparation of sulpho-aluminate belite cement from fly ash. *Cement and concrete research*, Volume 24, pp. 1065-1072.
- Saikia, N. & Brito, J. d., 2013. Waste polyethylene terephthalate as an aggregate in concrete. *Materials research*, 16(2), pp. 341-350.
- Salumkhe, T. V. & Mandal, J. N., 2014. Behaviour of fly ash at different mix ratios with plastic recycled polymers. *International Journal for Research in Applied Science and Engineering Technology (IJRASET)*, Volume 2.
- Sarkar, A. et al., 2012. A comprehensive analysis of the particle size and shape of fly ash from different fields of ESP of a super thermal power plant. *Energy sources, Part A: Recovery, utilization, and environmental effects*, 34(5), pp. 385-395.
- Sathish, S., Ganapathy, T. & Bhoopathy, T., 2014. Experimental testing on hybrid composite materials. *Applied mechanics and materials*, 592(594), pp. 339-343.
- Saxena, J. & Saxena, A., 2015. Enhancement the strength of conventional concrete by using nylon fibre. *International journal of engineering and science*, 5(2), pp. 56-59.

- Scheetz, B. E. & Earle, R., 1998. Utilization of fly ash. *Current opinion in solid state and material science*, Issue 3, pp. 510-520.
- Schroeder, L., 1994. The Use of recycled materials in highway construction. *Public Roads*, 58(2).
- Sciubidlo, A., Kuceba, M. I. & Niedzieslska, M., 2015. Comparison of fly ash from co-combustion of coal/solid recovered fuel (SRF) and coal/refuse derived fuel (RDF).. *Journal of Physics*., Volume 1398, pp. 1-8.
- Seghiri, M., Boutoutaou, D., Kriker, A. & Hachani, M. I., 2017. The Possibility of making a composite material from waste plastic. *Energy procedia*, Volume 119, pp. 163-169.
- Seijo, R. A. et al., 2017. Histopathological and molecular effects of microplastics in *Eisenia andrei* Bouche. *Environmental Pollution*, Volume 220, pp. 495-503.
- Selmy, A. I., El-baky, M. A. & Hegazy, D., 2019. Mechanical properties of inter-ply hybrid composites reinforced with glass and polyamide fibres. *Journal of Thermoplastic Composite Materials*, 32(2), pp. 267-293.
- Senneca, O., 2008. Burning and physico-chemical characteristics of carbon in ash from a coal fired power plant. *Fuel*, Volume 87, pp. 1207-1216.
- Seslija, M. et al., 2016. Laboratory testing of fly ash. *Technicki vjesnik*, 23(6), pp. 1839-1848.
- Sevim, O. & Demir, I., 2019. Optimization of fly ash particle size distribution for cementious systems with high compactness. *Construction and building materials*, Volume 195, pp. 104-114.
- Shackelford, C. D., 2000. Effective use of fly ash slurry as fill material. *Journal of Hazardous Materials*, Issue 2, pp. 159-163.
- Shah, S. P., 1993. Concrete composites, fiber reinforced. In: *Handbook of composite reinforcements*. New York: VCH Publishers, pp. 155-170.
- Shaikh, F. U. & Taweel, M., 2015. Compressive strength and failure behaviour of fibre reinforced concrete at elevated temperatures. *Advances in Concrete Construction*, 3(4), pp. 283-293.
- Shaikuthali, S. A. et al., 2019. Workability and compressive strength properties of normal weight concrete using high dosage of fly ash as cement replacement. *Journal of Building Pathology and Rehabilitation* , 4(26), pp. 1-7.
- Sharma, H., 2017. Innovative and sustainable application of PET bottle a green construction overview. *Indian journal of science and technology*, 10(16), pp. 1-7.
- Shen, L., Worrell, E. & Patel, M., 2010. Open loop recycling: A LCA case study of PET bottle to fibre recycling. *Resources conservation and recycling journal*, Volume 55, pp. 34-52.
- Shim, Y. S., Rhee, S. W. & Lee, W. K., 2005. Comparison of leaching characteristics of heavy metals from bottom and fly ashes in Korea and Japan. *Waste Manage*, Volume 25, pp. 473-480.
- Shreya, N. et al., 2014. Fly ash characterization of Jharkhand (India) by laser. *Comunicacoes Geologicas*, Volume 101, pp. 851-854.
- Siddiquee, T., 2021. *Civil Engineering*. [Online] Available at: <https://civiltoday.com/civil-engineering-materials/sand/359-specific-gravity-of-sand> [Accessed 10 October 2021].
- Siddique, R., 2004. Performance characteristics of high volume Class F fly ash concrete. *Cement Concr Res*, Volume 34, pp. 487-93.

- Siddique, R. & Khan, M. I., 2011. *Supplementary cementing materials*. Verlag: Springer.
- Simon, M. J., 2003. *Concrete mixture optimization using statistical methods*, Georgetown: Infrastructure Research and development, Federal highway administration.
- Singh, A. & Singh, V., 2017. Effect on Compressive and Split Tensile Strength of Concrete by Partial Replacement with Coal Bottom Ash. *International Journal for Research Trends and Innovation*, 2(11), pp. 42-49.
- Singh, B. & Jasrotia, A., 2017. Strength and Cost Comparison of Normal and High Volume Fly Ash Concrete. *International Journal of Advanced Technology in Engineering and Science*, 5(5), pp. 119-127.
- Singh, D. N. & Kolay, P. K., 2002. Simulation of ash–water interaction and its influence on ash characteristics. *Progress in Energy and combustion science*, 28(3), pp. 267-299.
- Sinha, D., 2014. Thermal properties of concrete. *Indian journal of research*, 3(2), pp. 90-92.
- Sivakumar, S. & Kameshwari, B., 2015. Influence of Fly Ash, Bottom Ash, and Light Expanded Clay Aggregate on Concrete. *Advances in Materials Science and Engineering*, pp. 1-9.
- Siyal, A. A., Azizli, A. K., Man, Z. & Ullah, H., 2016. Effect of parameters on the setting time of fly ash based geopolymers using Taguchi method. *Procedia Engineering*, Volume 148, pp. 302-307.
- Smith, M., Love, D. C., Rochman, C. M. & Neff, R. A., 2018. Microplastics in seafood and the implications for human health. *Current environmental health*, 5(3), pp. 375-386.
- Smith, M., Love, D. C., Rochman, C. M. & Neff, R. A., 2018. Microplastics in seafood and the implications for human health. *Food, health and the environment*, Volume 1, pp. 1-12.
- Sohaib, N., Seemab, F., Sana, G. & Mamoon, R., 2018. *Using polypropylene fibers in concrete to achieve maximum strength*. Islamabad, s.n.
- Sohaib, N., Seemab, F., Sana, G. & Mamoon, R., 2018. *Using polypropylene fibres in concrete to achieve maximum strength*. s.l., Proceedings of the Eighth International Conference on Advances in Civil and Structural Engineering.
- Solanki, J. V. & Pitroda, J., 2013. Flexural strength of beams by partial replacement of cement with fly ash and hypo sludge in concrete. *International Journal of Engineering Science and Innovative Technology*, 2(1), pp. 173-179.
- Solanki, J. V. & Pitroda, J. K., 2013. Flexural strength of beams by partial replacement of cement with fly ash and hypo sludge in concrete. *International Journal of Engineering Science and Innovative Technology*, 2(1), pp. 173-180.
- Song, P. S., Hwang, S. & Sheu, B. C., 2005. Strength properties of nylon and polypropylene fibre reinforced concretes. *Cement Concrete Res*, Volume 35, pp. 1546-1550.
- Sovjak, R., Maca, P. & Imlauf, T., 2016. Effect of fibre aspect ratio and fibre volume fraction on the effective fracture energy of ultra high performance fibre reinforced concrete. *Acta Polytechnica*, 56(4), pp. 319-327.
- Sovjak, R., Maca, P. & Imlauf, T., 2016. Effect of fibre aspect ratio and fibre volume fraction on the effective fracture energy of ultra high performance fibre reinforced concrete. *Acta Polytechnica*, 56(4), pp. 319-327.
- Stawiski, B., 2012. Strength of Concrete in Slabs, Investigates along Direction of Concreting. *Open Journal of Civil Engineering*, Volume 2, pp. 22-26.

- Sudhikumar, G. S., Prakash, K. B. & Rao, S., 2014. Effect of aspect ratio of fibres on the strength characteristics of slurry infiltrated fibrous ferrocement. *Journal of civil and structural engineering*, Volume 3, pp. 29-37.
- Sulaimani, A. et al., 1994. Shear Repair for Reinforced Concrete by Fiberglass Plate Bonding. *ACI Structural Journal*, 91(4), pp. 458-564.
- Sumer, M., 2012. Compressive strength and sulfate resistance properties of concretes containing Class F and Class C fly ashes. *Construct Build Mater*, Volume 34, pp. 531-6.
- Sun, W., Handog, Y. & Bingem, Z., 2003. Analysis of mechanism of water reducing effect of fine ground slag, high calcium fly ash and low calcium fly ash. *Cem Concr Res*, Volume 33, pp. 1199-1225.
- Supit, S. W. & Shaikh, F. U., 2015. Durability properties of high volume fly ash concrete containing nano-silica. *Mater Stru*, Volume 34, pp. 1087-92.
- Takeshi, K., 2001. The method to determine the optimum refractive index parameter in the laser diffraction and scattering method. *Advanced Powder Technology*, 12(4), pp. 589-602.
- Talebi, H. R., Kayan, B. A., Asadi, I. & Hassan, Z. F., 2020. Investigation of Thermal Properties of Normal Weight Concrete for Different Strength Classes. *Journal of Environmental Treatment Techniques*, 8(3), pp. 908-914.
- Tandon, G. H., 2017. *Slideshare*. [Online] Available at: <https://www.slideshare.net/gauravhtandon1/hardened-concrete-72809827> [Accessed 29 April 2019].
- Tangchirapat, W., Rattanashotinunt, C., Buranasing, R. & Jaturapitakkul, C., 2013. Influence of fly ash on slump loss and strength of concrete fully incorporating recycled concrete aggregates. *Journal of materials in civil engineering*, Volume 25, pp. 243-251.
- Tanikella, P. & Olek, J., 2017. *Updating Physical and Chemical Characteristics of Fly Ash for Use in Concrete*, Indiana: Indiana Department of Transportation and Purdue University.
- Taylor, H. F. et al., 1984. The hydration of tricalcium silicate. *Materials and Structures*, 17(6), pp. 457-468.
- Taylor, P. C., Kosmatka, S. H. & Voigt, G. F., 2006. Integrated materials and construction practices for concrete pavement. In: *A state of the practice manual*. s.l.:s.n.
- Tebbal, N. & Rahmouni, Z. E. A., 2016. Influence of Local Sand on the Physicomechanical Comportment and Durability of High Performance Concrete. *Advances in Civil Engineering*, pp. 1-11.
- Tehrani, D. M., Nosrati, H. & Rajabzadeh, M. H., 2015. Effects of plies stacking sequence and fibre volume ratio on flexural properties of basalt/nylon epoxy hybrid composites. *Fibre Polym*, Volume 16, pp. 918-925.
- Telli, A. & Ozdil, N., 2015. Effect of recycled PET fibres on the performance properties of knitted fabrics. *Journal of Engineered fibers and fabrics*, 10(2), pp. 47-60.
- Thomas, M., 2007. Optimizing the use of fly ash in concrete. *Portland Cement Association*, Issue 548, pp. 1-24.
- Thurumurugan, S. & Sivakumar, A., 2013. Compressed strength index of crimped Polypropylene fibres in high strength cementitious matrix. *World applied sciences journal*, 24(6), pp. 698-702.
- Tonet, K. G. & Proszek, G. J., 2013. Polymer concrete with recycled PET: The influence of the addition of industrial waste on flammability. *Construction and Building Materials*, Volume 40, pp. 378-389.

- Truong, D. G., 2012. An experimental study of the influence of PP fibers used in concrete to limit the crack widths in bending reinforced concrete structures., *MSC-2012 Conference*,.
- Turner, T., 2015. *Good News Network*. [Online] Available at: <https://www.goodnewsnetwork.org/bulletproof-fireproof-eco-friendly-homes-are-made-of-plastic-bottles/> [Accessed 28 April 2020].
- Tutuallo, G. & Mallisa, H., 2018. Using cementitious materials such as fly ash to replace a part of cement in producing high strength concrete in hot weather. *Materials Science and Engineering*, Volume 316, pp. 1-6.
- Umbria, A., Galan, M. & Munoz, M. J., 2004. Characterization of atmospheric particles: Analysis of particles in the Campo de Gibraltar. *Atmosfera*, Volume 17, pp. 191-206.
- Upadhyay, A. & Kamal, M., 2007. *Characterization and utilization of fly ash*, 2007: Naional Institute of Technology.
- Upadhyay, R., Srivastava, V., Herbert, A. & Mehta, P. K., 2014. Effect if fly ash on flexural strength of portland pozzolona cement concrete. *Journal of academia and industrial research*, 3(5), pp. 218-211.
- Van der Merwe, E. M. et al., 2014. Surface and bulk characterization of an ultrafine South African coal fly ash with reference to polymer applications. *Applied Surface Science*, Volume 317, pp. 73-83.
- Vassilev, S. V., 1992. Phase mineralogy studies of solid waste products from coal burning at some Bulgarian thermoelectric power plants. *Fuel*, Volume 71, pp. 625-633.
- Vassilev, S. V. & Vassileva, C. G., 1996. Mineralogy of combustion wastes from coal fired power stations. *Fuel Processing Technology*, Issue 47, pp. 261-280.
- Vazquez, A. & Pique, T. M., 2016. Biotech admixtures for enhancing portland cement hydration. In: *Biopolymers and Biotech Admixtures for Eco-Efficient Construction Materials*. s.l.:Elsevier, pp. 88-110.
- Verma, C., Medan, S. & Hussain, A., 2016. Heavy metal contaminantion of groundwater due to fly ash disposal of coal fired thermal power plant Parichha, Jhansi, India. *Cogent Engineering*, 3(1).
- Vinodsinh, J. S. & Pitroda, J., 2013. Flexural strength of beams by partial replacement of cement with fly ash and hypo sludge in concrete. *Internation journal of engineering science and innovative technology*, 2(1), pp. 173-179.
- Vishnu, D. C., 2016. *Fly Ash Concrete*. [Online] Available at: <https://www.slideshare.net/brajeshmeena9807/concrete-design-with-fly-ash> [Accessed 7 May 2020].
- VTS, 2018. *WAW-2000E 2000kN Rebar Universal Testing Machine*. [Online] Available at: www.vts-testing.com [Accessed 19 May 2019].
- Vu, H. H., Truong, D. G. & Nguyen, T. T., 2020. The application of polypropylene fiber for reinforced concrete beams and slabs. *Materials Science and Engineering* , Volume 869.
- Walton, P. L., 1978. Properties of cement composites with Kevlar fibres. *Journal of Materials Science*, 13(5), pp. 1075-1083.

- Wang, X. et al., 2019. The Effects of Fiber Length and Volume on Material Properties and Crack Resistance of Basalt Fiber Reinforced Concrete (BFRC). *Advances in Materials Science and Engineering*, pp. 1-17.
- Ward, C. R. & French, D., 2005. *Relation between coal and fly ash mineralogy, based on quantitative X-Ray diffraction methods*. Kentucky, World of Coal Ash (WOCA).
- Ward, C. R. & French, D., 2006. Determination of glass content and estimation of glass composition in fly ash using quantitative X-ray diffractometry. *Fuel*, 85(16), pp. 2268-2277.
- watch, S., 2016. *Rooiwai power station*. [Online] Available at: https://www.sourcewatch.org/index.php/Rooiwai_power_station [Accessed 13 May 2019].
- Webb, H. K., Arnott, J., Crawford, R. J. & Ivanova, E. P., 2013. Plastic degradation and its environmental implications with special reference to Poly(ethylene terephthalate). *Polymers*, 5(2073-4360), pp. 1-18.
- Wilinski, D., Lukowski, P. & Rokicki, G., 2016. Application of fibres from recycled PET bottles for concrete reinforcement. *Journal of Building Chemistry*, Volume 1, pp. 1-*
- Wills, B. A. & Finch, J. A., 2015. Particle size analysis. In: *Will's Minerals Processing Technology*. Pennsylvania: Butterworth-Heinemann, pp. 91-107.
- Wongkeo, W., Thongsanitgarn, P., Ngamjarurojana, A. & Chaipanich, A., 2014. Compressive strength and chloride resistance of self compacting concrete containing high level fly ash and silica fume. *Materials and Design*, 64(9), pp. 261-269.
- Won, J. P. et al., 2010. Long term performance of recycled PET fibre reinforced cement composites. *Construction and Building Materials*, Volume 24, pp. 660-665.
- Wright, S. L. & Kelly, F. J., 2017. Plastic and human health: A micro issue. *Environ Sci Technol*, Volume 51, pp. 6634-6647.
- Wright, S. L. & Kelly, F. J., 2017. Threat to human health from environmental plastics. *MBJ*, pp. 1-2.
- Wu, P., Wang, J. & Wang, X., 2016. A critical review of the use of 3D printing un the construction industry. *Automation in construction*, Volume 68, pp. 21-31.
- Yadav, V. K. & Fulekar, M. H., 2018. THE CURRENT SCENARIO OF THERMAL POWER PLANTS AND FLY ASH: PRODUCTION AND UTILIZATION WITH A FOCUS IN INDIA. *International Journal of Advance Engineering and Research Development*, 5(4), pp. 768-777.
- Yang, H. et al., 2017. Experimental study on permeability of concrete. *Earth and Environmental Science*, Volume 108.
- Yao, Z. T. et al., 2015. A comprehensive review on the applications of coal fly ash. *Earth Scie Rev*, Volume 141, pp. 105-21.
- Yao, Z. T. et al., 2015. A comprehensive review on the applications of coal fly ash. *Earth Science Rev*, pp. 105-121.
- Yao, Z. et al., 2014. Mix proportion design and mechanical properties of recycled PET concrete. *Journal of testing and evaluation*, 43(2), pp. 1-9.
- Yazici, S. & Arel, H. S., 2012. Effects of fly ash fineness on the mechanical properties of concrete. *Indian Academy of Sciences*, Volume 37, pp. 389-403.

- Yazici, S. & Arel, H. S., 2012. Effects of fly ash fineness on the mechanical properties of concrete. *Sadhana*, 37(3), pp. 389-403.
- Yeh C, 2006. Exploring concrete slump model using artificial neural networks. *Journal of computing in civil engineering*, 20(3), pp. 217-221.
- Yeh, I. C., 1998. Modelling of strength of high performance concrete using artificial neural networks. *Cement and concrete research*, 28(12), pp. 1797-1808.
- Yeh, I. C., 2006. Exploring concrete slump model using artificial neural networks. *Journal of computing in civil engineering*, 20(3), pp. 217-221.
- Yeh, I. C., 2007. Computer aided design for optimum concrete mixtures. *Cement and concrete composites*, 29(3), pp. 193-202.
- Yeh, I. C., 2007. Modeling slump flow of concrete using second order regressions and artificial neural networks. *Cement and concrete composites*, 29(6), pp. 474-480.
- Yeh, I. C., 2007. Modelling slump flow of concrete using second order regressions and artificial neural networks. *Cement and concrete composites*, 29(6), pp. 474-480.
- Yeh, I. C., 2009. Optimization of concrete mix proportioning using a flattened simplex-centroid mixture design and neural networks. *Engineering with computers*, 25(2), pp. 179-190.
- Yoo, D. Y. et al., 2018. Fiber Reinforced Cement Composites: Mechanical Properties and Structural Implications. *Advances in Materials Science and Engineering*, Volume 1, pp. 1-2.
- Zain, M. F., Mahmud, H. B., Ilham, A. & Faizal, M., 2002. Prediction of splitting tensile strength of high performance concrete. *Cement and Concrete Research*, 32(8), pp. 1251-1258.
- Zhang, S. P. & Zong, L., 2014. Evaluation of relationship between water absorption and durability of concrete materials. *Advances in Materials Science and Engineering*, pp. 1-8.
- Zhang, X. L. et al., 2011. Characterization of individual fly ash particles in surface snow at Urumqi Glacier No. 1, Eastern Tianshan. *Chinese Science Bulletin*, 56(32), pp. 3464-3473.
- Zhang, Y., Sun, W. & Liu, S., 2002. Study on the hydration heat of binder paste in high performance concrete. *Cement and concrete research*, 32(9), pp. 1483-1488.
- Zollo, R. F., 1982. *Collated fibrillated polypropylene fibres in FRC*. Detroit, s.n.
- Zollo, R. F., 1984. Collated fibrillated polypropylene fibers in FRC. *Fiber reinforced concrete international symposium*, pp. 397-409.
- Zollo, R. F., 1997. Fibre reinforced concrete: an overview after 30 years of development. *Cement Concrete Composite*, Volume 1, pp. 107-122.
- Zollo, R. F., 1997. Fibre reinforced concrete: an overview after 30 years of development. *Cement Concrete Composite*, Volume 1, pp. 107-122.
- Zulu, S. & Allopi, D., 2015. *Optimising the usage of fly ash in concrete in the construction in the construction of roadworks*. Johannesburg, Proceedings of the 34th Southern African Transport Conference.

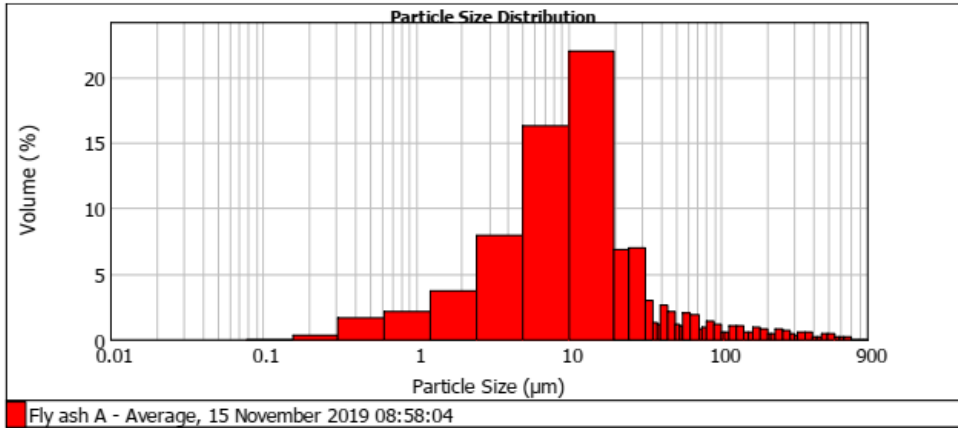
APPENDIX A: MASTERSIZER REPORT 1



Result Analysis Report

Sample Name: Fly ash A - Average	SOP Name: Fly Ash	Measured: 15 November 2019 08:58:04	
Sample Source & type: Paris	Measured by: ChanceT	Analysed: 15 November 2019 08:58:05	
Sample bulk lot ref: 123-ABC	Result Source: Averaged		
Particle Name: Fly Ash	Accessory Name: Hydro 2000G (A)	Analysis model: General purpose	Sensitivity: Enhanced
Particle RI: 1.730	Absorption: 1	Size range: 0.020 to 2000.000 um	Obscuration: 10.25 %
Dispersant Name: Water	Dispersant RI: 1.330	Weighted Residual: 1.259 %	Result Emulation: Off
Concentration: 0.0080 %Vol	Span : 6.635	Uniformity: 2.28	Result units: Volume
Specific Surface Area: 0.998 m ² /g	Surface Weighted Mean D[3,2]: 6.014 um	Vol. Weighted Mean D[4,3]: 48.174 um	

d(0.1): 3.183 um d(0.5): 17.610 um d(0.9): 120.029 um



Fly ash A - Average, 15 November 2019 08:58:04

Size (µm)	Volume In %	Size (µm)	Volume In %	Size (µm)	Volume In %	Size (µm)	Volume In %	Size (µm)	Volume In %	Size (µm)	Volume In %
0.078	0.00	25.000	6.91	63.000	1.82	140.000	0.59	300.000	0.24	630.000	0.17
0.156	0.35	32.000	2.99	71.000	0.77	150.000	0.54	315.000	0.54	710.000	0.00
0.310	1.67	36.000	1.30	75.000	0.86	160.000	0.96	355.000	0.49	800.000	0.00
0.625	2.16	38.000	1.19	80.000	1.45	180.000	0.83	400.000	0.24	850.000	0.00
1.250	3.74	40.000	2.58	90.000	1.17	200.000	0.44	425.000	0.22	900.000	0.00
2.500	7.90	45.000	2.13	100.000	0.61	212.000	0.40	450.000	0.40		
5.000	16.24	50.000	1.11	106.000	0.55	224.000	0.74	500.000	0.40		
10.000	22.01	53.000	1.00	112.000	1.04	250.000	0.68	560.000	0.23		
20.000	6.85	56.000	1.99	125.000	1.01	280.000	0.37	600.000	0.15		
25.000		63.000		140.000		300.000		630.000			

Operator notes:

APPENDIX B: MASTERSIZER REPORT 2



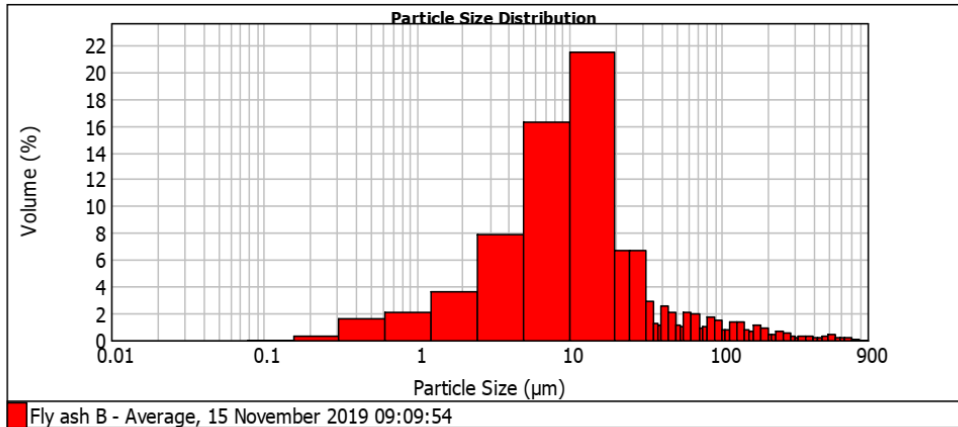
Result Analysis Report

Sample Name: Fly ash B - Average	SOP Name: Fly Ash	Measured: 15 November 2019 09:09:54
Sample Source & type: Paris	Measured by: ChanceT	Analysed: 15 November 2019 09:09:55
Sample bulk lot ref: 123-ABC	Result Source: Averaged	

Particle Name: Fly Ash	Accessory Name: Hydro 2000G (A)	Analysis model: General purpose	Sensitivity: Enhanced
Particle RI: 1.730	Absorption: 1	Size range: 0.020 to 2000.000 um	Obscuration: 10.39 %
Dispersant Name: Water	Dispersant RI: 1.330	Weighted Residual: 0.741 %	Result Emulation: Off

Concentration: 0.0083 %Vol	Span : 6.552	Uniformity: 2.21	Result units: Volume
Specific Surface Area: 0.975 m ² /g	Surface Weighted Mean D[3,2]: 6.153 um	Vol. Weighted Mean D[4,3]: 48.137 um	

d(0.1): 3.306 um d(0.5): 18.039 um d(0.9): 121.502 um



Size (µm)	Volume In %	Size (µm)	Volume In %	Size (µm)	Volume In %	Size (µm)	Volume In %	Size (µm)	Volume In %	Size (µm)	Volume In %
0.078	0.00	25.000	6.68	63.000	1.93	140.000	0.79	300.000	0.16	630.000	0.22
0.156	0.34	32.000	2.87	71.000	0.85	150.000	0.70	315.000	0.35	710.000	0.07
0.310	1.62	36.000	1.25	75.000	0.97	160.000	1.16	355.000	0.33	800.000	0.00
0.625	2.09	38.000	1.14	80.000	1.71	180.000	0.89	400.000	0.17	850.000	0.00
1.250	3.57	40.000	2.49	90.000	1.47	200.000	0.43	425.000	0.17	900.000	0.00
2.500	7.84	45.000	2.07	100.000	0.73	212.000	0.37	450.000	0.33		
5.000	16.27	50.000	1.09	106.000	0.73	224.000	0.62	500.000	0.36		
10.000	21.49	53.000	0.99	112.000	1.42	250.000	0.50	560.000	0.22		
20.000	6.66	56.000	2.02	125.000	1.38	280.000	0.25	600.000	0.15		
25.000		63.000		140.000		300.000		630.000			

Operator notes:

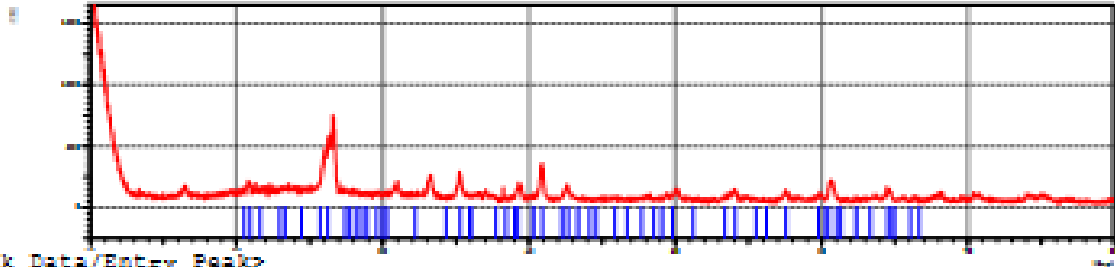
APPENDIX C: XRD REPORT

***** SEARCH / MATCH RESULT *****

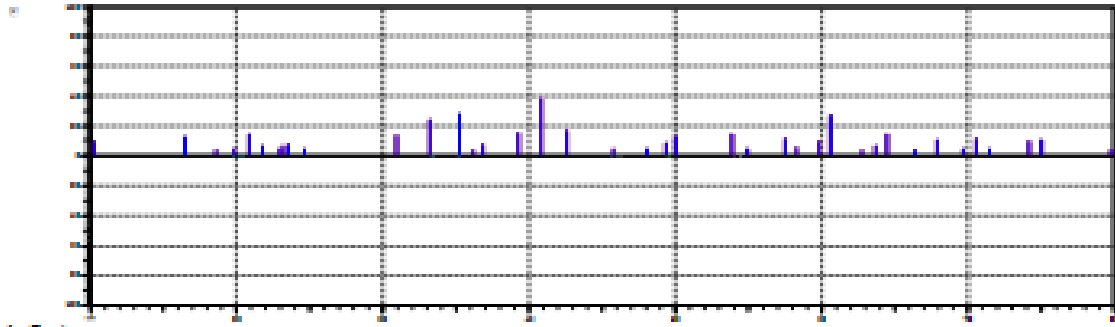
<Unknown Data>

Group Name : Standard
Data Name : Nkomo
File Name : Nkomo.PKR
Sample Name : Flyash2
Comment :
Date & Time : 02-10-20 09:17:25

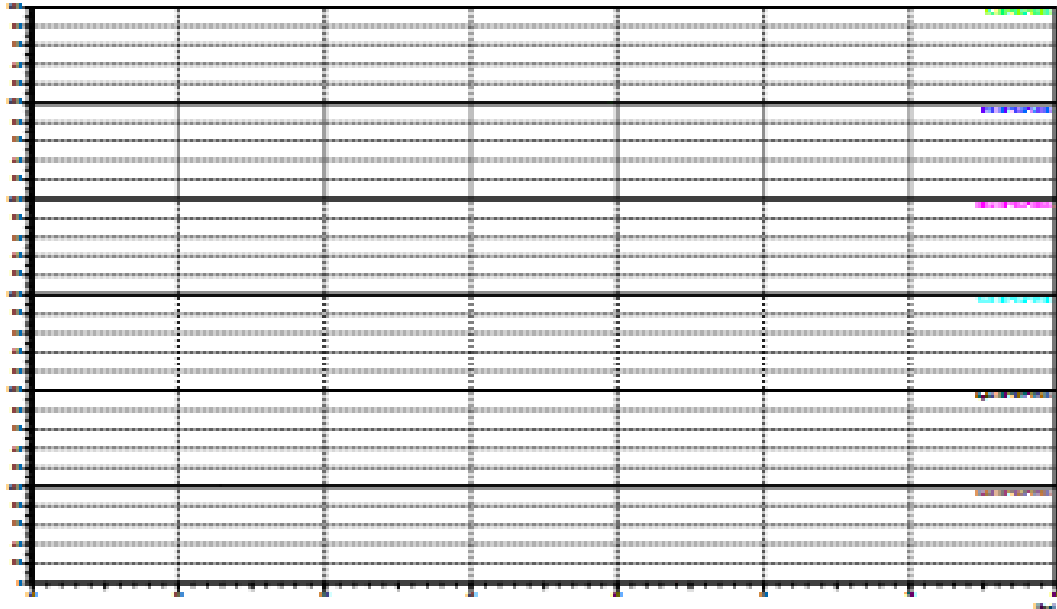
<Raw Data>



<Peak Data/Entry Peak>



<Card Data>



Group Name : Standard
 Data Name : Nkomo
 File Name : Nkomo.PKR
 Sample Name : Flyash2
 Comment :

<Entry Card>

No.	Card	Chemical Formula Chemical Name (Mineral Name)	S	L	d	I	R
				Dx	WT%	S.G.	
1	00-034-0529	Fe Iron (Hexaferrum, syn)	0.000	0.800 (4/ 6) 9.08	0.653	----- P63/mmc	0.523
2	00-055-1908	C70 Carbon	0.000	0.857 (6/ 7) -----	0.590	----- F	0.506
3	00-024-0835	KC24 Potassium Carbide	0.000	0.875 (7/11) 2.72	0.562	----- P	0.492
4	00-015-0783	TiS3 Titanium Sulfide	0.000	0.722 (13/18) 3.25	0.676	----- P21/m	0.488
5	00-027-0759	MgO4 Magnesium Oxide	0.000	0.778 (7/11) 3.70	0.612	----- R	0.476
6	00-012-0708	SiO2 Silicon Oxide	0.000	0.636 (7/11) 2.55	0.648	----- P3221	0.412
7	00-046-1045	SiO2 Silicon Oxide (Quartz, syn)	0.000	0.591 (13/58) 2.65	0.677	----- P3221	0.400
8	00-056-0457	Al2O3 Aluminum Oxide	0.000	0.667 (8/22) 3.76	0.561	----- Fd-3m	0.374
9	00-033-0664	Fe2O3 Iron Oxide (Hematite, syn)	0.000	0.650 (13/45) 5.27	0.570	----- R-3c	0.371
10	00-059-0333	Ca8OCl2(Si2O7)2 Calcium Oxide Chloride Silicate (Unnamed	0.000	0.657 (23/49) 2.88	0.560	----- Fdd2	0.368
11	00-022-1069	C Carbon (Chaoite)	0.000	0.667 (12/22) 3.56	0.506	----- P	0.337

Group Name : Standard
 Data Name : Nkomo
 File Name : Nkomo.PKR
 Sample Name : Flyash2
 Comment :

<Card List>

No.	Card	Chemical Formula Chemical Name (Mineral Name)	S	L	d	I	R
				Dx	WT%	S.G.	
1	00-043-0596	SiO2 Silicon Oxide	0.000	1.000(6/ 6)	0.762	-----	0.762
				2.68	-----	P3221	
2	00-047-1376	SiS2 Silicon Sulfide	0.000	0.846(11/13)	0.683	-----	0.578
				4.06	-----	P3221	
3	00-039-0973	Si Silicon	0.000	0.889(8/14)	0.631	-----	0.561
				2.34	-----	P41212	
4	00-034-0529	Fe Iron (Hexaferrum, syn)	0.000	0.800(4/ 6)	0.653	-----	0.523
				9.08	-----	P63/mmc	
5	00-055-1908	C70 Carbon	0.000	0.857(6/ 7)	0.590	-----	0.506
				-----	-----	F	
6	00-024-0835	KC24 Potassium Carbide	0.000	0.875(7/11)	0.562	-----	0.492
				2.72	-----	F	
7	00-015-0783	TiS3 Titanium Sulfide	0.000	0.722(13/18)	0.676	-----	0.488
				3.25	-----	P21/m	
8	00-049-1446	Al3Ti Aluminum Titanium	0.000	0.667(4/12)	0.714	-----	0.476
				3.41	-----	Pm-3m	
9	00-027-0759	MgO4 Magnesium Oxide	0.000	0.778(7/11)	0.612	-----	0.476
				3.70	-----	R	
10	00-052-0859	AlTi3 Aluminum Titanium	0.000	0.684(13/19)	0.661	-----	0.452
				4.20	-----	P63/mmc	
11	00-050-0927	C Carbon	0.000	0.800(8/10)	0.556	-----	0.444
				-----	-----	R	
12	00-036-1337	TiS3 Titanium Sulfide	0.000	0.846(11/13)	0.518	-----	0.438
				3.26	-----	P21/m	
13	00-023-0441	Na2S Sodium Sulfide	0.000	0.700(7/20)	0.615	-----	0.431
				1.85	-----	Pm-3m	
14	00-015-0776	Al6Si2O13 Aluminum Silicate (Mullite, syn)	0.000	0.509(27/63)	0.841	-----	0.428
				3.17	-----	Pbam	
15	00-031-0274	CaFe3O5 Calcium Iron Oxide	0.000	0.667(14/21)	0.621	-----	0.414
				4.50	-----	-----	
16	00-012-0708	SiO2 Silicon Oxide	0.000	0.636(7/11)	0.648	-----	0.412
				2.55	-----	P3221	
17	00-031-0967	KAl3Si2O8 Potassium Aluminum Silicate	0.000	0.667(8/12)	0.613	-----	0.409
				2.39	-----	Ia-3d	
18	00-055-0892	Mg0.93Ca0.07TiO3 Calcium Magnesium Titanium Oxide (Geikiel	0.000	0.786(11/14)	0.519	-----	0.407
				-----	-----	R-3	
19	00-049-1855	Ca8Mg(SiO4)4Cl2 Calcium Magnesium Chloride Silicate (Rond	0.000	0.667(20/60)	0.604	-----	0.403
				3.04	-----	Fd-3	
20	00-030-0900	K-Al-Fe-PO4 Potassium Aluminum Iron Phosphate	0.000	0.714(5/ 7)	0.561	-----	0.400
				-----	-----	-----	

Group Name : Standard
 Data Name : Nkomo
 File Name : Nkomo.PKR
 Sample Name : Flyash2
 Comment :

<Card List>

No.	Card	Chemical Formula	S	L	d	I	R
		Chemical Name (Mineral Name)		Dx	WT%	S.G.	
21	00-038-0903	O2 Oxygen	0.000	1.000(4/ 4)	0.400	-----	0.400
22	00-046-1045	SiO2 Silicon Oxide (Quartz, syn)	0.000	0.591(13/58)	0.677	-----	0.400
23	00-056-0457	Al2O3 Aluminum Oxide	0.000	0.667(8/22)	0.561	-----	0.374
24	00-050-1546	CaSMg(SiO4)4Cl2O Calcium Magnesium Oxide Chloride Silicate	0.000	0.647(22/47)	0.574	-----	0.371
25	00-033-0664	Fe2O3 Iron Oxide (Hematite, syn)	0.000	0.650(13/45)	0.570	-----	0.371
26	00-044-1154	Al0.58Mg0.42 Aluminum Magnesium	0.000	0.583(7/12)	0.632	-----	0.369
27	00-059-0333	Ca8OC12(Si2O7)2 Calcium Oxide Chloride Silicate (Unnamed	0.000	0.657(23/49)	0.560	-----	0.368
28	00-022-0945	Ti17P10 Titanium Phosphide	0.000	0.500(7/14)	0.730	-----	0.365
29	00-034-0673	Mg2Si Magnesium Silicon	0.000	0.550(11/20)	0.658	-----	0.362
30	00-047-1771	Al2O3 Aluminum Oxide (Unnamed mineral (NR))	0.000	0.684(13/25)	0.529	-----	0.362
31	00-041-0248	CaSMg(SiO4)4Cl2 Calcium Magnesium Chloride Silicate (Rond	0.000	0.615(16/26)	0.587	-----	0.361
32	00-063-0243	(Ca11.91Na0.06)(Al13.89Fe0.16Ti0.01 Sodium Calcium Aluminum Iron Titanium Oxid	0.000	0.579(22/62)	0.608	-----	0.352
33	00-011-0252	SiO2 Silicon Oxide	0.000	0.588(10/18)	0.597	-----	0.351
34	00-047-1698	Na2S Sodium Sulfide	0.000	0.600(6/23)	0.581	-----	0.348
35	00-010-0423	AlPO4 Aluminum Phosphate (Berlinite, syn)	0.000	0.621(18/70)	0.558	-----	0.346
36	00-045-0568	Ca12Al14O32Cl2 Calcium Aluminum Oxide Chloride (Chlormay	0.000	0.500(16/37)	0.689	-----	0.345
37	00-056-0458	Al2O3 Aluminum Oxide	0.000	0.727(8/22)	0.474	-----	0.345
38	00-059-0189	SiTi3C2 Silicon Titanium Carbide	0.000	0.583(14/29)	0.589	-----	0.344
39	00-016-0867	Ti3.3Al Aluminum Titanium	0.000	0.667(14/35)	0.512	-----	0.341
40	00-022-1069	C Carbon (Chaocite)	0.000	0.667(12/22)	0.506	-----	0.337

Group Name : Standard
 Data Name : Nkomo
 File Name : Nkomo.PKR
 Sample Name : Flyash2
 Comment :

<Card List>

No.	Card	Chemical Formula Chemical Name (Mineral Name)	S	L	d	I	R
			Dx	WT%	S.G.		
41	00-004-0345	C16K Potassium Graphite	0.000	0.545(6/13)	0.610	-----	0.333
				2.07	-----	P	
42	00-016-0728	CaP Calcium Phosphide	0.000	0.571(8/14)	0.579	-----	0.331
				-----	-----	-----	
43	00-042-1401	SiO2 Silicon Oxide (Tridymite-O)	0.000	0.500(11/23)	0.657	-----	0.328
				2.45	-----	F	
44	00-009-0413	Ca12Al14O33 Calcium Aluminum Oxide	0.000	0.548(17/36)	0.582	-----	0.319
				2.68	-----	I-43d	
45	00-025-1112	NaS2 Sodium Sulfide	0.000	0.472(25/55)	0.668	-----	0.315
				2.13	-----	I-42d	
46	00-061-0035	SiO2 Silicon Oxide	0.000	0.490(25/56)	0.634	-----	0.311
				2.64	-----	P3121	
47	00-043-0745	SiO2 Silicon Oxide	0.000	0.500(11/22)	0.618	-----	0.309
				-----	-----	-----	
48	00-047-1625	P Phosphorus	0.000	0.565(13/23)	0.545	-----	0.308
				2.42	-----	P2/c	
49	00-026-0031	Al2O3 Aluminum Oxide	0.000	0.556(10/32)	0.552	-----	0.307
				3.74	-----	P63mc	
50	00-042-1360	SiC Silicon Carbide (Moissanite-SH)	0.000	0.619(13/43)	0.494	-----	0.306
				3.26	-----	P	
51	00-017-0061	Mg2Si Magnesium Silicon	0.000	0.556(5/ 9)	0.539	-----	0.300
				2.10	-----	P-62c	
52	00-029-1194	NaCa(PO4) Sodium Calcium Phosphate (Buchwaldite)	0.000	0.529(9/22)	0.565	-----	0.299
				3.26	-----	Pmn21	
53	00-041-0753	CaFeO3 Calcium Iron Oxide	0.000	0.412(7/17)	0.726	-----	0.299
				4.45	-----	-----	
54	00-009-0427	Fe3+2Al2(SiO4)3 Iron Aluminum Silicate (Almandine)	0.000	0.563(9/28)	0.519	-----	0.292
				4.31	-----	Ia-3d	
55	00-017-0424	TiSi Titanium Silicon	0.000	0.565(13/38)	0.517	-----	0.292
				4.24	-----	Pnma	
56	00-018-1207	C32Na Sodium Carbon	0.000	0.500(5/12)	0.574	-----	0.287
				-----	-----	-----	
57	00-033-1381	TiO2 Titanium Oxide	0.000	0.600(6/10)	0.478	-----	0.287
				5.07	-----	P63	
58	00-053-0899	Na3(Mg3Fe+3Ti+4)Si8O22O2 Sodium Magnesium Iron Titanium Oxide	0.000	0.455(10/22)	0.628	-----	0.286
				3.15	-----	C2/m	
59	00-052-0861	Al2Ti Aluminum Titanium	0.000	0.500(15/30)	0.569	-----	0.285
				3.53	-----	I41/amd	
60	00-018-1170	SiO2 Silicon Oxide (Tridymite-M, syn)	0.000	0.411(23/56)	0.685	-----	0.281
				2.25	-----	Cc	

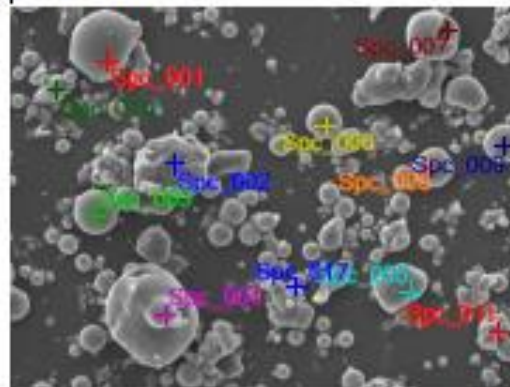
APPENDIX D: EDS ANALYSIS OF FLY ASH SAMPLE

Smp_FlyAsh



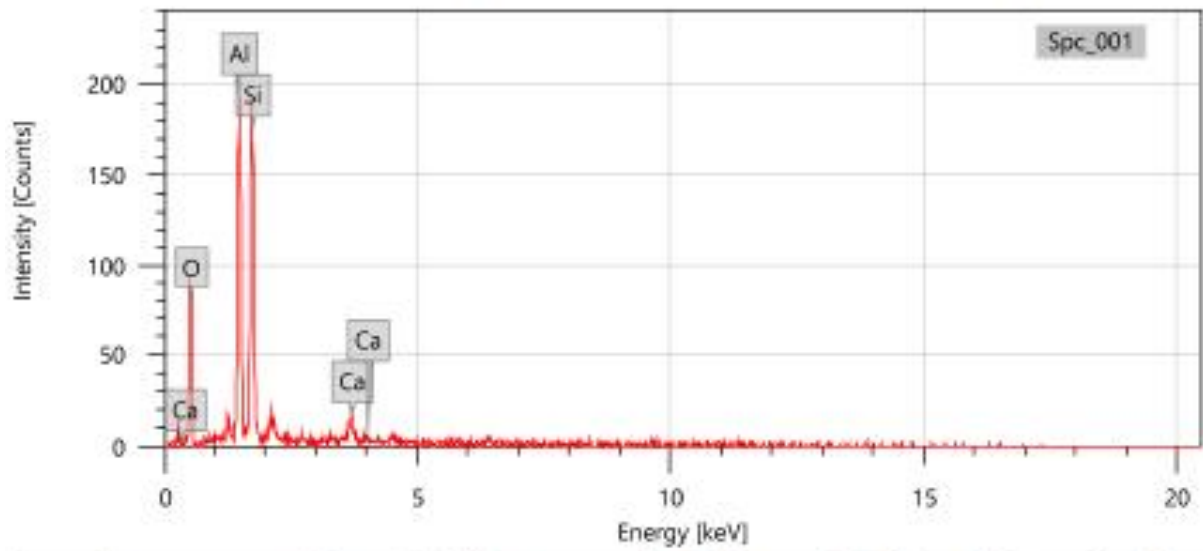
20 mm

Sem_SED_002



Signal SED
Landing Voltage 15.0 kV
WD 16.2 mm
Magnification x650
Vacuum Mode HighVacuum

20 μm



Items	Value
measurement conditions	
Acceleration voltage	20.00 kV
Probe current	-
Magnification	x 850
Process time	T3
Measurement detector	First
Live time	30.00 seconds
Real time	30.25 seconds
Dead time	1.00 %
Count rate	317.00 CPS

Display name	Standard data	Quantification method	Result Type
Spc_001	Standardless	ZAF	Metal
Element	Line	Mass%	Atom%
O	K	43.05±1.48	57.14±1.96
Al	K	22.73±0.72	17.89±0.57
Si	K	30.29±0.96	22.90±0.72
Ca	K	3.92±0.40	2.08±0.21
Total		100.00	100.00
Spc_001			Fitting ratio 0.2171

APPENDIX E: REBOUND NUMBER

Code	A	B	1	2	3	4	5	6	7	8	9	10	Avg
S3	0	0	19,00	25,00	23,00	15,00	17,00	23,00	23,00	23,00	22,00	21,00	21,10
S4	0,5	15	19,00	19,00	17,00	24,00	19,00	30,00	19,00	16,00	20,00	17,00	20,00
S5	1.0	15	13,00	10,00	18,00	16,00	16,00	15,00	15,00	14,00	17,00	22,00	15,60
S6	1,5	15	15,00	14,00	16,00	14,00	17,00	13,00	11,00	15,00	12,00	11,00	13,80
S7	2.0	15	10,00	10,00	10,00	15,00	10,00	16,00	12,00	11,00	12,80	11,80	11,86
S8	0,5	20	18,00	16,00	24,00	16,00	20,00	18,00	22,00	20,00	26,00	20,00	20,00
S9	1.0	20	18,00	19,00	15,00	17,00	15,00	20,00	15,00	15,00	20,00	16,00	17,00
S10	1,5	20	18,00	17,00	16,00	16,50	15,00	16,00	17,00	17,50	19,00	17,00	16,90
S11	2.0	20	18,00	16,00	20,00	16,00	17,00	16,00	20,00	15,00	18,00	17,00	17,30
S12	0,5	25	22,00	28,00	24,00	18,00	24,00	22,00	18,00	19,00	18,00	22,00	21,50
S13	1.0	25	10,00	14,00	11,00	14,00	14,00	13,00	14,00	12,00	12,00	11,00	12,50
S14	1,5	25	22,00	20,00	28,00	24,00	22,00	20,00	20,00	18,00	20,00	20,00	21,40
S15	2.0	25	16,00	16,00	16,00	14,00	14,00	14,00	15,00	14,00	14,00	14,00	14,70
S16	0,5	30	14,00	15,00	20,00	17,00	21,00	17,00	12,00	12,00	16,00	16,00	16,00
S17	1.0	30	11,00	24,00	15,00	15,00	14,00	16,00	12,00	16,00	16,00	17,00	15,60
S18	1,5	30	20,00	22,00	17,00	16,00	16,00	18,00	15,00	14,00	14,00	14,00	16,60
S19	2.0	30	12,00	18,00	14,00	12,00	14,00	13,00	11,00	16,00	14,00	10,00	13,40
S20	0	15	26,00	22,00	26,00	28,00	25,00	30,00	20,00	24,00	22,0	25,00	24,80
S21	0	20	20,00	19,00	26,00	20,00	25,00	25,00	21,00	24,00	24,00	19,00	22,30
S22	0	25	26,00	16,00	26,00	26,00	33,00	22,00	24,00	21,00	22,00	24,00	24,00
S23	0	30	20,00	24,00	25,00	24,00	25,00	24,00	20,00	22,00	21,00	22,00	22,70
S24	0,5	0	21,00	16,00	21,00	18,00	21,00	20,00	18,00	12,00	18,00	18,00	18,30
S25	1.0	0	16,00	13,00	12,00	14,00	13,00	16,00	17,00	12,00	21,00	13,00	14,70
S26	1,5	0	12,00	13,00	13,00	15,00	15,00	16,00	18,00	22,00	16,00	14,00	15,40
S27	2.0	0	14,00	15,00	14,00	14,00	12,00	10,00	14,00	10,00	10,00	10,00	12,30

A – Fibre Mass Fraction (%); B – Fly Ash Mass Fraction (%); Avg – Average Rebound Number

APPENDIX F: TURNITIN REPORT

Thesis Turnitin

ORIGINALITY REPORT

14%

SIMILARITY INDEX

7%

INTERNET SOURCES

11%

PUBLICATIONS

3%

STUDENT PAPERS

PRIMARY SOURCES

1	T.F. Awolusi, O.L. Oke, O.O. Akinkurolere, A.O. Sojobi. "Application of response surface methodology: Predicting and optimizing the properties of concrete containing steel fibre extracted from waste tires with limestone powder as filler", Case Studies in Construction Materials, 2019 Publication	1%
2	www.hindawi.com Internet Source	<1%
3	Adib Fikri Abdul Manaf, Shahiron Shahidan, Shamrul-Mar Shamsuddin, Najamuddin Falakh Sharif et al. "Chapter 21 Properties of Concrete Containing Recycled Polyethylene Terephthalate (PET) Fibre", Springer Science and Business Media LLC, 2021 Publication	<1%
4	H. Ataei, K. Kalbasi Anaraki, Rui Ma. "Mechanical Properties of Polyethylene Terephthalate Particle-Based Concrete: A	<1%